Lysine acetyltransferase and deacetylase in normal and abnormal brain development

Lin Li

Division of Experimental Medicine

Department of Medicine

McGill University

Montreal, Quebec, Canada

October 2018

A thesis submitted to Graduate and Postdoctoral Studies Office of McGill University in partial fulfillment of the requirements of the degree of Doctor of Philosophy

ABSTRACT

Lysine acetyltransferases and deacetylases are not only important for regulating cellular programs (such as cell proliferation, differentiation and gene transcription), but also involved in developmental control and different diseases. As the most complex organ in mammals, the brain is controlled by intracellular and extracellular signaling pathways to maintain its developmental homeostasis. In these pathways, lysine acetylation plays an essential role. To understand the functions of this modification during brain development, I have investigated the roles of *a*lpha-*t*ubulin *a*cetyl*t*ransferase 1 (ATAT1) and *h*istone *deac*etylase 3 (HDAC3) during mouse brain development. Moreover, we have identified four clinical cases with heterozygous *de novo HDAC3* mutations associated with a novel neurodevelopmental disorder and determined the pathogenicity, establishing the first link of this enzyme to a genetic disease.

ATAT1 is an α-tubulin acetyltransferase responsible for acetylation of lysine 40 of α-tubulin on microtubules. Identified in the 1980s, the acetylation is conserved from protists to humans and the only posttranslational modification in the lumen of microtubules. Although it has been implied in regulating microtubule assembly and motor-based transport *in vitro*, the real biological function of this modification remains controversial. The function *in vivo* was largely unknown until ATAT1 was identified a few years ago. We examined the role of tubulin acetylation in mouse development using a mouse strain carrying an inactivated *Atat1* gene (Chapter II). We show that loss of *Atat1* does not affect mouse survival but leads to hypoplasia of the striatum and septum in the brain. However, development of many other tissues such as the hematopoietic system is normal. While proliferation, differentiation, apoptosis and autophagy are not affected in the mutant brain, our data suggest that the hypoplasia in the striatum and septum is due to defective neuronal migration. Further behavioral tests indicate that mice lacking ATAT1 display a mild motor coordination deficit.

HDAC3 is a class I deacetylase that forms tetrameric complexes containing two small subunits and the nuclear receptor co-repressor NCoR or SMRT, either of which is essential for embryonic brain development. Although some evidence indicates that HDAC3 is important in the adult mouse brain, its roles in the embryonic mouse brain and the human brain are entirely unclear. To investigate this, we have adopted two strategies. In the first one, we engineered and

analyzed a mouse model with *Hdac3* specifically deleted in the cerebrum (Chapter III). In the second strategy, we identified and analyzed *HDAC3* germline mutations in human patients (Chapter IV). In Chapter III, we show that mouse *Hdac3* inactivation affects embryonic development of the neocortex and hippocampus and induces anxiety and hyperactivity in the resulting pups. We found that the defects are due to abnormal development of neural stem and progenitor cells. Moreover, inhibition of HDAC3 activity by a selective small-molecule inhibitor in cell-based assays *in vitro* confirmed that the enzymatic activity is essential for neural stem cell development. Using transcriptomic analysis of neurospheres originated from *Hdac3*-deficient cerebral cortices and neural stem cells, we observed altered expression of multiple genes, including increased transcription of neurogenesis-promoting genes (such as *Dlx* family genes) and decreased mRNA levels of neurogenesis-inhibiting genes (such as *Id* and *Hes* family genes). By transcriptomic analysis and co-immunoprecipitation, we demonstrated that multiple transcription factors, such as NFIB, COUP-TFI, RP58 and SOX4, are highly expressed in the cerebrum and interact with HDAC3. In Chapter IV, we present data on *HDAC3* mutations identified in 4 patients with a new neurodevelopmental disorder. We show that these patient-derived *HDAC3* mutations do not affect formation of the SMRT tetrameric complex, but the enzymatic activity is compromised for the resulting variants. These results make the first direct link of HDAC3 to a genetic disease.

In summary, I have uncovered a novel role of ATAT1 in mouse brain development and demonstrated that HDAC3 regulates mouse cerebral development via neural stem/progenitor cells. I have also obtained evidence that *HDAC3* mutations cause a novel neurodevelopmental disorder. This study thus yields original insights into how lysine acetylation affects mammalian brain development and sheds new light on abnormal brain development in related patients.

RÉSUMÉ

Les lysine acétyltransférases et désacétylases ne sont pas seulement importantes pour la régulation des programmes cellulaires (tels que la prolifération cellulaire, la différenciation et la transcription génique), mais aussi impliqués dans le contrôle du développement et de différentes maladies. En tant qu'organe le plus complexe chez les mammifères, le cerveau est contrôlé par des voies de signalisation intracellulaires et extracellulaires pour maintenir l'homéostasie durant le développement. Dans ces voies, l'acétylation de la lysine joue un rôle essentiel. Pour comprendre les fonctions de cette modification au cours du développement cérébral, j'ai étudié les rôles de l'*a*lpha-*t*ubuline *acét*yltransférase 1 (ATAT1) et de l'*h*istone *dés*a*c*étylase 3 (HDAC3) dans le développement du cerveau murin. De plus, nous avons identifié quatre cas cliniques avec des mutations hétérozygotes *de novo* HDAC3 associées à un nouveau trouble neurodéveloppemental et déterminé la pathogénicité, établissant ainsi le premier lien de cette enzyme avec une maladie génétique.

L'ATAT1 est une α-tubuline acétyltransférase responsable de l'acétylation de la lysine 40 de l'α-tubuline sur les microtubules. Identifiée dans les années 1980, l'acétylation est conservée des protistes à l'homme et est la seule modification post-traductionnelle dans la lumière des microtubules. Bien qu'elle ait été impliquée dans la régulation de l'assemblage des microtubules et du transport moteur *in vitro,* la fonction biologique réelle de cette modification reste controversée. La fonction *in vivo* était largement inconnue jusqu'à ce que ATAT1 ait été identifié il y a seulement quelques années. Nous avons examiné le rôle de l'acétylation de la tubuline dans le développement de la souris en utilisant une souche de souris portant un gène *Atat1* inactivé (Chapitre II). Nous montrons que la perte d'*Atat1* n'affecte pas la survie de la souris mais entraîne une hypoplasie du striatum et de la cloison dans le cerveau. Cependant, le développement de nombreux autres tissus tels que le système hématopoïétique est normal. Alors que la prolifération, la différenciation, l'apoptose et l'autophagie ne sont pas affectées dans le cerveau mutant, nos données suggèrent que l'hypoplasie dans le striatum et le septum est due à une migration défectueuse. D'autres tests comportementaux indiquent que les souris dépourvues d'ATAT1 présentent un léger déficit de coordination motrice.

HDAC3 est une déacétylase de classe I qui forme des complexes tétramériques contenant deux petites sous-unités et le co-répresseur du récepteur nucléaire NCoR ou SMRT, dont l'un ou l'autre est essentiel dans le développement cérébral embryonnaire. Bien que certaines données indiquent que HDAC3 est importante dans le cerveau de la souris adulte, son rôle dans le cerveau embryonnaire murin et dans le cerveau humain est totalement inconnu. Pour étudier cela, nous avons adopté deux stratégies. Nous avons premièrement conçu et analysé un modèle de souris avec *Hdac3* spécifiquement supprimé dans le cerveau (Chapitre III). Dans la deuxième stratégie, nous avons identifié et analysé les mutations *HDAC3* dans la lignée germinale chez les patients humains (Chapitre IV). Au Chapitre III, nous montrons que l'inactivation de *Hdac3* chez la souris affecte le développement embryonnaire du néocortex et de l'hippocampe et induit une anxiété et une hyperactivité chez les souriceaux. Nous avons constaté que les défauts sont dus au développement anormal des cellules souches et progénitrices neurales. De plus, l'inhibition de l'activité de HDAC3 par un inhibiteur sélectif de petites molécules *in vitro* a confirmé que l'activité enzymatique est essentielle au développement de cellules souches neurales. Nous avons observé une altération de l'expression de plusieurs gènes, notamment une transcription accrue des gènes promoteurs de la neurogenèse (tels que les gènes de la famille *Dlx*) et une diminution des niveaux d'ARNm des gènes inhibant la neurogenèse (tels que les gènes de la famille *Id* et *Hes*). Par l'analyse transcriptomique et la co-immunoprécipitation, nous avons démontré que plusieurs facteurs de transcription, tels que NFIB, COUP-TFI, RP58 et SOX4, sont fortement exprimés dans le cerveau et interagissent avec HDAC3. Au Chapitre IV, nous présentons des données sur les mutations HDAC3 identifiées chez 4 patients atteints d'un trouble neurodéveloppemental. Nous montrons que ces mutations HDAC3 dérivées du patient n'affectent pas la formation du complexe tétramère SMRT, mais l'activité enzymatique est compromise pour les variants résultants. Ces résultats font le premier lien direct entre HDAC3 et une maladie génétique.

En résumé, j'ai découvert un nouveau rôle de ATAT1 dans le développement du cerveau de la souris et a démontré que HDAC3 régule le développement cérébral embryonnaire chez les souris via des cellules souches/progénitrices neurales. J'ai également obtenu des preuves montrant comment les mutations HDAC3 provoquent un nouveau trouble neurodéveloppemental chez l'humain. Cette étude donne donc des indications originales sur la

façon dont l'acétylation de la lysine affecte le développement du cerveau des mammifères et jette une nouvelle lumière sur le développement anormal du cerveau chez les patients apparentés.

ACKNOWLEDGEMENTS

I am truly grateful to many people who have helped me in the past several years. First, I want to sincerely thank my supervisor, Dr. Xiang-Jiao Yang, for giving me the opportunity to study in his lab, and for his great guidance on—and support for—my study. His passion for science and his trail-blazing spirit in tireless exploration at scientific frontiers have inspired me to work harder, think bigger and aim higher, which I am sure will be beneficial for the rest of my scientific career.

Second, I want to thank the present and past members of Yang lab for collaboration and help. I need to express my sincere thanks to Ms. Go-Woon Kim, a former graduate student who guided me when I first joined the lab. Special thanks go to Kezhi, for his great help in experiments, as well as friendly invitations to holiday parties. Heartful thanks also go to Mohammad and Michael, who are always ready for help; Michael also translated the abstract into French for me. I also must thank Harvey Li for critical reading of this thesis. I would like to acknowledge different colleagues, including Linya You, Tarek Sabri, Ji Ji, Xin Liu, Hansong Du, Pengyong Han, Rami Alasiri, and Xiuli Bi, for their help and friendship. In particular, I collaborated fruitfully with Linya in an exciting project, which led a co-first author *J Clin. Invest.* paper (2016) for me. I also need to thank one of my best friends, Kezhuo, with whom I went through undergraduate and then PhD studies together, for numerous enjoyable and stimulating discussions. I must thank Drs. Hong Zhao and Ming Yan for their help in my study and friendly invitations to various parties. I also want to thank many other friends, whose names are not listed here, for being with me and supporting me in my life and during my education.

Third, I collaborated with Dr. Phillipe M. Campeau's lab at University of Montreal and would thus like to thank him, his lab members, and many other clinicians who identified the patients with *HDAC3* mutations. I also need to thank Lisa-Marie Legault and her supervisor Dr. Serge McGraw from CHU Sainte-Justine for generous help with the open field test analysis; Sriram Jayabal and his supervisor Dr. Alanna Watt for their kind help with the rotarod test; and Li-Ting Wang from Dr. Luke McCaffrey's lab for helping me take neurosphere images. Lisa-Marie Legault proofread my French translation as well. I would also like to thank Julien Leconte, Camille Stegen and Dr. Vinicius Motta for kind help with flow cytometry, as well as

Jo-Ann Bader, Cleber Moraes and Caroline Therien for their friendly help with histological analyses.

Fourth, I must thank my committee members, Drs. Maxime Bouchard, John White and Alan Peterson, for making their constructive suggestions and writing recommendation letters in a timely manner. I also need to thank Drs. Richard Roy, Jean-Jacques Lebrun and Luke McCaffrey for serving faithfully as members of my oral qualifying exam committee.

Last but not the least, I whole-heartedly thank my respectful father and mother for their natural love, great inspiration and unwavering support; my elder brother and younger sister for all their support and friendship along the way; and also my loving wife, Ding, and my dear daughter, Ruosi, for their companionship, encouragement and unconditional love. It is these members of my extended family who make my life joyful with purpose and meaning, so I would like to dedicate this doctoral thesis to them all.

PREFACE

I have chosen to write a manuscript-based thesis according to McGill University Guidelines for Thesis Preparation:

"As an alternative to the traditional thesis style, the research may be presented as a collection of papers of which the student is the author or co-author (i.e., the text of one or more manuscripts, submitted or to be submitted for publication, and/or published articles (not as reprints) but reformatted according to thesis requirements). These papers must have a cohesive, unitary character making them a report of a single program of research."

PUBLICATIONS ARISING FROM PHD STUDY

Publications presented in the thesis

1) Kim, G.W., Li, L., Ghorbani, M., You, L., and Yang, X.-J. (2013) Mice lacking α-tubulin acetyltransferase 1 are viable but displays dentate gyrus distortion. **J. Biol. Chem**. *288*, 20334-50.

2) Li, L. and Yang, X.-J. (2015) Tubulin acetylation: responsible enzymes, biological functions and human diseases. **Cell Mol. Life Sci.** *72*, 4237-4255.

3) You, L.*, Li, L.*, Zou, J., Yan, K., Belle, J., Nudnik, A., Wang, E., and Yang, X.-J. (2016) BRPF1 is essential for development of fetal hematopoietic stem cells. **J. Clin. Invest.** *126*, 3247–3262 (* co-1st authors).

4) Li, L., Jayabal, S., Legault, L., Ghorbani, M., McGraw, S., Watt, A, and Yang, X.-J. (2018) Tubulin acetyltransferase regulates septal and striatal development in the mouse brain. (Submitted).

5) Li, L. and Yang, X.-J. (2018) Histone deacetylase 3 governs perinatal cerebral development via neural stem and progenitor cells. (Submitted).

6) Li, L.*, Rousseau, J.*, …, Campeau, P.M., and Yang, X.-J. (2018) Heterozygous *HDAC3* mutations cause epilepsy and brain anomalies. (Manuscript in preparation for submission, *, co-1st authors).

7) Li, L.*, Rousseau, J.*, …, Campeau, P.M., and Yang, X.-J. (2018) Mutations of *GPS2* cause developmental delay, microcephaly and intellectual disability. (Manuscript in preparation for submission, *, co-1st authors).

Publications indirectly related to the thesis

1) Yan, K., You, L., Degerny, C., Ghorbani, M., Liu X., Chen L., Li, L., Miao, D. and Yang, X.J. (2015) The chromatin regulator BRPF3 preferentially activates the HBO1 acetyltransferase but is dispensable for mouse development and survival. **J. Biol. Chem.** *291*, 2647-63.

2) Li, L. and Yang, X.J. (2016) Molecular and Functional Characterization of Histone Deacetylase 4 (HDAC4). **Methods Mol. Biol.** *1436*, 31-45

3) Yan, K., Rousseau, J., Littlejohn, R.O., Kiss, C., Lehman, A., Rosenfeld, J.A., Stumpel, C.T.R., Stegmann, A.P.A., Robak, L., Scaglia, F., Nguyen, T.T.M., Fu, H., Ajeawung, N.F., Camurri, M.V., Li, L., Gardham, A., Panis, B., Almannai, M., Sacoto, M.J.G., Baskin, B., Ruivenkamp, C., Xia, F., Bi, W., Cho, M.T., Potjer, T.P., Santen, G.W.E, Parker, M.J., Canham, N., McKinnon, M., Potocki, L., MacKenzie, J.J., Roeder, E.R., Campeau, P.M., Yang X.-J. (2017) Mutations in the chromatin regulator gene BRPF1 cause syndromic intellectual disability and deficient histone acetylation. **Am. J. Hum. Genet**. *100*, 91-104

4) Li, L.*, Ghorbani, M.*, Rousseau, J.*, Campeau, P.M., and Yang, X.-J. (2018) KAT8 mutations cause intellectual disability and disrupt cerebral development. (Manuscript in preparation for submission, *, co-1st authors).

5) Li, L., …, and Yang, X.-J. (2018) BRPF1 governs transcriptomes in hematopoietic stem and progenitor cells. (Manuscript in preparation).

CONTRIBUTION TO ORIGINAL KNOWLEDGE

CHAPTER II

- ATAT1 and tubulin acetylation affect striatum and septum development in the mouse brain.
- Loss of *Atat1* affects brain functions such as motor coordination.
- ATAT1 has minor effects on mouse embryonic fibroblast properties and is not essential for hematopoiesis but loss of *Atat1* leads to platelets overproduction.
- There might be a minor tubulin acetyltransferase(s) other than ATAT1 in certain tissues.

CHAPTER III

- Cerebrum-specific loss of mouse *Hdac3* leads to developmental defects in the neocortex and hippocampus.
- HDAC3 is critical for neural stem cell fate determination through transcriptional regulation of multiple genes which include but not limited to *Dlx*, *Id* and *Hes* family genes.
- Several transcription factors (including NFIB, COUP-TFI, RP58 and SOX4), highly expressed in the mouse embryonic cerebral cortex and neural stem/progenitor cells, interact with HDAC3.

CHAPTER IV

- Characterized 4 human *HDAC3* mutations linked to a new neurodevelopmental disorder.
- Patient-derived *HDAC3* mutations compromise HDAC3 enzymatic activity while do not affect formation of a tetrameric complex with SMRT, GPS2 and TBL1Y.

APPENDIX A

- ATAT1 is the major *bond fide* tubulin acetyltransferase in mice.
- Loss of *Atat1* causes distortion in the dentate gyrus of hippocampus.

APPENDIX B

- BRPF1 is essential for mouse hematopoietic stem cell (HSC) development.
- Loss of mouse *Brpf1* reduces histone acetylation, diminishes HSCs, and leads to bone marrow failure.

CONTRIBUTION OF AUTHORS

CHAPTER I

A part of Chapter I is adapted from a review already published in *Cell. Mol. Life Sci.* I drafted the review and Dr. Yang finalized it.

CHAPTER II

I designed and carried out all the experiments except the one on iPS reprogramming of wild-type and *Atat1*$^{-/-}$ MEFs, which was carried out by Mohammad Ghorbani. Sriram Jayabal helped me with setting up the rotarod test. I analyzed all the data and wrote the manuscript. Dr. Yang provided overall supervision of the project.

CHAPTER III

I designed and carried out all the experiments, analyzed the data and wrote the manuscript. Dr. Yang helped analyze the RNA-seq data originated from the neurospheres and cerebral cortices. Dr. Yang provided overall supervision of the project.

CHAPTER IV

Dr. Yang and I designed the experiments. Dr. Philippe M. Campeau (University of Montreal) and several other clinicians (whose names will appear on the author list of publication resulting from Chapter IV) identified the patients, provided the mutation information, and collected the clinical information, consents and clinical samples.

APPENDIX A

The project was initiated by a former graduate student. I performed experiments for Figs. 6, 7 and 8, and also participated in experimental design, writing and revision of the manuscript. I am the 2nd author on the paper presented in Appendix A.

APPENDIX B

The project was initiated by a former doctoral student. I carried out experiments and the results were used in Figs. 8A-D, S1, S2, S6, S8, S10, S11 and S12, as well as Table S2. I participated in experimental design, data analysis, and revision of the manuscript. I am the co-1st author on the paper presented in Appendix B.

TABLE OF CONTENTS

LIST OF ABBREVIATIONS

ATAT1: alpha-tubulin acetyltransferase 1

ADHD: attention deficit hyperactivity disorder

BRPF1: bromodomain and PHD finger-containing protein 1

BRD: bromodomain

CNS: central nervous system

COUP-TFI: chicken ovalbumin upstream promoter transcription factor I

CP: cortical plate

ChIP: chromatin immunoprecipitation

Co-IP: co-immunoprecipitation

CBC: complete blood counting

DLX: distal-less homeobox

DAD: deacetylase activating domain

DNA: deoxyribonucleic acid

Esa1: essential Sas2-related acetyltransferase 1

FPKM: fragments per kilobase of transcript per million mapped reads

GPS2: G protein pathway suppressor 2

GNATs: Gcn5-related N-acetyltransferases

HAT: histone acetyltransferase

HDAC: histone deacetylase

HES: hairy and enhancer of split-1

HSC: hematopoietic stem cell

HPC: hematopoietic progenitor cell

HSPC: hematopoietic stem and progenitor cells

ID: inhibitor of DNA-binding/differentiation proteins

KAT: lysine (K) acetyltransferase

KDAC: lysine (K) deacetylase

LPS: lipopolysaccharides

MEFs: mouse embryonic fibroblasts

MOF: males absent on the first

MPP: multipotent progenitor

MSNs: medium spiny neurons

MeCP2: Methyl-CpG-binding protein 2

MiDAC: mitotic deacetylase complex

NS-DADm: mutations in the NCOR1 and SMRT-DAD domains

NSC: neural stem cell

NSPC: neural stem and progenitor cell

NCoR1: nuclear receptor co-repressor 1

NuRD: nucleosome remodeling and deacetylase complex

NODE: Nanog and Oct4-associated deacetylase complex

NFIB: nuclear factor IB

NR2F1: nuclear receptor subfamily 2 group F member 1

NCoA: nuclear receptor co-activators

PTM: posttranslational modification

PHD: plant homeodomain

RP58: transcriptional repressor 58

RNA: ribonucleic acid

RGCs: radial glial cells

SMRT: silencing mediator of retinoic acid and thyroid hormone receptor

SOX2: SRY (sex determining region Y)-box 2

SRC: steroid receptor co-activators

SANT: SWI3/ADA2/N-CoR/TFIII-B domains

TUNEL: Terminal deoxynucleotidyl transferase dUTP nick end labeling

TBL1Y: transducin beta like 1, Y-linked

VZ/SVZ: ventricular zone/subventricular zone

YEATS: Yaf9, ENL, AF9, Taf14, Sas5

ZNF238: zinc finger protein 238

ZFP238: zinc finger protein 238

ZBTB18: zinc finger and BTB domain-containing protein 18

LIST OF FIGURES AND TABLES

Chapter I

Chapter II

Chapter III

CHAPTER I: Literature review

1.1 General introduction

1.1.1 Lysine acetylation

After synthesis and for functional regulation, proteins are subject to covalent modifications. These post-translational modifications (PTMs) include phosphorylation, acetylation, methylation, ubiquitination, succinylation, crotonylation, propionylation, hydroxylation, ubiquitination, and sumoylation (1). Chemically, acetylation refers to the process of adding an acetyl group to amino acid residues in proteins. There are two types of protein acetylation, namely N^{α}-terminal acetylation and N^{ε}-lysine acetylation. N^{α}-terminal acetylation is very common occurring in about 85% of mouse proteins (2) and 57%-68% of yeast proteins (3). This type of acetylation is co-translational and irreversible; it regulates protein synthesis, stabilization and subcellular localization (4, 5). N^{ε}-lysine acetylation is another type of acetylation that involves the addition of an acetyl moiety to the ε-amino group of lysine residues in proteins. Different from N^{α}-terminal acetylation, N^{ε}-lysine acetylation is post-translational and reversible. Its levels are dynamically regulated in various cellular processes (4). Hereafter in this thesis, acetylation refers to N^{ε}-lysine acetylation.

Lysine acetylation and deacetylation are controlled by lysine acetyltransferases (KATs) and lysine deacetylases (KDACs), respectively (Fig. 1.2). Lysine acetylation occurs on both histones and non-histone proteins. Histone acetylation is found on all histones. A list of histone acetylation sites and their responsible enzymes are shown in Table 1.1. Histone acetylation and deacetylation regulate gene expression, with specific acetylation marks producing distinct outcomes. It appears that not all the acetylated sites have specific functions, with the exception of H4K16ac (acetylation of histone H4 at lysine 16). This modification has a specific role for chromatin condensation and folding (6).

Non-histone lysine acetylation, on the other hand, is found in many different categories of proteins. For instance, acetylation is found in cytoskeletal proteins such as α-tubulin in assembled microtubules (7); transcription factors and transcriptional co-regulators such as GATA proteins, STAT proteins, YY1, PGC1, Rb, c-Myc and p53 (4, 8, 9); chaperone proteins

such as Hsp90 and α-crystallin (10); and inflammatory signaling related proteins such as p38 MAPKs (11). In a most recent proteomic study, over 3600 lysine residues on about 1750 proteins were found to be acetylated. A majority of these proteins belong to non-histone proteins (12). More protein acetylation sites might be identified as high-resolution mass spectrometry develops rapidly.

Lysine acetylation exerts its effects through different mechanisms. For histone acetylation, the classical model is that the addition of an acetyl group neutralizes the positive charge on the unmodified lysine residues. This neutralization loosens the interaction between histone tails and phosphate backbones of DNA and leads to chromatin relaxation, promoting transcription (13-16) (Fig. 1.1). A more recent theory is the "histone code" hypothesis (13, 16). According to this hypothesis, histone modifications, such as methylation, acetylation, ubiquitination and phosphorylation, coordinate with each other to regulate chromatin structure and gene transcription. Moreover, this hypothesis also posits that histone modifications alter chromatin structure and regulates transcription by interacting with reader proteins (14-17). For histone acetylation, these proteins are now known to possess "reader" domains, including the bromodomain (BRD), double PHD zinc finger (DPF), and YEATS domain (18) (Fig. 1.2).

The bromodomain is a conserved domain possessed by many chromatin-associated proteins such as the BET family proteins, BRPF family proteins, CBP, p300, GCN5 and PCAF (18, 19). DPF domains are structurally conserved modules that selectively recognize histone acetylation (20) as well as histone methylation (21, 22). DPF3, MOZ and MORF contain this domain. YEATS is another domain that recognizes and binds to acetylated lysine residues (23), although recent studies imply that the YEATS domain has preference for crotonylation over acetylation (24). YEATS domain-containing proteins include AF9, ENL and GAS41(18). DNA-PKcs is a non-canonical BRD-containing protein that specifically recognizes H2AX acetylated at lysine 5 (25). However, no acetylation cascades have been firmly identified (26, 27).

Acetylation of lysine residues in non-histone proteins also modulate enzymatic activity. For example, acetylation of lysine 19 in hGLYATL2 decreases its enzymatic activity (28). Lysine acetylation occurs in evolutionarily conserved lysine residues in catalytic domains of enzymes in central carbon metabolism. Acetylation in these sites inhibit the enzymatic activity

of these proteins (29). In recent studies, it was shown that interactions between nearby acetyl moieties on lysine residues also exert effects on proteins. In the case of microtubules, the interactions between nearby acetyl groups in α-tubulin enhance the flexibility of microtubules under physical pressure (30, 31). Lysine acetylation regulates protein folding as well. Acetylation of Hsp70 at lysine 77 favors its binding to the co-chaperone Hop to allow protein refolding (32). Lysine acetylation also affects protein-DNA interaction. Acetylation in proteins such as p53, p50, NF-kappa B, E2F, EKLF and PC4 enhances sequence-specific DNA binding (33), while acetylation in FoxO1, HMGI, p65, *etc.*, decreases DNA binding capacity (34).

1.1.2 Lysine acetyltransferases (KATs)

Based on structural and functional similarities of their catalytic domains, the currently known KATs (about 15 in humans) are categorized into three major families (35) (Fig. 1.3). The first is the GNAT (GCN5-related N-acetyltransferases) superfamily, which is so named for sequence similarities to the GCN5 enzyme. Members of this family have a common domain that contains 4 conserved motifs. Many proteins in this family also contain a bromodomain or chromodomain which can bind to acetylated or methylated lysine residues, respectively (35, 36). Members of this family include Gcn5, PCAF, HAT1, ESCO1, ESCO2, Elp3 and ATAT1 (37, 38). Of note, HAT1 acetylates cytoplasmic histones and is responsible for histone H4 acetylation at lysine residues 5 and 12 (39, 40), while the other HATs may be recruited to promoters and generate a localized domain of histone acetylation. The MYST family is the second type because of the possession of a common MYST domain. The name “MYST” comes from the 4 founding members: MOZ, Ybf2 (a.k.a. Sas3), Sas2 and TIP60. While MOZ and TIP60 are human proteins, Sas2 and Sas3 are from yeast. Members of this family share a highly conserved MYST domain composed of an acetyl-CoA binding motif and a zinc finger. Some family members also contain other common domains such as chromodomains and plant homeodomain-linked (PHD) zinc fingers. The other three members of this family of human proteins include MOF, MORF and HBO1, whereas Esa1 is the third member in yeast (41, 42). The third family of HATs is smaller, composed of p300 and CBP family (35, 43).

Many KATs form multisubunit protein complexes that are stoichiometric and highly stable. For example, MOZ (as well as MORF and HBO1) forms a tetrameric protein complex with

BRPF1, ING5 and EAF6 (42, 44). HAT-containing complexes are recruited to target genetic loci by other transcription factors. For example, RUNX recruits the complex containing MOZ/MORF to the MIP-1α promotor and facilitates transcription of MIP-1α (42). Some HATs are not specific for an individual lysine site but could still fulfill specific functions. One possible mechanism to achieve this is through distinct genome localization via non-catalytic domains such as the bromodomain, chromodomain, PHD finger, WD40 domain and tudor domain on these enzymes and/or their associated subunits (45). In some cases, KATs have functions that are independent of their enzymatic activity. For example, KAT3A activates β-catenin, which is a transcription factor involved in inflammatory regulation, independent of its enzymatic capacity (46).

Non-histone proteins are catalyzed by HATs as well, with some exceptions. For instance, ATAT1 acetylates α-tubulin on assembled microtubules but cannot acetylate histones (47). Similarly, ESCO1 and ESCO2 acetylate cohesion but not histones (48-50). Acetylation of non-histone proteins regulates transcription, as well as mRNA and protein stability, cell cycle, circadian rhythms, metabolism, *etc.* (8, 9). In many cases, non-histone acetylation is relevant for tumorigenesis, cancer proliferation and immune functions (9). More non-canonical proteins might be identified to possess intrinsic lysine acetyltransferase activity. As an example, TAU, which is a protein involved in Alzheimer's disease, was unexpectedly identified to be a lysine acetyltransferase (51).

1.1.3 Lysine deacetylases (KDACs)

KDACs in humans are classified into 4 classes according to their sequence homology to the yeast histone deacetylases (Fig. 1.3). Class I KDACs have a similar domain structure to the yeast Rpd3 and its members include HDAC1, -2, -3 and -8. Class II KDACs share similar domain structure to the yeast Hda1. Class IIa KDACs are composed of HDAC4, -5, -7 and -9, and class IIb comprises HDAC6 and -10. Sir2 (silent information regulator-2) and sirtuin (Sir2-like protein) are NAD^+-dependent and form class III. In humans, class III KDACs include SIRT1-7. HDAC11 shows similar homology to both Rpd3 and Hda1 and is thus classified into a new class, the class IV HDAC. Compared to sirtuin proteins, class I, II and IV KDACs were found earlier and are zinc-dependent, thus referred to as the "classical family" of KDACs (52).

Like HATs, some KDACs exist in large protein complexes. For example, HDAC1/2 is found in 3 distinct multisubunit protein complexes, which include the NuRD, Sin3 and Co-REST/REST complexes (53-55). Moreover, three other types of complexes containing HDAC1/2 were also identified, namely, the SHIP, NODE and MiDAC complexes (56-58). In contrast, HDAC3 is found in only one type of complexes, namely the NCoR/SMRT complexes (59-61).

HDACs can function through its enzymatic activities as well as function independent of its enzymatic activities. Through their enzymatic capacity, deacetylation of histones leads to condensed chromatin (heterochromatin) and thus represses transcription. For example, histone deacetylase activity is essential for HDAC1-mediated transcriptional repression (62). HDAC7 associates with Runx2 and represses Runx2 transcriptional activity in a deacetylase-independent manner (63). Typically, individual HDAC has enzymatic activity towards multiple lysine residues. HDACs together with their complexes could be recruited to specific promoters and thus achieves specific functions.

Deacetylation of non-histone proteins is usually catalyzed by KDACs. Although bearing the name “histone”, HDAC6 is a lysine deacetylase that has a unique substrate specificity mainly for nonhistone proteins (64), including α-tubulin (65). The dynamic balance of non-histone protein acetylation and deacetylation regulates various cellular activities as mentioned above in section 1.1.1.

1.1.4 KATs and KDACs in mouse brain development

Brain development is regulated by transcriptional factors and epigenetic regulators, as well as by environmental signals including growth factors and signaling molecules (Fig. 1.4). The mammalian brain is the most complicated organ. During the early embryonic stage, the nervous system derives from the ectoderm germ layer, which consists 3 parts: external ectoderm, neural crest and neural tube (66). The central nervous system (CNS) continues to develop with the closure of neural tube and formation of brain vesicle which contains neuroepithelium (66). Neuroepithelial cells are the first neural stem cells (NSCs). At the beginning, neuroepithelial cells undergo symmetric proliferative division, and later, these cells differentiate into radial glial cells (RGCs) (which is a mixture of neural stem and progenitor cells) and undergo

neurogenesis (Fig. 1.4) (66). Neurogenesis produces neurons as well as other progenitor cells. In mice, neurogenesis starts at around embryonic day 10 and slows down rapidly at around day 18 (67). Gliogenesis is inhibited during the embryonic neurogenesis stage and starts to erupt at around the neonatal stage (68). Neurogenesis is very limited in adult mice and humans, compared with embryos. The development of embryonic NSPCs is important as it is near irreversible after reaching the adulthood.

The spatial and temporal development of the brain is tightly regulated by the transcriptional machinery, containing transcription factors and epigenetic regulators. The molecular mechanisms that control embryonic neurogenesis have been extensively studied. Transcription factors, such as Notch, TGF and β-catenin, are the master regulators that regulate neural stem cell self-renewal and differentiation (69). Epigenetic regulators, which regulate DNA and histone modifications, play a vital role in the development of neural stem cells as well. For example, conditional deletion of *Ezh2* gene, which is a histone H3K27 methyltransferase, in the mouse forebrain disrupts the balance between self-renewal and differentiation in the cerebral cortex (70). Some KATs and KDACs have also been shown to be essential for brain development, regulating differentiation, proliferation or survival of neural stem and/or progenitor cells. For instance, absence of p300 or CBP leads to neural tube closure defects (71, 72). Double knockout of HDAC1 and 2 leads to neurodevelopmental defects (73). These KATs and KDACs regulate neural stem cell development through control of gene expression. In the case of HDAC1/2, neuron-restrictive silencing factor/RE-1 silencing transcription factor (NRSF/REST) binds to its DNA response element (RE-1) and recruits the complex containing Sin3a and HDAC1/2 to promote transcriptional repression (74). These studies support the importance of KATs and KDACs in early brain development.

1.1.5 KATs and KDACs in neurodevelopmental disorders

Abnormalities in CNS development lead to a variety of sensory, motor and cognitive disorders, including Rett syndrome, Down syndrome and intellectual disability. Some neurodevelopmental disorders are found to be single-gene Mendelian diseases, caused by mutations either inherited from parents or acquired *de novo* during early gestation. For example, Rett syndrome is a rare neurological and developmental disorder that affects brain development

and leads to progressive inability in using muscles that control movement, coordination and communication. Frequently, it also causes seizures and intellectual disability. Rett syndrome is due to X-linked *MeCP2* mutations and almost exclusively occurred in girls as the mutation in the male is lethal. For 99.5% of all cases, Rett syndrome is sporadic and due to *de novo* mutations in the gene (75).

The dynamic process of lysine acetylation and deacetylation links the extracellular signals to intracellular responses (76). Until recently, ~30 chromatin modifiers have been associated with human diseases, a lot of which show symptoms such as neurodevelopmental delay, microcephaly and intellectual disability. For KATs, gene mutations for CREBBP, EP300, KAT6A, KAT6B and ESCO2 have been identified in these disorders so far (77-85). For KDACs, only HDAC4 and HDAC8 mutations are implicated in human diseases directly (86, 87). Epigenetic "readers" are also involved in human diseases. Mutations of *BRPF1*, which is a histone acetylation "reader" and a subunit of the MOZ protein complex, are implied in developmental delay and brain disorders (88). HDAC inhibitors such as valproic acid have been used in clinical treatment of epilepsy and bipolar disorders for over six decades (89, 90). Tapias *et al.* have published a comprehensive review on the roles of KATs and KDACs in mouse brain development and human neurodevelopmental disorders (76).

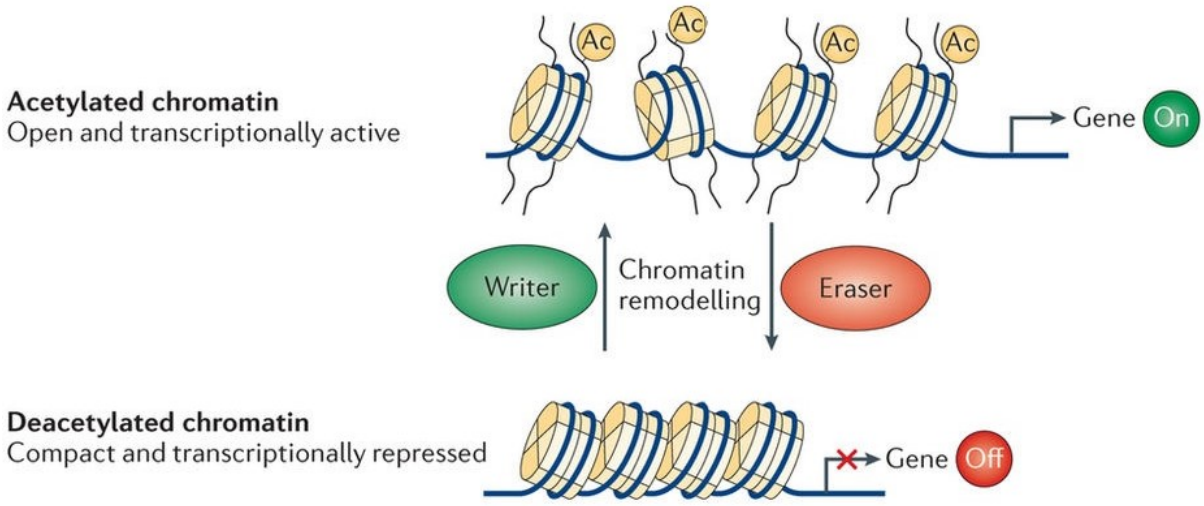

Figure 1.1. Histone acetylation and deacetylation mark an open and compact chromatin respectively.

Acetylation of histone tails by "writer" (HATs) leads to an open and transcriptionally active chromatin structure, while deacetylation by "eraser" (HDACs) results in a compact and transcriptionally repressed chromatin structure. Adapted from Verdin and Ott, Nature Reviews Molecular Cell Biology **16**, 258–264 (2015), doi:10.1038/nrm3931, with permission from Springer Nature.

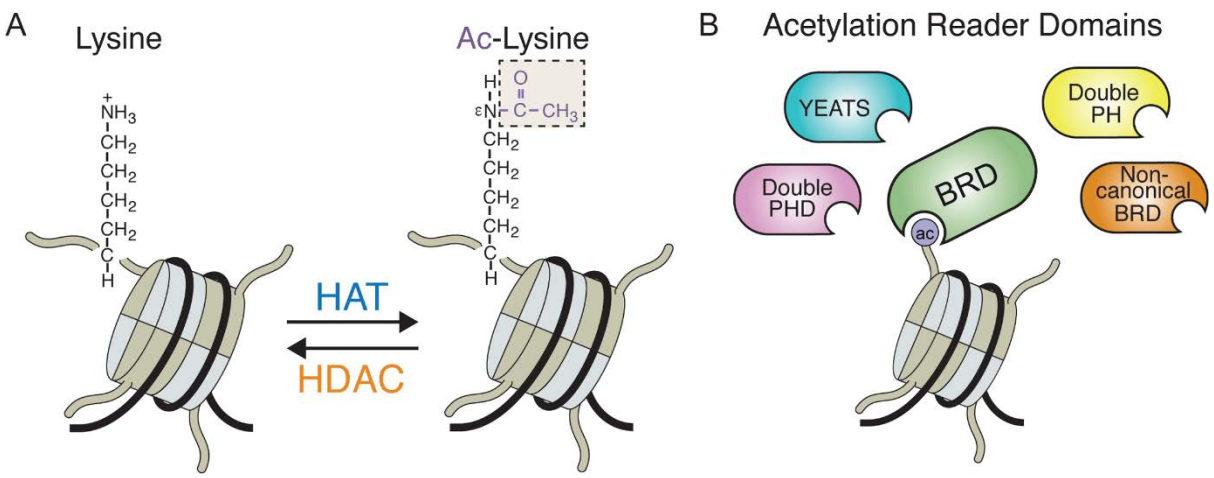

Figure 1.2. Histone acetylation and its reader proteins.

A, Histone acetylation refers to the addition of an acetyl moiety to the ε-amino group of a lysine residue catalyzed by a HAT, and the reversible process is catalyzed by a HDAC. B, Lysine acetylation "readers", such as the bromodomain (BRD), double plant homeodomain (PHD) finger, double pleckstrin-homology (PH) domain, YEATS domain and non-canonical BRD, could bind to acetylated histones and thus regulate transcription. Copyright: Gong *et al*., 2016, PLoS Genet 12(9): e1006272. ("This is an open access article distributed under the terms of the Creative Commons Attribution License, which permits unrestricted use, distribution, and reproduction in any medium, provided the original author and source are credited.")

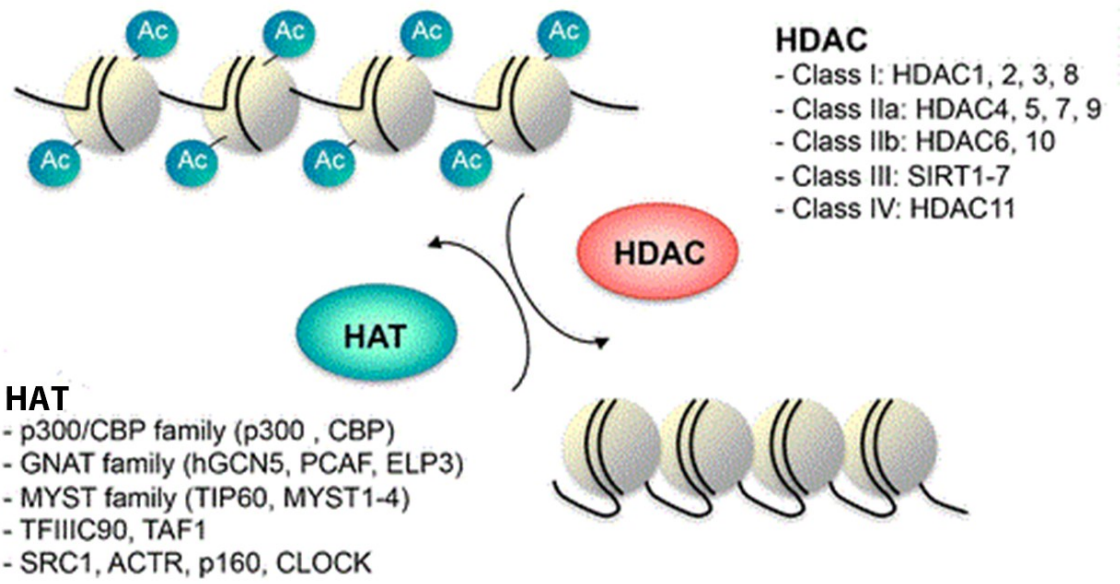

Figure 1.3. HAT and HDAC families.

HATs and HDACs regulate histone acetylation and deacetylation, respectively. The HATs are grouped into 3 families, including the p300/CBP family, GNAT family and MYST family. Additional studies are needed to verify the acetyltransferase activity reported for members of the remaining two families shown here. The HDACs are categorized into 4 classes, composed of class I (HDAC1, -2, -3 and -8), IIa (HDAC4, -5, -7 and -9), IIb (HDAC6 and -10), III (SIRT1-7) and IV (HDAC11). Adapted from Schneider *et al.*, Neurotherapeutics (2013) 10: 568, with permission.

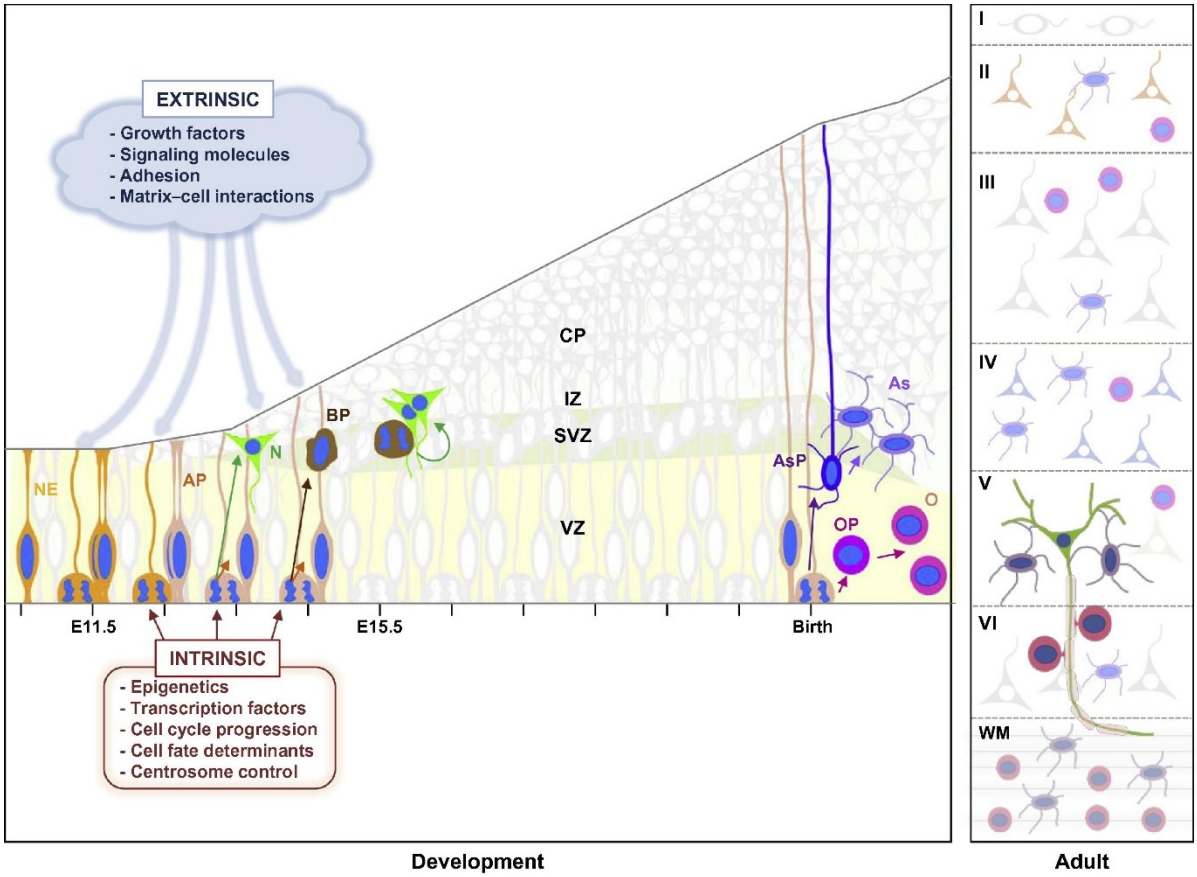

Figure 1.4. Intrinsic and extrinsic factors that regulate mouse cerebral cortex development.

Intrinsic factors include transcription factors, epigenetic regulators and other cellular regulators. Extrinsic factors include secreted growth factors, hormones and other signaling molecules. Neuroepithelium (NE) contains the first neural stem cells (blue) at around E10. The neural stem cells proliferate to populate themselves at the early stage (before E11.5) and then undergo self-renewal as well as differentiation to produce progenitor cells (astrocyte-like progenitor cells, AP, basal progenitor cells, BP) and neurons (N). These cells migrate to proper layers and form the ventricular zone (VZ), subventricular zone (SVZ), intermediate zone (IZ) and cortical plate (CP). Gliogenesis is inhibited between E10.5 to E18. At perinatal stage, neural stem and progenitor cells begin to produce astrocyte progenitor cells (AsP) and oligodendrocyte progenitor cells (OP), and further produce astrocyte (As) and oligodendrocyte (O) cells. The cerebral cortex further developed to form white matter (WM) layer and the other 5 layers (VI, V, IV, III, II, I from inside to outside) in the adult brain. Copyright: Tapias *et al*., Genomics, Proteomics & Bioinformatics, 15(1), February 2017, Pages 19-36. (Copyright distributed under a Creative Commons License which allows for free distribution for private use.)

Table 1.1. Histone acetylation sites, the responsible HATs and potential functions

Histone	Site	HATs	Proposed function
H2A	Lys4 (*S. cerevisiae*)	Esa1	transcriptional activation
	Lys5 (mammals)	Tip60, p300/CBP	transcriptional activation
	Lys7 (*S. cerevisiae*)	Hat1	Unknown
		Esa1	transcriptional activation
H2B	Lys5	p300	transcriptional activation
	Lys11 (S. cerevisiae)	Gcn5	transcriptional activation
	Lys12 (mammals)	p300/CBP	transcriptional activation
	Lys15 (mammals)	p300/CBP	transcriptional activation
	Lys16 (S. cerevisiae)	Gcn5, Esa1	transcriptional activation
	Lys20	p300	transcriptional activation
H3	Lys4 (S. cerevisiae)	Esa1	transcriptional activation
	Lys9	Unknown	histone deposition
		Gcn5, SRC-1	transcriptional activation
	Lys14	Unknown	histone deposition
		Gcn5, PCAF	transcriptional activation
		Esa1, Tip60	transcriptional activation, DNA repair
		SRC-1	transcriptional activation
		Elp3	transcriptional activation (elongation)
		Hpa2	Unknown
		hTFIIIC90	RNA polymerase III transcription
		TAF1	RNA polymerase II transcription
		Sas2	Euchromatin
		Sas3	transcriptional activation (elongation)
		p300	transcriptional activation
	Lys18	Gcn5	transcriptional activation, DNA repair
		p300/CBP	DNA replication, transcriptional activation
	Lys23	Unknown	histone deposition
		Gcn5	transcriptional activation, DNA repair
		Sas3	transcriptional activation (elongation)
		p300/CBP	transcriptional activation
	Lys27	Gcn5	transcriptional activation
	Lys36	Gcn5	transcriptional activation
	Lys56(S. cerevisiae)	Spt10	transcriptional activation, DNA repair
H4	Lys5	Hat1	histone deposition
		Esa1, Tip60	transcriptional activation, DNA-repair
		ATF2	transcriptional activation
		Hpa2	Unknown
		p300	transcriptional activation
	Lys8	Gcn5, PCAF	transcriptional activation
		Esa1, Tip60	transcriptional activation, DNA-repair
		ATF2	transcriptional activation
		Elp3	transcriptional activation (elongation)

	p300	transcriptional activation
Lys12	Hat1	histone deposition, telomeric silencing
	Esa1, Tip60	transcriptional activation, DNA repair
	Hpa2	Unknown
	p300	transcriptional activation
Lys16	Gcn15	transcriptional activation
	MOF	transcriptional activation
	Esa1, Tip60	transcriptional activation, DNA repair
	ATF2	transcriptional activation
	Sas2	Euchromatin
Lys91 (S. cerevisiae)	Hat1/Hat2	chromatin assembly

Notes: Cited from Cell signaling "Histone Modification Table" which is reviewed and revised in March 2018.

1.2 ATAT1 and tubulin acetylation

1.2.1 Identification of lysine 40 of α-tubulin as the acetylation site

The journey started in 1981 when it was found that the flagella of the single-cell green alga *Chlamydomonas reinhardtii* contains a tubulin isoform distinct from those from the cytoplasm, as judged from their different isoelectric points (91). Importantly, it was subsequently shown that the difference is due to a post-translational modification rather than expression from a different gene (92), because the cytoplasmic precursor could be converted to the flagellar form (93). With tritiated acetate labelling, the α-tubulin protein from the flagella was found to contain tritium, indicating that the protein contains a modification due to a tritiated moiety (93). Addition of hydrazine to acetylated microtubules produced acetyl-hydrazine, indicating the involvement of acetylation, and subsequent analysis of proteolytic digests by thin-layer chromatography revealed that the acetyl group is linked to the epsilon-amino group of a lysine residue (94). In 1987, amino acid sequencing identified Lys-40 as the acetylation site (95). Two years earlier, a monoclonal antibody specific for the acetylated form was developed and found to recognize α-tubulin from various organisms, indicating that the acetylation is conserved in different species (96). Indeed, amino acid sequence comparison revealed that the acetylation site is conserved from protists to mammals such as mice and humans (96, 97) and is also present in flowering plants (98). However, the acetylation site is not conserved in yeast (99). Being commercially available for more than two decades, the monoclonal antibody clone 6-11B-1, specific to acetylated α-tubulin (96), has been widely used as a routine marker of stable microtubules.

A recent large-scale acetylome study identified other multiple acetylated sites on α- and β-tubulin (100), but these new sites need to be independently substantiated by other means. Lys-252 of β-tubulin is also acetylated, but the modification only exists in soluble α- and β-tubulin heterodimers (101). This acetylation is catalyzed by the acetyltransferase San and inhibits tubulin incorporation into microtubules to regulate microtubule dynamics (101). Currently, Lys-40 is the only acetylation site known to occur on polymerized microtubules (Fig. 1.5), so this modification has been widely referred to as tubulin or microtubule acetylation.

1.2.2 Tubulin acetyltransferases and deacetylases

Identification and analysis of tubulin acetyltransferases

In 1985, an acetyltransferase activity was detected in extracts isolated from *Chlamydomonas* flagella (102), but the identity of this enzyme remained obscure until recently. *In vitro* studies identified several candidates, including the transcriptional elongation regulator ELP3 (elongator protein 3) (103, 104), an N^{α}-acetyltransferase complex (105) and the histone acetyltransferase GCN5 (homolog of yeast general control nonderepressible 5) (106). Genetic screening for touch sensitivity defects in the soil nematode *Caenorhabditis elegans* identified various mutant alleles, one of which encodes Mec-17 (mechanosensory abnormality protein 17) (107, 108). Interestingly, Mec-17 displays sequence similarity to members of the GCN5 (general control non-derepressible 5) superfamily of histone acetyltransferases (109). In 2010, Mec-17 and the mammalian ortholog ATAT1 (alpha-tubulin acetyltransferase 1) were identified as α-tubulin acetyltransferases (47, 110). They possess intrinsic α-tubulin acetyltransferase activity and acetylate α-tubulin efficiently (47, 110). Moreover, ATAT1 functions as a *bona-fide* tubulin acetyltransferase *in vivo*, because deletion of the mouse *Atat1* gene leads to nearly complete loss of tubulin acetylation in embryos and various tissues (111-113). Thus, ATAT1 is now considered as a major tubulin acetyltransferase in mammals. The other three candidates (i.e., ELP3, GNC5 and an N^{α}-acetyltransferase) may be responsible for minor tubulin acetylation *in vivo*. In support of this, zebrafish embryos depleted of Mec-17 display loss of tubulin acetylation in neurons but not in cilia (110), and in *Atat1* knockout mice, there are also residual tubulin acetylation signals in some tissues (111).

At the amino acid sequence level, the Mec-17/ATAT1 family of proteins is conserved from *protists* to humans. There are two Mec-17 proteins in *C. elegans*, while in higher organisms there is only one ortholog (47, 110). Notably, tubulin acetylation is present in flowering plants (98), but no Mec-17 related proteins are encoded in genomes of model plants such as *Arabidopsis thaliana,* indicating that other proteins acetylate α-tubulin in angiosperms. Mec-17 or ATAT1 has four sequence motifs characteristic of the GCN5-related N-acetyltransferase family of acetyltransferases and is thus a member to this superfamily (109). In addition to catalyzing tubulin acetylation, ATAT1 interacts with microtubule-associated proteins such as

doublecortin (111) and destabilizes microtubules independent of its acetyltransferase activity (112).

Multiple structural studies have provided molecular insights into how human ATAT1 interacts with and specifically acetylates α-tubulin (in a heterodimeric form with β-tubulin) and microtubules (114-118). Consistent with their sequence similarity (109), the overall 3D structure of ATAT1 is very similar to that of the well studied acetyltransferase GCN5 (114-118). Different from GCN5, ATAT1 contains a basic substrate-binding pocket for recognition of four acidic residues (Asp-33, -39, -46 and -47) of α-tubulin (115). In support of this, mutagenesis analysis revealed that Asp-39 and Asp-46 of α-tubulin contribute to acetylation of Lys-40 (118). Interestingly, Ser-38 of α-tubulin is essential for acetylation of Lys-40 (118). Roughly, the acetylation site conforms to the consensus sequence xxxSDKxxxxxDxx, where S is essential, D is important and x is any residue (118).

Tubulin acetylation is a hallmark for long-lived microtubules and is a unique luminal modification on microtubules (Fig. 1.5) (119-122), so an interesting question is how tubulin acetyltransferase gains access to the luminal residue, Lys-40. It was shown that the acetylation of microtubules proceeds from both ends (Fig. 1.5), suggesting that enzymes diffuse through the microtubule lumen (110). This model seems problematic as through diffusion, an antibody that is specific for an interior epitope in microtubules would require years to approach the equilibrium (123). The acetylation reaction is not dependent on the length of microtubules (124) and the *Km* value of ATAT1 for free α-tubulin is almost identical to that for microtubules (47), indicating that ATAT1 binds to α-tubulin in microtubules in an unrestricted manner. It was proposed that ATAT1 reaches the luminal acetylation site through transient holes in the microtubule lattice (47). A new study indicates that ATAT1 acetylates the entire microtubule without a preference for the ends and that its catalytic activity rather than the substrate access is rate-limiting for microtubule acetylation (125).

To investigate whether there are other acetylation sites on α-tubulin than Lys-40, Shida *et al.* engineered the point mutant K40R (47). Wild-type α-tubulin but not the mutant is acetylated by ATAT1, confirming that Lys-40 is the only acetylation site (47). In a related study, a pan-acetyl-lysine antibody was used to detect tubulin purified from the *Atat1*-deficient mouse brain and almost no positive signals were detected (112), supporting that ATAT1 is a major α-tubulin

acetyltransferase and Lys-40 is the predominant acetylation site *in vivo*.

Genetically, loss of Mec-17 and its paralog Atat-2 in *C. elegans* leads to disappearance of tubulin acetylation and decreases touch sensitivity (110). While using morpholino oligomers to treat zebrafish embryos, tubulin acetylation is almost completely lost in neurons but not cilia and the treated embryos display developmental defects, including curved body shape, short body axis and hydrocephalus, as well as small head and eyes (110). By staining for β-galactosidase activity in $Atat1^{LacZ}$ mice, it was shown that *Atat1* is expressed in a variety of tissues, with the strongest expression in the central nervous system and ciliated tissues such as the testis, lung, eye and inner ear (Lin & Yang, unpublished data) (111). In knockout mice, *Atat1* deficiency leads to nearly total loss of tubulin acetylation but does not affect animal survival (111-113). Except for some brain and sperm abnormalities, mutant mice develop rather normally (111-113). The brain abnormalities include alteration of the dentate gyrus and dilation in the lateral ventricles (Lin & Yang, unpublished data) (111). In the mutant testis, apoptosis is activated (112). Unlike what was observed in zebrafish (110), these mouse genetic studies indicate that in mammals, ATAT1 is not essential for survival (111-113). As it is required for optimal hippocampus development, ATAT1 may be important for advanced functions such as learning and memory (111).

Identification and analysis of tubulin deacetylases

In 2002, Hubbert *et al*. first reported that histone deacetylase 6 (HDAC6) is an α-tubulin deacetylase co-localized with the microtubule network (65). It preferentially binds to and deacetylates α-tubulin that has been incorporated into microtubules (65). Independently, two other groups made similar discoveries (126, 127). HDAC6 is conserved from *C. elegans* from humans and similar proteins are also present in plants (99). Except for unicellular organisms such as *Tetrahymena* and green algae, this correlates well with the presence of α-tubulin acetylation in different organisms. Sirtuin 2 (SIRT2), a human ortholog of yeast Sir2 (silent information regulator 2), was identified as an NAD^+-dependent α-tubulin deacetylase (128), but deletion of the murine gene does not change the α-tubulin acetylation level *in vivo* (129, 130). By contrast, deletion of the mouse *Hdac6* gene leads to global α-tubulin hyperacetylation (131), indicating that HDAC6 is a major tubulin deacetylase *in vivo*. SIRT2 may function in special conditions. For example, the microtubule-associated protein Furry inhibits SIRT2

deacetylase activity and promotes α-tubulin acetylation in the mitotic spindle (132). In murine macrophages, SIRT2 but not HDAC6 is the responsible α-tubulin deacetylase during inflammasome activation (133). Interestingly, a recent study has identified HDAC5 as an injury-regulated tubulin deacetylase important for axon regeneration (134). Therefore, HDAC6 is the major α-tubulin deacetylase and other deacetylases such as SIRT2 and HDAC5 may function as tubulin deacetylases in special situations.

Human HDAC6 was initially considered to be exclusively cytoplasmic (135), but two recent studies have revealed that it is also present in the nucleus (136, 137). Related to this, mouse HDAC6 is subject to active nucleocytoplasmic trafficking (138). In addition to tubulin, HDAC6 deacetylates other proteins, including the molecular chaperone HSP90 (heat-shock protein 90 kDa) (10), the HSP70-interacting protein CHIP (carboxy terminus of HSP70-interacting protein) (139), the E3 ubiquitin ligase TRIM50 (tripartite motif containing protein 50) (140), the cytoskeletal protein cortactin (cortical actin binding protein) (141) and a DNA mismatch repair regulator (137). HDAC6 also regulates degradation of misfolded and aggregated proteins (142, 143) and modulates transcriptional co-repression (144). Moreover, HDAC6 is important for mitochondrial transport in hippocampal neurons (145) and has a role in neurodegenerative diseases (146). The diverse substrates and multiple roles of HDAC6 in different cellular processes have complicated the efforts to dissect out its role as a tubulin deacetylase *per se*.

In *Hdac6-null* mice, α-tubulin is hyperacetylated in almost all tissues tested (131). While the mutant mice are viable and fertile, they display only minor phenotypes such as moderately impaired immune responses (131), hyperactivity, decreased anxiety and lower depression tendency (147). Tubulin deacetylation by HDAC6 is not required for platelet activation, but tubulin hyperacetylation influences platelet spreading (148). Despite the lack of major phenotypes in the knockout mice, HDAC6 may fine-tune physiological and pathological processes. Alternatively, as the mutant mice are raised *ad libitum* under regulated cage environments, the situation may be different if the dietary and environmental conditions are changed or if the mice are challenged. For example, a recent study indicates that HDAC6 is important for inflammatory response (149).

1.2.3 Functions of tubulin acetylation

Tubulin acetylation as a marker of stable microtubules

Tubulin acetylation was first identified in flagellar axonemes of *Chlamydomonas reinhardtii* (93). Subsequent studies demonstrated that this modification is not restricted to axonemes, but also present in basal bodies and a subset of cytoplasmic microtubules (150). Moreover, tubulin acetylation was found mainly on stable microtubules resistant to depolymerization induced by cold shock and other treatments, but not on dynamic microtubules such as those in neuronal growth cones (151-153). In retina tissues, tubulin acetylation is more abundant in neurons than other cell types (154) and is enriched in axons when compared to dendrites (155). As it is often found on stable microtubules (150), tubulin acetylation has been widely used as an indicator for microtubule stability.

Notably, tubulin acetylation may be a consequence of, rather than a contributor to, microtubule stability (potential tubulin functions summarized in Fig. 1.6). Tubulin acetylation and detyrosination exist in stable microtubules such as those in axons and ciliary axonemes (155, 156). As other studies suggested that detyrosination alone does not promote microtubule stability *per se* (157-159), it was proposed tubulin acetylation might play a role in microtubule stabilization (152). Some early reports provided supporting evidence for this, but subsequent studies suggested that tubulin acetylation is likely to be a consequence rather than a cause of enhanced microtubule stability (112, 125, 160, 161). Related to this, a recent study indicates that detyrosination but not acetylation is important for chromosome congression (i.e., aligning chromosomes on the spindle) during mitosis (162).

Overexpression of HDAC6 significantly increases cell motility, and it was proposed that this is due to decreased microtubule stability caused by reduced tubulin acetylation (65). Pallazzo *et al.* challenged this conclusion and demonstrated that tubulin acetylation induced by HDAC6 inhibition does not lead to increased resistance to nocodazole, a drug that induces microtubule depolymerization (160). Another *in vitro* study demonstrated that highly acetylated microtubules exhibit delay in drug-induced depolymerization and that overexpression of HDAC6 promotes the depolymerization (127). However, it is unclear whether it is due to tubulin deacetylation or other functions of HDAC6 contribute to

microtubule instability. Related to this, the stability of microtubules is determined by the extent of HDAC6 binding to microtubules, but not by the level of tubulin acetylation (163). Selective inhibition of HDAC6 increases microtubule acetylation and significantly reduces microtubule growth and shrinkage, whereas siRNA knockdown of HDAC6 increases microtubule acetylation but does not affect microtubule growth velocity (163).

ATAT1 overexpression destabilizes microtubules, but it is its interaction with microtubules rather than its enzymatic activity regulates microtubule stability (112). Interestingly, in *C. elegans*, Mec-17 loss leads to microtubule instability and axon degeneration, independent of its acetyltransferase activity (164). This is not consistent with the observation that microtubules in *Atat1*$^{-/-}$ mouse embryonic fibroblasts (MEFs) are more resistant to nocodazole treatment than those in wild-type MEFs (112). Whether expression or loss of ATAT1 is beneficial for microtubule stability remains unclear, but both studies showed that microtubule instability is not caused by tubulin acetylation *per se*. Moreover, tubulin acetylation exerts no effects on microtubule structure in biochemical experiments (161), supporting that tubulin acetylation does not intrinsically affect microtubule stability. It was reported that ATAT1 has suboptimal enzymatic activity on microtubules and concluded that acetylation accumulates on stable microtubules because they exist for hours whereas dynamic microtubules have a much shorter half-life (125). Thus, tubulin acetylation accumulates in stable microtubules, rather than directly contribute to enhanced microtubule stability (160), which also explains why tubulin acetylation is enriched in long-lived microtubules in axons (155).

Tubulin acetylation, microtubule architecture, and mechanosensation

Microtubules are cyclinders comprising linear polymers (termed protofilaments) of α- and β-tubulin heterodimers (Fig. 1.7). In many cells and organisms, microtubules are composed of 13 protofilaments (Fig. 1.7) (165, 166). However, in some special situations, the protofilament number is different. Pillar and phalangeal cells in the mammalian inner ear contain mainly 15-protofilament microtubules (167). Moreover, 12- and 16-protofilament microtubules have been found in lobster neurons and insect sperms, respectively (166, 168). In *C. elegans*, most cells contain 11-protofilament microtubules, but sensory cilia possess 13-protofilament microtubules and neurites of touch receptor neurons are filled with 15-protofilament microtubules (169). Thus, the protofilament number in microtubules varies from 11 to 16 and

is cell type-specific. An important question is how this specificity is achieved.

Microtubule assembly experiments *in vitro* have shed some light on this question. While protofilaments are restricted to specific numbers in different cells *in vivo*, microtubule assembly *in vitro* yields heterogeneous populations (161, 170, 171). For example, tubulin preparations from the crayfish nerve cord and porcine brain generate a mixture of 13- and 14-protofilament microtubules, with the ratio dependent on the buffer conditions (161, 170). Interestingly, even under the same buffer condition, tubulin from bovine brain forms mainly 13-protofilament microtubules with a small portion containing 12- and 14-protofilaments, but tubulin from *C. elegans* leads to formation of mixed microtubules with the protofilament number of 9, 10, 11 and 12, at 30, 22, 43 and 17%, respectively (171). The protofilament number difference between microtubules assembled from bovine and worm tubulins is in rough agreement with the observation that microtubules in bovine and worm tissues are mainly composed of 13- and 11-protofilaments, respectively (165, 166, 169). Thus, in addition to buffer conditions, tubulin sequences and perhaps also post-translational modifications and microtubule-associated proteins affect the protofilament number of microtubules assembled *in vitro*. Interestingly, the microtubule-stabilizing anti-cancer drug Taxol (a.k.a. Paclitaxel) promotes formation of 12-protofilament microtubules (172). Moreover, the microtubule stabilizing protein doublecortin stimulates assembly of 13-protofilament microtubules *in vitro* and the intracellular transport motor protein kinesin is also in favor of 13-protofilament microtubules (161, 173, 174), indicating that microtubule-association proteins directly affect the protofilament number of microtubules.

In addition to *in vitro* microtubule assembly experiments, genetic studies in *C. elegans* have yielded insights into the question why touch receptor neurons contain mainly 15-protofilament microtubules. Within the simple nematode nervous system, there are six touch receptor neurons to mediate touch sensitivity (108, 175). Strikingly, the long neurites are filled with staggered arrays of ~20-μm long 15-protofilament microtubules (as many as 50 per neurite section) (169, 176, 177). As revealed by immunostaining with the monoclonal antibody (clone 6-11B-1 (96)) specific to acetylated α-tubulin, these microtubules are heavily acetylated (178, 179). Moreover, Mec-17 is highly expressed in these neurons (47). Thus, an interesting question is whether tubulin acetylation regulates the protofilament number of microtubules in

C. elegans. Two genetic and structural studies have demonstrated that this is the case (177, 180). In one study, loss of Mec-17 was found to cause morphological defects in touch receptor neurons and loss of touch sensitivity (177). In terms of microtubules, loss of Mec-17 exerts dramatic impact on touch receptor neurons: 1) decreased microtubule number per neurite section (from 46.5 in the wild-type to 8.8-14.7 in two mutant strains), 2) reduced microtubule diameter and decreased protofilament number (from uniform 15-protofilament microtubules in the wild-type to heterogeneous 11-15-protofilament microtubules in the two mutants, with 60% of the mutant microtubules comprising 13-protofilaments), 3) loss of mysterious darkly-stained material inside microtubules, and 4) appearance of microtubule hooks and bending (177). As a result of microtubule defects, axonal processes display periodic swellings, where severe microtubule bending occurs (177). Related to this, loss of mouse *Atat1* leads to formation of similar swellings on sperm flagella (112). Loss of the Mec-17 paralog Atat-2 in *C. elegans* has similar impact although it is not as dramatic as loss of Mec-17 itself (177). The acetyltransferase activity of Mec-17 is essential for microtubule integrity but not touch sensitivity (177).

In the other study, it was found that loss of either Mec-17 or Atat-2 reduces the number of microtubules per neurite section and shortens microtubule length in touch receptor neurons (180). In addition, loss of Mec-17 but Atat-2 alters the protofilament number (from >95% 15-protofilament and <5% 11-protofilament microtubules in the wild-type or *Atat-2* mutant worms to heterogeneous 10-16-protofilament microtubules in *Mec-17* mutants) (180). In addition, microtubules in *Mec-17* mutants display lattice openings (~150 nm wide, equivalent to ~20 tubulin heterodimers) that are not present in microtubules from wild-type or *Atat-2* mutant worms (180). Thus, these two studies are consistent with each other and support that loss of Mec-17 promotes loss of microtubules, alters the protofilament number and shortens microtubule length, thereby disrupting microtubule integrity in touch receptor neurons (177, 180). According to molecular modeling, Lys-40 of α-tubulin may form a salt bridge with Glu-55 and prevent it from engaging in an intermolecular salt bridge with His-283 of a neighbouring α-tubulin monomer (180). Acetylation at Lys-40 may make Glu-55 available for the intermolecular salt bridge, thereby facilitating formation of 15-protofilament microtubules (180).

These genetic and structural studies using *C. elegans* as an elegant model system (177, 180) raise two important questions. The first is whether the conclusion can be extrapolated to other organisms such as mammals. This question is important, especially when considering that even under the same assembly conditions *in vitro*, tubulins from bovine brain and *C. elegans* form microtubules containing different numbers of protofilaments (171). The availability of *Atat1*$^{-/-}$ and *Hdac6*-null mice should help address this question (111, 112, 131). For example, electron microscopy employed to analyze *C. elegans* (177, 180) can be used to interrogate tissue sections from wild-type and *Atat1*-null mice. The two *C. elegans* studies show that tubulin acetylation is *necessary* for maintaining microtubule structure in touch captor neurons (177, 180), but the question whether tubulin acetylation is *sufficient* for the maintenance remains unaddressed. In a recent study, *in vitro* microtubule assembly was carried out with porcine brain tubulin to investigate whether acetylation *per se* affects microtubule structure (161). Different from what was observed with mutant worms lacking Mec-17 (177, 180), acetylation does not have a major effect on microtubule structure *in vitro* (161). Under the conditions used, non-acetylated tubulins form a mixture of 13- and 14-protofilament microtubules (Fig. 1.7) (161). Notably, there is a small fraction of 15-protofilament microtubules (~8%) (161). With acetylation, this fraction increases by ~2-fold (161). In the presence of kinesin, acetylation enhances the ratio of 13-protofilament microtubules (161). Thus, acetylation exerts some minor effects on microtubule structure. However, it is clear that acetylation does not promote formation of uniform 15-protofilament microtubules *in vitro* (161), which is in stark contrast to what was observed in touch receptor neurons *in vivo* (177, 180).

Different outcomes from structural studies of microtubules from *C. elegans* (177, 180) and *in vitro* assembly experiments (161) reiterate that acetylation is necessary but not sufficient for regulating microtubule architecture. As shown with the *Mec-17* gene, mutation of the *Mec-12* and *Mec-7* genes (encoding α- and β-tubulin isoforms, respectively) also affect microtubule structure in touch receptor neurons (108, 179), supporting that acetylation is not sufficient for formation of 15-protofilament microtubules in touch receptor neurons. Based on this, it is tempting to propose that acetylation facilitates interaction of an unknown protein(s), which in turn regulates microtubule structure (Fig. 1.7). Related to this, kinesin and doublecortin affect

the protofilament number of microtubules assembled *in vitro* (161, 173, 174). Moreover, deletion of the *Mec-17* gene leads to loss of mysterious darkly-stained material inside microtubules (177). The mysterious material may represent the unidentified protein(s) that binds to acetylated tubulin (Fig. 1.7). If so, identification of the mysterious protein(s) shall shed novel light on how acetylation regulates microtubule architecture *in vivo*.

Like touch receptor neurons in *C. elegans*, pillar and phalangeal cells in the mammalian inner ear contain densely packed 15-protofilament microtubules (167). In addition, as touch receptor neurons mediate mechanosensing, pillar and phalangeal cells are integral parts of the organ of Corti in the inner ear. The stiffness of 15-protofilament microtubules in pillar cells may contribute to mechanosensation by the organ of Corti (181). Moreover, similar to touch receptor neurons in *C. elegans,* 15-protofilament microtubules in pillar cells are heavily acetylated (182). By analogy to touch receptor neurons (177, 180), it is reasonable to suggest that acetylation may regulate formation of 15-protofilament microtubules in pillar and phalangeal cells. If so, acetylation may also contribute to mammalian hearing sensation. *Atat1*$^{-/-}$ mice (111, 112) should be valuable for investigating these two interesting issues.

Tubulin acetylation and intracellular transport

Tubulin acetylation has been proposed to participate in subcellular and intraflagellar transport. Loss of microtubule acetylation was reported to reduce the binding and motility of the molecular motor kinesin-1 *in vitro* (183). Related to this, kinesin-1 and a kinesin-like protein preferably bind to stable microtubules marked by acetylation and detyrosination (184, 185). Increased tubulin acetylation by HDAC6 inhibition causes recruitment of dynein and kinesin-1 to microtubules, thereby compensating intracellular transport deficits in Huntington's disease (186). While these studies support that tubulin acetylation recruits kinesin-1 and regulates intracellular transport in cell-based assays, enrichment or loss of acetylation on microtubules in a purified system does not result in significant changes in the kinesin-1 loading rate while detyrosination causes a moderate increase in the rate (187). Similarly, increased tubulin acetylation alone without changing the status of other modifications does not alter the selectivity of kinesin-1 accumulation in polarized cells, while global enhancement of tubulin acetylation, detyrosination, and polyglutamylation by treatment with or by inhibition of glycogen synthase kinase 3β (GSK3β) decreases the selectivity of kinesin-1 translocation and

leads to formation of multiple axons (188). Microtubule stabilization by Taxol promotes initial neuronal polarization (189). For investigating whether this polarization is caused by tubulin acetylation, neurons were treated with the deacetylase inhibitors tubacin and trichostatin A. The treatment leads to clear elevation of microtubule acetylation, but the polarity is not altered (189). As treatment with Taxol or inhibition of GSK3β increases global tubulin modifications, and both increase kinesin-1 selectivity (188). Also prior acetylation dampens detyrosination, which itself leads to a moderate enhancement of kinesin-1 binding (187). Thus, the observation that tubulin acetylation alone does not result in significant changes in the kinesin-1 loading rate (187) may be due to the possibility that tubulin acetylation and detyrosination, or even with other tubulin modifications, affect kinesin-1 binding in a concerted fashion. If true, this would suggest a crosstalk of tubulin acetylation with other microtubule modifications.

Tubulin acetylation in regulating cell motility and polarity

As discussed above, it was reported that HDAC6-mediated tubulin deacetylation enhances microtubule-dependent motility and was proposed that this enhanced motility is due to reduced microtubule stability caused by decreased tubulin acetylation (65). Related to this, the ETS transcription factor ERG [E-twenty-six (ETS)-related gene product] directly regulates HDAC6 expression and tubulin acetylation during endothelial cell migration (190). Another group suggested that HDAC6-mediated enhancement of cellular motility is due to tubulin acetylation itself rather than microtubule stability as tubulin acetylation does not necessarily enhance microtubule stability (160). Knockdown *Atat1* and *Elp3* expression revealed that tubulin acetylation is important for neuronal migration (103, 191). However, ELP3 is unlikely a major tubulin acetyltransferase *in vivo* (111-113), so impaired neuronal migration observed in *Elp3*-deficient mice may be due to other mechanisms (103). Of note, ELP3 proteins from different organisms are able to modify the anticodon of tRNA (192).

Interestingly, the focal adhesion scaffold protein Paxillin interacts with HDAC6 and inhibits its deacetylase activity to upregulate microtubule acetylation for cell invasion and migration (193). Moreover, by interacting the clathrin adaptor AP2 with ATAT1, clathrin-coated pits control microtubule acetylation, which in turn ensures microtubule acetylation at the leading edge and promotes directional cell migration (194). It was also reported that tubulin acetylation is required for cell-cell contact inhibition and cell adhesion (113). Decreased

dynamics of acetylated microtubules induced by HDAC6 inhibition inhibits turnover of cellular focal adhesion (195). α-Tubulin acetylation was also shown to regulate breast cancer invasion (196). Because invasion inhibitory protein 45 (IIp45) and G protein-coupled receptor kinase 2 (GRK2) modulate cell motility by interacting with HDAC6 (197, 198), so this deacetylase itself may also be involved in regulating migration. These studies support tubulin acetylation, or perhaps also its responsible enzymes, may regulate cell migration. As tubulin acetylation is almost totally lost in various tissues in *Atat1* knockout mice (111-113), these mice should serve as a good model for investigating whether tubulin acetylation indeed regulates cell migration and promotes cancer metastasis *in vivo*.

Tubulin acetylation is also important for regulating cell polarity. As discussed above, for polarized epithelial cell migration, Paxillin binds to HDAC6 and stimulates microtubule acetylation (193). Moreover, expression of two phospho-defective mutants of NIMA (never in mitosis A)-related kinase 3 (NEK3) decreases tubulin acetylation, reduces neuronal polarity and alters cell morphology (199). Pharmacological inhibition of HDAC6 reverses this effect (199), suggesting that through tubulin deacetylation, HDAC6 modulates neuronal polarity. Therefore, tubulin acetylation plays important roles in regulating cell polarity and motility.

Tubulin acetylation and cilia

Cilia are subcellular structures differentiating from centrioles in non-proliferating cells and contain microtubule bundles constituting the axoneme. Cilia are evolutionarily related to flagella of lower eukaryotes like the green algae *Chlamydomonas*. Thus, it is not surprising that cilia were the first subcellular structures that were discovered to harbour tubulin acetylation (96). Since then, this modification has been widely used to mark cilia and related structures. However, it remains not so clear whether tubulin acetylation plays a causal role in cilium formation (Fig. 1.6). Ciliary assembly and disassembly require intraflagellar transportation. Considering tubulin acetylation may be important for cargo transportation, an interesting question is whether this modification regulates dynamics of ciliary assembly and disassembly. Growth of human telomerase-expressing retinal pigment epithelial cells in the OptiMEM media stimulates cilia formation and addition of serum induces ciliary disassembly (200). The prometastastic scaffolding protein HEF1 (human enhancer of filamentation 1; a.k.a. Cas-L and NEDD9) interacts with and activates Aurora kinase A, which then phosphorylates and activates

HDAC6, leading to ciliary disassembly. Knockdown or inhibition of Aurora kinase A, depletion of its activator HEF1, or inhibition of the downstream target HDAC6 prevents ciliary disassembly.

Inhibition of mouse HDAC6 by a specific inhibitor stimulates cilia formation in mouse embryos cultured *in vitro* (201). Treatment of human KD diploid fibroblasts with 25-50 mM LiCl promotes α-tubulin acetylation and elongation of primary cilia (202). siRNA-mediated depletion ATAT1 expression showed that ATAT1 is required for induced α-tubulin acetylation in these cells (202). Similar depletion of ATAT1 expression in human telomerase-expressing retinal pigment epithelial cells slows down the kinetics of ciliary disassembly (47). Primary cilium dysfunction affects the development and homeostasis of many organs in Bardet-Biedl syndrome (a ciliopathic genetic disorder) and seven conserved Bardet-Biedl syndrome proteins form a stable complex that functions in membrane trafficking to and inside the primary cilium (203). Interestingly, one small subunit of this complex promotes microtubule acetylation (203). In addition, ceramide inhibits HDAC6 activation by Aurora kinase A and promotes tubulin acetylation of tubulin in primary cilia in human neural stem cells *in vitro* (204).

The cylindromatosis (a.k.a. turban tumor syndrome) gene product CYLD is a tumor suppressor with intrinsic deubiquitinating enzyme (205). Interestingly, it associates with microtubules and appears to stabilize microtubules. In agreement with this, it interacts with and inactivate HDAC6 (205). Thus, in keratinocytes from *Cyld*$^{-/-}$ mice, tubulin acetylation is elevated (205). A recent study indicates that CYLD is located at the basal bodies (206). Upon Cyld knockdown, tubulin acetylation is reduced and ciliary length decreases in mouse embryonic fibroblasts (207). Moreover, treatment with selective HDAC6 inhibitors partially rescues ciliary defects in *Cyld*$^{-/-}$ mice (207). Thus, CYLD interacts with HDAC6 and regulates ciliogenesis.

From above, numerous studies indicate that tubulin acetylation has a critical role in cilium assembly and disassembly. However, it is often assumed that HDAC6-mediated tubulin deacetylation destabilizes microtubules and leads to ciliary disassembly. As discussed above, tubulin acetylation does not contribute to microtubule stability and *Hdac6* knockout mice do not display major phenotypes (131). Cilia are essential for vertebrate development (208, 209), so tubulin acetylation may only play a fine-tuning rather than important role in cilia during

animal development. In support of this, cilia are not affected in *Atat1*$^{-/-}$ mice although sperm flagella are slightly impaired (112). Different from the *Hdac6* and *Atat1* knockout mice (111, 112, 131), a majority of studies that support a role of tubulin acetylation in ciliary assembly are based on cells or embryos cultured *in vitro.*

Tubulin acetylation in immune and viral responses

Multiple studies have linked tubulin acetylation to immunity. As mentioned above, *Hdac6* knockout mice display a moderately impaired immune response (131). Under unchallenged conditions, serum IgM and IgG levels of *Hdac6*$^{-/y}$ mice (the murine *Hdac6* gene is X-linked) are close to what was observed in wild-type littermates (131). When mice are immunized with a T-cell-dependent antigen, a robust normal response of antigen-specific IgG is induced in wild-type mice, but not in *Hdac6*$^{-/y}$ mice, the response is ~4-fold weaker (131). In addition, deletion of the *Hdac6* gene or inhibition of its deacetylase activity enhances regulatory T cell functions in inflammation and autoimmunity, suggesting that HDAC6 inhibition is beneficial for treating colitis and suppressing allograft rejection (210). *Atat1*$^{-/-}$ mice display normal peripheral blood parameters (112), but roles of this acetyltransferase in the immune system remain to be examined.

Macrophages are major effector cells mediating innate immune responses. Activation of murine RAW264.7 macrophages by lipopolysaccharide (LPS) and IFN-γ *in vitro* enhances microtubule acetylation and secretion of matrix metalloproteinase-9, which then facilitates the cells migration across the subendothelial basement membrane and the interstitial matrix composed mainly of collagen to reach target tissues and initiate an inflammatory attack (211). Upon infection, pattern-recognition receptors in effector cells such as macrophages form protein complexes termed inflammasomes for maturation pro-inflammatory cytokines like interleukin 1β (IL-1β) to engage innate immune defense (212). During screening for regulators of inflammasome activation, it was found that microtubule depolymerization suppresses IL-1β production in response to nigericin, an antibiotic derived from *Streptomyces hygroscopicus* and known to promote inflammasome activation (133). Interestingly, tubulin acetylation by ATAT1 is required for inflammasome activation (133), whereas the natural diphenol resveratrol inhibits tubulin acetylation and inflammasome activation (213). Pharmacological inhibition revealed that mouse SIRT2 instead of HDAC6 is the responsible tubulin deacetylase (133), but it will

be important to substantiate this with related knockout mice. In addition to production of pro-inflammatory molecules such as matrix metalloproteinase-9 and IL-1β, tubulin acetylation is also essential for production of an anti-inflammatory cytokine, IL-10, which may serve a feedback mechanism to control inflammation. When challenged by LPS, RAW264.7 macrophages display extensive tubulin acetylation and induced production of IL-10 (149). Knockdown of *Atat1* expression suppresses LPS-induced tubulin acetylation and inhibits IL-10 induction, whereas in *Hdac6*-deficient macrophages and mice, LPS induces hyper-production of IL-10 (149). Tubulin acetylation is required for LPS-induced activation of p38 kinases (149), but it remains unclear why this modification is required for p38 kinase activation. It should be noted that LPS inhibits tubulin acetylation in human pulmonary macrovascular endothelial cells (214), indicating that LPS effects on tubulin acetylation are cell type-specific.

Upon T cell stimulation, the transcription factor NF-AT (nuclear factor of activated T-cells) is dephosphorylated by the phosphatase calcineurin, promoting interaction with importin β and nuclear translocation (215). Interestingly, α-tubulin binds to the N-terminal region of NFAT and stimulates complex formation with importin β for nuclear translocation, whereas α-tubulin acetylation inhibits this (215). Acetate upregulates tubulin acetylation and hinders NF-AT nuclear translocation (215). Of relevance, through increasing tubulin acetylation, acetate suppresses IL-8 production in epithelial cells induced by the bacterial flagellar protein flagellin. Tubulin hyperacetylation by treatment with an HDAC inhibitor also suppresses IL-8 production induced by flagellin, highlighting the role of tubulin acetylation in regulating IL-8 expression (216). Thus, tubulin acetylation is important for both innate and acquired immunity.

In addition, this modification is important for viral responses. Human immunodeficiency virus (HIV) infection stabilizes microtubules and stimulates tubulin acetylation in host cells (217). Overexpression of HDAC6 inhibits HIV infection (218). Similar to HIV, influenza A virus induces microtubule acetylation (219). In addition, HDAC6 inhibits release of this virus (220). Tubulin acetylation is also important for infection by herpes viruses. Just 30 minutes after infection, Kaposi's sarcoma-associated herpes virus enhances significant tubulin acetylation (221). About 4 hours post infection, herpes simplex virus type 1 (HSV-1) increases tubulin acetylation, which in turn enhances HSP90 binding to microtubules and facilitates nuclear localization of viral capsid protein (222). Notably, this effect is completely opposite

from that on NF-AT nuclear localization (215), indicating that effects of tubulin acetylation nuclear import are context-dependent.

Tubulin acetylation in stress and other signalling pathways

Chemical exposures, such as high salt concentration (e.g., NaCl and NiCl), H_2O_2 and Taxol, as well as physical insults like UV irradiation, dramatically elevate tubulin acetylation (97, 223). However, H_2O_2 inhibits tubulin acetylation in human pulmonary macrovascular endothelial cells (214), indicating that the effects on tubulin acetylation are cell-specific. Tubulin hyperacetylation in cultured cell is beneficial for cell survival after exposure to 0.25 M NaCl (224). KCl depolarization in neurons increases acetylation of α-tubulin in *Cornu Ammonis* 1 (CA1) of the hippocampus (225). Moreover, expression of microtubule-associated proteins increases tubulin acetylation (226). As the experiments were performed with cultured cells, the significance of tubulin hyperacetylation *in vivo* under stressing conditions remains unclear. Interestingly, a pathological study on alcoholics revealed significant increase of tubulin acetylation in the prefrontal cortex (227).

Merlin, encoded by the neurofibromatosis type 2 (NF2) gene and acting as an upstream component of the Hippo signalling pathway, is normally associated with acetylated microtubules, so loss of tubulin acetylation redistributes merlin to the cytosol, thereby impairing Hippo signalling (113). Increased tubulin acetylation enhances sensitivity of microtubule disruption catalyzed by the microtubule-severing AAA protein katanin in neurons and fibroblasts (228). Tubulin acetylation has been reported in regulating Na^+ and K^+-ATPase activity (229-233). Expression of an acetylation-resistant α-tubulin mutant significantly inhibits adipogenesis (234), suggesting that adipocyte differentiation is dependent on tubulin acetylation. In *Atat1*-null mice, there are no significant adipocyte-related phenotypes (111, 112), so studies with altered dietary conditions are needed to investigate this issue more thoroughly. Tubulin acetylation is also involved in regulating autophagy. Tubulin acetylation is required for fusion of autophagosomes with lysosomes (235), and starvation-induced tubulin hyperacetylation is required for autophagy activation by nutrient deprivation (236). Thus, tubulin acetylation plays a role in regulating stress and other signalling pathways.

1.2.4 Tubulin acetylation, human diseases and therapeutic implications

Pathologically, tubulin acetylation is associated with several neurological disorders. Charcot-Marie-Tooth disease affects approximately 1 in 2,500 individuals and is the most common inherited disorder of the peripheral nervous system (237). Mutations in the 27-kDa small heat-shock protein (HSPB1) gene cause axonal Charcot-Marie-Tooth disease or distal hereditary motor neuropathy (237). Mice expressing HSPB1 exhibit axonal transport defects, axonal loss and decreased tubulin acetylation (237). Importantly, HDAC6 inhibitors reverse these abnormalities (237). Inflicting roughly one in 80,000 newborns, Joubert syndrome is a genetic disease affecting mainly the cerebellum. A recent study identified related mutations in the kinesin 7 gene and found that this kinesin is required for optimal tubulin acetylation (238). Parkinson's disease is a common neurodegenerative condition affecting the motor system in the central nervous system, and mutations of the *LRRK2* (leucine-rich repeat kinase 2) gene are the most common genetic cause of this disease (239). At subcellular level, defective microtubule-based axonal transport is one possible cause. Related to this, LRRK2 interacts directly with β-tubulin and inhibits α-tubulin acetylation (240), indicating that in normal cellular contexts, this kinase acts as a negative regulator of microtubule acetylation. Unlike wild-type LRRK2, two mutants carrying Parkinson's disease-associated mutations form filamentous subcellular structures (241). Either expression of ATAT1 or inhibition of HDAC6 prevents formation of such structures (241). Amyotrophic lateral sclerosis (a.k.a. Lou Gehrig's disease) involves degenerative death of motor neurons in the motor cortex of the cerebrum, and transgenic mice expressing the G93A point mutant of superoxide dismutase 1 are known models of this disease (130). Loss of *Hdac6* significantly extends survival of these mice and maintains motor axon integrity (130). The protective effect of *Hdac6* deletion is associated with increased tubulin acetylation (130). Roles of tubulin acetylation in these four neurological disorders also yield therapeutic implications (Table 1.2).

Moreover, HDAC6 has been implicated in aging-related dementia such as Alzheimer's disease (Table 1.2). Reduced expression of HDAC6 ameliorates cognitive deficits in a mouse model for this disease (242). Inhibition of HDAC6 activity improves memory and reduces the level of the microtubule-associated protein Tau, a key marker for Alzheimer's disease (243).

As HDAC6 is the major tubulin deacetylase *in vivo*, tubulin acetylation may be important in these processes. However, this can also be due to other HDAC6 functions, such as its ubiquitin-binding ability (99). Inhibition of HDAC6 with selective inhibitors promotes tubulin acetylation and significantly improves learning-based performance in mice with β-amyloid-induced hippocampal lesions (244, 245).

Axon regeneration is crucial for recovery of neurological functions following injury and axon injury induces tubulin deacetylation in peripheral neurons in a mouse model (134). Moreover, tubulin deacetylation is required for axonal growth and regeneration in the mouse model (134). It is unclear, however, whether tubulin acetylation by ATAT1 is also required for the regeneration program. On the other hand, Mec-17 loss in *C. elegans* leads to axon degeneration (164). These two studies suggest that while tubulin acetylation is important for axon maintenance, tubulin deacetylase is required for axon regeneration. Possibly, it is the fine balance between tubulin acetylation and deacetylation that is required for axon maintenance and regeneration.

In addition to neurological disorders, tubulin acetylation has been linked to cancer development (Table 1.2). This modification is a prognostic marker for squamous cell carcinoma of the head and neck (246). Elevated tubulin acetylation in primary tumors from breast cancer patients is linked to the basal-like subtype and an increased risk of disease progression and death (247). Mechanistically, elevated tubulin acetylation promotes adhesion and invasion of breast cancer cells (247). Ectopic ATAT1 expression in cultured cells increases tubulin acetylation and enhances formation of microtentacles, membrane protrusions in detached breast cancer cells (247). ATAT1 is also associated with pancreatic cancer-initiating cells (248). The turban tumor syndrome protein CYLD acts as a tumor suppressor and inhibits cell-cycle progression by inactivating HDAC6 and elevating tubulin acetylation (205). In these three cases, inhibition of tubulin acetylation would be beneficial (Table 1.2). However, the neurofibromatosis type 2 (NF2) gene product merlin is a tumor suppressor upstream of the Hippo signalling pathway and is normally associated with acetylated microtubules (113). Loss of tubulin acetylation impairs Hippo signalling and affects cell-cell contact inhibition (113). Therefore, although the impact of tubulin acetylation is context-dependent, multiple lines of evidence suggest that it plays a role in cancer initiation and progression (Table 1.2). Moreover,

in combination with the proteasome inhibitor bortezomib, low doses of a specific HDAC6 inhibitor displays anti-multiple myeloma activity (249), setting the stage for further clinical trials.

Proteotoxicity is an important mechanism in heart diseases. Transgenic expression of an αB-crystallin mutant in mouse cardiomyocytes causes cardiomyopathy due to aggregation of the mutant protein (250). Tubulin hyperacetylation by pharmacological inhibition of mouse HDAC6 activity or knockdown of *Hdac6* expression ameliorates the aggregation process (250). Atrial fibrillation is a significant contributor to cardiovascular morbidity and mortality. Tachypacing, rapid pacing of the heart by an artificial electronic pacemaker, induces contractile dysfunction in cardiomyocytes, and interestingly, it also induces tubulin deacetylation (251). HDAC6 activation contributes to tachypacing-induced contractile dysfunction in experimental and human atrial fibrillation (251). These two studies suggest that human HDAC6 is a potential therapeutic target for cardiovascular diseases (Table 1.2).

In addition to neurologic disorders, cancer and heart diseases, tubulin acetylation plays a role in other pathological conditions (Table 1.2). Furthermore, chronic obstructive pulmonary disease (COPD) involves abnormal airway inflammatory responses to cigarette smoke, which inhibits ciliary tubulin acetylation (252). As discussed above, tubulin acetylation is important for viral entry, inflammation and other immune responses (Fig. 1.6). Moreover, the spore-forming bacterium *Clostridium difficile* is a causative pathogen of antibiotic-associated diarrhea and pseudomembranous colitis in humans (253). Toxin A from the bacterium inhibits tubulin acetylation and activates acute inflammation, whereas inhibition of HDAC6 ameliorates colitis in a mouse model injected with toxin A (253). Similarly, HDAC6 inhibition is beneficial for inhibiting murine colitis induced by dextran sodium sulfate (210). Therefore, altered tubulin acetylation is linked to different human diseases and the responsible enzymes constitute two novel molecular targets for drug development and therapeutic intervention (Table 1.2).

1.2.5 Rationale and hypothesis for the study in Chapter II

Lysine 40 of α-tubulin is the only acetylation site on assembled microtubules. This modification was found three decades ago and implied in many cellular functions such as

microtubule assembly and intracellular cargo transportation (254). However, these studies are based on indirect methods such as mutagenesis which converts lysine 40 to arginine to remove the effects of acetylation. Several enzymes were proposed to be the tubulin acetyltransferases, but none was confirmed *in vivo* until the identification of Mec-17 in *C. elegans* a few years ago (47, 110). Loss of *Atat1*, a mammalian homolog of *mec-17*, abolishes almost total tubulin acetylation in MEFs and various tissues in the mice (112, 255). In lower eukaryotes such as in the zebrafish, knockdown of Mec-17 by morpholinos showed striking phenotypes such as curved body shape, short body axis, hydrocephalus, small heads, small eyes and neuromuscular dysfunction (110). These studies raise the interesting question whether tubulin acetylation is also important in mammals. The identification of ATAT1 opens a window for exploring the roles of tubulin acetylation *in vivo* in a direct and thus reliable way. Based on these *in vitro* studies, and studies in lower eukaryotes, we propose tubulin acetylation may be important in cell functions as well as mouse development. We and others identified ATAT1 is identified as a major tubulin acetyltransferase in mice (Appendix 1) (255). In Chapter II, I continued this line of research.

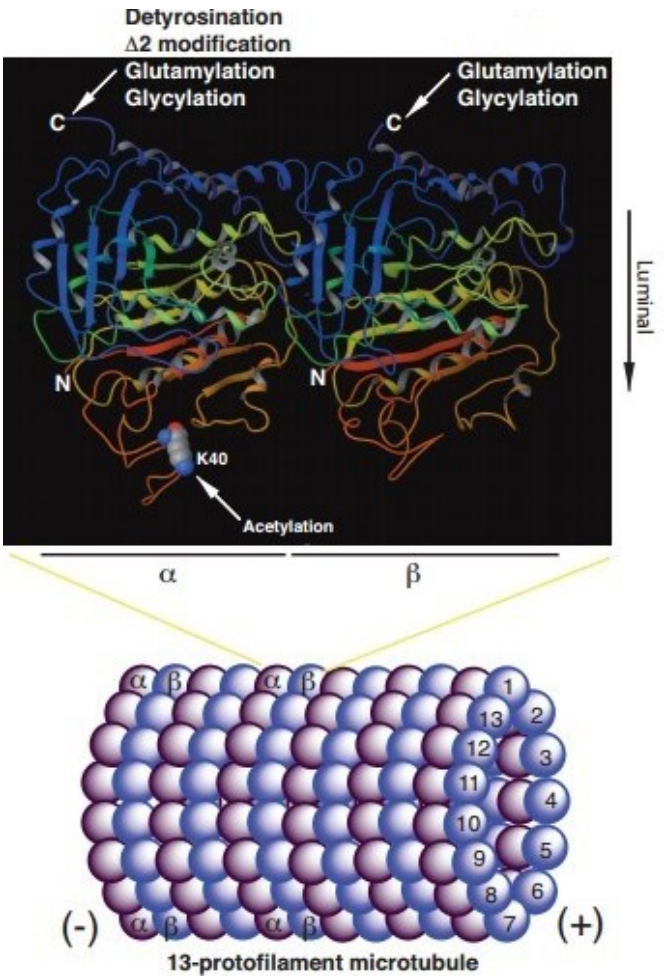

Figure 1.5. Schematic cartoon illustrating microtubule structure and the location of acetylation of α-tubulin and other post-translational modifications (PTMs).

While lysine-40 (K40) of α-tubulin resides at the luminal side of microtubules, whereas the C-terminal tails of α- and β-tubulin are located at the outer surface of microtubules (161, 256-258). Thus, acetylation is on the luminal side of microtubules, but PTMs at the C-terminal tails are on the outer surface of microtubules. Such PTMs include detyrosination, Δ2 modification, glutamylation and glycylation (119-122). Detyrosination and Δ2 modification occur only with α-tubulin, whereas glutamylation and glycylation modify both α- and β-tubulin. These two modifications occur at both mono- and poly-forms. Not illustrated here are other tubulin PTMs, including phosphorylation of β-tubulin at serine 172, polyamination of α- and β-tubulin, palmitoylation, ubiquitination and sumoylation (122, 259). The α- and β-tubulin heterodimer structure shown in the upper panel is adapted from reference (260) and their flexible acidic C-terminals in different isoforms are not present in the structures (256-258). Note that the helical nature of microtubules is not reflected in the lower panel.

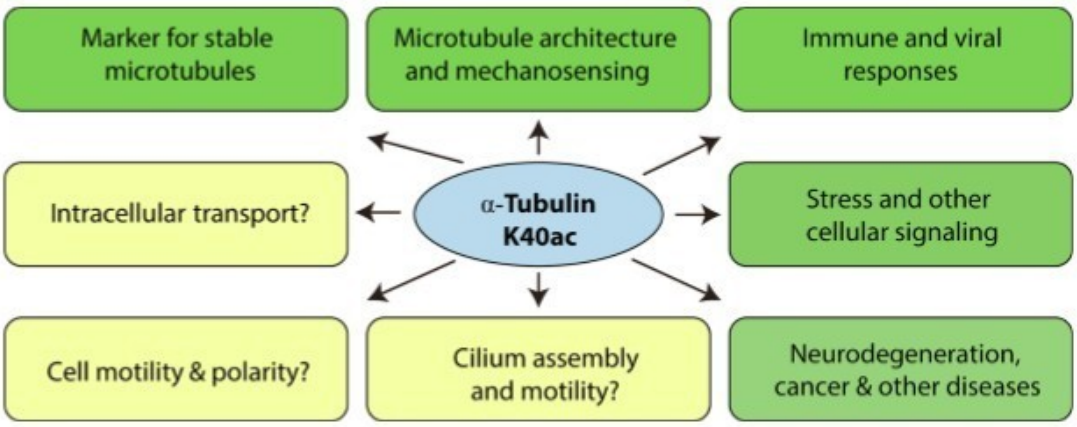

Figure 1.6. Known and potential roles of α-tubulin acetylation.

This modification serves as a marker for stable microtubules, regulates microtubule architecture and controls stress and immune responses. In addition, the modification has potential roles in various other cellular processes, including intracellular transport, cilium assembly, cellular signalling, cell migration and neurodegeneration. Questions marks denote that functions of α-tubulin acetylation in the processes remain to be firmly established. K40ac, Lys-40 acetylation.

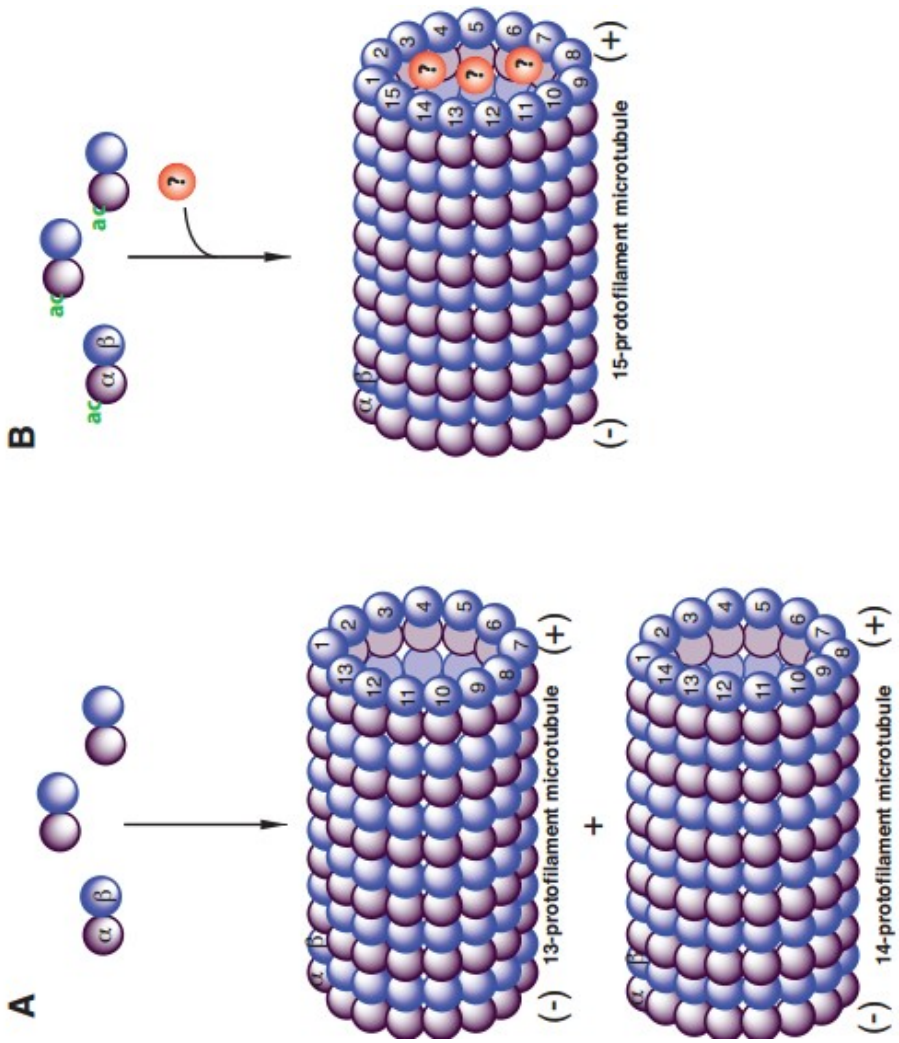

Figure 1.7. Hypothetical models on how α-tubulin acetylation may affect microtubule structure.

(**A**) In the absence of acetylation, α- and β-tubulin heterodimers form 13- or 14-protofilament microtubules *in vitro*. However, in most cells, microtubules contain 13-protofilaments, so some cellular proteins may promote formation of such microtubules. (**B**) In the presence of acetylation (ac), α- and β-tubulin heterodimers are in favour of formation of 15-protofilament microtubules such as those in touch neuron receptors in *C. elegans* and pillar cells in the mammalian inner ear. However, acetylation is not sufficient for promoting formation of 15-protofilament microtubules. Acetylation may form a specific docking site for an unidentified protein(s), which may in turn promote formation of 15-protofilament microtubules. As 15-protofilament microtubules are not common, some acetylation-specific proteins may promote assembly of microtubules with a different number of protofilaments. The question mark refers to an unidentified protein(s).

Table 1.2 Links of altered tubulin acetylation to human diseases

Human diseases	Tubulin acetylation [References]	Predicted therapeutic strategy
Neurologic disorders		
Charcot-Marie-Tooth disease	Decrease (237)	HDAC6i
Joubert syndrome	Decrease (238)	HDAC6i
Parkinson's disease	Decrease (240, 241)	HDAC6i
Amyotrophic lateral sclerosis	Decrease (130)	HDAC6i
Alzheimer's disease	Decrease? (242, 243)	HDAC6i
Axon injury	Increase (134)	ATAT1i?
Axon degeneration	Decrease? (164)	HDAC6i
Cancer		
Head and neck squamous cell carcinoma	Increase (246)	ATAT1i
Breast Cancer	Increase (247)	ATAT1i
Pancreatic cancer	Increase? (248)	ATAT1i
Cylindromatosis	Decrease (205)	HDAC6i
Breast Cancer	Increase (247)	ATAT1i
Neurofibromatosis type 2	Increase? (113)	ATAT1i?
Multiple myeloma	Decrease? (113)	HDAC6i
Heart diseases		
Heart failure due to proteotoxicity increase	HDAC6 induction (250)	HDAC6i
Atrial fibrillation	Decrease? (251)	HDAC6i
Lung disease		
COPD	Decrease (252)	HDAC6i
Inflammation & immunity		
Inflammasome activation	Increase (133)	HDAC6i
Colitis	Decrease (210, 253)	HDAC6i
Allograft rejection	Decrease (210)	HDAC6i
Virus entry	Decrease (210)	HDAC6i

ATAT1i, ATAT1 inhibitor; COPD, chronic obstructive pulmonary disease; HDAC6i, HDAC6 inhibitor. While no ATAT1 inhibitors are available yet, selective HDAC6 inhibitors have been developed and evaluated in preclinical studies (249, 261).

1.3 HDAC3

1.3.1 Identification of HDAC3 as a class I member

HDAC3 was identified based on its sequence homology to yeast Rpd3 as well as to Hdac1/2 (262, 263). It is highly conserved from flies to humans. While HDAC1 and HDAC2 share 83% amino acid sequence identity, there is only 56% identity between HDAC1 and HDAC3 (264). HDAC3 shares a conserved HDAC domain in the N-terminal part with other HDACs (Fig. 1.8). This domain is essential for its deacetylase activity. HDAC3 has a more variable C-terminus, showing no apparent similarity to other HDACs. This C-terminal region is required for transcriptional repression and enzymatic activity (265). In the cells, HDAC3 is found mainly in the nucleus, but can also be found in the cytoplasm and the plasma membrane (266). In contrast to HDAC3, the other class I HDACs are exclusively in the nucleus. HDAC3 possesses a nuclear localization (NLS) and export (NES) motif, different from other class I HDACs (265). This explains the subcellular distribution difference between HDAC3 and other class I HDACs. HDAC3 is ubiquitously expressed.

1.3.2 HDAC3 in the NCoR/SMRT tetrameric complexes

Except HDAC8, the other class I HDACs function within multisubunit protein complexes. Biochemical purification of NCoR, SMRT or HDAC3 followed by mass spectrometry identified NCoR or SMRT as subunits associated with HDAC3 (267-269). *In vitro* studies in Hela cells showed that majority of the cellular HDAC3 associates with NCoR and SMRT complexes (269). Further studies established stoichiometric association with GPS2, TBL1 and SMRT, confirming GPS2 and TBL1 as stable and integral components of the NCoR or SMRT complexes (270). These studies link HDAC3 to the NCoR/SMRT co-repressor complexes and imply that the complexes repress transcription at least in part through histone deacetylation by the HDAC3 subunit (61). NCoR and SMRT have similar domain structures with multiple domains and are functionally interchangeable *in vitro* (271). GPS2 and TBL1 interact with repression domain 1 (RD1) of NCoR or SMRT to form a heterotrimeric structure. GPS2 and TBL1 indirectly link to HDAC3 via the extended SANT domain of NCoR or SMRT (270). Recently, structural analysis of HDAC3 complexes identified ins(1,4,5,6)P4 as a small

compound binding to the complexes (272). A recent study reported that USP44 is also an integral component of the NCoR/SMRT complexes, linking them directly to histone H2B deubiquitination (273).

In addition to forming highly stable tetrameric complexes with NCoR/SMRT, GPS2 and TBL1 (Fig. 1.9), HDAC3 interacts weakly but functionally with many other transcription factors in a tissue-specific manner. These transcription factors recruit NCoR/SMRT complexes to regulatory regions in the genome via interaction with HDAC3 or with other components of the NCoR/SMRT complexes. For instance, HDAC3 and its complex were recruited by MEF2 to regulate muscle differentiation (274). HDAC3 interacts with the osteoblast master protein, Runx2, to regulate osteoblast differentiation and bone formation (275). HDAC3 directly associates with the hematopoietic transcription factor, GATA2, and suppresses its key transcriptional activity (276). HDAC3 interacts with HDAC4 and 5 in the nucleus to repress gene expression (277). HDAC3 also interacts with YY1 and p300 to repress c-Myc expression (278).

1.3.3 Regulation of HDAC3 enzymatic activity

HDAC3 possesses very weak enzymatic activity by itself (279). In fact, the enzymatic activity of most class I HDACs (except HDAC8) requires formation of multisubunit protein complex (279). In the NCoR/SMRT complexes, the enzymatic activity of HDAC3 is stimulated by the deacetylase activating domain of NCoR or SMRT (280). The interaction of the SANT domain of SMRT or NCoR with HDAC3 results in a large structural rearrangement that facilitates the complex formation and activation of the HDAC3 enzymatic activity (272). Ins(1,4,5,6)P4 is essential for the NCoR/SMRT complex assembly and regulates HDAC3 enzymatic activity at least *in vitro* (272). HDAC3 enzymatic activity is undetectable in mice bearing point mutations in the deacetylase activating domain of both NCoR1 and SMRT, demonstrating an essential role for the domain in activating the HDAC3 activity *in vivo* (281).

The HDAC3 enzymatic activity is also regulated by phosphorylation. Serine 424 of HDAC3 is phosphorylated by protein kinase CK2. Phosphorylation at this site increases the HDAC3 enzymatic activity while mutation of this residue decreases its enzymatic activity (282). Phosphorylation of HDAC3 associated members, such as SMRT, disrupts the complex

formation and compromises the enzymatic activity (283). HDAC3 activity is negatively regulated by the nuclear protein DBC1. It interacts with HDAC3, inhibits its deacetylase activity specifically and alters its subcellular distribution (284). HDAC3 subcellular distribution is also regulated by Igboα. Nuclear translocation of HDAC3 is coupled with IκBα degradation. IκBα might regulate HDAC3 functions by controlling its distribution (285).

1.3.4 Substrates for HDAC3

Unlike other class I HDACs, HDAC3 is found in the nucleus, cytoplasm and cell membrane (266). Consistent with this, substrates of HDAC3 are found both in the nucleus and cytoplasm. Histones, including H2A, H2B, H3 and H4, are the primary substrates for HDAC3. Non-histone proteins, including nuclear proteins such as MEF2, SRY, PCAF (274, 286) and cytoplasmic proteins such as NF-κB, are also deacetylated by HDAC3 (287).

1.3.5 Comparison of HDAC3 with other class I HDACs

Class I HDACs share a common HDAC domain. However, HDAC3 contains a more variable C-terminus. HDAC1 and 2 are found in 6 complexes (i.e., the NuRD, Co-REST/REST, Sin3, NODE, SHIP, and MiDAC complexes), while HDAC3 is found in only one complex (i.e., the NCoR/SMRT complex) (57, 58, 288, 289). Class I HDACs play a critical role in controlling cell cycle progression, cell differentiation and tissue development. For instance, both HDAC1/2 and HDAC3 are shown to inhibit multipotent cell differentiation (290), but these three HDACs have both overlapping and distinct promotor occupancy, indicating different mechanisms used for HDAC1/2 and HDAC3 to regulate cell differentiation (291). It seems that their structure similarities determine their function redundancy. HDAC1 and -2 are 83% identical in amino acids, while HDAC1 and HDAC3 share only 53% identify. Indeed, a single allele of *Hdac1* or *Hdac2* is enough to rescue their double knockout phenotypes (292, 293). Though in redundancy, HDAC1 has broader functions than HDAC2. Germline deletion of HDAC1, but not HDAC2, causes early embryonic lethality in the mice (73, 294). While germline knockout of HDAC3 in the mouse is sufficient to cause lethality as early as E9.5, indicating its roles could not be compensated by the other HDACs. The bigger difference of HDAC1/2 from HDAC3 in amino acid sequence identity determines that they have distinct

binding proteins and form different multisubunit protein complexes. Global deletion of HDAC8 leads to perinatal lethality as well, due to skull instability (295). In contrast to HDAC1, -2 and -3, which form multisubunit protein complexes and deacetylate histones globally as well as locally, HDAC8 acts alone and is fully active by itself. These lines of evidence support that although class I HDACs have similar functions such as in regulating apoptosis, differentiation and cell cycles, they probably utilize different mechanism in achieving these. Moreover, HDAC3 has distinct functions that could not be compensated by others. Thus, HDAC3 is a unique deacetylase both *in vitro* and *in vivo*.

1.3.6 Cellular functions of HDAC3

HDAC3 regulates global deacetylation of H3K9ac, H3K14ac, H3K27ac, H4K5ac, H4K12ac, H4K16ac (Li & Yang, unpublished observations) as well as locus-specific deacetylation of H3K9-K14ac (296). Deletion of *Hdac3* in the mouse embryonic fibroblasts (MEFs) blocks S-phase progression, induces apoptosis, and alters chromatin structure and genome stability (296, 297). Of note, the induced apoptosis is due to impaired S-phase progression and DNA double strand breaks, rather than altered transcription in the *Hdac3*-deficient cells (297). On the contrary, HDAC3 affects cell proliferation and differentiation through regulating transcriptional programs via the protein complex containing NCoR and SMRT (298).

1.3.7 HDAC3 in mouse embryo and tissue development

At the organismal level, HDAC3 is essential for the development of embryos and various tissues. Germline deletion of *HDAC3* leads to embryonic lethality as early as E9.5 due to defects in gastrulation (299). Loss of hepatic *Hdac3* leads to defective metabolism of lipid, cholesterol and carbohydrate (300). In the adult liver, HDAC3 associates with Rev-erbα to regulate lipid metabolism and loss of *Hdac3* causes hepatic steatosis (301). Deletion of *Hdac3* in the first or second heart field progenitor cells by the *Nkx2-5-Cre* or *Isl1-Cre* mouse strain leads to early embryonic lethality (302, 303). Intestinal epithelial cells (IECs) lacking HDAC3 showed deregulated gene expression and loss of Paneth cells, which further impaired IEC function and altered the intestinal composition of commensal bacteria (304). In the

hematopoietic system, inactivation of *Hdac3* mediated by *Vav-iCre* leads to failure in hematopoietic stem cell proliferation and differentiation (305).

However, the functions of HDAC3 are not necessarily dependent on its enzymatic capacity for all cases. In NS-DADm mice which bear a single-amino-acid mutation in the DAD domains of NCoR and SMRT, histone acetylation is elevated to a level that is comparable to the *Hdac3* liver-specific knockout mice (281). Although germline deletion of NCoR, SMRT and HDAC3 leads to embryonic lethality (297, 306), the NS-DADm mice are viable (300), indicating the essential role of NCoR, SMRT and HDAC3 interaction in development independent of their roles in mediating histone deacetylation.

1.3.8 HDAC3 in human disease and treatment

In humans, HDAC3 has not been linked to any developmental disorders. This could be attributed to early lethality in case of severe HDAC3 dysfunction. However, we have indeed identified several cases of *HDAC3* mutations linked to a novel brain disorder (Li *et al*., unpublished data). On the contrary, HDAC3 has been associated with a range of cancers (307, 308). There are 5 HDAC inhibitors that are licensed for use in treating cutaneious T-cell lymphoma, peripheral T-cell lymphoma and multiple myeloma (309). Other than cancers, HDAC inhibitors are used in treating brain and psychiatric disorders as well. For example, valproic acid, a class I HDAC selective inhibitor, has been used in treating epilepsy, bipolar disorders and to prevent migraine headaches (310).

1.3.9 Rationale and hypothesis for the studies in Chapters III and IV

Chapter III

HDAC3 is a histone deacetylase functioning within the NCoR/SMRT complexes. Molecularly, the NCoR/SMRT complexes are recruited to specific promoters to regulate transcription. NCoR and SMRT are both essential for embryonic brain development (306, 311). HDAC3 is also shown to be important in the neonatal and adult brain development (312, 313). However, role of HDAC3 in embryonic brain development is unclear. In the cells, HDAC3 is known to regulate DNA damage repair, apoptosis and genome stability independent of its roles in transcription (296, 297). HDAC3 is also important in proliferation and differentiation

relating to its roles in regulating transcriptional programs (291, 314, 315). At the organismal level, HDAC3 is shown to be important for hematopoiesis, development and/or functioning of heart, liver, muscle and fat (305, 316-319). We propose that HDAC3 is important in embryonic brain development and HDAC3 might regulate the transcriptional programs of neural stem cells. *Emx1-Cre* is expressed in neuroepithelial cells as early as E10.5, and thus would be sufficient in deleting *Hdac3* in the neural stem cells in the very early embryonic stage. In Chapter III, we generated a *Hdac3*$^{f/f}$; *Emx1Cre* mouse model and dissect the role of HDAC3 in cerebral development.

Chapter IV

We show in Chapter III that HDAC3 is important in embryonic cerebral development through regulating the transcriptional programs of neural stem and progenitor cells. We further show that inhibition of HDAC3 enzymatic activity with a selective HDAC3 inhibitor affects formation of neurospheres. Based on these findings, we wonder whether malfunction of HDAC3 is involved in human brain developmental disorders. We collaborated with clinical doctors and searched patients with potential *HDAC3* mutations and identified 4 patients who carry heterozygous *HDAC3* mutations and display developmental delay, intellectual disability and epilepsy. All these 4 mutations are within the core domain of HDAC3, suggesting the enzymatic activity of HDAC3 might be affected in these patients. In Chapter IV, we analyzed the impact of the patient-derived *HDAC3* mutations on the enzymatic activities.

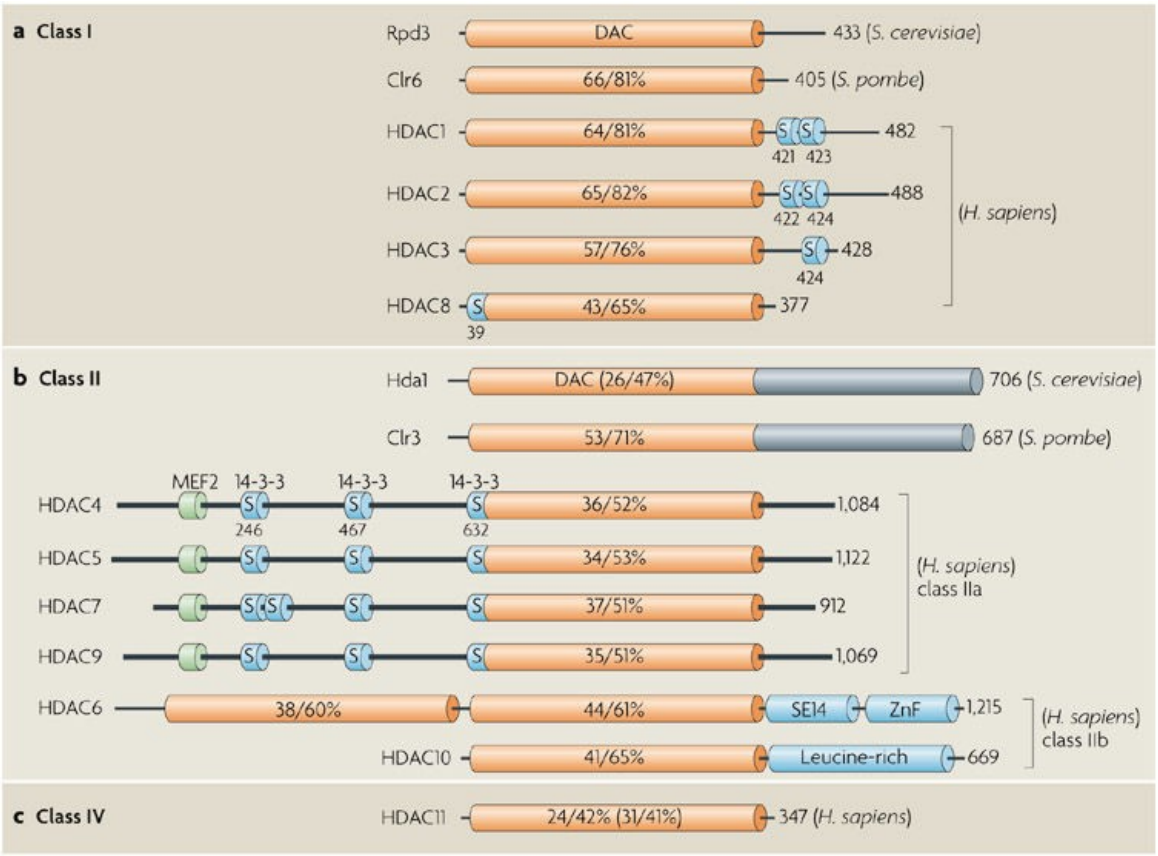

Figure 1.8. Structural illustration of classical HDACs.

The classical HDACs include class I HDACs (HDAC1, -2, -3 and -8), class IIa HDACs (HDAC4, -5, -7 and -9), class IIb HDACs (HDAC6 and -10), class IV HDAC (HDAC11). The amino acid identity and similarity compared with Rpd3 are shown as percentage. The other domains and motifs are shown as well. Copyright: Yang and Seto, Nature Reviews Molecular Cell Biology 9, 206-218 (2008), doi: 10.1038/nrm2346. Permission obtained from Springer Nature.

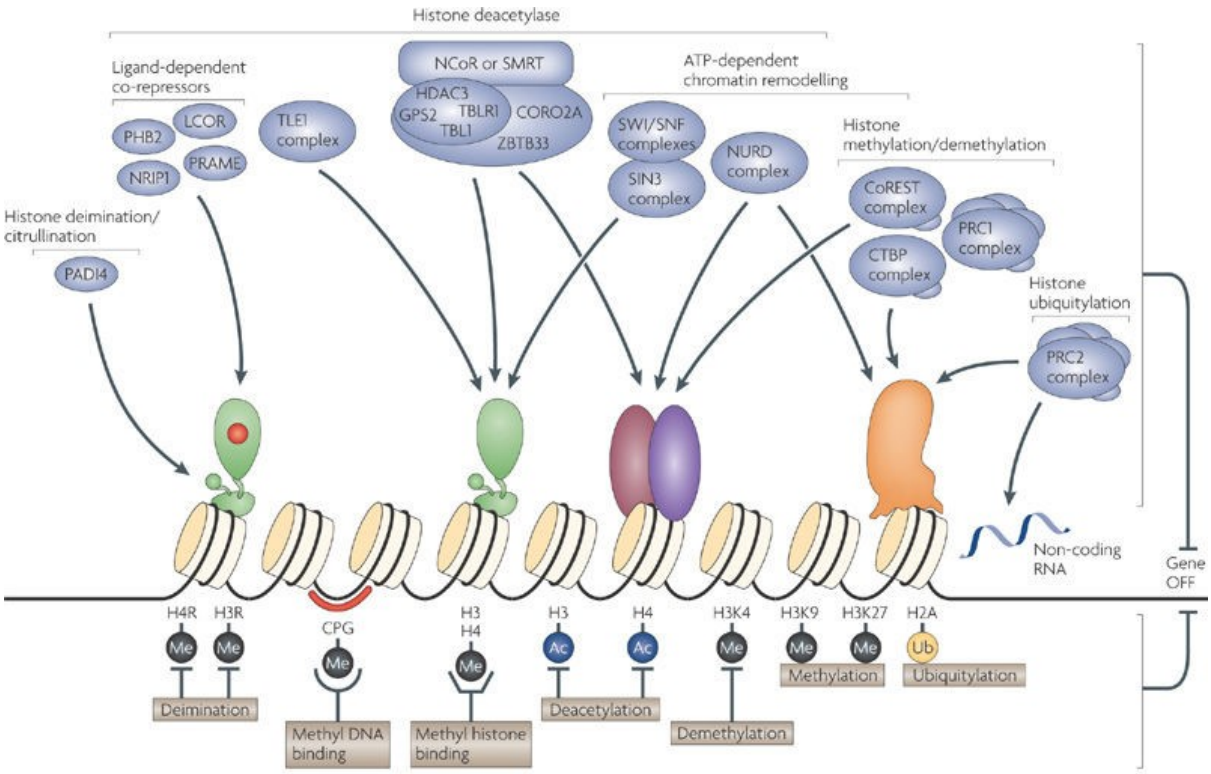

Figure 1.9. Class I HDACs as well as many other epigenetic regulators form multisubunit protein complexes.

Epigenetic regulators such as histone "modifiers" are usually recruited into multisubunit protein complexes. For instance, HDAC3 forms a complex with NCoR/SMRT, GPS2 and TBL1 to regulate transcription. Copyright: Perissi *et al.*, Nature Reviews Genetics 11, 109–123 (2010) doi:10.1038/nrg2736. Permission obtained from Springer Nature.

Bridging text between Chapters I and II

In Chapter I, I presented a general review on lysine acetylation and their responsible enzymes and provided overview of the literature on ATAT1 and HDAC3, two proteins to be studied in the following chapters. In Chapter II, I will investigate the role of ATAT1 in mouse development, mainly in the forebrain.

CHAPTER II: Tubulin acetyltransferase regulates septal and striatal development in the mouse brain

Lin Li[1,2], Sriram Jayabal[3], Mohammad Ghorbani[1,2], Lisa-Marie Legault[4], Serge McGraw[4], Alanna Watt[3] and Xiang-Jiao Yang[1,2,5,6,*]

[1]The Rosalind & Morris Goodman Cancer Research Center, and Departments of [2]Medicine, [3]Biology, and [5]Biochemistry, McGill University; and [6]McGill University Health Center, Montreal, Quebec, Canada

[4] Department of Obstetrics and Gynecology, Faculty of Medicine, Université de Montréal, Montreal, Quebec, Canada

Running Title: Brain development and tubulin acetylation

[*]To whom correspondence should be addressed: Goodman Cancer Centre, 1160 Pine Avenue West, Montreal, QC H3A 1A3, Canada; email: xiang-jiao.yang@mcgill.ca; Tel: 514-398-5883

Keywords: Lateral ventricle; ventricular dilation; ventriculomegaly; septum; striatum; hematopoiesis; platelet; tubulin acetylation; osmotic stress

2.1 ABSTRACT

α-Tubulin acetyltransferase 1 (ATAT1) catalyzes α-tubulin acetylation at lysine-40. Despite its suggested importance based on studies *in vitro*, mouse *Atat1* is dispensable for survival, raising the question what functions the enzyme has i*n vivo*. Thus, we systematically analyzed a mutant mouse strain in which *Atat1* is inactivated. These analyses revealed that starting at postnatal day 5, the mutant mice display enlarged lateral ventricles in the forebrain. The ventricular dilation resembles ventriculomegaly observed in patients. We found that in the mutant mice, the dilation is due to hypoplasia in the septum and striatum. Behavioral tests demonstrated that the mutant mice exhibit deficits in motor coordination. Birth-dating experiments showed that neuronal migration to striatum and septum is impaired in the mutant brain. As it is unclear about the role of *Atat1* in hematopoiesis, we analyzed this systematically. The results indicated that except for platelets, the hematopoietic system remains unaltered in mutant mice. In addition, we investigated the role of mouse *Atat1* in embryonic fibroblasts. These cells display minor defects in proliferation and primary cilia formation. Importantly, tubulin hyperacetylation is induced in wild-type but not *Atat1*-deficient embryonic fibroblasts in response to high salt and other cellular stresses. Furthermore, although tubulin acetylation is completely lost in a majority of mutant mouse tissues, residual levels were observed in the mutant trachea, oviduct, thymus and spleen. Therefore, this study not only establishes the importance of ATAT1 in forebrain development, platelet production and cellular stress responses, but also suggests the existence of an additional α-tubulin acetyltransferase(s).

2.2 INTRODUCTION

Acetylation of α-tubulin was first identified in the early 1980s with the flagella of the single-cell green alga *Chlamydomonas reinhardtii* (94). Amino acid sequencing subsequently identified Lys-40 as the acetylation site (95). The acetylation site is conserved from protists to mammals (96, 97) and is also present in flowering plants (98), but not in yeast (99). A monoclonal antibody specific for the acetylated form was then developed and found to recognize α-tubulin from various organisms (96). Commercially available for over two decades, this monoclonal antibody (known as clone 6-11B-1) has been widely used as a marker of stable microtubules. Tubulin acetylation is a marker for long-lived stable microtubules and is

abundant in axons and structures such as flagella and cilia. Numerous studies have been carried out using cells cultured *in vitro* and from these studies, it was concluded that acetylation of α-tubulin is important for various cellular and perhaps also developmental processes. For example, tubulin acetylation was proposed to play roles in regulating microtubule architecture (177, 180), intracellular transport (183, 186). Such conclusions were first challenged ~10 years ago when the responsible deacetylase, HDAC6 (65, 126, 127), was genetically inactivated in mice and no major phenotypes were observed (131).

Compared to the deacetylases, the responsible acetyltransferase was identified much later. Mec-17 was first identified in 2010 as the α-tubulin acetyltransferase in lower eukaryotes (47, 110). The importance of tubulin acetylation *in vivo* has been implied by the study which showed that knockdown of *mec-17* expression by morpholinos led to zebrafish developmental defects that include curved body shape, short body axis, hydrocephalus, small heads, small eyes and neuromuscular dysfunction (110). Two other studies either using shRNA to knockdown MEC-17 or deleting *Elp3* in the mice showed that loss of tubulin acetylation affected neuronal migration and differentiation in the mouse cerebral cortex (7, 191, 320). These studies suggested a major role for tubulin acetylation in development of higher mammals. However, genetic deletion of *Atat1*, which is a mouse homolog of *mec-17*, leads to a near complete tubulin acetylation loss in many tissues, confirming ATAT1 as the *bona fide* α-tubulin acetyltransferase in mice (112, 255). Surprisingly, the mice are viable and fertile, displaying only minor phenotypes including a mild distortion in the dentate gyrus, a mild impairment of sperm motility and slightly reduced litter size (112, 255). While contradicting the important roles of tubulin acetylation based on various studies using cultured cells, these results are consistent with the knockout studies of HDAC6 (131). Thus, an important question is what roles tubulin acetylation and its enzymes play *in vivo*.

A preliminary observation from our previous study is that *Atat1*$^{-/-}$ mice show enlarged lateral ventricles in the brain (255). As the abnormality has not been characterized (255), we followed this initial lead to understand the function of ATAT1 *in vivo*. We have systematically analyzed serial sections from the mutant brain. The analyses confirmed the ventricular dilation and revealed that it starts at postnatal day 5 due to hypoplasia in the septum and striatum. We

further showed that the anomaly is because of defective neuronal migration. Related to the striatal defects, behavioral tests confirmed poor motor coordination in the mutant mice.

Moreover, the role of *Atat1* in the blood system remains elusive, so we have also analyzed different hematopoietic cells. Flow cytometry indicated that composition of these cells is similar in the wild-type and *Atat1*$^{-/-}$ bone marrows, indicating that ATAT1 is dispensable for hematopoiesis. Interestingly, total blood counts uncovered an increase of platelet production in the mutant mice, so this enzyme is important for platelet biogenesis. In the MEFs, we found loss of *Atat1* has minor effects on proliferation and primary cilia formation. Stress conditions, such as treatment of cultured cells with high-concentration salt (or glucose) and exposure to H_2O_2, were recently reported to induce tubulin hyperacetylation (161). As reported (161), these stimuli cause tubulin hyperacetylation in wild-type MEFs. Importantly, the stimuli failed to induce any tubulin acetylation in *Atat1*$^{-/-}$ MEFs, indicating tubulin hyperacetylation in response to cellular stresses acts through ATAT1. Furthermore, while ATAT1 is the *bone fide* α-tubulin acetyltransferase in many tissues (112, 255), we observed residual tubulin acetylation in the mutant trachea, oviduct, thymus and spleen, indicative of another α-tubulin acetyltransferase(s) in these tissues.

2.3 RESULTS

Atat1 inactivation causes ventricular dilation

Atat1$^{-/-}$ mice are born normally and also fertile, with few obvious defects from appearance (112, 255). From the previous sagittal brain sections, we noticed that the lateral ventricles are larger in the mutant forebrain (255). To verify and extend this preliminary but promising observation, we carried out Nissl staining on serial wild-type and *Atat1*$^{-/-}$ brain sections. For this, we systematically compared sagittal sections from three pairs of wild-type and mutant brains at 24 days and 8 months after birth. Shown in Fig. 2.1A-B are two pairs of representative sagittal sections. At both timepoints, we observed significantly larger lateral ventricles in the mutant forebrain. Consistent with this, the transverse and coronal brain sections also displayed a larger lateral ventricle in the *Atat1*$^{-/-}$ mice at 2 and 12 months (Fig. 2.2A-B and data not shown). Of note, this dilation is the most obvious in the middle part of serial sections. The dilation of lateral ventricles observed in the mutant mice differs from the dilation in typical

hydrocephalus. While a bulge is frequently observed on the head of mice with hydrocephalus symptoms (321), no such bulges were observed in 12-month old *Atat1*$^{-/-}$ mice (Fig. 2.1C). To trace the developmental origin of the defect, we investigated when dilation of the lateral ventricle becomes obvious during brain development, we carried out Nissl staining using serial transverse sections from wild-type and mutant brains at E17.5, P1, P5 and P15. Larger lateral ventricles were observed as early as P5 (Fig. 2.2C-F). We asked whether this dilation affects overall health and life-span of *Atat1*$^{-/-}$ mice. However, no overall differences were observed regarding body weight and general health condition for wild-type and mutant littermates for up to 24 months of age (data not shown). Thus, *Atat1* deletion causes ventricular dilation in the forebrain as early as P5.

***Atat1* loss causes hypoplasia in the septum and striatum of the forebrain**

From the stained transverse brain sections, we observed a thinner septum (Fig. 2.2A, lower panel) and a smaller striatum (Fig. 2.2A, indicated by a red asterisk) in the *Atat1*$^{-/-}$ brain, while the other brain structures such as the cerebral cortex and cerebellum appear normal (Fig. 2.2A). To confirm this quantitatively, we measured the size of the whole brain, thickness of the neocortex, size of the striatum, and width at the bottom part of the septum using paired wild-type and *Atat1*$^{-/-}$ transverse brain sections. In serial stained sections, those that displayed the most obvious lateral ventricle dilation were used for measurement. While thickness of the overall brain and neocortex are comparable between the wild-type and mutant mice (Fig. 2.2G and H), the septum is dramatically thinner (Fig. 2.2I) in the mutant brain. Albeit less dramatic, the striatum is significantly smaller (Fig. 2.2J) in the mutant forebrain (Fig. 2.2A).

Ependymal cilia in the brain ventricles are important for the circulation of cerebrospinal fluid. Dysfunction of ependymal cilia in the ventricles causes a blockade in the cerebrospinal fluid circulation and leads to larger ventricular dilation in the brain (322). Tubulin acetylation is abundant in the cilia and might have roles in cilia functioning (254). A knockin *LacZ* reporter is harbored within the mutant allele of the heterozygous *Atat1*$^{+/-}$ mice (255), so we used the reporter to detect *Atat1* expression by β-galactosidase staining. We found that *Atat1* is highly expressed throughout the brain, not only in the ependymal cells of the lateral ventricle, where ependymal cilia reside, but also in the septum, striatum, and cerebral cortex (Fig. 2.1D). We

showed that tubulin acetylation was detectable in the wild-type but not mutant ependymal cilia (Fig. 2.1E). However, the length of ependymal cilia is comparable between wild-type and mutant mice (Fig. 2.1F), indicating that a loss of *Atat1* and tubulin acetylation does not affect ependymal cilia assembly in lateral ventricles. Thus, loss of *Atat1* and tubulin acetylation leads to larger lateral ventricles due to hypoplasia in the septum and striatum.

Atat1 loss does not affect neocortical development

It has been reported that knockdown of *Atat1* by shRNAs (191) or loss of tubulin acetylation by inactivating *Elp3* (103) causes neuronal migration and differentiation defects in the mouse cerebral cortex. By Nissl staining, we found that the thickness of cerebral cortex is not affected in the mutant brain (Fig. 2.2H). To investigate whether loss of *Atat1* affects neocortical development, we performed indirect immunofluorescence microscopy using antibodies against the neural stem and progenitor cell (NSPC) markers such as Sox2 and Tbr2. As shown in Fig. 2.3A-D, NSPC development is not affected in the mutant neocortex. We also tested antibodies specific to the cortical lamination markers such as Cux1, Cux2, Tbr1 and Ctip2. As shown in Fig. 2.3E-F, similar patterns of these lamination markers were observed in the wild-type and mutant neocortices, indicating that neocortical lamination is unaffected in the mutant. Golgi staining revealed no obvious abnormalities in the neuronal structure and organization of the *Atat1* mutant cerebral cortices (Fig. 2.3G-H). Thus, loss of *Atat1* and tubulin acetylation does not affect neocortical development.

Impaired neuronal migration to the *Atat1*$^{-/-}$ septum and striatum of the forebrain

Neurogenesis reaches its peak at the mid gestation. To trace how neurons are produced and then migrate in the brain, we injected bromodeoxyuridine (BrdU) intraperitoneally into pregnant mice at E13.5 and recovered the brain at day 10 after pups were born. This timepoint was chosen because ventricular dilation is already obvious in the mutant brain by then (Fig. 2.2A-F). After immunohistochemical staining with an anti-BrdU monoclonal antibody, we counted positively stained cells in the striatum, septum and neocortex. For the latter, we divided the neocortical layer from the subventricular zone to the molecular zone equally into 10 sub-layers (Fig. 2.4D) to count BrdU^{+} cells in each sub-layer. When counting positively stained cells in the striatum, septum and neocortex, we considered those with darkly stained nuclei as

dense labels and those with lightly stained nuclei as light labels. We found that there are significantly fewer $BrdU^+$ cells (both densely and lightly labelled) in the mutant striatum (Fig. 2.4A-B) and septum (Fig. 2.4A and C). By contrast, no major difference was observed between the wild-type and mutant neocortices (Fig. 2.4D-F); consistent with this, no neocortical laminatfion defects were present in the mutant brain (Fig. 2.3E-F).

To investigate whether loss of *Atat1* affects the NSPC proliferation, we injected BrdU intraperitoneally into P10 pups. After 1 h, the brains were recovered for immunohistochemical staining against an anti-BrdU monoclonal antibody and counting $BrdU^+$ cells close to the subventricular zone. As shown in Fig. 2.4G-H, the number of $BrdU^+$ NSPCs is comparable between the wild-type and *Atat1*$^{-/-}$ subventricular zones, indicating that loss of *Atat1* does not affect the S-phase of NSPCs. To substantiate this, we stained E14.5 embryonic and P0 brain sections using an anti-Ki67 antibody. As shown in Fig. 2.4I, we observed no difference between wild-type and *Atat1*$^{-/-}$ mice, supporting NSPC proliferation is not affected by loss of *Atat1* and tubulin acetylation.

Atat1 loss was reported to promote apoptosis in the seminiferous tubules (323). To test whether the frequency of apoptosis is affected in the mutant brain, we carried out TUNEL staining using brain sections from wild-type and *Atat1*$^{-/-}$ mice. No significant difference was observed regarding the number of $TUNEL^+$ cells in the striatum between the two groups at both E14.5 and P24 (Fig. 2.4J). Although it was suggested that there is enhanced apoptosis in *Atat1*$^{-/-}$ testis (112), we didn't observe significant difference (data not shown). Tubulin acetylation was suggested to regulate autophagy (235, 236, 324). Taken together, these results support that loss of *Atat1* and tubulin acetylation cause defective cell migration to the striatum and septum but do not affect other NSPC properties.

Atat1 loss leads to motor coordination deficits

To determine possible functional impact of hypoplasia in the mutant striatum and septum, we carried out a battery of behavioral tests. The open field test revealed no overall difference between control and *Atat1*$^{-/-}$ mice (Fig. 2.5A-C). The time the mice spent in the center area (Fig. 2.5A) and total distance travelled (Fig. 2.5B) in the arena were comparable between two groups. The feces during the open field test are indicators for an anxious status of the mice. We thus

counted the feces as well, but no significant difference was observed (Fig. 2.5C). The tail suspension test revealed no statistically significant difference regarding immobile time, which is an indicator for depression, between wild-type and *Atat1*$^{-/-}$ mice (Fig. 2.5D).

Accelerated rotarod tests were utilized to check the motor coordination ability of the mice (325). For these test, each mouse was subjected to 4 tests per day (with a break of at least 20 min between 2 tests) for 4 consecutive days. The latent time for each test in a single day (Fig. 2.5E-G) and the average latent time for each mouse in 4 days were recorded (Fig. 2.5H). As shown by a shorter average latent time (Fig. 2.5E-G), the *Atat1*$^{-/-}$ mice were prone to fall. This trend was more obvious in 6-month-old mice (Fig. 2.5F). Thus, loss of *Atat1* and tubulin acetylation results in mild defects in motor coordination.

Atat1 deletion exerts minor effects on MEFs

We next investigated how loss of *Atat1* and tubulin acetylation might affect characteristics of MEFs. In *Atat1*$^{-/-}$ MEFs, while the overall microtubule networks are normal as shown by immunofluorescence using an anti-tubulin antibody (Fig. 2.6A, left panel), tubulin acetylation is completely lost as shown by immunofluorescence staining against the anti-acetyl-tubulin monoclonal antibody (Fig. 2.6A, right panel). 20,000 MEF cells were seeded per well in 12-well plates and the growth rate was measured by the IncuCyte Imaging System. *Atat1*-deficient MEFs grew faster than the wild-type in the first couple of days but showed no difference from wild-type MEFs afterwards (Fig. 2.6B).

Primary cilium is important in cell signaling and tubulin acetylation is enriched in this organelle (200). Using type III adenylyl cyclase (ACIII), a marker for primary cilia, we found that tubulin acetylation is totally lost in the mutant primary cilia (Fig. 2.6C). Serum starvation or growth to confluency induces primary cilia formation, whereas heat shock for a short time induces primary cilia resorption (326). To study how tubulin acetylation affects primary cilia formation, we grew MEFs to confluency and treated them with either the EBSS media (for serum starvation) for 4 h or incubation at 42°C for up to 30 min. In the no-treatment group, there were comparable numbers of wild-type and mutant MEFs possessing primary cilia (WT 38% vs KO 45%, p=0.29), and the length of primary cilia was also comparable between wild-type and mutant MEFs (Fig. 2.6D). However, after serum starvation or heat shock, the mutant

primary cilia were longer in the *Atat1*-deficient MEFs although the difference was small (Fig. 2.6D), indicating tubulin acetylation slightly affects primary cilia formation. In the treatment groups, number of MEFs possessing primary cilia is comparable as well (WT 58% vs KO 59% for EBSS starvation, p=0.79, and WT 50% vs KO 42% for heat shock, p=0.16). In comparison, the length of ependymal cilia in the lateral ventricle is comparable between wild-type and *Atat1*$^{-/-}$ mice (Fig. 2.1I). Thus, loss of tubulin acetylation exerts minor effects on primary cilia formation.

It was reported that tubulin acetylation regulates autophagy (235, 327). To verify this, Western blotting was carried out using MEF extracts against LC3 antibodies. There were no differences regarding the LC3b-II/LC3b-I ratio (Fig. 2.6E-F), indicating that autophagy is not affected in mutant MEFs. Tubulin acetylation is reduced during differentiation of stem cells or iPS cells (328). To check whether iPS reprogramming is related to tubulin acetylation, we reprogrammed wild-type and *Atat1*$^{-/-}$ MEFs to iPS cells; no difference was found between the two groups (data not shown).

Atat1 is required for stress-induced tubulin hyperacetylation

A recent study demonstrated that cellular stress stimuli, such as exposure to or H_2O_2 or high concentration of NaCl induces tubulin hyperacetylation (161). As shown in Fig. 2.7A, upon treatment with 0.25 M NaCl or exposure to 5 mM H_2O_2 or 100 mM glucose for 30-60 min, tubulin acetylation increased by 2.8 to 11 folds in wild-type MEFs (Fig. 2.7A, compare lanes 1, 3, 5 and 7). By contrast, in *Atat1*$^{-/-}$ MEFs, there was no tubulin acetylation detected, with or without treatments (lanes 2, 4, 6 and 8). After treatment with these stimuli, we observed no overall morphological difference between wild-type and *Atat1*$^{-/-}$ MEFs (Fig. 2.7B, left two panels). Indirect immunofluorescence microscopy with an anti-acetyl-tubulin antibody confirmed that NaCl treatment and EBSS starvation induced tubulin hyperacetylation in the wild-type but not mutant MEFs (Fig. 2.7B). Thus, tubulin hyperacetylation is induced in wild-type MEFs in response to cellular stress, but this response is lost in *Atat1*$^{-/-}$ MEFs.

Enhanced platelet production and residual tubulin acetylation in *Atat1*$^{-/-}$ mice

As it remains entirely unclear about the role of *Atat1* in the blood system, we analyzed hematopoietic cells systematically. As shown in Table 2.1, complete blood counts revealed that

various blood cells were not affected. Notably, the platelet number significantly increased in the mutant mice (Table 2.1). In addition, biochemical analyses revealed no difference between the wild-type and mutant blood (Table 2.2). To explore how hematopoiesis is affected upon *Aata1* deletion, we accrued out systematic flow cytometric analyses of cells in the bone marrow compartment. As shown in Fig. 2.8A-G, hematopoietic stem cells, progenitors and other cells in were not affected in the mutant bone marrow compartment. In light of residual levels of histone acetylation in the thymus, spleen and other tissues, we investigated whether tubulin acetylation is affected in the mutant bone marrow. We showed that tubulin acetylation is totally lost in the *Atat1*$^{-/-}$ bone marrows (data not shown). Taken together, these results indicate that except for platelet production, hematopoiesis is not affected in the mutant mice.

While ATAT1 is the sole tubulin acetyltransferase in in the brain and many other tissues (112, 255), we observed residual signals of tubulin acetylation in the mutant trachea and oviduct by immunofluorescence microscopy (Fig. 2.9A-B). By contrast, the acetylation was completely absent in the mutant lateral ventricles (Fig. 2.1E), MEFs (Fig. 2.7A) and olfactory ependyma (Fig. 2.9C). Moreover, immunoblotting confirmed the residual levels of tubulin acetylation in the mutant trachea and oviduct (Fig. 2.9E-F). Moreover, such residual levels were also detected in the mutant thymus, spleen and skeletal muscle (Fig. 2.9E-F). These results indicate the existence of a minor tubulin acetyltransferase(s) in the tissues with residual tubulin acetylation after *Atat1* is deleted.

2.4 DISCUSSION

This study extends the previous preliminary finding that *Atat1*$^{-/-}$ mice show enlarged lateral ventricles in the brain (255). We have confirmed the ventricular dilation in the mutant brain starting at P5 (Figs. 2.1, 2.2), demonstrated that the dilation is due to septal and striatal hypoplasia in the forebrain (Figs. 2.1, 2.2), and identified defective neuronal migration as the underlying cause (Fig. 2.4). The role of *Atat1* in the blood system remains elusive, so we have also analyzed hematopoietic cells systematically. Total blood counts uncovered more platelets in the mutant mice (Table 2.1). We observed similar cellular composition in the wild-type and *Atat1*$^{-/-}$ bone marrows (Fig. 2.8), indicating ATAT1 is not essential for hematopoiesis in that compartment. In the MEFs, we found loss of *Atat1* has minor effects on proliferation and

primary cilia formation (Fig. 2.6). As reported (161), stress conditions, such as high salt or glucose concentration and H_2O_2 exposure, induces tubulin hyperacetylation in cultured cells (Fig. 2.7). Importantly, these stimuli fail to induce any tubulin acetylation in *Atat1*$^{-/-}$ MEFs, so tubulin hyperacetylation in response to cellular stress stimuli acts through ATAT1 (Fig. 2.7). While ATAT1 is the major *bone fide* tubulin acetyltransferase (112, 255), there are residual signals of tubulin acetylation in the mutant trachea, oviduct, thymus and spleen, so we propose another tubulin acetyltransferase(s) is responsible for the residual tubulin acetylation in these tissues.

Previously, tubulin acetylation was reported to have a role in neuronal migration and differentiation in the cerebral cortex (103, 191). Our results using *Atat1*$^{-/-}$ mice show that although tubulin acetylation is totally depleted, the cerebral cortex development is not affected (Fig. 2.1E, Fig. 2.3). One previous study utilized shRNA to knockdown ATAT1 (191), which might produce off-target effects. Another previous study (103) described neuronal migration and differentiation defects, but they might be caused by Elp3 itself but rather than its relation to tubulin acetylation. Although we did not observe abnormality in the cerebral cortex, we observed smaller striatum and thinner septum in the *Atat1*$^{-/-}$ brain (Figs. 2.1, 2.2). The striatum is a critical component of the motor and reward system in mice. It receives glutamatergic and dopaminergic inputs from sources such as the motor cortex, and outputs to the rest parts of the basal ganglia (329). Using the accelerated rotarod test, we revealed that mice lacking *Atat1* have a mild defect in motor coordination (Fig. 2.5E-H). The defective motor coordination might be due to the hypoplasia in the striatum and septum of the *Atat1*-deficient mice, but we cannot exclude the possibility that the other parts such as muscle function might also be affected. The open field test showed that the mutant mice travelled similar distance compared wild-type mice (Fig. 2.5B), indicating it is less likely that the muscle function is compromised. The striatum and septum are also involved in anxiety behaviors. However, we observed no difference using the open field and tail suspension tests (Fig. 2.5A-D). This study thus links ATAT1 and tubulin acetylation not only to striatum and septum development, but also to brain functions such as motor coordination.

Unexpectedly, the motor coordination defects observed in the mutant mice somewhat resemble Huntington's disease, an inherited neurodegenerative disorder characterized by

massive loss of medium spiny neurons, which constitute 95% of the cells in the striatum (330). The disease shows a lack of coordination and increased mental abnormalities as the disease progresses. In the *Atat1*$^{-/-}$ mice, we performed immunofluorescence microscopy against an anti-Ctip2^{+} antibody. The results showed fewer Ctip2^{+} cells, which is consistent with to the reduced striatum area (data not shown). *Atat1*$^{-/-}$ mice also show a mild motor coordination defect (Fig. 2.5E-H), which is common in Huntington's disease patients.

Tubulin acetylation is associated with Huntington's disease, and levels of tubulin acetylation are reduced in the patients' brains (186). Many studies associated HDAC6 with Huntington's disease (186, 331-333). As HDAC6 is the major tubulin deacetylase, it remains possible that tubulin acetylation might have a role in Huntington's disease. Our study on ATAT1 established a link between tubulin acetylation loss and hypoplasia in the striatum, and thus further support the hypothesis that disturbance of tubulin acetylation might relate to HD. It has been shown that inhibition of HDAC6 (the tubulin deacetylase) increases the transport of the cortico-striatal derived neurotrophic factor BDNF, which is neuroprotective for striatal neurons both *in vitro* and *in vivo*, through elevated tubulin acetylation (186). BDNF is neuroprotective for striatal neurons both *in vitro* and *in vivo*. It seems possible that tubulin acetylation affects the striatum through its regulation of BDNF. However, in another study, it was shown that elevated tubulin acetylation levels did not affect the efficiency of BDNF transport from the cortex to the striatum (334). We did not detect any significant difference regarding cell survival in the striatum as indicated by TUNEL staining. The role of tubulin acetylation in BDNF transport remains elusive and further investigation is needed.

The role of *Atat1* in the blood system remains entirely unclear (112, 255), so we analyzed mutant hematopoietic cells systematically. Complete blood counts revealed that the platelet number significantly increased in the mutant mice (Table 2.1). Related to the platelet overproduction in the mutant mice, the tubulin deacetylase HDAC6 has been shown to regulate platelet maturation and activation (148, 335). Thus, tubulin acetylation is likely to play an important role in platelet homeostasis. Notably, platelets are important in hemostasis and thrombosis, so they are highly relevant to different clinical conditions such as hypercholesterolemia (336). In addition, platelet overproduction is characteristic of essential thrombocythemia, a rare chronic blood condition (337). No patients with *ATAT1* mutations

have been identified, but the forebrain defects and platelet abnormalities should help identify and characterize patients with such mutations.

Many *in vitro* studies have implied that tubulin acetylation has important roles in cellular functions such as intracellular transport, microtubule assembly, and cell motility (254). Knockdown of ATAT1 using shRNA revealed tubulin acetylation is essential for neuronal migration (338). With this evidence, it is unexpected that the *Atat1*-deficient mice are viable and fertile and show no obvious defects. We further showed that loss of *Atat1* in MEFs does not affect MEF properties in a significant way, indicating ATAT1 and tubulin acetylation does not have a critical role in cell proliferation, differentiation and survival. In agreement with this, we did not observe any developmental defects in various tissues including in the hematopoietic system (Fig. 2.8 and Table 2.1). While we observed hypoplasia in the striatum and septum, the proliferation, differentiation, apoptosis and autophagy are not affected in the brain. By contrast, we observed fewer $BrdU^+$ cells in the mutant striatum and septum (Fig. 2.5A-C), indicating a possible migration defect.

Atat1$^{-/-}$ mice and cells provide a valuable tool for dissecting the roles of tubulin acetylation under normal and pathological conditions. Tubulin acetylation has been shown important for touch sensitivity in *C. elegans* (110). A recent study show that tubulin acetylation is essential for touch sensation in mice as well (339). Loss of MEC-17 and tubulin acetylation has been shown to disrupt microtubule organization (177, 180). However, none of these proposed functions of tubulin acetylation affect mouse development significantly. We observed hypoplasia in the striatum and septum, but it does not affect mouse survival as well. A very recent study showed that ATAT1 and tubulin acetylation was critical for cell proliferation, as cell growth rate increased more than 5 folds in the absence of *Atat1* (340). However, in our *Atat1*$^{-/-}$ MEFs, we observed a slight increase in proliferation for the first few days in cultured plates but overall there is no significant difference between wild-type and *Atat1*$^{-/-}$ MEFs (Fig. 2.7B). This discrepancy might relate to cell types. However, in another study, it was shown that genetic disruption of *Atat1*, inhibits proliferation and invasion of colon cancer cells, while restoring the levels of ATAT1 in *Atat1*-deficient cells restores the cancer cell invasive characteristics (341). These two studies showed a contradicting role of ATAT1 and tubulin

acetylation in cell proliferation. Whether the role of tubulin acetylation in proliferation is dependent on cell types and their growing environment needs further investigation.

On the other hand, the role of tubulin acetylation has been inadequately analyzed under stress conditions. It was shown that stimuli such as exposure to a higher concentration of NaCl could induce tubulin hyperacetylation (236). This observation implies that tubulin acetylation might have a role in anti-stressing stimuli, which needs further investigation. As reported (236), we observed that stressing stimuli such as treatment with high concentration of NaCl induces tubulin hyperacetylation in wild-type MEFs (Fig. 2.7). Interestingly, no tubulin acetylation was observed in *Atat1*$^{-/-}$ MEFs no matter with or without stimuli treatment (Fig. 2.7). Tubulin hyperacetylation caused by high-concentration salt might be due to the rapid activation of TAK1, which is osmotic-inducible and activates ATAT1 in a rapid manner (340). Microtubule hyperacetylation could be induced by lipopolysaccharides treatment as well. This induced tubulin acetylation is found necessary for the production of the anti-inflammatory cytokine IL-10 (342). Two recent studies have shown that tubulin acetylation enhances the flexibility of microtubules under physical pressure (30, 31). Elucidating the role of tubulin hyperacetylation in response to cellular stress might reveal the role of ATAT1 under stressing or pathological conditions.

As expected, *Atat1* is highly expressed in the ciliated tissues such as in the ependymal cells of the lateral ventricle (Fig. 2.2G), the nasal cavity, and in the ganglion cell layer of the eyes (Fig. 2.9D). While tubulin acetylation is found totally lost in the ependymal cilia (Fig. 2.1E), residual levels were detected in the trachea, oviduct, thymus and spleen (Fig. 2.9). These results indicate that while ATAT1 is the acetyltransferase governing tubulin acetylation in the brain and many other tissues (112, 255), there is another tubulin acetyltransferase in certain tissues such as the trachea, oviduct, thymus and spleen. Prior to the identification of ATAT1, three other enzymes have been shown to possess acetyltransferase activity against microtubules (103-106). It will be interesting to investigate whether one of them or another protein is the elusive tubulin acetyltransferase responsible for the residual tubulin acetylation observed in the trachea, oviduct, thymus and spleen.

In conclusion, this study uncovers ventricular dilation due to septal and striatal hypoplasia in the *Atat1*$^{-/-}$ brain, identifies platelet overproduction in the mutant blood system, and shows

that ATAT1 is essential for tubulin hyperacetylation in stress responses. No patients with *ATAT1* mutations have been reported yet, but the forebrain defects and platelet anomalies in *Atat1*$^{-/-}$ mice should help identify and characterize such human mutations. This study also provides evidence for existence of a new α-tubulin acetyltransferase in certain tissues.

2.5 MATERIALS AND METHODS

Animals and mouse genotyping

Atat1$^{-/-}$ mice were initially obtained from the Knockout Mouse Project (KOMP) repository (Project ID: VG14032), as previously described (255). The DNA sequence between first exon and last exon was replaced by a sequence containing the *LacZ* and *Neo* genes (255). The *Neo* gene was flanked by two LoxP sites and removal of this gene had no impact on the phenotype. Mice were on the C57BL/6J background and maintained in the animal facility of Goodman Cancer Centre of McGill University. All procedures involved in the experiments relating to mice were performed according to the guidelines and protocols approved by the McGill Animal Use Committee.

Tissue extract preparation and Western blotting

Tissues were taken from 2-month-old littermates of wild-type and *Atat1*$^{-/-}$ mice. Tissues were weighted and homogenized with a plastic pestle in Eppendorf tubes by adding 3 volumes of the RIPA buffer (25 mM Tris-HCl pH 7.6, 150 mM NaCl, 1% nonidet P-40, 1% sodium deoxycholate, and 0.1% SDS, supplemented with a protease inhibitor cocktail composed of phenylmethylsulfonyl fluoride, aprotinin, pepstatin and leupetin). After additional homogenization by sonication with a Virsonic 100 sonicator (Virtis, Inc) at setting 5 for 6 times (5 seconds each), the suspension was centrifuged at ~20,000 g and 4°C for 10 min. The supernatant was collected as whole protein extracts. 1 µl of protein extract was used for protein concentration measurement by the Bradford assay reagent (Bio-Rad) and the rest was flash-frozen in a dry ice and methanol mixture for further storage at -80°C.

For Western blotting, tissue extracts were mixed with a 3x reducing sample buffer (188 mM Tris-HCl pH6.8, 6% SDS, 30% glycerol, 0.3% bromophenol blue, 16% β-mercaptoethanol) and boiled for 3-5 min before SDS-PAGE and Western transfer. The membranes were blocked

in 0.15% Tween-20/PBS solution containing 5% non-fat skimmed milk. Primary antibodies used were as follows: anti-α-tubulin antibody (Sigma, T5168) (1:2500 dilution), anti-acetylated tubulin (Sigma, T7451, clone 6-11B-1) (1:5000), and anti-LC3b I/II antibody (Novusbio, NB100-2220) (1:1000). The membranes were incubated overnight at 4°C with agitation. The membranes were then washed for 3 times, 10 min each time, followed by incubation in the horseradish peroxidase-conjugated sheep anti-mouse IgG secondary antibody (GE Healthcare Life Sciences, NA931V; diluted at 1:5000) for 1 h. After washing for 3 times, 10 min each time, protein bands were detected with the WEST-ZOL plus Western Blot Detection System (iNtRON Biotechnology, Seoul, Korea).

MEF isolation and culture

MEFs were isolated from E13.5 mouse embryos. Briefly, E13.5 embryos were dissected out of pregnant mice; the head and internal organs of the embryos were removed. The rest parts of the embryos were minced with scissors and digested with 0.25% Trypsin-EDTA for 10 min in a 37 ℃ shaker. After centrifugation, the supernatant was removed, and the pellet was resuspended in complete medium (DMEM supplemented with 15% fetal bovine serum, non-essential amino acids (Thermo Fisher Scientific, Cat No. 11140050), penicillin and Streptomycin (Thermo Fisher Scientific, Cat No. 15140122)). The cell suspension was cultured in a low oxygen incubator (4% O_2). MEF protein extract and Western blotting were carried out as described for mouse tissues.

Frozen section preparation

Mice were anesthetized and perfused first with 50 ml cold PBS, followed by 50 ml cold 2% PFA in PBS, as previously described (255). The brains were then dissected out under a chemical hood. For embryos, whole embryos or dissected embryonic brains were collected. The tissues were fixed at 4°C for 2-16 h in the fixative solution (0.1 M phosphate buffer [pH7.4], 2% PFA, 0.2% glutaraldehyde, 5 mM EGTA [pH 8.0], 2 mM $MgCl_2$ and 0.2% nonidet-P40), and subsequently equilibrated first with 15% sucrose in PBS for 8 h and then with 30% sucrose in PBS overnight at 4 °C till the tissues sunk down to the bottom of the container. The tissues were taken out from the fixative solution and blotted with wipe paper to remove extra solution. Afterwards, the tissues were incubated with the OCT compound (Tissue-Tek) in a cassette at

4 °C for 30 min. The direction of the tissues was arranged properly, and then the cassettes were snap-frozen on a dry ice and methanol mixture. The blocks were sectioned on a cryostat (Thermo Shandon, A77210167), and 15-μm sections were collected onto glass slides (Fisher Scientific). The sections were air-dried at room temperature (RT) for about 1 h and then stored at -80°C.

β-Galactosidase staining of frozen sections

Frozen sections were taken out from -80°C freezer and put in RT for 10 min to recover. The sections were then post-fixed in a fixative (0.2% PFA in 0.1 M PIPES, pH 6.9, 2mM $MgCl_2$, and 5 mM EGTA) on ice for 10 min, then rinsed and washed in PBS containing 2mM $MgCl_2$ for 10 min. Sections were permeabilized by incubation in the detergent solution (PBS containing 0.3% Triton X-100) on ice for 10 min, and then changed to the β-gal staining solution (add components here) and incubated at 37 °C in the dark until the desired color was reached (vary from 1 hour to overnight). The slides were then washed in PBS containing 2 mM $MgCl_2$ for 3 times, 5 min each time, followed by washing in distilled water for 5 min. Sequential dehydration was performed with 70%, 95% and 100% ethanol (5 min each). Sections were incubated in xylene for two times, 5 min each, and mounted with the ClearMount mounting medium (American Master Tech, MM0126).

BrdU labeling

BrdU was injected into E13.5 pregnant mice or P10 mice via the peritoneum at a dose of 50 μg BrdU per g of body weight as previously described (343, 344). For cell tracking, after BrdU injection into E13.5 pregnant mice, brains of the new pups were collected at P10. For S-phase assays, brains of the P10 mice were collected 1 h after BrdU injection. The collected brains were fixed in 4% paraformaldehyde (PFA) overnight, followed by paraffin processing and embedding.

Paraffin section preparation

The tissues were collected same as above, fixed in 4% PFA/PBS overnight, and proceeded for paraffin processing and embedding. The paraffin blocks were sectioned on a Leica Rotary

Microtome (Leica RM2125RTS). 5-μm sections were collected onto glass slides (Fisher Scientific) and baked 2 h at 37 °C. The slides were kept at 4°C for long-term storage.

Histological analysis and immunotaining of brain sections

For histological analysis, Nissl staining were carried out as described previously (255, 343, 344). For immunohistochemical staining of BrdU, the paraffin sections were dewaxed, rehydrated, and exposed to 2 N HCl at 37 °C for 30-60 min before antigen-retrieval by boiling in 10 mM of sodium citrate (pH 6.0) for 20 min. After cooldown, sections were incubated in blocking buffer (2% BSA in 0.2% Triton X-100/PBS solution) at RT for 30-60 min before incubation with a rat anti-BrdU antibody (Abcam, AB6326, 1:200) in the blocking buffer at 4 °C overnight. After wash twice in 0.2% Triton/PBS, sections were incubated with biotin-SP-conjugated AffiniPure donkey anti-rat IgG(H+L) antibody (Jackson ImmunoResearch, 712-065-153, 1:500). The signal was developed with the Vector ABC and DAB substrate kits (Vector Labs, PK-4001, SK-4100). For immunofluorescence staining, after deparaffinization, rehydration and antigen-retrieval, the sections were incubated in blocking buffer for 30-60 min, followed by incubation with primary antibodies for overnight at 4 °C and secondary antibodies for 1 hour at RT (111). The following antibodies were used: goat anti-Sox2 (R&D systems, AF2018, 1:200), rabbit anti-Tbr2 (Abcam, ab23345, 1:400), rabbit anti-Cux1 (1:200) (345), rat anti-Ctip2 (Abcam, ab18465, 1:400), rabbit anti-Cux2 (1:200) (346), rabbit anti-Tbr1 (1:400), mouse anti-α-tubulin antibody (Sigma, T5168) (1:1000 dilution), mouse anti-acetylated tubulin (Sigma, T7451, clone 6-11B-1) (1:1000), rabbit anti-ACIII (Abcam, ab125093, 1:1000), Alexa Fluor 488-conjugated goat-anti-rabbit IgG (Invitrogen, A-11008, 1:500), Alexa Fluor 488-conjugated donkey-anti-goat IgG (Invitrogen, A-11055, 1:500), Alexa Fluor 568-conjugated goat-anti-rabbit IgG (Invitrogen, A-11011, 1:500), Alexa Fluor 488-conjugated goat-anti-rat IgG (Invitrogen, A-11006, 1:500), Alexa Fluor 568-conjugated goat-anti-mouse IgG (Invitrogen, A-11004, 1:500). Golgi staining was described in (347). TUNEL assay was carried out using DeadEnd™ Fluorometric TUNEL System (Promega, G3250) according to the kit manual.

Behavioral tests

The open field test was carried out in a box (40 x 40 x 40 cm) described somewhere else (348). Briefly, the cages with mice were taken to a quiet room 1 h before the experiment started. Each mouse was put in the center of the arena and recorded for 10 min while avoiding disturbance during the whole testing process. Between each test, the bottom of the box was cleaned with 75% alcohol and paused for 5 min before starting the next test. The recorded videos were analyzed by the SMART 3.0 video-tracking system (Pan-Lab, Harvard Apparatus). Rotarod tests were carried out as previously described (325). Mice were placed on a rotarod (Stoelting Europe) using an accelerating rotarod protocol. The rod accelerates from 4 to 40 rpm in 5 min, and then maintains at 40 rpm for another 5 min. The latency to fall was recorded for each mouse as an indicator for motor coordination. Each mouse was tested 4 times per day, with at least a 20-min break between two trials. All the mice were tested for 4 consecutive days. For the tail suspension test, cages with mice were brought to a quiet room where the experiment will be carried out 1 hour before the experiment starts. Each mouse was suspended by the tail for 5 min and was recorded with a video camera while avoiding disturbance during the test. The immobile time (as an indicator for depression) was measured later with the recorded videos.

Complete blood counting and flow cytometry

For complete blood counting, whole blood was collected into tubes containing anticoagulants via heart puncture from anesthetized 2-month-old mice as described (349). The whole blood was then send to blood testing lab (Animal center of McGill University) for complete blood counting. Multicolor flow cytometry was carried out as previously described (350). Specifically, bone marrows were flushed out from femurs and tibias with DMEM containing 2% FBS. The bone marrows were pipetted up and down with a 1-ml tip and then passed through a 40-μm cell strainer (StemCell Technologies). Red blood cells were removed using the Red Blood Cell (RBC) Lysis Buffer (eBioscience). FVD-eFluor 506 (eBioscience) was used for labeling of dead cells, which were excluded during flow cytometric analysis. Cell surface markers, such as CD3, B220, Gr1, Ter119 and Mac1 (all from eBioscience), were used for labeling of lineage-specific cells. For hematopoietic stem and progenitor cells, lineage markers were combined with the cell surface markers Scal1, cKit, CD48 and CD150. The

labeled cells were analyzed with a BD FACSAria sorter and analyzed by FlowJo software (Treestar).

Statistical analysis

Statistical analysis was performed with unpaired 2-tailed Student's *t* test. $p<0.05$ was considered to be statistically significant. Graphs were generated with GraphPad Prism 6 (Graphpad Software).

Acknowledgement: This work was supported by research grants from Canadian Institutes of Health Research, Natural Sciences and Engineering Research Council of Canada, and the Canadian Cancer Society (to X.-J.Y.). L.L. received stipend support from the China Scholarship Council, the Clifford C.F. Wong Fellowship program, a CIHR/FRSQ training grant in cancer research for the McGill Integrated Cancer Research Training Program, and the Canderel Foundation.

Conflict of interest: The authors declare that they have no conflicts of interest with the contents of this article.

Author contribution: L.L. carried out the entire project and wrote the manuscript; S.J. & A.W. supervised the rotarod tests; M.M. performed the iPS cell experiment; L.-M.L & S.M. helped with open-field test tests; X.J.Y. supervised the project and finalized the manuscript.

Table 2.1 Complete blood counts for the control and mutant mice

		Control	Knockout	Significance
Erythroid	RBCs $x10^{12}$/L	8.8±0.6	9.0±0.9	ns
	MCV fL	44.7±0.5	46.0±0.7	ns
	Hemoglobin g/L	138.3±7.9	141.0±13.4	Ns
	Hematocrit L/L	0.4±0.03	0.42±0.04	Ns
	MCH pg	15.7±0.3	15.7±0.2	Ns
	MCHC g/L	350.0±7.5	340.8±4.6	Ns
Leukocytes	WBCs $x10^{9}$/L	2.6±1.1	3.6±1.1	Ns
	Neutrophils %	15.3±9.8	12.0±3.5	Ns
	Lymphocytes %	67.0±16.9	86.0±3.4	Ns
	Monocytes %	0.0±0.0	0.3±0.4	Ns
	Eosinophils %	1.0±0.8	1.5±0.5	Ns
	Platelets $x10^{9}$/L	345.7±272.3	865.5±83.0	*

Note: Values represent mean±s.d., calculated from 3 wild-type and 4 knockout mice at 2 months of age. ns, not statistically significant; *, $p<0.05$. RBC, red blood cells; MCV, mean corpuscular volume; MCH, mean corpuscular hemoglobin; MCHC, mean corpuscular hemoglobin concentration; WBC, white blood cell.

Table 2.2 Biochemical analysis of blood from the control and mutant mice

	Units	Control	Knockout	Significance
Total Protein	g/L	52±1	50.25±1.3	Ns
Albumin	g/L	26±0	25.5±1.1	Ns
Albumin/Globulin ratio		1±0	1.05±0.05	ns
Glucose	mmol/L	11±0.8	17.6±5.1	ns
BUN Urea	mmol/L	7.8±0.3	7.45±0.78	ns
Creatinine	µmol/L	7±0	11.25±0.83	ns
Total Bilirubin	µmol/L	20.5±4.5	12.25±2.95	ns
ALT	U/L	34.5±1.5	50.5±5.89	ns
AST	U/L	209.5±2.5	149.5±26.51	ns
Alkaline Phosphase	U/L	69.5±17.5	87±3.08	ns
GGT	U/L	14#	NA	NA
CK	U/L	753.5±49.5	394±120.35	NA
Cholesterol	mmol/L	2.865±0.135	3.05±0.28	ns
Sodium	mmol/L	154#	153.3±1.8	NA
Potassium	mmol/L	7.1#	8.325±3.05	NA
Chloride	mmol/L	115#	112.5±1.12	NA
Calcium	mmol/L	2.36±0.09	2.65±0.07	ns
Phosphorus	mmol/L	3.31±0.17	3.57±0.39	ns
Magnesium	mmol/L	1.535±0.025	1.62±0.10	ns

Note: Values represent mean±s.d., calculated from 2 wild-type and 4 knockout mice at 2 months of age. ns, not statistically significant; NA, not available; #, indicate value from one WT mouse as value from another one is not available. BUN, Blood Urea Nitrogen; ALT, alanine aminotransferase; AST, aspartate aminotransferase; GGT, gamma-glutamyl transferase; CK, Creatine kinase.

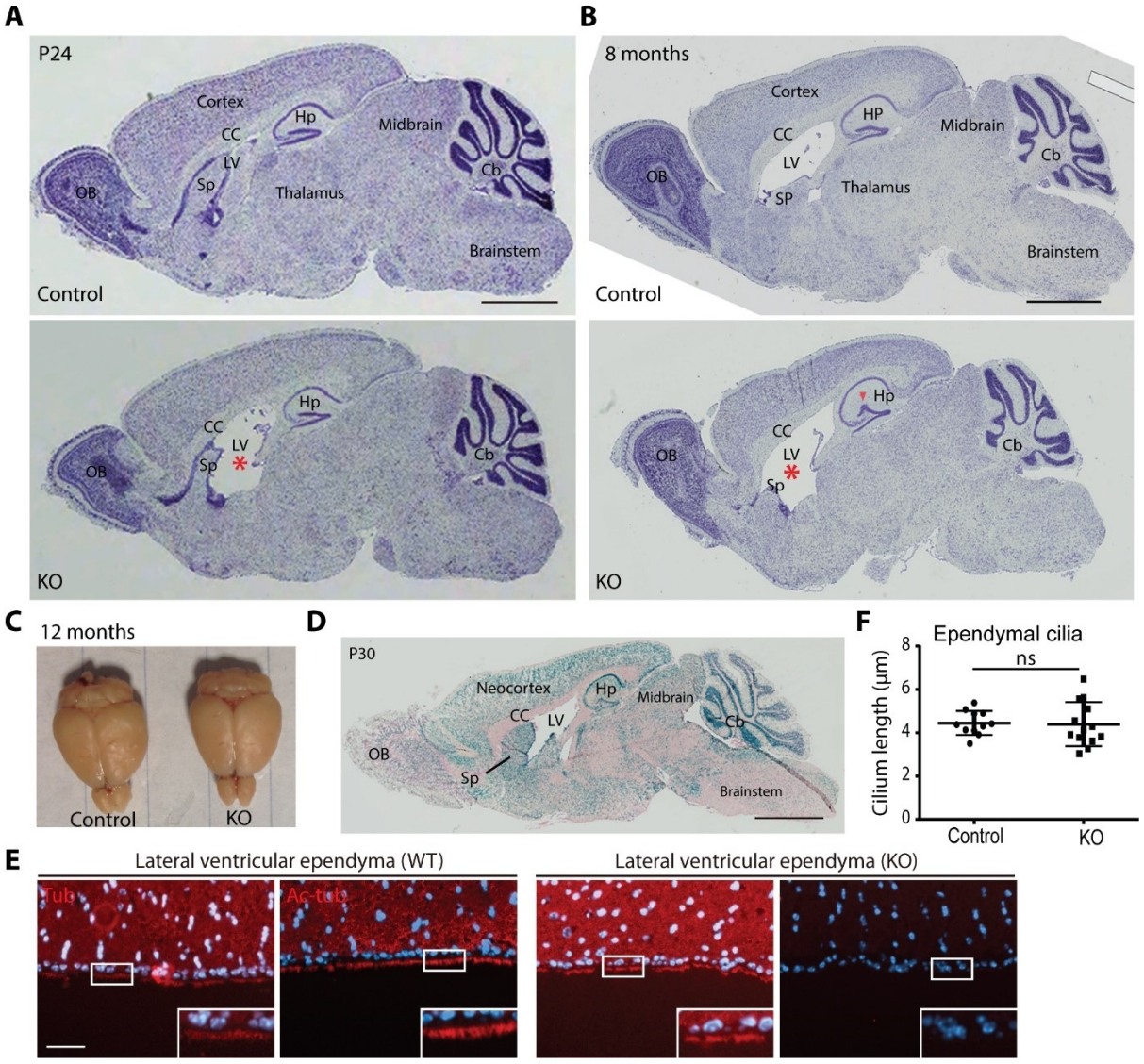
A
P24
Cortex
Hp
CC
LV
Sp
OB
Thalamus
Midbrain
Cb
Brainstem
Control
KO
B
8 months
Cortex
HP
CC
LV
SP
OB
Thalamus
Midbrain
Cb
Brainstem
Control
KO
C
12 months
Control
KO
D
P30
Neocortex
Hp
CC
LV
OB
Sp
Midbrain
Cb
Brainstem
F
Ependymal cilia
ns
Cilium length (µm)
8
6
4
2
0
Control
KO
E
Lateral ventricular ependyma (WT)
Lateral ventricular ependyma (KO)
Tub
Ac-tub

Figure 2.1. *Atat1* loss causes ventricular dilation in the mutant mouse forebrain.

A-B, Nissl staining for sagittal brain sections from 24 day- or 8 month-old mice. Lateral ventricles are larger in the *Atat1*$^{-/-}$ (KO) brain. Red asterisks mark hypoplasia in the septum. A red arrowhead denotes a distorted dentate gyrus that we have reported previously (255). Other structures of the brain, including the neocortex, corpus callosum, cerebellum, thalamus, and middle brain are similar between wild-type and *Atat1*$^{-/-}$ mice. Scale bar, 1 mm. **C**, representative top view of the whole brain for 12-month-old wild-type and *Atat1*$^{-/-}$ mice. **D**, β-Gal staining of a sagittal brain section from *Atat1*$^{-/-}$ mice at P30. Scale bar, 1 mm. **E**, immunostaining of lateral ventricular ependyma with anti-tubulin and anti-acetyl-tubulin antibodies. Images for ependymal cilia were enlarged and shown in the right bottom. Scale bar, 30 μm. **F**, length of ependymal cilia in lateral ventricles (as in panel **E**; multiple positions were measured from 2 pairs of mice). ns, not statistically significant. Abbreviations: Cb, cerebellum; CC, corpus callosum; Hp, hippocampus; LV, lateral ventricle; OB, olfactory bulb; Sp, septum.

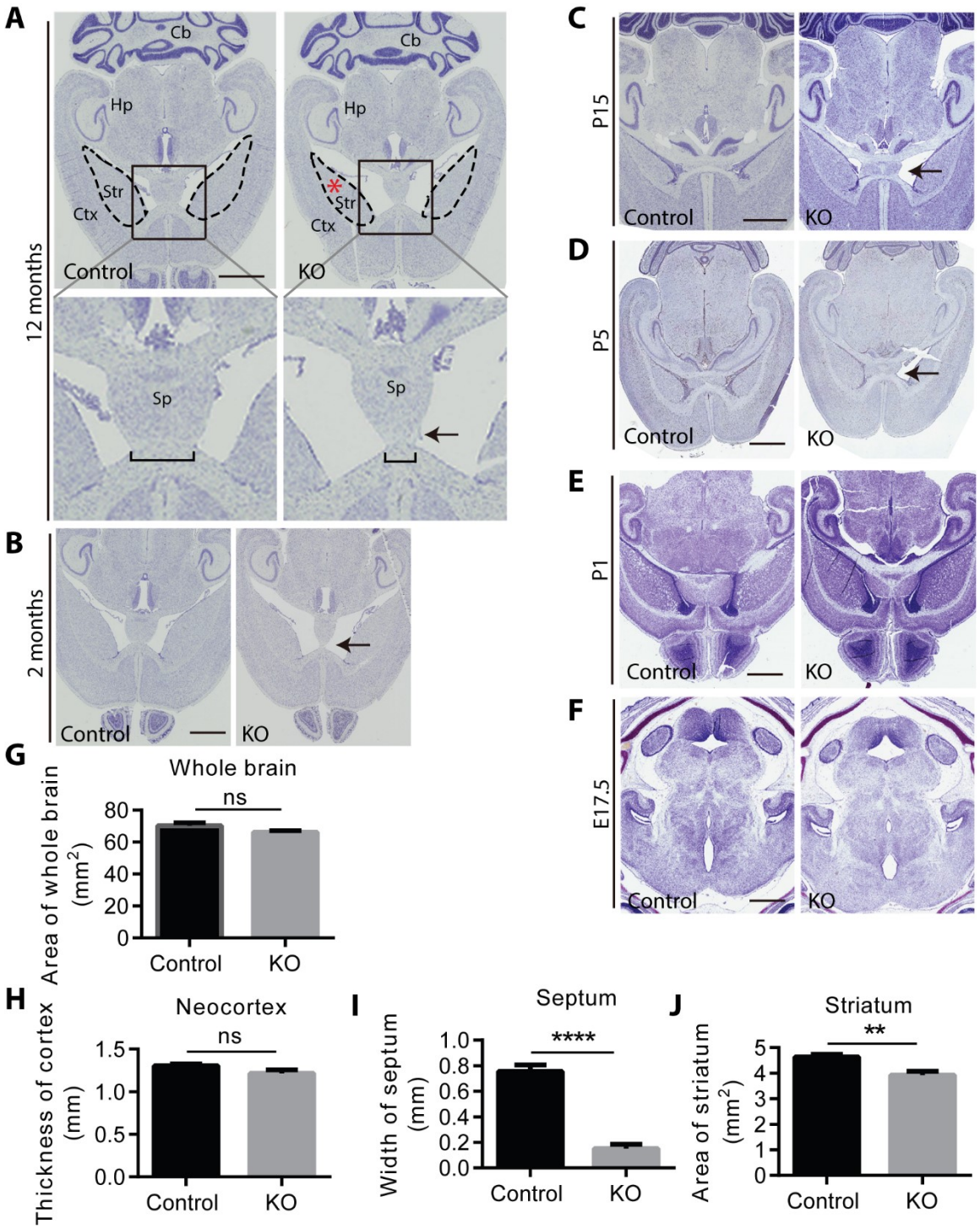
A
12 months
Cb
Hp
Str
Ctx
Control
KO
Sp
B
2 months
C
P15
D
P5
E
P1
F
E17.5
G
Whole brain
ns
Area of whole brain (mm2)
H
Neocortex
ns
Thickness of cortex (mm)
I
Septum
****
Width of septum (mm)
J
Striatum
**
Area of striatum (mm2)

Figure 2.2. Ventricular dilation in the mutant mice are due to septal and striatal hypoplasia.

A-F, Nissl staining for transverse brain sections from adult mice at 12 and 2 months of age (**A-B**) or pups at P1, P5 and P15 (**C-E**), or from embryos at E17.5 (**F**). Arrows in **A-D** denote that the bottom part of the mutant septum is thinner, and the mutant lateral ventricles are larger in *Atat1*$^{-/-}$ mice than the counterparts in the wild-type mice. The boundary of the striatum is indicated by dotted curves. The red asterisk in panel **A** marks a smaller striatum in the *Atat1*$^{-/-}$ brain. All the brain samples were serially sectioned; wild-type and mutant sections from similar position were used for Nissl staining. Scale bar, 2 mm (**A-B**), 1 mm (**C-D**), 500 μm (**E-F**). Cb, cerebellum; Hp, hippocampus; Ctx, neocortex; Str, striatum; Sp, septum. **G**, area of whole brain measured from transverse brain sections (3 pairs of mice, 2 sections for each biological sample). ns, not statistically significant. **H**, thickness of neocortex in the middle part was measured from transverse brain sections (3 pairs of mice, 2 sections for each biological sample). **I**, area of striatum measured from transverse brain sections (3 pairs of mice, 2 sections for each biological sample). **J**, width of septum measured at the bottom part of septum (3 pairs of mice, 2 sections for each biological sample). Paraffin-embedded brains were serially sectioned to obtain paired transverse sections, with sections showing the most obvious ventricular dilation used for measurement. For **G-J**, data are represented as mean±sem; ns, not statistically significant; **, $p<0.01$; ****, $p < 0.0001$.

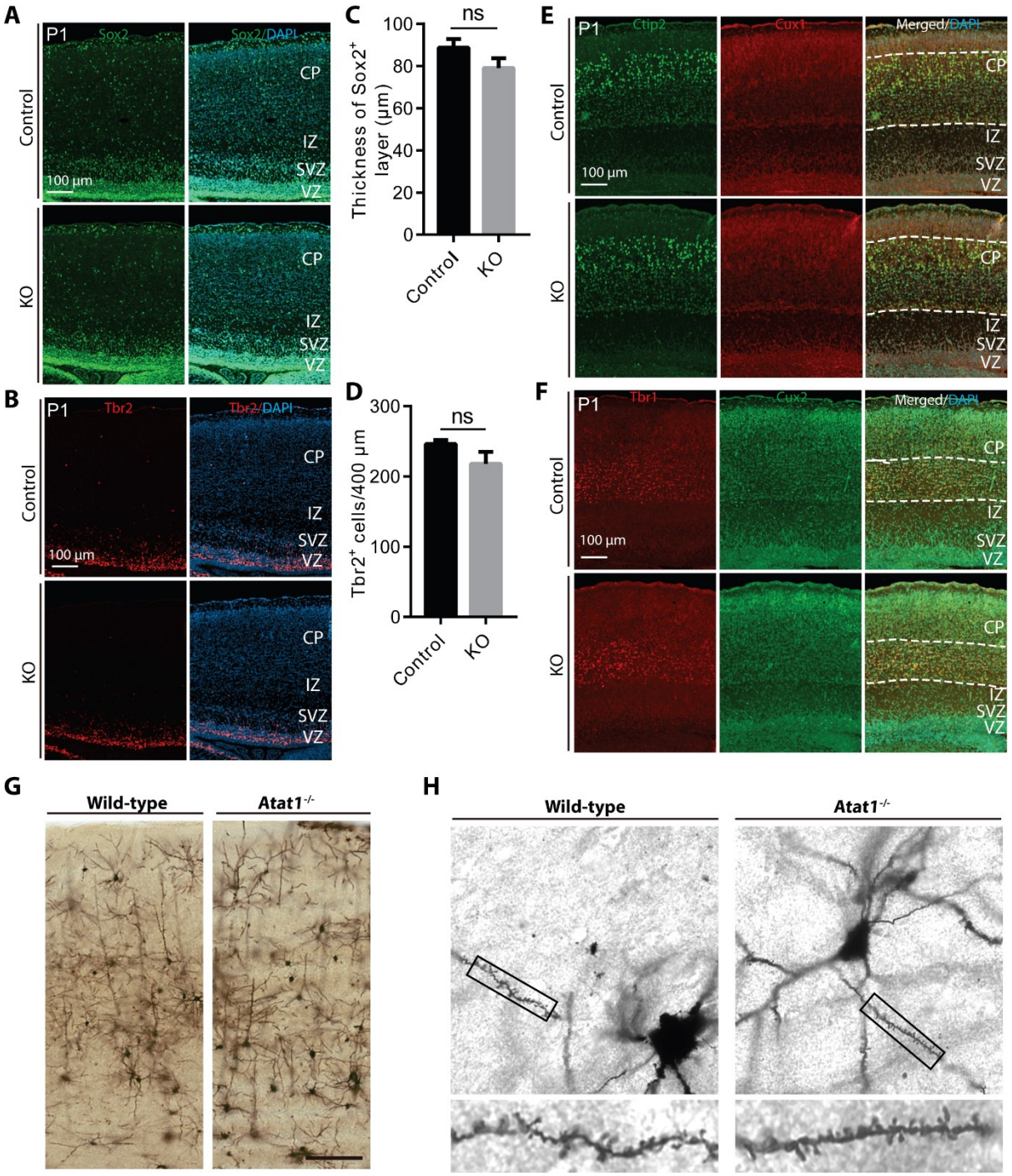
A
P1
Sox2
Sox2/DAPI
Control
KO
CP
IZ
SVZ
VZ
100 µm
B
P1
Tbr2
Tbr2/DAPI
C
ns
Thickness of Sox2+ layer (µm)
100
80
60
40
20
0
Control
KO
D
ns
Tbr2+ cells/400 µm
300
200
100
0
E
P1
Ctip2
Cux1
Merged/DAPI
F
P1
Tbr1
Cux2
G
Wild-type
Atat1-/-
H
Wild-type
Atat1-/-

Figure 2.3. Cerebral cortex development is not affected in the *Atat1*-deficient mice.

A-B, immunofluorescence microscopy to detect $Sox2^+$ neural stem cells (NSCs) and $Tbr2^+$ neural progenitor cells (NPCs) on P1 brain sections. The thickness of $Sox2^+$ layer was measured and shown in **C** (2 pairs of mice, 2 sections from each mice), the number of $Tbr2^+$ cells was counted and shown in **D** (2 pairs of mice, 2 sections from each mice). Data are represented as mean±sem; ns, not statistically significant. **C** and **D**, statistical analysis for results from **A** and **B**, respectively. **E**, immunofluorescence detection of $Cux1^+$ and $Ctip2^+$ neurons. White dotted line indicates the $Ctip2^+$ layer. **F**, immunofluorescence detection of $Tbr1^+$ and $Cux2^+$ neurons. A white dotted line indicates the $Tbr1^+$ layer. **G**, representative views of the wild-type and knockout neocortices from Golgi-stained brain sections. **H**, enlarged views of the areas boxed in **G**. VZ, ventricular zone; SVZ, subventricular zone; IZ, intermediate zone; CP, cortical plate.

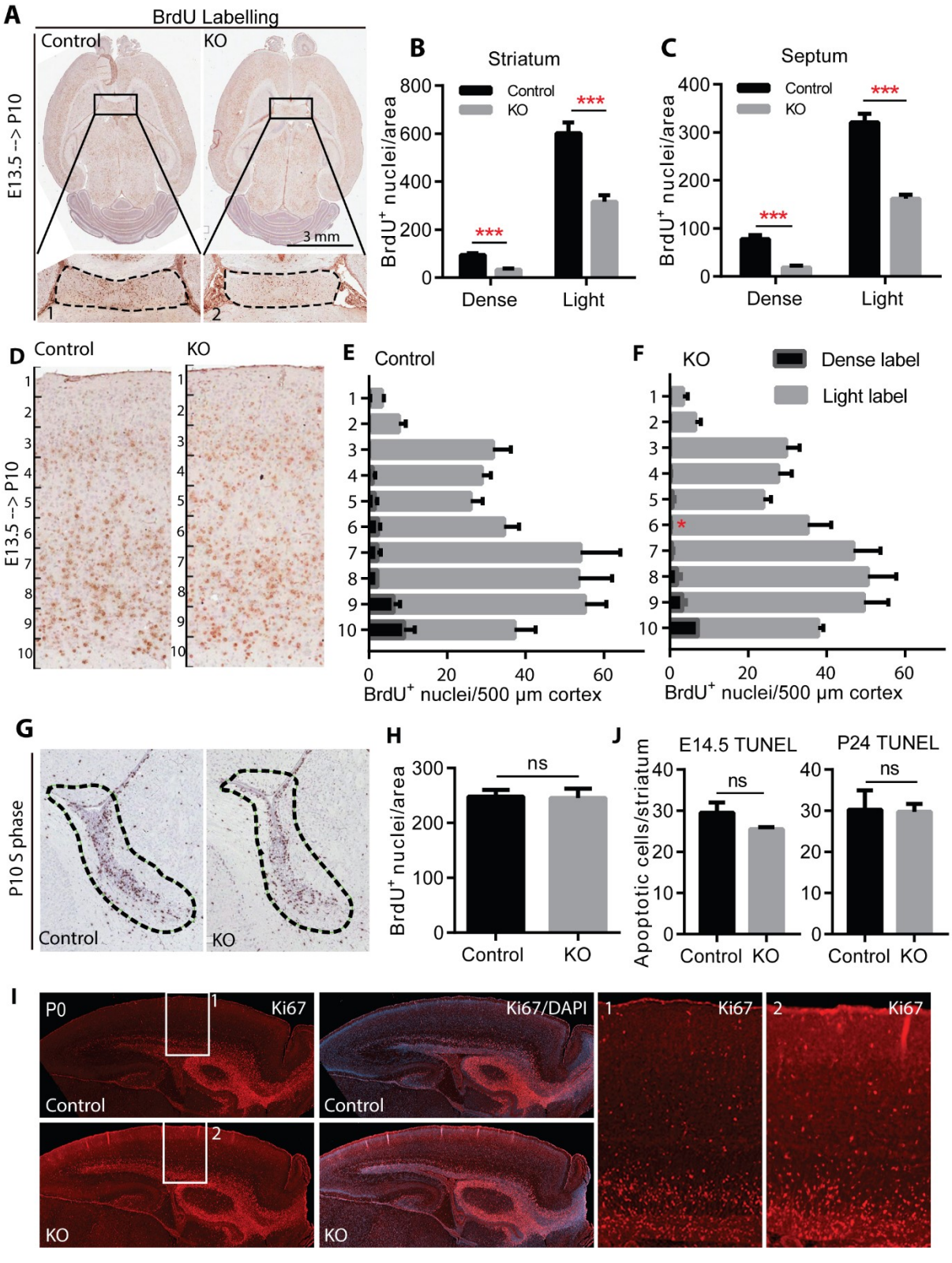
A
BrdU Labelling
Control
KO
E13.5 --> P10
3 mm
1
2
B
Striatum
Control
KO
***
***
BrdU+ nuclei/area
800
600
400
200
0
Dense
Light
C
Septum
Control
KO
***
***
BrdU+ nuclei/area
400
300
200
100
0
Dense
Light
D
Control
KO
E13.5 --> P10
1
2
3
4
5
6
7
8
9
10
E
Control
1
2
3
4
5
6
7
8
9
10
0
20
40
60
BrdU+ nuclei/500 µm cortex
F
KO
Dense label
Light label
1
2
3
4
5
6
*
7
8
9
10
0
20
40
60
BrdU+ nuclei/500 µm cortex
G
P10 S phase
Control
KO
H
ns
BrdU+ nuclei/area
300
200
100
0
Control
KO
J
E14.5 TUNEL
P24 TUNEL
Apoptotic cells/striatum
40
30
20
10
0
ns
ns
Control
KO
Control
KO
I
P0
1
Ki67
Control
Ki67/DAPI
Control
1
Ki67
2
Ki67
2
KO
KO

Figure 2.4. BrdU tracing of neuronal migration in the wild-type and *Atat1*$^{-/-}$ mouse brains. **A**, BrdU was injected into E13.5 pregnant mice intraperitoneally, and the brains from new pups were collected at P10. The septum in the box of the upper panel in A was enlarged and shown in the lower panel. **B-C**, quantification of BrdU^{+} dense labelled and light labelled cells in the striatum and septum (n=3, 2 sections for each mouse). ***, $p<0.001$. The boundary of septum was indicated by black dotted line. If the cellular nucleus is fully dark, it was counted as a dense label; otherwise the cell was considered as a light label. **D-F**, cerebral cortex above the hippocampus was divided into 10 layers. BrdU^{+} cells in each layer were counted and shown in panel **E** (control) and **F** (KO) (n=3, 2 sections for each mouse). **G-H**, 1-h BrdU incorporation in the neural stem and progenitor cells in wild-type and *Atat1*$^{-/-}$ brains. One hour after BrdU injection, P10 pups were sacrificed for immunohistochemical analysis using an anti-BrdU monoclonal antibody. Representative images were shown in **G**. The incorporated BrdU^{+} cells near the lateral ventricle area (indicated by black dotted line) are counted and shown in **H** (n=3, 2 sections for each mouse). **I**, Representative images showing Ki67 signal was comparable between control and mutant neonatal brain sections. The neocortices were enlarged and shown in the right two panels. All quantitative data are represented as mean±sem; ns, not statistically significant.

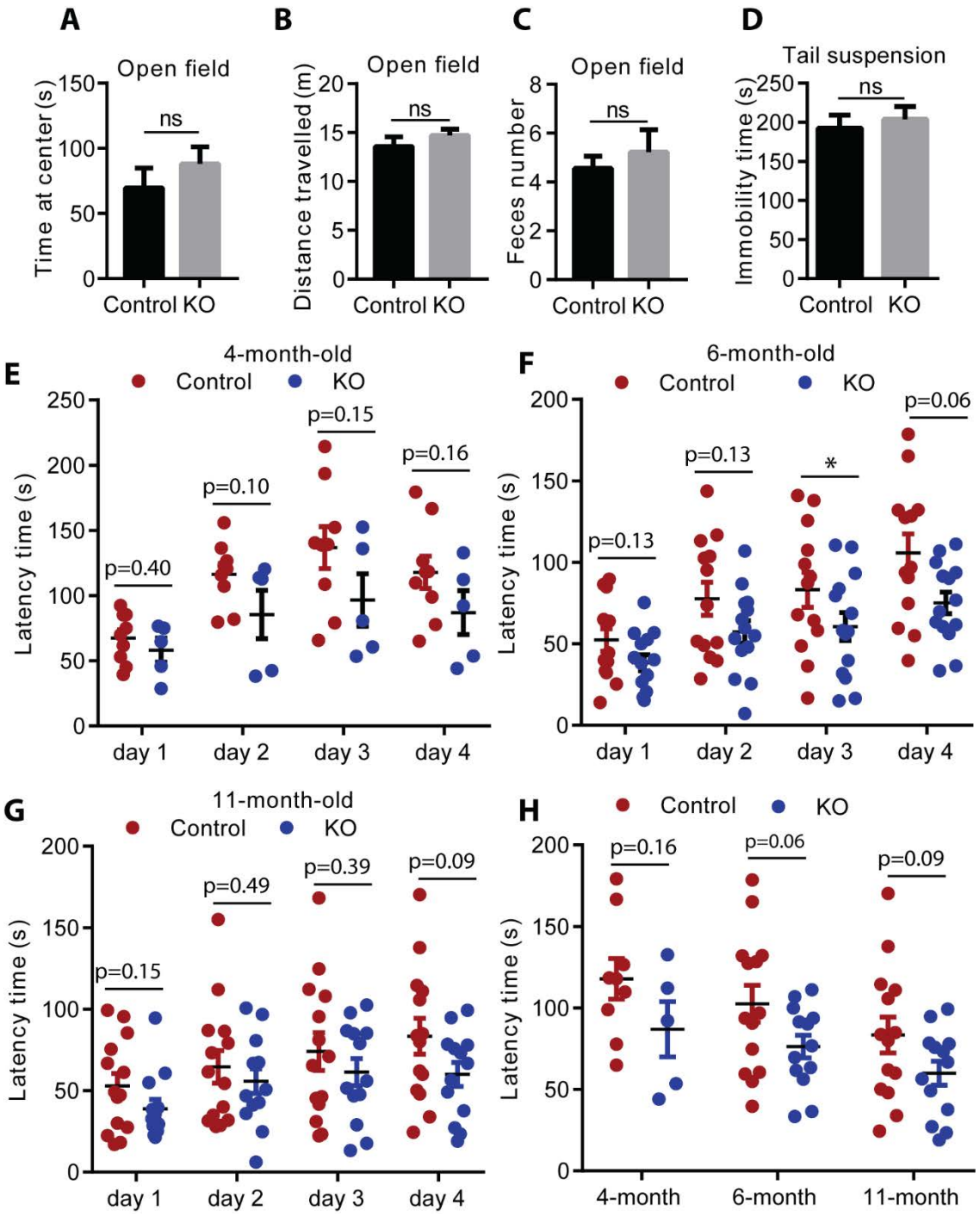
A
Open field
Time at center (s)
150
100
50
0
ns
Control KO
B
Open field
Distance travelled (m)
20
15
10
5
0
ns
Control KO
C
Open field
Feces number
8
6
4
2
0
ns
Control KO
D
Tail suspension
Immobility time (s)
250
200
150
100
50
0
ns
Control KO
E
4-month-old
Control
KO
Latency time (s)
250
200
150
100
50
0
p=0.40
p=0.10
p=0.15
p=0.16
day 1
day 2
day 3
day 4
F
6-month-old
Control
KO
Latency time (s)
200
150
100
50
0
p=0.13
p=0.13
*
p=0.06
day 1
day 2
day 3
day 4
G
11-month-old
Control
KO
Latency time (s)
200
150
100
50
0
p=0.15
p=0.49
p=0.39
p=0.09
day 1
day 2
day 3
day 4
H
Control
KO
Latency time (s)
200
150
100
50
0
p=0.16
p=0.06
p=0.09
4-month
6-month
11-month

Figure 2.5. Behavioral tests of wild-type and *Atat1*$^{-/-}$ mice.

A-C, open field tests were carried out in a 40 x 40 x 40 cm arena (n=9 for the control or *Atat1*$^{-/-}$ mice). Time of the mice in the center of the arena (20 x 20 cm) (each mouse was tested for 10 min) is shown in **A**, whereas the distance travelled in the arena is presented in **B**. Feces per mouse in the open field tests were counted and the number is shown in **C**. Data are represented as mean±sem. ns, not statistically significant. **D**, immobility time of the mice during the tail suspension tests (each mouse was tested for 5 min) (n=9 for the control and 12 for the KO). **E-G**, accelerated rotarod test for mice of 4-month-old (n=9 for control and 5 for KO), 6-month-old (n=14 for control and 13 for KO) and 11-month-old (n=14 for control and 13 for KO) mice as indicated. Mice were tested 4 times per day (with a 20-min break between 2 trials) for 4 consecutive days. The average of the 4 repeats in each day is calculated as the latency time for each mouse in that day. **H**, latency time of the mice in the 4th day is shown for 4-, 6-, and 11-month-old mice. *, $p < 0.05$. The p values for all the timepoints are shown, no matter whether they are statistically significant or not. For graphs in **E**-**H**, "Latency time" refers to the latency to fall from the rotarod.

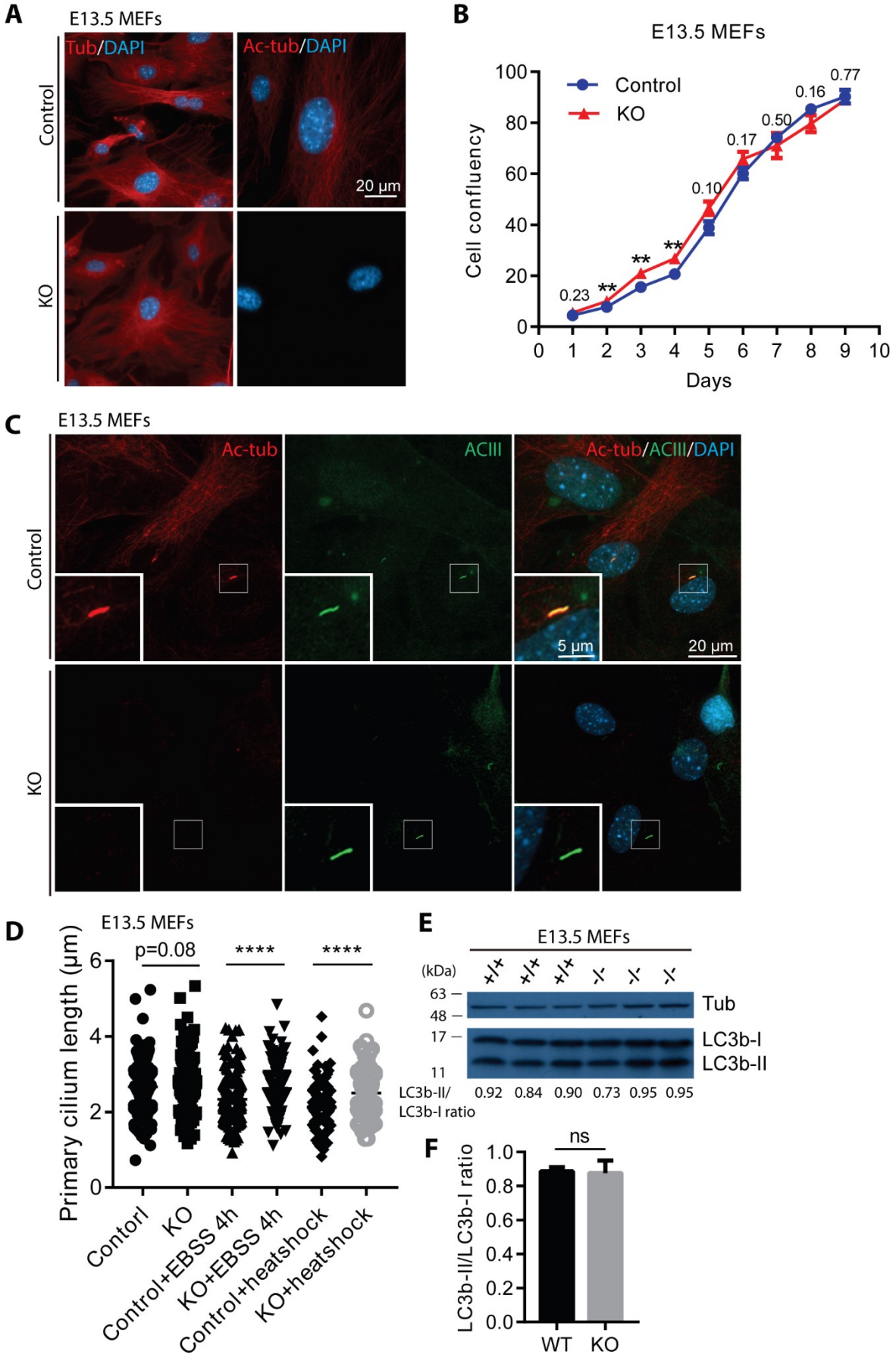
A
E13.5 MEFs
Tub/DAPI
Ac-tub/DAPI
Control
KO
20 μm
B
E13.5 MEFs
Control
KO
Cell confluency
Days
0.23
0.10
0.17
0.50
0.16
0.77
**
C
E13.5 MEFs
Ac-tub
ACIII
Ac-tub/ACIII/DAPI
Control
KO
5 μm
20 μm
D
E13.5 MEFs
p=0.08
****
****
Primary cilium length (μm)
Contorl
KO
Control+EBSS 4h
KO+EBSS 4h
Control+heatshock
KO+heatshock
E
E13.5 MEFs
(kDa)
+/+
+/+
+/+
-/-
-/-
-/-
63
48
17
11
Tub
LC3b-I
LC3b-II
LC3b-II/
LC3b-I ratio
0.92
0.84
0.90
0.73
0.95
0.95
F
ns
LC3b-II/LC3b-I ratio
WT
KO

Figure 2.6. Loss of tubulin acetylation exerts minor effects on MEF properties.

A, immunostaining to detect α-tubulin and its acetylation in MEFs from wild-type and *Atat1*$^{-/-}$ embryos at E13.5. Notably, the acetylation was detectable in the wild-type but not mutant MEFs. **B**, growth curve of control and *Atat1*$^{-/-}$ MEFs measured using IncuCyte imaging system (n=4). **C**, primary cilia in MEFs were detected using immunostaining with anti-ACIII and anti-acetyl-tubulin antibodies. Images of single primary cilium were enlarged and shown at bottom-left corners. **D**, length of primary cilia with or without EBSS treatment or heat shock were measured. For each group, 50-200 primary cilia were measured. **E**, Western blotting with the LC3b I/II antibody to detect autophagy in wild-type and *Atat1*$^{-/-}$ MEFs. **F**, the LC3b-II/LC3b-I ratio (indicative of autophagy) is not affected (n=3). All quantitative data are represented as mean±sem. ns, not statistically significant; **, $p<0.01$; ****, $p<0.0001$.

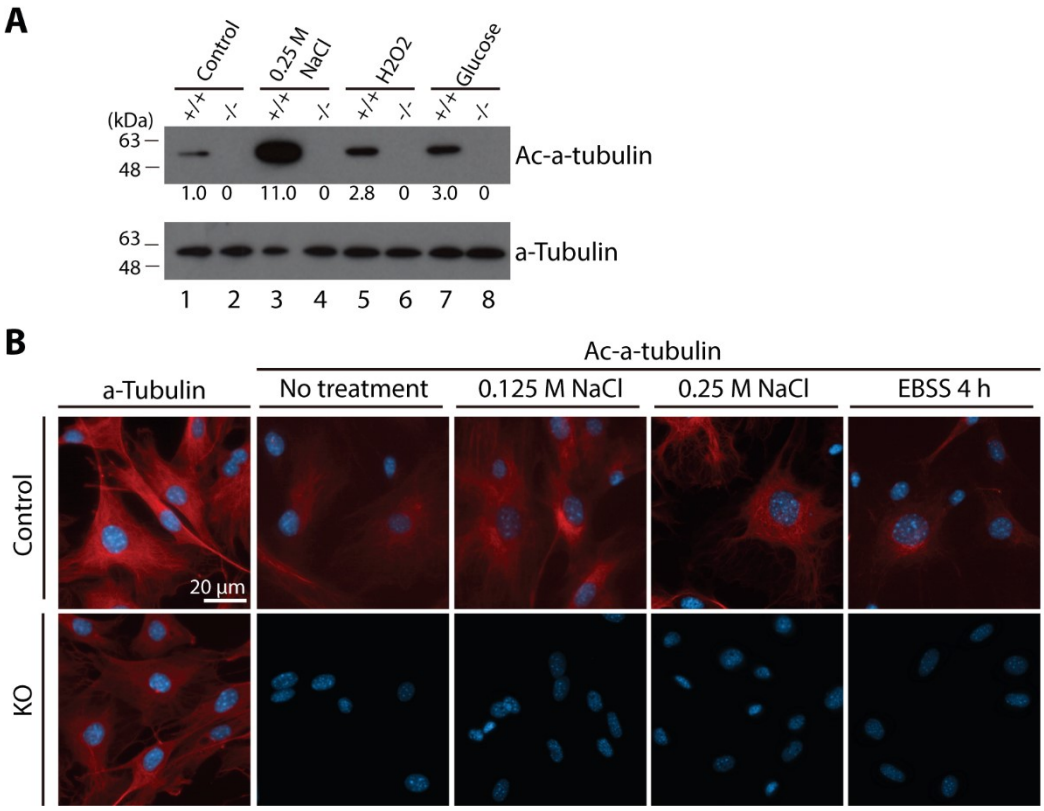

Figure 2.7. Lack of stress-induced tubulin hyperacetylation in *Atat1*$^{-/-}$ MEFs.

A, Western blots showing that treatment with 0.25 M NaCl, 5 mM H_2O_2 or 100 mM glucose for 30-60 min, stimulated tubulin acetylation in the wild-type but not mutant MEFs. The intensity of bands relative to the wild-type MEFs without any treatment (lane 1) was shown in values. **B**, immunostaining with anti-α-tubulin and anti-acetyl-α-tubulin antibodies confirmed that NaCl treatment stimulated tubulin acetylation in the wild-type but not mutant MEFs.

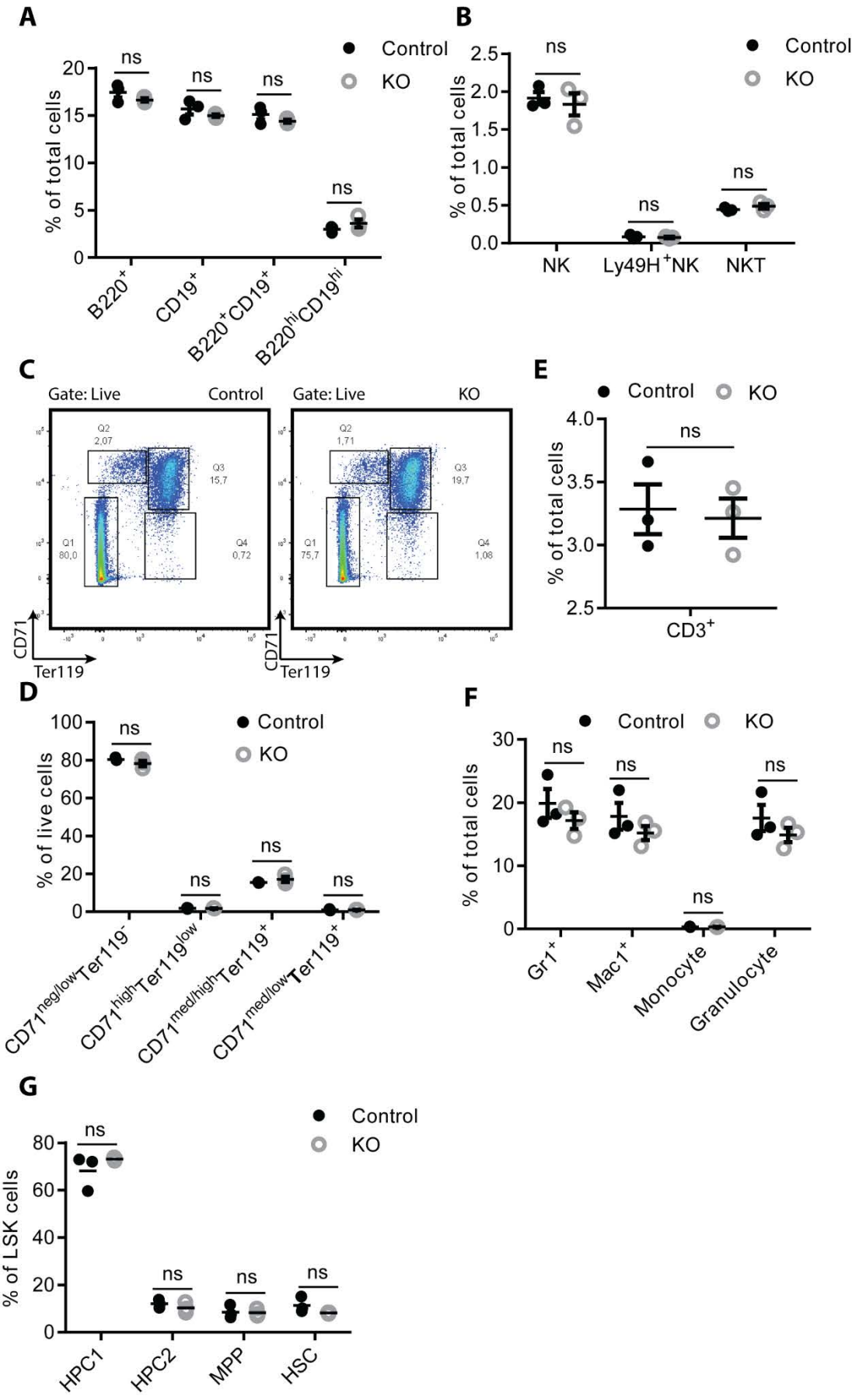
A
Control
KO
% of total cells
ns
B220+
CD19+
B220+CD19+
B220hiCD19hi
B
NK
Ly49H+NK
NKT
C
Gate: Live
Control
KO
Q1 80,0
Q2 2,07
Q3 15,7
Q4 0,72
Q1 75,7
Q2 1,71
Q3 19,7
Q4 1,08
CD71
Ter119
D
% of live cells
CD71neg/lowTer119-
CD71highTer119low
CD71med/highTer119+
CD71med/lowTer119+
E
CD3+
F
Gr1+
Mac1+
Monocyte
Granulocyte
G
% of LSK cells
HPC1
HPC2
MPP
HSC

Figure 2.8. Cytometric analysis of wild-type and *Atat1*$^{-/-}$ bone marrow cells from 2-month-old mice.

A, ratio of B220^{+} cells, CD19^{+} cells, B220^{+}CD19^{+} cells and B220^{hi}CD19^{hi} cells in total nucleated cells from bone marrows. **B**, ratio of NK cells (NK1.1^{+}CD3^{-}), Ly49H^{+} NK cells and NKT cells (NK1.1^{+}CD3^{+}) in total nucleated cells from bone marrows. **C**, gating of nucleated cells from bone marrows using CD71 and Ter119 antibodies. **D**, quantification of cell populations shown in **C**. **E**, ratio of CD3^{+} cells in total nucleated cells from bone marrows. **F**, ratio of Gr1^{+}, Mac1^{+}, monocyte (Gr1^{lo}Mac1^{hi}), and granulocyte (Gr1^{hi}Mac1^{h}) cells in the total nucleated cells from bone marrows. **G**, ratio of hematopoietic stem and progenitor cells (HSC, HPC1, HPC2 and MPP) in total LSK (Lin^{-}Sca1^{+}c-Kit^{+}) cells. HSC, LSKCD48^{-}CD150^{+}; HPC1, LSKCD48^{+}CD150^{-}; HPC2, LSKCD48^{+}CD150^{+}; MPP, LSKCD48^{-}CD150^{-}; n=3 for all groups. The cell marker abbreviations are used as described (351). All data are represented as mean±sem; ns, not statistically significant.

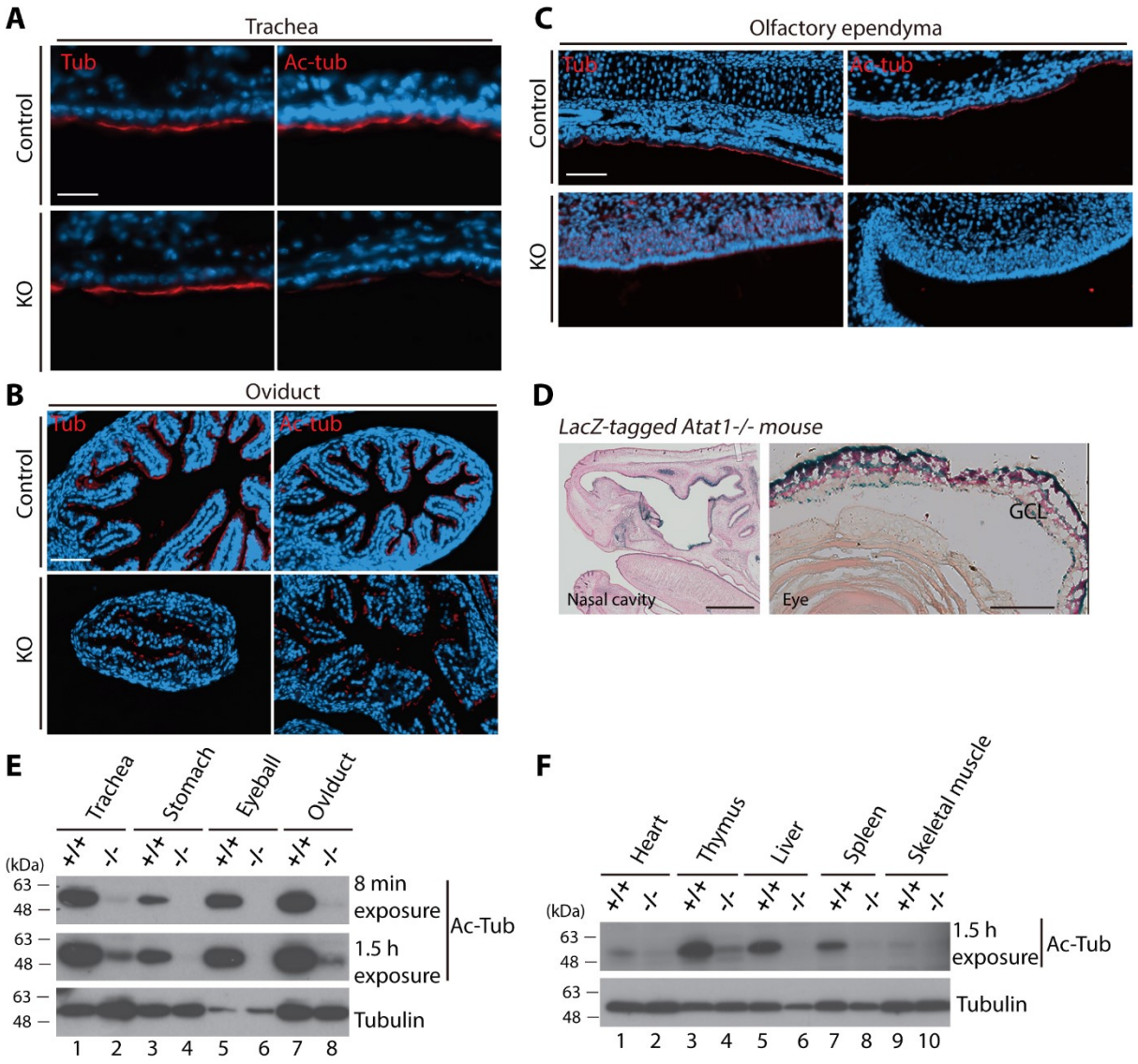

Figure 2.9. Residual tubulin acetylation in some tissues from the *Atat1*$^{-/-}$ mice.

A-C, immunostaining with anti-tubulin and anti-acetyl-tubulin antibodies of the trachea, olfactory ependyma, and oviduct sections. Scale bars, 30 μm (**A**) and 50 μm (**B-C**). **D**, β-Gal staining of sagittal brain sections from *Atat1*$^{-/-}$ mice at P30 as in Fig. 2.1D. Scale bar, 1 mm for nasal cavity and 200 μm for eye. **E-F**, detection of tubulin and acetylated tubulin by Western blotting in various tissue extracts.

Bridging Text between Chapters II and III

In Chapter II, I studied the role of ATAT1, which is a non-histone lysine acetyltransferase that acetylates lysine 40 of α-tubulin on assembled microtubules. During the initial stage of my thesis project, we were not sure how far the research direction on ATAT1 could lead, so as a backup plan and taking the suggestion from the advisory committee, I started to work on another project, which is related to HDAC3, a deacetylase that reverses acetylation of histone and non-histone proteins. This backup plan has been much more promising than the project from Chapter II has yielded. Thus, in Chapter III, I will describe the study about how HDAC3 regulates embryonic cerebral development.

CHAPTER III: Histone deacetylase 3 governs perinatal cerebral development via neural stem and progenitor cells

Lin Li[1,2] and Xiang-Jiao Yang[1,2,3,4,*]

[1]The Rosalind & Morris Goodman Cancer Research Center, and Departments of [2]Medicine and [3]Biochemistry, McGill University and [4]McGill University Health Center, Montreal, Quebec, Canada

[*]Correspondence: xiang-jiao.yang@mcgill.ca; Tel: 514-398-5883

Running Title: Regulation of brain development by HDAC3

Keywords: Intellectual disability**;** forebrain development; cerebrum; neocortex; hippocampus; neural stem cell; histone deacetylation; NCoR; SMRT; TBL1; GPS2

3.1 ABSTRACT

Intellectual disability affects 2–3% of the general population. Related to the nature vs nurture hypothesis, both genetic and epigenetic factors contribute to intellectual development. Histone deacetylase 3 (HDAC3) is a unique epigenetic regulator forming stoichiometric complexes with several other proteins. Patients with mutations in one such protein display intellectual disability, implying an important role of HDAC3 in this prevalent but poorly understood disease. Here we report that cerebrum-specific inactivation of the mouse gene causes striking developmental defects in the neocortex, hippocampus and corpus callosum; post-weaning lethality; and abnormal behaviors, including hyperactivity and anxiety. The developmental defects are due to rapid loss of neural stem and progenitor cells (NSPCs), starting at E14.5. Premature neurogenesis and abnormal neuronal migration in the mutant brain alter NSPC homeostasis. Mutant cerebral cortices display augmented DNA damage, massive apoptosis, and histone hyperacetylation. In agreement with these results, mutant NSPCs are impaired in forming neurospheres *in vitro,* and treatment of wild-type NSPCs with the HDAC3-specific inhibitor RGFP966 abolishes neurosphere formation. Transcriptomic analyses of neonatal cerebral cortices and cultured neurospheres support that HDAC3 regulates various transcriptional programs through interaction with multiple transcription factors, including NFIB. These findings establish HDAC3 as a major deacetylase critical for perinatal development of the mouse cerebrum and NSPCs, thereby supporting a direct link of this enzymatic epigenetic regulator to human intellectual (dis)ability.

3.2 INTRODUCTION

Histone acetylation is critical for regulating and maintaining all eukaryotic epigenomes (260, 352, 353). This reversible modification is controlled by the opposing actions of acetyltransferases and deacetylases. There are 18 mammalian histone deacetylases (HDACs) (354, 355). Different from the other 15 deacetylases, HDAC1, HDAC2 and HDAC3 are catalytic subunits of stoichiometric multiprotein complexes, which are highly stable, even enough for purification via conventional chromatography (354). These complexes serve as functional cores for additional interaction with other partners to exert gene-specific histone deacetylation and subsequent functional impact (354). While HDAC1 and HDAC2 are part of at least three different complexes containing >15 other proteins (354), HDAC3 is the catalytic subunit of paralogous tetrameric complexes, composed of the nuclear receptor corepressor N-COR (or its paralog SMRT), the WD40 protein TBL1 (a.k.a. TBL1X; or its paralogs TBL1XR1 and TBL1Y, the latter of which is Y-chromosome associated and thus male-specific) and the cell-signaling regulator GPS2 (356, 357). Thus, HDAC3 is unique among the HDAC superfamily. Within the complexes, N-CoR and SMRT serve as the scaffolds for complex assembly by using deacetylase-activating domains for HDAC3 interaction and other domains for association with TBL1 and GPS2 (272, 357, 358). Such complex formation is crucial for the maximal deacetylase activity of HDAC3 (359, 360).

HDAC3 has been subject to various genetic studies in mice. Germline deletion of *Hdac3* leads to embryonic lethality at E9.5, indicating an essential role in mouse embryo development (297). Conditional deletion of *Hdac3* in the liver, hematopoietic system, heart, muscle and fat, causes abnormal development or metabolism in these tissues (299, 305, 317, 361, 362). The results show that HDAC3 is crucial for development and homeostasis of these tissues (301, 363-366). By comparison, much less is known about its role in brain development (367). While the mouse genetic studies suggest that HDAC3 is also critical for human development, direct evidence for this important issue remains limited. One patient with neonatal epileptic encephalopathy and a heterozygous *de novo HDAC3* mutation has been reported (368). Multiple patients with *TBL1XR1* germline mutations have been shown to display intellectual disability (369-371), supporting the role of the HDAC3 complexes in human cerebral and

intellectual development. Clinical features in these patients suggest that the HDAC3 complexes are critical for early brain development. To substantiate this, we carried out cerebrum-specific deletion of mouse *Hdac3* to investigate its role in perinatal cerebral development. Here we report that the mutant mice show severe cerebral defects resulting from impaired NSPC development, altered histone acetylation and deregulated gene expression.

3.3 RESULTS

Hdac3 is highly expressed in the developing cerebrum

To understand the role of HDAC3 in mouse brain development, we first determined the expression pattern of *Hdac3* in the developing cerebral cortex. Indirect immunofluorescence microscopy using a specific anti-HDAC3 antibody at P0, E16.5 and E12.5 indicated that *Hdac3* is abundantly expressed in the developing ventricular zone, subventricular zone, cortical plate (or preplate) and hippocampus (Fig. S3.1a,c,e). In addition, RNA-Seq showed that the FPKM value for *Hdac3* mRNA is higher than 30 in the neonatal cerebral cortex and the neurospheres cultured from E16.5 embryos (Fig. S3.1g), indicating high-level expression of this deacetylase in the developing cerebral cortex and embryonic NSPCs. The expression data suggest that HDAC3 may have an important role in regulating perinatal brain development.

Cerebrum-specific *Hdac3* deletion leads to early lethality and abnormal behaviors

To evaluate directly the function of HDAC3 in cerebral development, we generated cerebrum-specific knockout mice by using the *Emx1-Cre* line, which expresses the Cre recombinase specifically in the cerebrum and its precursors as early as E10.5 (372, 373). Mating of this line with $Hdac3^{f/f}$ mice produced the $Hdac3^{f/f}$; *Emx1-Cre* knockout (or cKO) mice. The knockout pups were born at a normal Mendelian ratio (Table S3.1) and appeared grossly normal. However, starting from week 2, the pups failed to thrive and became significantly smaller than the wild-type (Fig. 3.1a). In week 3, some of the mutant pups were runted and subsequently died, with a majority unable to survive through the week after (Fig. 3.1a,b). At P21, the mutant pups started to show obvious abnormalities in walking and were overactive (supplemental videos from one representative pair of P24 wild-type and cKO pups). Moreover, 2- or 3-week-old mutant pups were also easily irritated when touched. We thus

carried out open field tests, to assess the anxious and hyperactive status of mice (374, 375). Paired control and cKO mice at P22 were tested in an arena for 10 min and recorded by a video tracking system (supplemental videos of one representative pair of P22 wild-type and cKO mice in open field arena). The results showed that compared to the wild-type counterparts, the mutant pups spent significantly more time at the border (Fig. S3.2a,c) and travelled much more (Fig. S3.2b,c). The heterozygous mice did not display such developmental defects (data not shown). Thus, the homozygous mutant pups displayed hyperactivity and an increase in anxiety.

In the mutant mice, the brain weight of the mutant pups was comparable to the wild-type counterparts at P7 but showed significant reduction at P17 and P23 (Fig. 3.1c). As shown in Fig. 3.1d, the brain/body weight ratio was comparable between the wild-type and mutant pups, even at P17 and P23. Thus, the mutant brain remained proportional to the body weight (Fig. 3.1c,d), indicative of no microcephaly in the mutant pups.

We verified that *Hdac3* is efficiently and specifically deleted in the mutant cerebrum. For this, we carried out Western blotting analysis of cerebral extracts from wild-type and mutant pups. As shown in Fig. 3.1e, HDAC3 was specifically detected in the wild-type cerebral cortices at P4 (lanes 1-3). Importantly, the protein level was greatly reduced in the mutants (lanes 4-6). To investigate whether the deletion is also efficient at early development timepoints, we performed immunofluorescence microscopy to analyze expression of HDAC3 on brain or embryonic sections at P0, E16.5 and E12.5. As shown in Fig. S3.1a-b, *Hdac3* was efficiently deleted at a majority of cells in the neocortex or hippocampus, but not the striatum at P0. A small number of cells remained positive in the cKO mutant neocortex (Fig. S3.1a,b). They are interneurons that migrate in a parallel manner from the ganglionic eminence (GE) (376), and the Cre recombinase in the *Emx1-Cre* line is not expressed in these cells (372, 373). Similar results were obtained at E16.5 (Fig. S3.1c,d). As for E12.5, HDAC3 was lost in the mutant cortical plate but not the GE (Fig. S3.1e,f). Thus, the *Emx1-Cre* line induces efficient and specific *Hdac3* deletion in the cerebrum and its embryonic precursors, starting at E12.5.

HDAC3 is crucial for development of the neocortex, hippocampus and corpus callosum

Unexpectedly, during brain dissection, we noticed prominent cysts at the caudal part of the mutant brain from 3-week old pups (Fig. 3.1f). Nissl staining of serial brain sections revealed

thin neocortices and large lateral ventricles in the mutant forebrain (Fig. 3.1g). Moreover, the mutant hippocampus was poorly developed, with the dentate gyrus barely visible (Fig. 3.1h). Such neocortical and hippocampal defects were also similarly present in the mutant pups at earlier timepoints, such as P7 (Fig. 3.1i,j) and P0 (Fig. 3.1k,l). Moreover, Nissl staining of serial brain sections from P0 showed that the corpus callosum was underdeveloped, with no clear boundaries between the corpus callosum and the adjacent tissues (Fig. 3.1m). In contrast, the heterozygous mice did not display such developmental defects (data not shown).

To substantiate the above histological observations, we carried out immunostaining to examine the defects at the molecular and cellular levels. For this, we used various antibodies specific to makers (such as Cux1, Cux2, Ctip2 and Tbr1) for different layers of the neocortex. As shown in Fig. S3.3a,b, neocortical lamination was altered in the mutant brain at birth. This alteration was also observed at P7 (Fig. S3.3c,d) and E16.5 (Fig. S3.3e,f). There was no clear boundary for the mutant Ctip2$^+$ layer (Fig. S3.3a, lower panel). In the mutant neocortex, the number of Tbr1$^+$ cells was significantly reduced (Fig. S3.3b, lower panel). Moreover, the distribution pattern of these cells was also altered (Fig. S3.3b, lower panel). The Cux1$^+$ and Cux2$^+$ layers were obvious in the wild-type neocortices but missing in the mutant neocortices (Fig. S3.3a,b). Thus, cerebrum-specific deletion of *Hdac3* results in severe developmental defects in the neocortex.

The above immunostaining experiments also confirmed hippocampal abnormalities in the embryonic, neonatal and postnatal mutant brain (Fig. S3.3). To substantiate this, we utilized two other markers, NeuroD and GFAP. As shown in Fig. S3.4a,c, immunostaining with antibodies against these two markers supported the abnormal morphology of the mutant hippocampus at P0, with fewer NeuroD$^+$ cells but more GFAP$^+$ cells than the wild-type. As shown in Fig. S3.4b,d, the abnormality was even more dramatic in the mutant hippocampus at P7. Thus, these results support that cerebrum-specific deletion of *Hdac3* leads to profound developmental defects in the hippocampus.

HDAC3 is required for development of neural stem and progenitor cells

During DAPI and Nissl staining, we observed that the ventricular/subventricular zone is thin in the mutant brain at E16.5 (Fig. S3.1h) and almost missing at P0 (Fig. 3.1k). The embryonic

ventricular/subventricular zone is the area where radial glia cells (the precursors of neural stem and progenitor cells) reside (377). To investigate whether these cells are affected, we first carried out immunofluorescence staining of embryonic and brain sections using an antibody against Sox2, a specific marker of NSCs (378). At P0, the $Sox2^+$ layer was dramatically reduced in the mutant (Fig. 3.2a,b), indicating that loss of *Hdac3* exhausts the NSC compartment. Moreover, we observed ectopic $Sox2^+$ cells outside of the ventricular/subventricular zone (Fig. 3.2a). At E16.5, the $Sox2^+$ layer was also dramatically reduced in the mutant (Fig. 3.2c,d), and ectopic $Sox2^+$ cells were observed outside of the ventricular/subventricular zone (Fig. 3.2c). Thus, at both P0 and E16.5, HDAC3 is critical for development of the $Sox2^+$ cell layer. By contrast, although HDAC3 was efficiently deleted at E12.5 (Fig. S3.1e-f), the thickness of the $Sox2^+$ cell layer was not significantly affected in the mutant (Fig. 3.2e,f), indicating that HDAC3 is not important for formation of the $Sox2^+$ cell layer at this embryonic stage.

We next analyzed different embryonic and brain sections using an antibody specific to the transcription factor Tbr2, a marker of neuronal progenitors critical for neocortex as well as hippocampus development (379, 380). As shown in Fig. 3.3a,b, the $Tbr2^+$ progenitor cell number was reduced profoundly in the mutant ventricular/subventricular zone at P0. Reminiscent of what was observed with the mutant $Sox2^+$ cells, $Tbr2^+$ cells were found outside the ventricular/subventricular zone of the mutant brain (Fig. 3.3a, lower panel). Similar to the mutant ventricular/subventricular zone, the $Tbr2^+$ progenitor cell number was greatly reduced in the mutant hippocampus (Fig. 3.3a). Consistent with this, few $Tbr2^+$ progenitor cells were detected in the mutant hippocampus at P7 (Fig. S3.5c). Moreover, at both E16.5 (Fig. 3.3c,d) and E14.5 (Fig. 3.3e,f), the $Tbr2^+$ progenitor cell number was significantly decreased in the mutant neocortices. As with the neonatal mutant brain, ectopic $Tbr2^+$ cells were also observed outside the ventricular/subventricular zone at both E16.5 (Fig. 3.3c) and E14.5 (Fig. 3.3e), indicating impaired migration of the progenitors in the mutant brain. In stark contrast to what observed at P0, E16.5 and E14.5, the $Tbr2^+$ progenitor cell number remained comparable between the wild-type and mutant neocortical primordium at E12.5 (Fig. S3.5a), indicating that HDAC3 is not required for formation of the $Tbr2^+$ progenitor cell layer at this embryonic stage. Thus, loss of *Hdac3* reduces the number of neural stem and progenitor cells required for neocortical development starting at E14.5.

The hippocampal fissure is formed at E17.5, and its boundary with the CA1-CA3 regions starts to emerge at this timepoint (381). As described above (Fig. 3.2a), at P0, the upper blade of the dentate gyrus was almost missing and there were fewer $Sox2^+$ cells in the dentate gyrus. At E16.5, noticeably fewer $Sox2^+$ cells were present in the hippocampal neuroepithelium area (Fig. 3.2b, indicated by red arrowheads). The hippocampus (or its primordium) in the mutant cerebral cortices at P0 and E16.5 were smaller when compared to the wild-type (Fig. 3.2a,c). At P0, there were fewer $Tbr2^+$ cells in the mutant hippocampus than the wild-type (Fig. 3.3a). One week later, this population of $Tbr2^+$ cells disappeared in the mutant hippocampus (Fig. S3.5a). Thus, cerebrum-specific loss of *Hdac3* reduces the number of NSPCs required for hippocampus development.

Hdac3 deletion induces premature neurogenesis and disrupts neuronal migration

Embryonic NSPCs either proliferate to replenish the population or differentiate to generate new neurons for proper brain development (382). To investigate whether neurogenesis from NSPCs is affected, we performed immunostaining of embryonic brain sections using an anti-Tuj1 antibody recognizing Tuj1, a neuron-specific β-tubulin (343, 344). As shown in Fig. S3.6a,b, thickness of the $Tuj1^+$ cell layer was similar between the wild-type and mutant brains at E13.5. By contrast, this became different at E14.5: while the entire neocortex remained similar between the wild-type and mutant brain, this cell layer was thicker in the mutant than the wild-type E14.5 (Fig. S3.6c,d), indicating that in the absence of *Hdac3*, neurogenesis is enhanced at this developmental stage. One day later at E15.5, even though the $Tuj1^+$ cell layer was comparable between the wild-type and mutant brains, the entire neocortex was thinner in the mutant (Fig. S3.6e,f), indicating that the ratio of the $Tuj1^+$ cell layer to the neocortex is still higher in the mutant than the wild-type. These results indicate that the neurogenic zone expands at both E14.5 and E15.5. Related to this, at both developmental stages, the ventricular/subventricular zone was compressed in the mutant (Fig. S3.6c,e, areas labelled with green asterisks). Moreover, ectopic distribution of $Tuj1^+$ neurons was also observed in the mutant (Fig. S3.6c,e, areas labelled with green asterisks), indicative of aberrant birth of $Tuj1^+$ neurons from NSPCs. These results indicate that *Hdac3* deletion causes premature neurogenesis.

Embryonic NSPCs are subject to delicate balance between self-renewal (proliferation) and differentiation (neurogenesis). To investigate whether NSPC proliferation is affected, we examined the S phase by carrying out BrdU labeling *in vivo* for subsequent immunostaining with a monoclonal antibody recognizing this label (343, 344). For the assay, BrdU was injected into pregnant mice at E12.5 or E13.5 for embryo retrieval 1 h later. Indirect immunofluorescence microscopy was then performed with embryonic sections using anti-BrdU and -Ki67 antibodies. As shown in Fig. S3.7, no difference was observed between the mutant and wild-type at both developmental timepoints. Considering that total $Sox2^+$ radial glial cells and $Tbr2^+$ progenitor cells are comparable in the wild-type and mutant neocortices at E12.5 (Fig. 3.2e,f & S3.5b) and E13.5 (data not shown), these results indicate that NSPC proliferation is not affected.

For neurogenesis, NSPCs exit the cell cycle for neuronal differentiation. To gain mechanistic insights into the above observations about premature neurogenesis, we analyzed cell cycle progression of NSPCs by carrying out BrdU labeling (343, 344). For this, BrdU was injected into pregnant mice at E12.5 or E14.5 for embryo retrieval 24 h later. Indirect immunofluorescence microscopy was then performed with anti-BrdU and -Ki67 antibodies as described above. As shown in Fig. S3.8a,b, compared to the wild-type, there were significantly more $BrdU^+Ki67^-$ cells (green) in the mutant ventricular zone at E12.5 and E14.5, indicating that more NSPCs exit the cell cycle with 24 h after BrdU injection, further supporting enhanced neurogenesis in the mutant brain.

During immunofluorescence staining, we observed ectopic distribution of $Sox2^+$ NSCs (Fig. 3.2), $Tbr2^+$ neuronal progenitors (Fig. 3.3), $Tuj1^+$ neurons (Fig. S3.6) and cortical layer-specific neurons (Fig. S3.3). These observations suggest that neuronal migration might be affected. To evaluate this directly, we injected BrdU into pregnant mice at E12.5 or E14.5 for embryo retrieval 2-4 days later at E16.5. As shown in Fig. S3.8a,b, neuronal migration was significantly compromised in the mutant neocortex. Specifically, for BrdU tracing from E12.5 to E16.5, a majority of the $BrdU^+$ cells were observed in the cortical plate in the wild-type neocortex (Fig. S3.8a, upper panel), whereas such cells were rather evenly distributed throughout the mutant neocortex (Fig. S3.8a, lower panel). For BrdU tracing from E14.5 to E16.5, a majority of $BrdU^+$ cells were localized to the wild-type ventricular/subventricular zone

(Fig. S3.8b, upper panel), whereas while such cells were quite evenly distributed throughout the mutant neocortex, with lots of $BrdU^+$ cells in the cortical plate (Fig. S3.8b, lower panel). Thus, these results indicate severe impairment of neuronal migration in the mutant cerebral cortex.

Hdac3 deletion augments DNA damage and triggers massive apoptosis

Because global deletion of *Hdac3* in embryonic fibroblasts was reported to induce DNA damage and trigger apoptosis (297), so we investigated whether cerebrum-specific loss of *Hdac3* causes similar defects. For this, immunostaining of embryonic and brain sections with an anti-γH2A.X antibody was used to detect DNA damage, and TUNEL assays was employed to assess apoptosis. As shown in Fig. 3.4a,b, the number of $\gamma H2A.X^+$ cells increased dramatically in the neonatal mutant neocortex. Interestingly, such increase was found even at E12.5 (Fig. 3.4c), when the NSPC number was found to be normal (Figs. 3.2e,f & S3.5b,c). TUNEL assays revealed that apoptosis was dramatically increased in the mutant at both E14.5 (Fig. 3.4d,e) and P0 (Fig. 3.4g,h). Specifically, massive apoptosis in the neocortex was observed in the mutant VZ/SVZ at E14.5 (Fig. 3.4d,e), indicating that *Hdac3* deletion drastically reduces embryonic NSPCs. Moreover, immunostaining with an antibody recognizing activated caspase 3 corroborated these findings (Fig. 3.4f,i). Together, these results indicate that DNA damage and apoptosis contribute to NSPC depletion in the mutant.

Mutant NSPCs are impaired in forming neurospheres *in vitro*

To investigate whether the remaining mutant NSPCs are still functional, we conducted neurosphere formation assays, which have been widely used to determine NSPC potential *in vitro* (383). For these assays, we collected cerebral cortices from wild-type and mutant embryos at E16.5 to prepare single cell suspension for subsequent neurosphere formation in an NSC culture medium *in vitro*. Like the wild-type, single cells from the E16.5 mutant cerebral cortex formed round neurospheres during the first 4 days (Fig. 3.5a), but the mutant neurospheres became irregular at day 6 and afterwards (Fig. 3.5b). Even at day 4, more dead cells were visible in the medium for culturing the mutant neurospheres than the wild-type (data not shown). Quantification revealed that at this timepoint, there were significantly fewer mutant neurospheres than the wild-type (Fig. 3.5c). Measurement of neurosphere sizes indicated that

at day 4 and day 7, the mutant neurospheres were significantly smaller than the wild-type (Fig. 3.5d). Moreover, the total cell number was much lower in the mutant neuropheres than the wild-type (Fig. 3.5e), while there was no difference between wild-type and heterozygous groups (Fig. 3.5e).

We also collected cerebral cortices from wild-type and mutant embryos at E18.5 to grow neurospheres. More strikingly, neurospheres from the E18.5 mutant embryos were irregular even at day 4 (Fig. 3.5f). To examine the NSC nature of the neurospheres, we immunostained them using the anti-Sox2 antibody. As shown in Fig. 3.5g, there was a high ratio of $Sox2^+$ cells in both wild-type and mutant neurospheres. Together, these results indicate that at both E16.5 and E18.5, neurosphere formation is impaired in the mutant cerebral cortex.

To investigate the impact of *Hdac3* inactivation on NSC self-renewal, we analyzed formation of secondary neurospheres. For this, primary neurospheres were cultured as described above and used for preparation of single-cell suspension through pipetting. 20,000 cells were used for neurosphere formation in the NSC medium. As shown in Fig. 3.5h, single cells prepared from the mutant neurospheres yielded a much smaller number of neurospheres, indicating impairment of self-renewal in mutant NSCs.

HDAC3 is a transcription coregulator with intrinsic deacetylase activity (384), so we took a pharmacological approach to substantiate the above conclusions drawn from genetically modified NSPCs. For this, we utilized a selective HDAC3 inhibitor, RGFP966 (385). Single cell suspension was prepared from E16.5 wild-type cerebral cortex for neurosphere formation in the presence or absence of this inhibitor. As shown in Fig. 3.5i, treatment with this inhibitor even at the IC50 value of 0.08 μM was sufficient for impairing neurosphere formation, indicating that HDAC3 inhibition of its enzymatic activity abolishes neurosphere formation. These results support that the deacetylase activity of HDAC3 is essential for NSPC development.

Hdac3 deletion alters epigenetic marks differently in the cerebrum and neurospheres

To shed light on how *Hdac3* deletion affects cerebral development and NSPC homeostasis, we asked whether and how cerebrum-specific *Hdac3* deletion alters the epigenome. We thus determined levels of histone marks. For this, we performed Western blotting by using various

histone modification-specific antibodies. Protein extracts of cerebral cortices were prepared from wild-type and mutant pups at P4, because at this stage the mutant pups were still grossly normal (Fig. 3.1b,c). For histone H3, levels of the histone acetylation marks H3K9ac, H3K18ac and H3K27ac, but not at H3K4ac, H3K14ac and H3K23ac, increased greatly in the mutant cerebral cortex (Fig. 3.6a, left and middle panels). Consistent with the increased levels of H3K9ac and H3K27ac, trimethylation at both sites, but not H3K4, decreased (Fig. 3.6a, middle panels). Notably, the decrease in the H3K27me3 level was much more dramatic than the H3K9me3 level (Fig. 3.6a, middle panels). Consistent with this, immunostaining of brain sections revealed H3K27me3 levels dramatically decreased in the mutant cerebral cortex, while the change of the H3K9me3 level was not so obvious (Fig. S3.9). As with histone H3, histone H4 was also hyperacetylated (Fig. 3.6a, right top panel). In support of this, the H4K16ac level increased dramatically in the mutant cerebral cortex (Fig. 3.6a, right bottom panel). These results indicate that cerebrum-specific *Hdac3* deletion causes histone hyperacetylation and deregulates histone modifications.

We also performed Western blotting with protein extracts of wild-type and mutant neurospheres. As shown in Fig. 3.6b (top left two panels), *Hdac3* was efficiently deleted in neurospheres. This is consistent with the results for the cerebral cortex (Fig. 3.1e) and its embryonic precursors (Fig. S3.1b,d,f). As expected, H3K4 acetylation slightly increased whereas H3K9 acetylation dramatically increased in the mutant neurospheres (Fig. 3.6b, top left panels). Such increase was also observed with wild-type neurospheres treated with the HDAC3-specific inhibitor (Fig. 3.5j). However, instead of hyperacetylation observed with the mutant cerebral cortex (Fig. 3.6a), H3K14, H3K18 and H3K23 acetylation decreased in the mutant neurospheres (Fig. 3.6b, middle left panels). As for methylation, the H3K4me3 level decreased, the H3K9me3 level increased, and the K3K27me3 level remained unaltered in the mutant neurospheres (Fig. 3.6b, bottom left panels). About histone H4, its total acetylation level decreased in the mutant neurospheres whereas the H4K16ac level was not altered (Fig. 3.6b, right panels). Thus, unlike what was observed with cerebral cortex (Fig. 3.6a), *Hdac3* deletion causes histone hypoacetylation at some histone sites in neurospheres (Fig. 3.6b).

HDAC3 regulates different transcription programs in the cerebrum and neurospheres

To identify the molecular mechanisms by which *Hdac3* deletion affects cerebral development and NSPC homeostasis, we analyzed transcriptomes. For this, we extracted total RNA from cerebral cortices from wild-type and mutant newborns (P0). Poly(A) RNA-profiling revealed altered transcription of multiple genes related to NSPC or lineage cell development (Fig. 3.6c; Table S3.4). Especially, we observed a dramatic increase in *Gfap* expression, consistent with our immunofluorescence staining in P0 brain sections showing increased gliogenesis (Fig. S3.4c,d), and a previous study (312).

To further identify the molecular mechanism in the NSPCs, we extracted total RNA from E16.5 primary neurospheres cultured at day 4 (at this date the morphology was similar between the wild-type and mutant neurospheres, Fig. 3.5a). Poly(A) RNA-profiling and gene differential analysis identified 73 upregulated (fold change>2) and 76 downregulated (fold change<0.5) genes ($p<0.001$) (Table S3.2, S3.3), including increased transcription of pro-neurogenesis genes such as the *Dlx* family genes and decreased transcription of anti-neurogenesis genes such as the *Id* and *Hes* family genes (Fig. 3.6d, Table S3.5). Transcript levels of many other neurogenesis-promoting genes (such as *Sox1*, *Pbx*, *Lhx6*, *Gad1*, *Gad2*, *Cux2*, *Tbr1*, *Dcx*, *Erbb4*, *NeuroD1* and *NeuroD2*) increased, whereas the levels of anti-neurogenesis genes (such as *Notch3*, *Sox10*, *Ascl1*, *Fabp7, Tnc and Nes*) decreased as well (Fig. 3.6d). These results indicate that *Hdac3* deletion promotes premature neurogenesis through upregulating expression of multiple pro-neurogenesis genes and inhibiting expression of anti-neurogenesis genes.

Consistent with anti-BrdU and -Ki67 staining at E12.5 and E13.5 (Fig. S3.7), expression of cell cycle inhibitors such as *p27*, *p57*, *p15* and *p53* was not affected in the *Hdac3*-deficient P0 cerebral cortex or cultured E16.5 neurospheres (Fig. S3.10a,b). However, *p21* was increased in the *Hdac3*-deficient P0 cerebral cortex (Fig. S3.10a) while *p18* decreased in the *Hdac3*-deficient E16.5 neurospheres (Fig. S3.10b). The *p53* transcript level was comparable between control and mutant groups, and the *Ki67* transcript level was not significantly affected either (Fig. S3.10a,b). These results indicate proliferation is not significantly affected in the cerebral cortex or mutant neurospheres.

HDAC3 binds multiple transcription factors abundant in the cerebrum and neurospheres

As an enzymatic transcriptional coregulator (270, 386), HDAC3 is recruited to specific promotors for gene-specific actions. To identify DNA-binding transcription factors that target this deacetylase to specific genetic loci during cerebral development, we analyzed previous ChIP-seq datasets for HDAC3 in different tissues (318, 319, 387-390). DNA sequence motif analysis identified multiple potential candidates, including MEF2, COUP-TFI, nuclear factor-I (such as NFIB and NFIC), C/EBPγ and SOX4. Important for brain development (391, 392), RP58 contains a POZ domain, known to interact with the NcoR/SMRT corepressors (393), so we also included this repressor as an candidate. As shown in Fig. S3.3.11a,b, *Rp58*, *Nfib*, *Coup-tfi*, and *Sox4* were highly expressed in the cerebral cortex (Fig. S3.11a) and in the neurospheres (Fig. S3.11b). Immunostaining showed that NFIB is highly expressed in the cortical plates and SVZ/VZ zone (Fig. S3.11c, topper panel). Serendipitously, we found that *Hdac3* deletion altered this distribution pattern (Fig. S3.11c, lower panel), corresponding to the altered cortical layers (Fig. S3.1h). These results indicate that HDAC3 affects NFIB expression in different cerebral areas during brain development.

We next assessed the interaction of HDAC3 with NFIB and the three other transcription factors identified above. FLAG-tagged HDAC3 was thus expressed with HA-tagged NFIB, -C/EBPγ, -SOX4, and -RP58 in HEK293 cells for co-immunoprecipitation. As shown in Fig. S3.11e, HDAC3 co-immunoprecipitated NFIB, NFIC, and SOX4. Moreover, HDAC3 interacted with a truncated form of NFIB containing its N-terminal 200 residues (Fig. S3.11e, lane 3). This region is conserved among NFIB, NFIC and other NFI proteins (Fig. S3.11c), suggesting that HDAC3 interacts with different members of the NFI family. We also expressed FLAG-tagged HDAC3 alone in HEK293 cells to detect interaction with endogenous COUP-TFI, NFIB, and RP58 proteins by using antibodies against these proteins. As shown in Fig. S3.11f-j, FLAG-tagged HDAC3 co-immunoprecipitated these endogenous proteins. The results suggest that multiple transcription factors (such as NFIB, COUP-TFI, RP58, and SOX4) recruit HDAC3 for gene-specific gene regulation during cerebral development.

3.4 DISCUSSION

This study uncovers an important role of *Hdac3* in governing perinatal cerebral development through NSPCs. Immunostaining revealed that HDAC3 is highly expressed in the

developing mouse brain (Fig. S3.1). Cerebrum-specific inactivation of the gene induces hyperactivity, anxiety and early lethality in the pups, along with severe developmental defects such as neocortical disorganization, hippocampal hypoplasia and callosal agenesis (Fig. 3.1). As for the underlying cellular mechanisms, immunofluorescence microscopy revealed rapid loss of NSCs (Fig. 3.2) and neuronal progenitors (Fig. 3.3), resulting from premature neurogenesis (Fig. S3.6) and enhanced DNA damage and apoptosis (Fig. 3.4). Moreover, the mutant NSPCs are defective in forming neurospheres (Fig. 3.5a-f) and the HDAC3-specific inhibitor RGFP966 is capable of abolishing neurosphere formation by wild-type NSPCs (Fig. 3.5i). Related to the molecular mechanisms (Fig. 3.6), immunoblotting unveiled altered histone acetylation in the mutant cerebral cortex or neurospheres (Fig. 3.6a,b & 5j). Furthermore, RNA-Seq not only revealed perturbation of transcription programs in the mutant cerebral cortex and NSPCs (Fig. 3.6c,d) but also unmasked high expression of multiple HDAC3-interacting transcription factors in the wild-type cerebrum and neurospheres (Fig. S3.11a,b). These results thus identify HDAC3 as a major deacetylase critical for perinatal cerebral and NSPC development (Fig. 3.6e).

The results also complements and extends a previous study that reported the role of *Hdac3* in brain development (312). The *Nestin-Cre* strain was used in the study and the resulting ablation induced neonatal lethality (312). The study was focused on the cerebellum, so neocortical disorganization was only briefly described for neonates, without any analyses of neocortical development at the prenatal stage and within the first two weeks after birth, when neocortical lamination occurs dynamically (394). The impact on development of the hippocampus and corpus callosum was not characterized either. The neonatal lethality is likely because of *Nestin-Cre* expression in the entire nervous system (312). The strain is inefficient for inducing excision at E12.5-14.5 (395, 396). By contrast, the *Emx1-Cre* strain used herein confers efficient excision specifically in the stem/progenitor cells and cortical neurons starting at E12.5 (Fig. S3.1f) (397). Due to cerebrum-specific expression, the resulting mutant pups survived for ~4 weeks (Fig. 3.1a), permitting systematic analysis of neocortical and hippocampal development at different timepoints before and after birth. In addition, direct involvement of NSPCs was also investigated (Figs. 3.2, 3.3). Several reports have described specific deletion of *Hdac3* in the adult brain and showed that HDAC3 is important for

regulating memory (313, 398), motor coordination (312, 313), social behaviors (313) and drug addiction (399). HDAC3 is also essential for myelin growth and regeneration (400). The present study focuses on perinatal cerebral and NSPC development, thus complementing these previous reports.

The present study uncovers an important role of HDAC3 in NSPC development (Figs. 3.2-3.4). The results showed that cerebrum-specific deletion of *Hdac3* promotes premature neurogenesis (Fig. S3.6). Moreover, in the mutant neurospheres, expression of pro-neurogenesis genes (such as *Dlx* family members) was upregulated, whereas expression of anti-neurogenesis genes was downregulated (such as *Id* and *Hes* family members) (Fig. 3.6d). These results are consistent with a recent report showing that *Hdac3* knockdown initiates a neuronal differentiation program *in vitro* (291). HDAC3 is the catalytic subunit of tetrameric complexes composed of N-COR (or SMRT), TBL1 (or its paralogs) and GPS2 (356, 357). These complexes function as transcriptional corepressors upon transcription factor-dependent recruitment to specific promotors. Consistent with the important role of HDAC3 in NSPCs (Figs. 3.2-3.4), $Smrt^{-/-}$ embryos display NSC defects (311), and $Ncor^{-/-}$ NSCs show enhanced gliogenesis *in vitro* (401). In agreement with premature gliogenesis upon *Ncor* deletion, *Gfap* transcription was elevated in $Hdac3^{-/-}$ neurospheres (1.9-fold) and mutant cerebral cortices (4.4-fold) (Tables S3.4 and S3.5). Moreover, immunostaining detected strong GFAP signals in $Hdac3^{-/-}$ cerebral cortices (Fig. S3.4c,d). As shown in Fig. S3.10c,d, both NcoR and SMRT are highly expressed in the wild-type cerebral cortex and neurospheres, suggesting redundant roles of these two paralogs. Together with the published reports on NcoR (401) and SMRT (311), the present study supports a model in which the HDAC3 complexes play important roles in regulating NSPC and cerebral development (Fig. 3.6e). Further mouse genetic studies are needed to pinpoint the exact roles of different subunits in cerebral development.

As for DNA-binding proteins that recruit these complexes for gene-specific actions, RNA-Seq and co-immunoprecipitation uncovered high expression of multiple HDAC3-interacting transcription factors in the wild-type cerebrum and neurospheres (Fig. S3.11a,b). These uncovered transcription factors are important in NSC maintenance and differentiation. For example, NFIB proteins are master regulators of neuronal differentiation (402). Disruption of both *Nr2f1* and *Nr2f2* (encoding COUP-TFI and COUP-TFII, respectively) promotes sustained

neurogenesis and prolonged generation of early-born neurons in NSPCs and the developing forebrain (403). COUP-TFI is also important for differentiation of oligodendrocytes (404) and directly binds to the *Fabp7* promotor (405). Related to this, reduced expression of *Fabp7* was found in *Hdac3*$^{-/-}$ neurospheres (FPKM of 580 in the wild-type to 374 in the mutant, Table S3.2). It is well established that the HDAC3 complexes interact with MeCP2 (313, 406). RNA-Seq revealed moderate expression of *Mecp2* in the developing cerebrum and cultured neurospheres (Fig. S3.11a,b). Moreover, developmental defects of *Mecp2*$^{-/-}$ mice are much milder (407, 408) than those of the *Hdac3* knockouts described herein (Fig. 3.1), suggesting that MeCP2 is not the sole DNA-binding partner recruiting HDAC3 complexes for genome-wide actions. Rev-ErbA and Rev-ErbB are important transcription factors in mediating function of HDAC3 in circadian clock and metabolism (409). However, RNA-seq implied low expression of *Rev-erba* and *Rev-erbb* in the cerebral cortex and neurospheres, indicating they may not be the main transcription factors for mediating HDAC3 function in the cerebrum. We propose that multiple DNA-binding proteins interact with and recruit HDAC3 complexes for epigenomic regulation during cerebral development (Fig. 3.6e). Further studies are needed to test this model and investigate how HDAC3 and its associated subunits are targeted to different genomic loci for governing perinatal development of the mouse cerebrum and NSPCs.

The important role of HDAC3 in mouse cerebral development (Fig. 3.1) begs the question whether this epigenetic regulator is also essential for human intellectual development. Consistent with the neocortical and hippocampal defects of the mutant *Hdac3* knockout mice, multiple patients with *TBL1XR1* germline mutations display intellectual disability (369-371), supporting a critical role of the HDAC3 complexes in regulating human cerebral and intellectual development. As for *HDAC3* itself, one patient with a heterozygous *de novo* mutation has been identified (368). The developmental defects described herein for the mutant mice will serve a valuable guide for identification of additional patients with *HDAC3* mutations. Clinical features of patients with mutations in genes for other subunits of the HDAC3 complexes, including *NCOR1* (encoding NCoR), *NCOR2* (encoding SMRT), *TBL1X*, and *GSP2* (Fig. 3.6e), will provide valuable information of the complexes in human development.

There are 18 human HDACs (354, 355), so a key question is how each HDAC contributes to epigenomic regulation during cerebral development. The results described herein highlight

the importance of HDAC3 for this regulation. Published studies have identified important roles of HDAC1, HDAC2, HDAC4 and HDAC8 in the brain (52, 87). Among them, HDAC4 shows little detectable deacetylase activity, and HDAC8 deacetylates cohesion rather than histones (52, 87), so HDAC1 and HDAC2 are two deacetylases targeting histones in the brain. Knockout studies established that mouse *Hdac1* and *Hdac2* have redundant roles in brain development (73). Inactivation of both genes disrupts cell-cycle progression, leaving few cells at the S phase (~3%) (73). In stark contrast, normal BrdU incorporation was observed in *Hdac3*$^{-/-}$ neuroepithelia at E12.5 and E13.5 (Fig. S3.7). In addition, neuronal progenitors lacking both *Hdac1* and *Hdac2* are defective in differentiation (73), whereas *Hdac3* deletion promotes premature neurogenesis and causes NSPC depletion. Related to this, haploinsufficiency of *SIN3A*, encoding a subunit of an HDAC1/HDAC2 complex, reduces cortical neurogenesis. These differences support that HDAC3 is complementary to HDAC1 and HDAC2 during cerebral development. Despite little impact on expression of these two and other HDACs (Fig. S3.10e,f), both histones H3 and H4 were hyperacetylated in the mutant cerebral cortex (Fig. 3.6a). Taken together, results from this study establish HDAC3 as a major histone-deacetylating epigenetic regulator that is important for perinatal cerebral and NSPC development in mice and perhaps also in humans.

3.5 MATERIALS AND METHODS

Methods, including statements of data availability and any associated accession codes and references, are available in the online version of the paper.

ONLINE METHODS

Mouse husbandry and generation of cerebrum-specific knockouts

The *Hdac3*^{f} allele was generated from a knockout-first strain from International Knockout Mouse Consortium (*Hdac3*$^{tm1a(EUCOMM)Wtsi}$) by excision of the FRT-flanked *LacZ-Neo* cassette with a *PGK1-Flp0* strain (The Jackson Laboratory, Stock No. 011065). The resulting *Hdac3*^{f} allele contains two loxP sites flanking the 3rd exon, which is common for different HDAC3 isoforms. To generate cerebrum-specific knockouts, the *Hdac3*$^{f/f}$ mice were mated with the *Emx1-Cre* strain (Jackson Laboratory, Stock No. 005628). E0.5 was defined as the noon after the morning when the plug was found. The mice were maintained in the McGill animal facility

operated under a 12-h light/12-h dark cycle and with food and water available *ad libitum*. All the experimental procedures related to the animal works were performed according to an animal use protocol approved by the McGill University Animal Care Committee.

Open field tests

The tests were carried out with a 40 cm x 40 cm x 40 cm translucent box as the testing arena (348). Mouse cages were taken to a quiet room 1 h before a test to allow mice to become familiar with the environment. Mice were put in the center of the arena in each test and video-recorded for 10 min. Disturbance for the mice was avoided during the testing period. After each test, the bottom of the box was wiped with 75% alcohol and air dry for 5 min before starting the next test. The recorded videos were analyzed by the SMART 3.0 video-tracking system (Pan-Lab, Harvard Apparatus).

Histology

The brain was dissected out and fixed in 4% PFA for 24-48 h. The tissues were then subject to dehydration and paraffin embedding. The paraffin blocks were sectioned to 5 μm and used for subsequent Nissl, H &E or immunohistochemical staining as described (255, 343, 344).

BrdU tracing *in vivo*

BrdU labeling was carried out as described (255, 343, 344). It was injected intraperitoneally into pregnant mice with a dosage of 50 mg per 1 kg body weight. The mice were sacrificed at different timepoints according to experimental goals. For S-phase analysis, mice were sacrificed 1 h after injection. For analysis of the cell-cycle exit, the waiting time after injection was 24 h, and for migration, the time was from 48 to 96 h.

Immunostaining

Antigen retrieval was carried out by boiling paraffin-section slides in the citrate buffer (10 mM sodium citric acid, 0.05% Tween 20, pH 6.0) for 20 min for immunostaining as described (255, 343, 344). For BrdU detection, followed by antigen retrieval, the sections were incubated in 2N HCl for 30-60 min. The nuclei were counterstained with DAPI or Hoechst 33342. The following antibodies were used: rabbit anti-HDAC3 (Abcam, ab7030, 1:2500), goat anti-Sox2

(R&D systems, AF2018, 1:200), rabbit anti-Tbr2 (Abcam, ab23345, 1:400), rabbit anti-Cux1 (1:200) (345), rat anti-Ctip2 (Abcam, ab18465, 1:400), rabbit anti-Cux2 (1:200) (346), rabbit anti-Tbr1 (Santa Cruz, sc-376258, 1:100), mouse anti-Tuj1 (Covance, MMS-435p, 1:1000), rat anti-BrdU (Abcam, ab6326, 1:400), mouse anti-Ki67 (BD Pharmingen, 550609, 1:200), rabbit anti-gamma H2A.X (Abcam, ab2893, 1:500), rabbit anti-H3K9me3 (EMD Millipore, 07-442, 1:500), mouse anti-H3K27me3 (Abcam, ab6002, 1:500), goat anti-NeuroD (Santa Cruz, sc1084, 1:100), rabbit anti-GFAP (Dako, Z0334, 1:2000), Alexa Fluor 488-conjugated goat-anti-rabbit IgG (Invitrogen, A-11008, 1:500), Alexa Fluor 488-conjugated donkey-anti-goat IgG (Invitrogen, A-11055, 1:500), Alexa Fluor 568-conjugated goat-anti-rabbit IgG (Invitrogen, A-11011, 1:500), Alexa Fluor 488-conjugated goat-anti-rat IgG (Invitrogen, A-11006, 1:500), Alexa Fluor 568-conjugated goat-anti-mouse IgG (Invitrogen, A-11004, 1:500).

Immunoblotting

On ice, mouse tissues or neurospheres were suspended in the cold RIPA buffer (150 mM NaCl, 1.0% Nonidet P-40 (or Triton X-100), 0.5% sodium deoxycholate, 0.1% SDS, 50 mM Tris-HCl, pH 8.0) containing a proteinase inhibitor cocktail, composed of 1 mM phenylmethylsulfonyl fluoride, 1 μg/ml pepstatin, 2 μg/ml aprotinin and 0.5 μg/ml leupeptin. After brief sonication (15s set at 5 with a VirSonic 100 sonicator) on ice, the suspension was centrifugated at 20,000 *g* and 4°C in an Eppendorf centrifuge for 10 min. The supernatant was transferred to a new tube on ice. The protein concentration was determined by a Bradford protein assay kit (Sigma). Protein extracts were mixed with a 3xRSB buffer (240 mM Tris-HCl pH 6.8, 6% SDS, 30% glycerol, 16% β-mercaptoethanol, 0.06% bromophenol blue) and boiled, for SDS-PAGE on 10-15% acrymide gels and subsequent transfer onto a Nitrocellulose membrane (Pall Corp., P/N66485). The membrane was incubated with the blocking buffer (TBS-T(0.1% Tween 20 in TBS) containing 5% nonfat milk powder) for 30 min at room temperature on a rocking platform and then incubated with the same buffer containing primary antibodies overnight at 4 °C on a rocking platform. After washing with TBS-T for 4 times (10 min each, with agitation), the membrane was incubated, on a rocking platform, with the blocking buffer containing the horse radish peroxidase-conjugated secondary antibodies at room temperature for 1 h. The membrane was washed above and developed with the enhanced

chemiluminescence substrates (FroggaBio, 16024). The following antibodies were used: Rabbit anti-HDAC3 (Abcam, ab7030, 1:10,000), rabbit anti-H3 (Abcam, ab1791, 1:100,000), rabbit anti-H3K4ac (EMD Millipore, 07-539, 1:2000), rabbit anti-H3K9ac (Abcam, ab4441, 1:2000), rabbit anti-H3K14ac (Abcam, ab52946, 1:1000), rabbit anti-H3K18ac (Abcam, ab1191, 1:10,000), rabbit anti-H3K23ac (EMD Millipore, 07-355, 1:20,000), rabbit anti-H3K27ac (EMD Millipore, 07-360, 1:1000), rabbit anti-H4 (Abcam, ab18253, 1:10,000), rabbit anti-H4K16ac (Abcam, ab109463, 1:1500), rabbit anti-H4ac (EMD Millipore, 06-866, 1:2000), rabbit anti-H3K14pr (PTM Biolabs, PTM-211, 1:1000), mouse anti-H3K23pr (PTM-208, 1:1000), mouse anti-H3K23cr (PTM-519, 1:2500), rabbit anti-H3K4me3 (EMD Millipore, 07-473, 1:5000), rabbit anti-H3K9me3 (EMD Millipore, 07-442, 1:500), mouse anti-H3K27me3 (Abcam, ab6002, 1:2000), rabbit anti-NFIB/B2 (Abcam, ab186738, 1:2000), rabbit anti-ZNF238/RP58 (Abcam, ab118471, 1:500), rabbit anti-COUP-TFI (Abcam, ab181137, 1:1000).

Neurosphere formation assays

All the procedures were done in the tissue-culture hood unless indicated. All the surgical instruments and solutions used were sterilized. Briefly, the pregnant mice at E16.5 or E18.5 were euthanized and the embryos were dissected out and put in PBS. The heads of the embryos were cut, washed in PBS and kept in PBS/2% glucose on ice for subsequent manipulations. Under a bench dissecting microscope, the head skin and skull were opened with surgical scissors, and the brain was dissected out using a pair of forceps in cold PBS/2% glucose solution. The cerebral cortices were segregated with forceps under the dissecting microscope and collected into Eppendorf tubes containing 1 ml of the neurosphere complete culturing medium (NeuroCult NSC Basal Medium (mouse) (StemCell Technologies, #05700) supplemented with 10% NeuroCult Proliferation Supplement (StemCell Technologies, #05701) and 20 ng/ml rhEGF (StemCell Technologies, #78006.1)) on ice. Once all the cortices were collected, the tubes were transferred into the hood and pipetted up and down with 1 ml tips for 8 times to prepare single cell suspension. Avoid air bubbles (set the pipette volume to 0.8 ml instead of 1 ml) during pipetting as excessive oxygen carried by bubbles would be deleterious for subsequent NSC growth. After pipetting, the tube was kept still at room temperature for 1

min, and the supernatant was then transferred to a new tube for centrifugation at 150 *g* for 5 min with a bench centrifuge at room temperature. The supernatant was discarded, and the pellet was gently mixed with 1 ml of the fresh neurosphere complete culture medium. The suspension was filtered through a 40-μm nylon cell strainer (Fisher Scientific, #22363547) and the resulting filtrate was considered as the single-cell preparation. After counting, wild-type and mutant cells were seeded into wells of a 6-well plate at the same number.

For treatment with the HDAC3 inhibitor RGFP966 (SelleckChem, #S7229), different concentrations were used (0, 0.08 or 0.8 μM). At different timepoints during culturing neurospheres, their size, numbers and total cell numbers were measured. For neurosphere size measurement, images were randomly taken. For counting neurospheres, a small aliquot of cultured neurospheres was diluted in a 96-well plate and the neurosphere number was counted under the regular light microscope. For counting of total cell numbers, an aliquot of neurospheres was taken and pipetted up and down to prepare single cell suspension; the total cell number was then counted. For immunostaining, cultured neurospheres were collected into a 15 ml tube, and kept for 10 min in the hood. The supernatant was aspirated and 4% PFA was added for incubation at room temperature for 10 min. After fixation, the upper supernatant was removed and neurospheres were washed in PBS for 3 times (to preserve the neurosphere morphology, for precipitation all the steps were done by putting still for 10 min instead of centrifugation). Neuropheres were then applied for immunofluorescence following standard protocol. For RNA-Seq, neurospheres were washed once with PBS for subsequent RNA preparation. For immunoblotting, neurospheres were washed once with PBS for extract preparation in the RIPA buffer as described below.

RNA isolation and sequencing

Total RNA was extracted from P0 neocortex and neurospheres cultured from E16.5 embryonic neocortex at day 4. The RNA quality and quantity were measured with an RNA Tapestation (Agilent). All RNA samples with a SIN score higher than 8 were used for subsequent RNA-Seq at Omega Biotek (Norcross, USA). Specifically, poly(A) RNA was purified for reverse transcription to cDNA and fragmentation to ~200 bp fragment, followed by amplification with PCR using random primers. The prepared cDNA library was loaded into

different lanes of the flow cell and sequenced by an Illumina sequencer. At least 40 million pair-end 100 bp sequences were obtained for each sample. The quality of the sequences was analyzed by FastQC to remove reads with scores lower than 20. The filtered sequences were mapped to the mouse genome (mm9) using STAR, and the reads were counted using FeatureCounts or Htseq-count, followed by differential analysis with DESeq2.

Statistical analysis

Statistical analysis was performed with unpaired 2-tailed Student's *t* test. $p<0.05$ was considered to be statistically significant. Graphs were generated with GraphPad Prism 6 (Graphpad Software).

ACKNOWLEDGEMENT

This work was supported by research grants from Canadian Institutes of Health Research, Natural Sciences and Engineering Research Council of Canada, and the Canadian Cancer Society (to X.-J.Y.). L.L. received stipend support from the China Scholarship Council, the Clifford C.F. Wong Fellowship program, a CIHR/FRSQ training grant in cancer research for the McGill Integrated Cancer Research Training Program, and the Canderel Foundation.

AUTHOR CONTRIBUTIONS

L.L. carried out all experiments, performed data analysis and wrote the manuscript; X.J.Y. supervised the project and finalized the manuscript.

COMPETING FINANCIAL INTERESTS

The authors declare no competing financial interests.

Table S3.1. Mendelian ratio for new born *Hdac3*-deficient pups is normal.

	Hdac3 f/f	Hdac3 f/+	Hdac3 f/f,Emx1-Cre	Hdac3 f/+,Emx1-Cre	Total	Chi-Test
Total	25	19	17	19	80	ns
Male	11	12	9	9	41	ns
Female	14	7	8	10	39	ns
Expected Ratio	25%	25%	25%	25%	100%	

Note: Male *Hdac3*$^{f/+}$; *Emx1-Cre* mice were mated with *Hdac3*$^{f/f}$, and pups were genotyped in the ensuing few days after birth. ns, not statistically significant.

Table S3.2 73 top upregulated genes with fold change >2.0 (i.e. log_2(FC)>1.0) and p<0.001 in E16.5 neurospheres

GeneSymbol	Base mean	log2(FC)	StdErr	Wald-Stats	p-value	p-adjust
Spp1	3806.59	4.59	0.19	-23.73	1.68E-124	2.17E-120
Col3a1	1971.16	4.24	0.23	-18.11	2.56E-73	1.10E-69
Col6a3	1551.65	3.81	0.20	-18.81	6.30E-79	4.07E-75
Col6a2	628.33	3.37	0.24	-13.84	1.37E-43	3.53E-40
Cyp1b1	297.67	3.35	0.28	-12.01	3.10E-33	4.99E-30
Col1a1	927.97	3.34	0.23	-14.25	4.32E-46	1.39E-42
Col6a1	716.63	2.65	0.24	-11.16	6.75E-29	8.70E-26
Mgp	146.75	2.30	0.29	-8.04	8.99E-16	4.14E-13
Col4a1	2834.91	2.27	0.17	-13.50	1.48E-41	3.19E-38
Tbx18	144.08	2.14	0.29	-7.50	6.36E-14	2.16E-11
Enpp1	256.80	2.01	0.28	-7.16	7.93E-13	2.27E-10
Sned1	339.60	1.99	0.27	-7.39	1.42E-13	4.69E-11
Postn	238.37	1.91	0.28	-6.82	8.95E-12	2.18E-09
Col4a2	2956.36	1.90	0.18	-10.27	9.82E-25	9.75E-22
Neat1	1062.06	1.81	0.22	-8.23	1.95E-16	1.14E-13
Nrk	175.16	1.75	0.29	-6.11	9.89E-10	1.66E-07
Nid1	372.09	1.71	0.26	-6.53	6.74E-11	1.50E-08
Rasgef1b	1511.34	1.61	0.20	-8.17	2.97E-16	1.60E-13
Dcn	420.78	1.57	0.27	-5.92	3.15E-09	4.83E-07
Anpep	157.51	1.57	0.28	-5.57	2.55E-08	3.26E-06
Ctsk	189.13	1.49	0.29	-5.22	1.77E-07	1.73E-05
Serpinf1	191.74	1.45	0.29	-5.07	3.98E-07	3.59E-05
Ednra	249.52	1.43	0.28	-5.09	3.50E-07	3.22E-05
Pdgfrb	345.65	1.42	0.28	-5.09	3.62E-07	3.29E-05
Ifi203	107.96	1.41	0.28	-5.00	5.70E-07	4.97E-05
Dnm3os	79.81	1.36	0.27	-4.97	6.73E-07	5.75E-05
Col5a1	838.21	1.36	0.23	-6.02	1.75E-09	2.76E-07
Cped1	177.47	1.35	0.29	-4.70	2.55E-06	0.000180687
Pbx3	1023.42	1.32	0.21	-6.40	1.54E-10	3.15E-08
Mmp9	125.78	1.31	0.28	-4.61	4.11E-06	0.000269063
Dlx2	1860.85	1.31	0.18	-7.39	1.45E-13	4.69E-11
Nrp2	3761.96	1.29	0.17	-7.63	2.38E-14	8.52E-12
Mmp2	231.56	1.27	0.28	-4.48	7.43E-06	0.000442568
Maf	4182.92	1.23	0.15	-8.46	2.78E-17	1.71E-14
Dlx6os1	3893.50	1.23	0.18	-6.84	8.10E-12	2.01E-09
Cp	364.42	1.22	0.27	-4.44	8.94E-06	0.000515079
Penk	613.57	1.22	0.26	-4.68	2.89E-06	0.00020259
Erbb4	4084.00	1.22	0.22	-5.56	2.75E-08	3.41E-06
Adamts12	343.90	1.21	0.27	-4.54	5.54E-06	0.000346748
Zfhx4	939.82	1.21	0.25	-4.76	1.92E-06	0.000145129
Gm14204	750.89	1.21	0.22	-5.38	7.56E-08	8.19E-06

Meg3	76063.34	1.19	0.18	-6.60	3.98E-11	9.18E-09
Gad2	3659.98	1.18	0.15	-7.81	5.65E-15	2.21E-12
Thbs1	919.90	1.18	0.22	-5.44	5.29E-08	5.99E-06
Dlx1as	1906.76	1.17	0.19	-6.29	3.09E-10	5.87E-08
Gm5607	538.81	1.17	0.26	-4.53	5.89E-06	0.000361918
Dlx1	1597.18	1.16	0.18	-6.35	2.21E-10	4.46E-08
Sp9	683.40	1.16	0.24	-4.81	1.50E-06	0.000115432
Col5a2	854.98	1.15	0.24	-4.74	2.18E-06	0.000159158
Tox2	1763.43	1.15	0.18	-6.52	6.91E-11	1.51E-08
Lama4	253.57	1.15	0.28	-4.06	4.81E-05	0.002154278
Sorl1	1750.45	1.15	0.18	-6.21	5.20E-10	9.45E-08
Gad1	12544.07	1.14	0.12	-9.12	7.20E-20	5.16E-17
Sez6	14235.09	1.13	0.15	-7.73	1.06E-14	3.92E-12
Adarb2	1978.04	1.12	0.20	-5.57	2.49E-08	3.21E-06
Bend4	1185.95	1.12	0.20	-5.75	9.15E-09	1.27E-06
Lhx6	6091.52	1.12	0.14	-8.13	4.16E-16	2.06E-13
Gsn	543.88	1.11	0.24	-4.60	4.28E-06	0.000278917
Sox1	1526.84	1.09	0.19	-5.74	9.34E-09	1.28E-06
Grik1	1266.82	1.08	0.20	-5.38	7.27E-08	7.95E-06
Fam222a	405.37	1.08	0.27	-4.03	5.54E-05	0.002414191
Plxna2	21912.03	1.06	0.14	-7.52	5.34E-14	1.86E-11
Col11a2	1094.09	1.05	0.21	-4.96	6.97E-07	5.92E-05
Slc32a1	1645.85	1.04	0.18	-5.78	7.37E-09	1.06E-06
Dlx5	1124.41	1.04	0.20	-5.12	3.05E-07	2.88E-05
Acan	648.63	1.03	0.25	-4.10	4.07E-05	0.001870094
Ephb1	1304.86	1.03	0.19	-5.32	1.06E-07	1.08E-05
Synpr	284.81	1.02	0.28	-3.67	0.000244342	0.007700865
Zfp804a	1882.81	1.02	0.19	-5.36	8.29E-08	8.84E-06
Nid2	607.40	1.01	0.25	-3.98	6.81E-05	0.002889772
Dock5	107.90	1.01	0.28	-3.56	0.000368511	0.010565613
Ptgds	332.15	1.01	0.27	-3.79	0.000151228	0.005345602
Agtr2	94.49	1.01	0.26	-3.88	0.000106448	0.004099689

Table S3.3 76 top downregulated genes with fold change <0.5 (i.e., $log_2FC<-1.0$) and p<0.001 in E16.5 neurospheres

GeneSymbol	Base mean	log2(FC)	StdErr	Wald-Stats	p-value	p-adjust
Slc16a3	266.42	-3.33	0.28	11.80	4.06E-32	5.82E-29
Mt2	1085.23	-2.46	0.22	11.04	2.49E-28	2.92E-25
Dio2	960.42	-2.02	0.23	8.81	1.30E-18	8.39E-16
Mt1	1579.12	-1.97	0.24	8.09	6.03E-16	2.88E-13
Bnip3	839.52	-1.79	0.22	8.16	3.37E-16	1.74E-13
Slc2a1	1527.65	-1.74	0.19	9.19	3.98E-20	3.02E-17
Cav1	813.44	-1.68	0.24	7.07	1.60E-12	4.30E-10
Dgkk	711.48	-1.67	0.23	7.14	9.58E-13	2.63E-10
Egln3	503.56	-1.67	0.24	6.81	9.85E-12	2.35E-09
P4ha2	308.71	-1.65	0.27	6.03	1.63E-09	2.60E-07
Ndufa4l2	108.14	-1.64	0.28	5.88	4.20E-09	6.23E-07
Hmox1	2923.72	-1.63	0.17	9.46	3.08E-21	2.48E-18
Ramp1	457.82	-1.53	0.26	5.89	3.76E-09	5.70E-07
Car9	88.64	-1.53	0.27	5.56	2.63E-08	3.33E-06
Gpi1	24383.69	-1.48	0.12	12.41	2.41E-35	4.44E-32
Pdk1	1416.13	-1.47	0.19	7.77	7.97E-15	3.02E-12
Grin2c	425.58	-1.47	0.26	5.56	2.75E-08	3.41E-06
Ldha	9453.70	-1.46	0.14	10.32	5.54E-25	5.95E-22
Fbln2	4435.15	-1.44	0.16	8.85	8.62E-19	5.85E-16
Ldb2	1650.97	-1.44	0.18	7.89	2.98E-15	1.24E-12
F2rl2	297.52	-1.44	0.27	5.32	1.07E-07	1.08E-05
Ero1l	3079.17	-1.40	0.17	7.99	1.30E-15	5.79E-13
Lipg	181.20	-1.38	0.29	4.81	1.49E-06	0.000115
Sparcl1	7092.27	-1.36	0.14	9.68	3.52E-22	3.03E-19
Fam162a	642.78	-1.36	0.25	5.35	8.86E-08	9.29E-06
Usp43	368.62	-1.35	0.28	4.85	1.24E-06	9.78E-05
Ptpru	732.79	-1.34	0.23	5.85	5.06E-09	7.43E-07
Sidt1	131.64	-1.34	0.29	4.67	2.96E-06	0.000205
Pcdh20	439.62	-1.33	0.25	5.26	1.48E-07	1.48E-05
Hk2	700.04	-1.33	0.24	5.53	3.20E-08	3.93E-06
Pgm2	1386.23	-1.32	0.19	6.86	6.66E-12	1.68E-09
Ccbe1	708.96	-1.32	0.23	5.78	7.61E-09	1.08E-06
Slc38a3	1632.07	-1.32	0.18	7.27	3.54E-13	1.09E-10
Id1	316.06	-1.31	0.28	4.68	2.91E-06	0.000203
Rgs6	283.12	-1.29	0.28	4.58	4.69E-06	0.000302
Necab1	1869.56	-1.29	0.20	6.40	1.51E-10	3.14E-08
P4ha1	1521.48	-1.26	0.19	6.52	7.11E-11	1.53E-08
Ephx1	2229.93	-1.24	0.22	5.76	8.46E-09	1.19E-06
Bhlhe40	1342.71	-1.21	0.20	6.12	9.24E-10	1.59E-07
Slc1a3	23062.92	-1.21	0.12	10.12	4.41E-24	4.07E-21
Rasl11a	336.29	-1.20	0.27	4.49	7.11E-06	0.000427

Lrfn5	741.08	-1.20	0.22	5.42	6.11E-08	6.79E-06
Mfge8	5595.41	-1.19	0.17	7.01	2.33E-12	6.13E-10
Rspo2	233.40	-1.19	0.29	4.16	3.12E-05	0.001515
3110035E14Rik	643.57	-1.18	0.25	4.62	3.92E-06	0.000261
Id3	665.51	-1.16	0.23	5.04	4.64E-07	4.07E-05
Ndrg1	2964.02	-1.16	0.18	6.32	2.67E-10	5.13E-08
Tpi1	5674.19	-1.16	0.16	7.30	2.93E-13	9.21E-11
Ntsr1	1452.35	-1.16	0.19	6.24	4.29E-10	7.91E-08
Galk1	370.34	-1.15	0.26	4.42	1.01E-05	0.000567
Slc16a1	744.15	-1.14	0.26	4.37	1.23E-05	0.000676
Ppp1r3c	873.17	-1.14	0.23	5.06	4.14E-07	3.69E-05
Aox1	251.59	-1.14	0.28	4.12	3.80E-05	0.001777
Nusap1	832.96	-1.13	0.23	4.91	9.18E-07	7.55E-05
Inhbb	479.88	-1.12	0.25	4.55	5.40E-06	0.000341
Rlbp1	1382.92	-1.11	0.19	5.71	1.13E-08	1.53E-06
Emp2	785.36	-1.10	0.24	4.62	3.87E-06	0.000259
Igfbp2	8149.82	-1.10	0.13	8.21	2.24E-16	1.26E-13
Cpne7	993.47	-1.09	0.24	4.54	5.58E-06	0.000348
Cth	185.59	-1.08	0.29	3.76	0.000169	0.005783
Tubb6	1319.01	-1.07	0.23	4.74	2.11E-06	0.000155
Grm2	792.76	-1.07	0.22	4.83	1.39E-06	0.000108
Kif18a	483.24	-1.06	0.27	3.91	9.23E-05	0.003697
Itga6	2248.11	-1.06	0.17	6.32	2.57E-10	5.03E-08
Thy1	3429.66	-1.06	0.16	6.79	1.14E-11	2.67E-09
Htr1a	105.71	-1.05	0.28	3.70	0.000214	0.006978
Gen1	148.36	-1.05	0.29	3.66	0.000252	0.007891
Vegfa	10233.43	-1.05	0.13	7.86	3.91E-15	1.57E-12
Klf10	1749.83	-1.04	0.19	5.50	3.72E-08	4.45E-06
Ctsc	1116.52	-1.03	0.23	4.52	6.07E-06	0.000371
E130114P18Rik	377.04	-1.03	0.26	3.97	7.33E-05	0.003063
Pgk1	5239.95	-1.03	0.14	7.15	8.73E-13	2.45E-10
Kbtbd11	1282.26	-1.02	0.21	4.98	6.40E-07	5.51E-05
Eya1	356.91	-1.01	0.28	3.68	0.000234	0.007422
Ccnd2	18189.63	-1.01	0.13	7.90	2.78E-15	1.19E-12
Cap2	890.96	-1.00	0.22	4.63	3.65E-06	0.000245

FIGURES AND LEGENDS

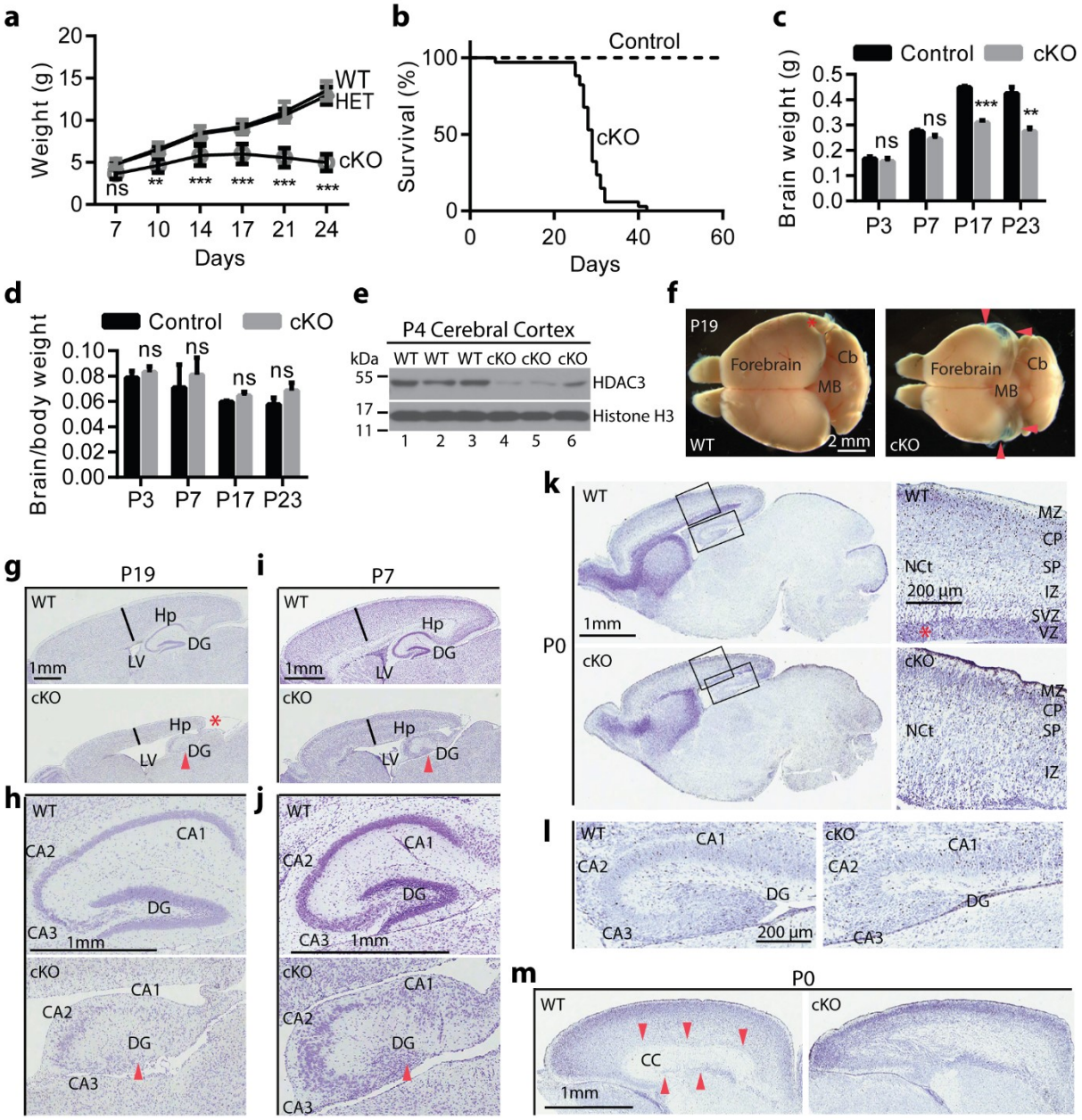

Figure 3.1. Cerebrum-specific loss of *Hdac3* causes severe defects in the neocortex, hippocampus and corpus callosum.

(**a**) Survival curves for control and homozygous mutant mice (n=40 and 38 for the control and cKO groups, respectively). (**b**) Growth curves for wild-type (WT), heterozygous (HET) and homozygous cerebrum-specific knockout (cKO) mice (n=12, 8 and 7 for the wild-type, heterozygous and cKO groups, respectively). cKO was compared with WT for statistical analysis. ns, not statistically significant; **, $p<0.01$; ***, $p<0.001$. (**c, d**) Brain weight and brain/body weight ratio at P3, P7, P17 and P23 (n>= 3 for all groups). (**e**) Western blotting showing efficient deletion of *Hdac3* in the cerebral cortex of mutant pups at P4. (**f**) Representative brain images of the wild-type and cKO mice at P19. Red arrowheads denote cysts in the cKO brain. In the wild-type, an asterisk denotes damage caused during dissection. Scale bar, 2 mm. **(g,i)** Representative images for Nissl staining of WT and cKO brain sections from pups at P19 (**g**) and P7 (**i**). Red arrowheads denote the underdeveloped mutant hippocampi. A red asterisk denotes the region corresponding to the cyst observed in (**f**). Scale bar, 1 mm. **(h,j)** Enlarged images of the hippocampal regions of brain sections shown in (**g,i**). Scale bar, 1 mm. (**k**) Nissl staining of brain sections indicated that the ventricular/subventricular zone almost disappears in the P0 mutant cerebrum. Red asterisk denotes the ventricular/subventricular zone in the wild-type. Scale bar, 1 mm. **(l)** Enlarged images of the hippocampal regions of brain sections shown in (**k**). (**m**) Representative images showing agenesis of the mutant corpus callosum at P0. Red arrowheads denote the boundary of the corpus callosum in the WT cerebral cortex. Scale bar, 1 mm. Abbreviations: CA1, Cornu Ammonis 1; CA2, Cornu Ammonis 2; CA3, Cornu Ammonis 3; Cb, cerebellum; CC, corpus callosum; CP, cortical plate; DG, dentate gyrus; Hp, hippocampus; IZ, intermediate zone; LV, lateral ventricle; MB, middle brain; MZ, marginal zone; NCt, neocortex; SP, subplate; SVZ, subventricular zone; VZ, subventricular zone.

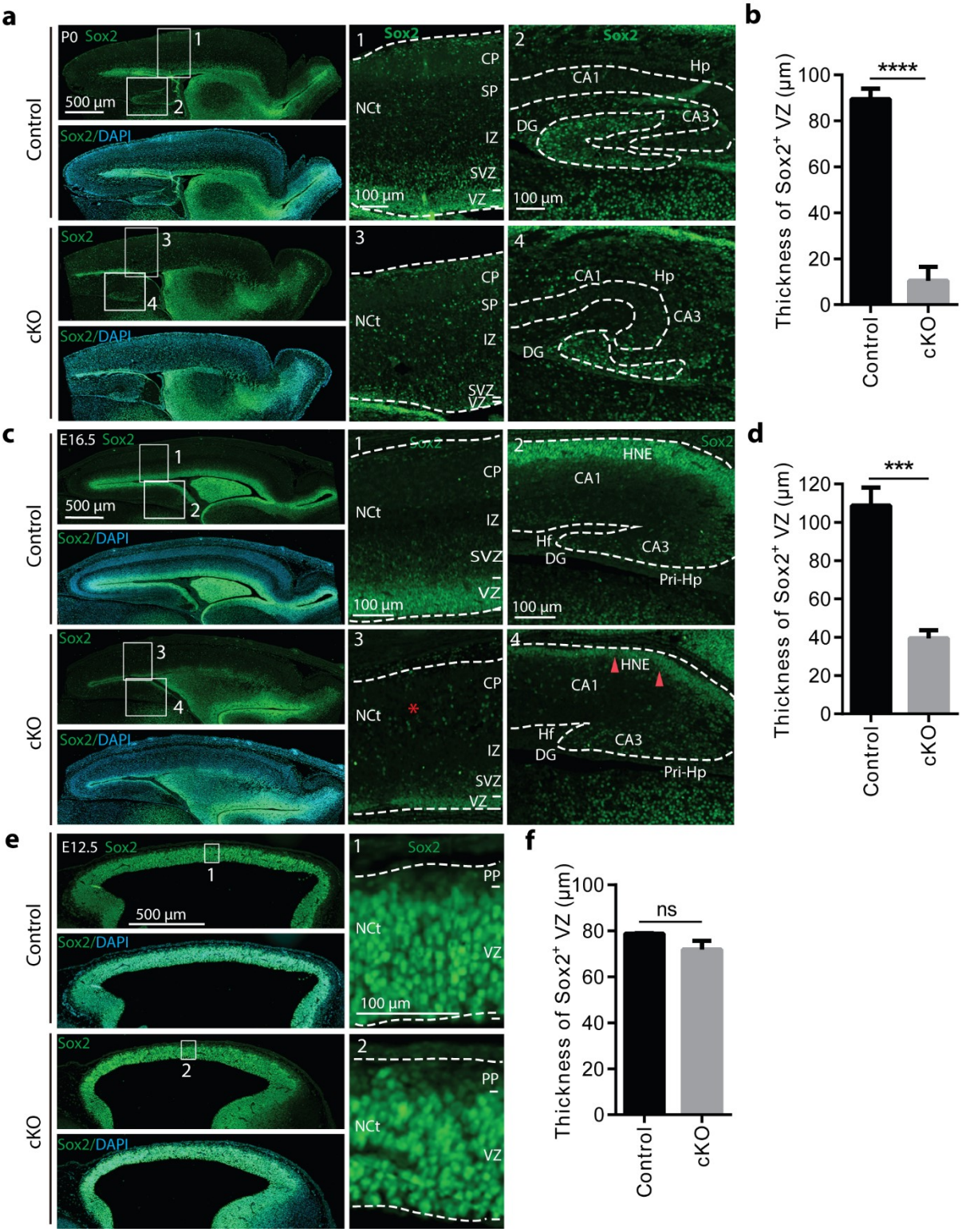
a
P0 Sox2
500 μm
Sox2/DAPI
Control
cKO
Sox2
CP
SP
NCt
IZ
SVZ
VZ
100 μm
CA1
Hp
CA3
DG
b
Thickness of Sox2+ VZ (μm)
****
Control
cKO
c
E16.5 Sox2
HNE
Hf
Pri-Hp
d
***
e
E12.5 Sox2
PP
f
ns

Figure 3.2. Cerebrum-specific *Hdac3* deletion compresses the NSC compartment.

(**a,b**) Immunostaining analysis with an anti-Sox2 antibody showed almost complete disappearance of $Sox2^+$ cells in the VZ of the mutant cerebral cortex at P0 (n=4 for both the wild-type and mutant). Scale bar, 500 μm for the left panels; 100 μm for the middle and right panels. (**c,d**) Immunostaining analysis revealed reduction of $Sox2^+$ cells in the VZ of mutant cerebral cortex at E16.5 (n=4 for both the wild-type and mutant). Scale bar, 500 μm for the left panels; 100 μm for the middle and right panels. Red arrowheads denote a thinner layer of the hippocampal neuroepithelium in the mutant. (**e**) Immunostaining analysis to compare the wild-type and mutant $Sox2^+$ cells at E12.5. Scale bar, 500 μm for left panel, 100 μm for right panel. (**f**) Thickness of the $Sox2^+$ layer at the VZ is comparable between control and cKO cerebral cortex at E12.5 (n=3 for both the wild-type and mutant). Red asterisk denotes the ectopic distribution of $Sox2^+$ cells. Abbreviations: Hf, hippocampal fissure; HNE, hippocampal neuroepithelium; Pri-Hp, primordial hippocampus. Other abbreviations are listed in the legend to Fig. 3.1. ns, not statistically significant; ***, $p<0.001$; ****, $p<0.0001$.

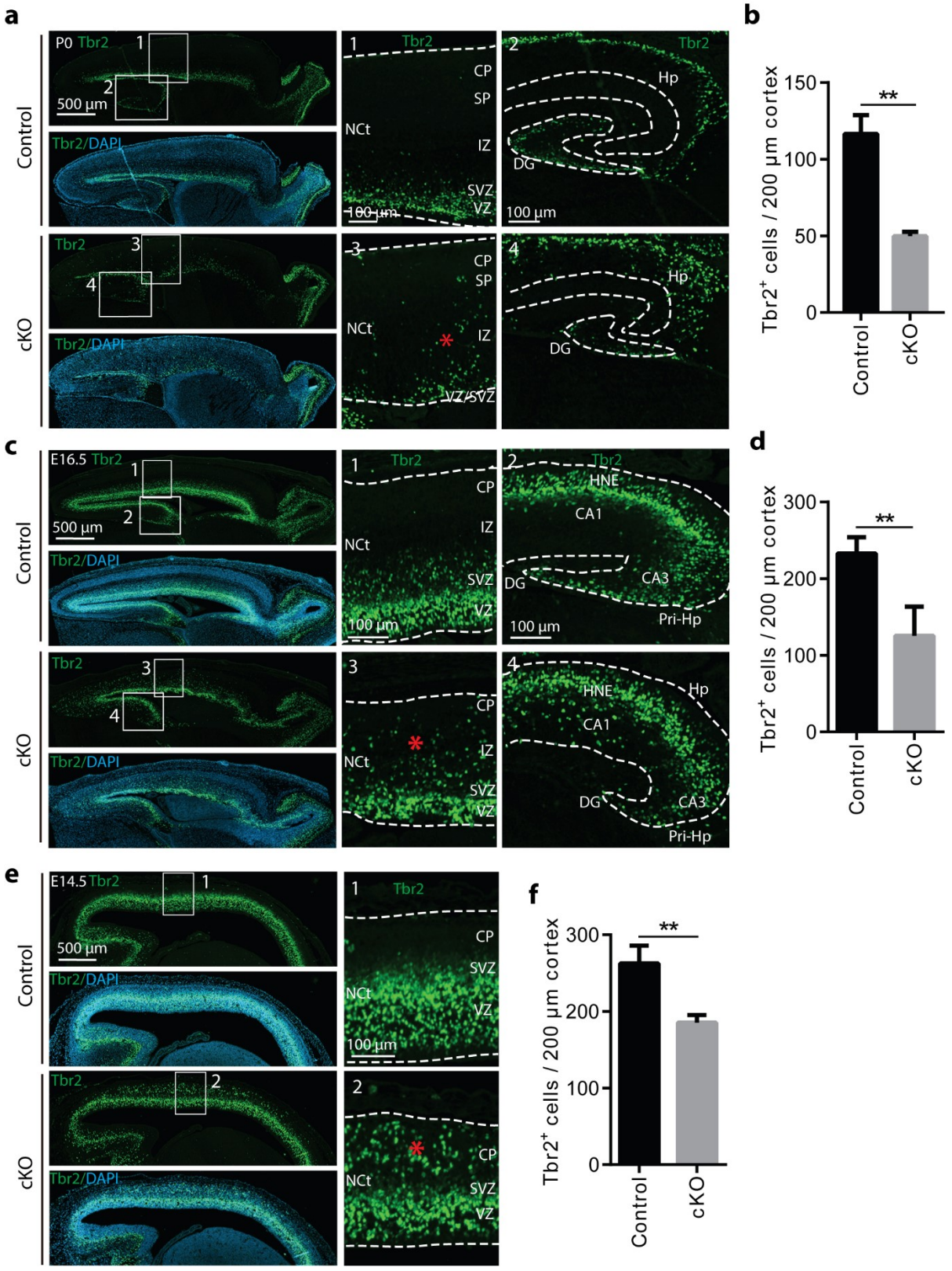
a
P0 Tbr2
500 µm
Tbr2/DAPI
Control
cKO
CP
SP
IZ
SVZ
VZ
NCt
Hp
DG
100 µm
b
Tbr2+ cells / 200 µm cortex
150
100
50
0
**
Control
cKO
c
E16.5 Tbr2
HNE
CA1
CA3
Pri-Hp
d
300
200
e
E14.5 Tbr2
f

Figure 3.3. Cerebral *Hdac3* inactivation depletes the Tbr2$^+$ neuronal progenitor population.

(**a**) Immunostaining analysis with an anti-Tbr2 antibody to detect Tbr2$^+$ progenitors in brain sections from wild-type and mutant neonates. Scale bar, 500 μm for left panels; 100 μm for middle or right panels. Red asterisks denote the ectopic distribution of Tbr2$^+$ progenitors. (**b**) Quantification of Tbr2$^+$ progenitors from sections as shown in (**a**) (n=4). (**c**) Same as in (**a**) except that E16.5 embryonic sections were analyzed. Scale bar 500 μm for left panel, 100 μm for middle or right panels. Red asterisks denote the ectopic distribution of Tbr2$^+$ progenitors. Dotted lines denote the boundary of the hippocampus and neocortex. (**d**) Quantification of Tbr2$^+$ progenitors from sections as shown in (**c**) (n=4). (**e**) Same as (a) except that E14.5 embryonic sections were analyzed. (**f**) Quantification of Tbr2$^+$ progenitors from sections as shown in (**e**). The number of Tbr2$^+$ progenitor cells is comparable at E12.5 (n=3) are significantly reduced at E14.5 and E16.5 (n=4). **, $p<0.01$.

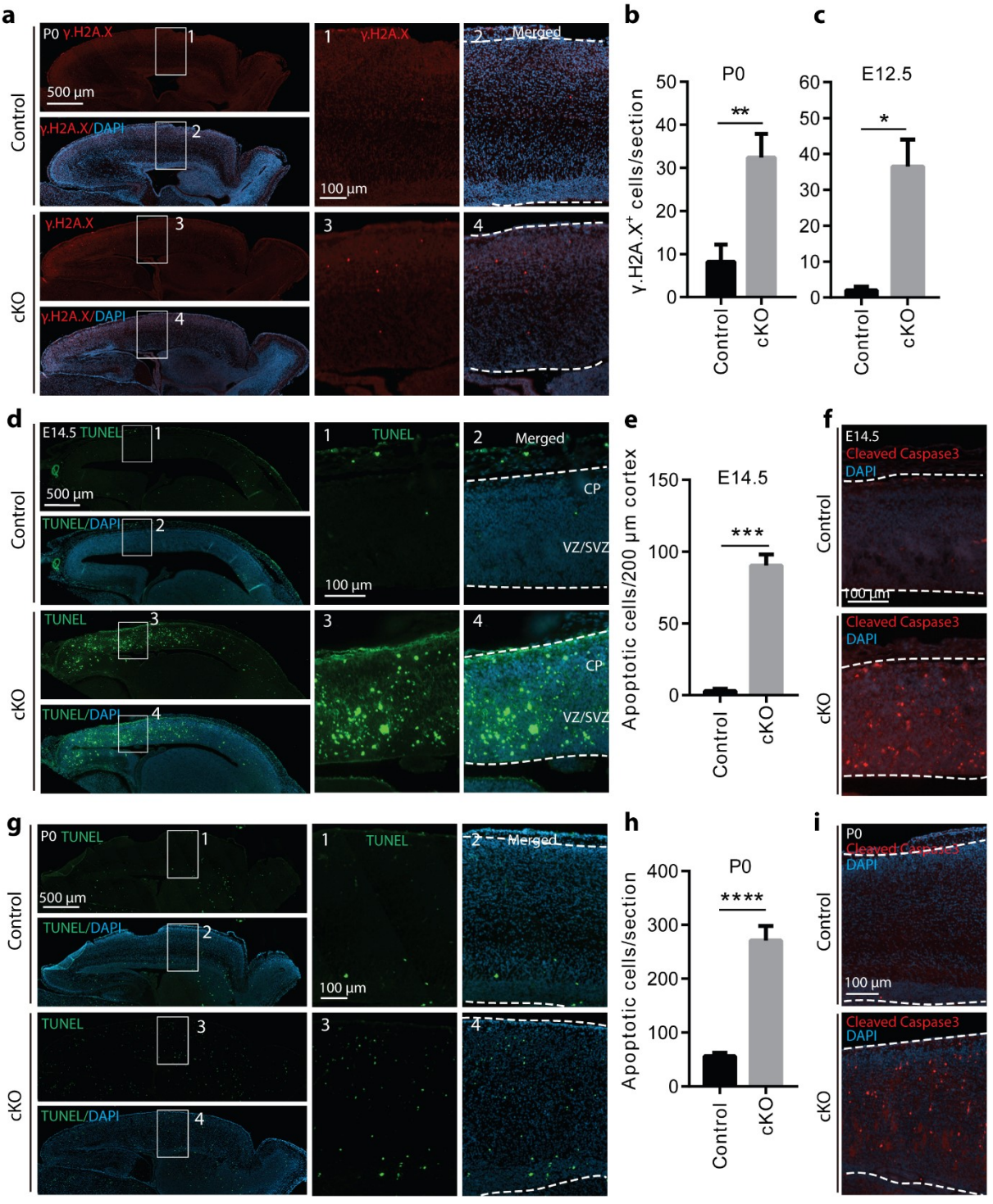
a
P0 γ.H2A.X
500 μm
γ.H2A.X/DAPI
Control
cKO
100 μm
Merged
b
P0
γ.H2A.X+ cells/section
**
Control
cKO
c
E12.5
*
d
E14.5 TUNEL
TUNEL/DAPI
TUNEL
CP
VZ/SVZ
e
E14.5
Apoptotic cells/200 μm cortex
***
f
E14.5
Cleaved Caspase3
DAPI
g
P0 TUNEL
h
P0
Apoptotic cells/section
****
i
P0

Figure 3.4. Cerebral *Hdac3* loss causes DNA damage and massive apoptosis.

(**a**) Immunostaining of wild-type and mutant neonatal brain sections with an anti-γH2A.X antibody. Scale bar, 500 μm for the left panels; 100 μm for the middle and right panels. (**b**) Quantification of sections shown in (**a**) showing that there are dramatically more γH2A.X^{+} cells in the mutant cerebral cortex than the wild-type (n=3). (**c**) Quantification of sections as in (**b**) except that E12.5 embryonic sections were analyzed (n=3). (**d**) TUNEL staining in control and cKO neonatal brain sections. Scale bar, 500 μm for left panel, 100 μm for middle and right panels. (**e**) Quantification of TUNEL-positive cells in neonatal brain sections as shown in (**d**). (**f**) TUNEL staining in control and cKO embryonic sections at E14.5. For (**d,f**), Scale bar, 500 μm for left panel, 100 μm for middle and right panels. (**g**) Quantification of TUNEL-positive cells in neonatal brain sections as shown in (**f**). *, $p<0.05$, **, $p<0.01$.

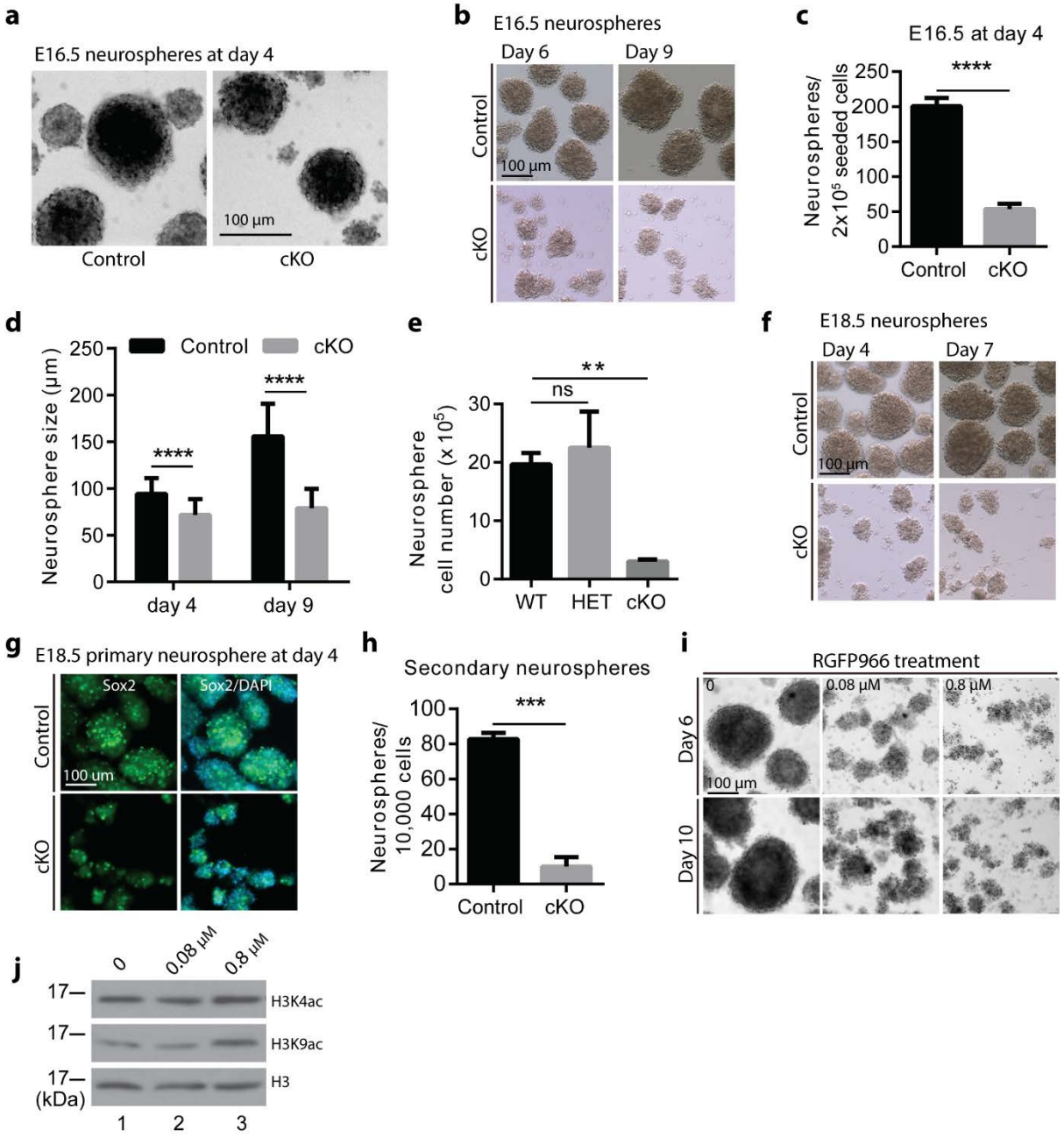
a
E16.5 neurospheres at day 4
100 µm
Control
cKO
b
E16.5 neurospheres
Day 6
Day 9
Control
cKO
100 µm
c
E16.5 at day 4
****
Neurospheres/ 2x10⁵ seeded cells
250
200
150
100
50
0
Control
cKO
d
Control
cKO
Neurosphere size (µm)
250
200
150
100
50
0
****
****
day 4
day 9
e
**
ns
Neurosphere cell number (x 10⁵)
30
20
10
0
WT
HET
cKO
f
E18.5 neurospheres
Day 4
Day 7
Control
cKO
100 µm
g
E18.5 primary neurosphere at day 4
Sox2
Sox2/DAPI
Control
cKO
100 µm
h
Secondary neurospheres
***
Neurospheres/ 10,000 cells
100
80
60
40
20
0
Control
cKO
i
RGFP966 treatment
0
0.08 µM
0.8 µM
Day 6
Day 10
100 µm
j
0
0.08 µM
0.8 µM
17—
H3K4ac
17—
H3K9ac
17—
H3
(kDa)
1
2
3

Figure 3.5. HDAC3 is essential for neurosphere formation *in vitro*.

(**a**) Normal round morphology of the mutant neurospheres at day 4. The suspended single cells from wild-type and cKO cerebral cortices were cultured in the complete NSC medium. In the first 4 days, the morphology of *Hdac3*-deficient neurospheres was similar to that of the wild-type counterparts. Scale bar, 100 μm. (**b**) Photos of wild-type and mutant neurospheres at day 6 and day 9. (**c**) Quantification of neurospheres formed from $2x10^5$ single cells prepared from the E16.5 wild-type or mutant cerebral cortex (n=3). (**c**) Numbers of neurospheres formed from 20,000 single cells originated from E16.5 primary neurospheres. (**d**) Diameter of neurospheres grown for 4 days from the cerebral cortices of control and mutant embryos at E16.5 (>50 neuropheres were measured for each group). (**e**) Total cell number in neurospheres from the wild-type, heterozygous and homozygous mutant cerebral cortices. n=5, 2 and 3 for the wild-type, heterozygotes and homozygous mutant cerebral cortices, respectively. (**f**) Morphology of E18.5 primary neurospheres at day 4 and day 7. The wild-type neuropheres were round sphere while the mutant ones were irregular. (**g**) Immunofluorescence staining of E18.5 neurospheres with an antibody against Sox2 and counterstained with DAPI. (**h**) Quantification of neurospheres formed from $2x10^5$ single cells prepared from the E18.5 wild-type or mutant primary neurospheres (n=3). (**i**) Treatment of E18.5 wild-type neurospheres using the selective HDAC3 inhibitor RGFP966 at concentrations of 0, 0.08 and 0.8 μM. The IC50 value of this inhibitor is 0.08 μM (410). The HDAC3 inhibitor was added to the initial culture medium for single cells prepared from cerebral cortices. ns, not statistically significant; **, $p<0.01$; ***, $p<0.001$; ****, $p<0.0001$. Scale bar, 100 μm. (**j**) Western blotting analysis of proteins extracts from wild-type neurospheres treated with RGFP966 at concentration of 0, 0,08 and 0.8 μM. Anti-histone H3 and two acetylation-specific antibodies were used to detect changes of acetylation.

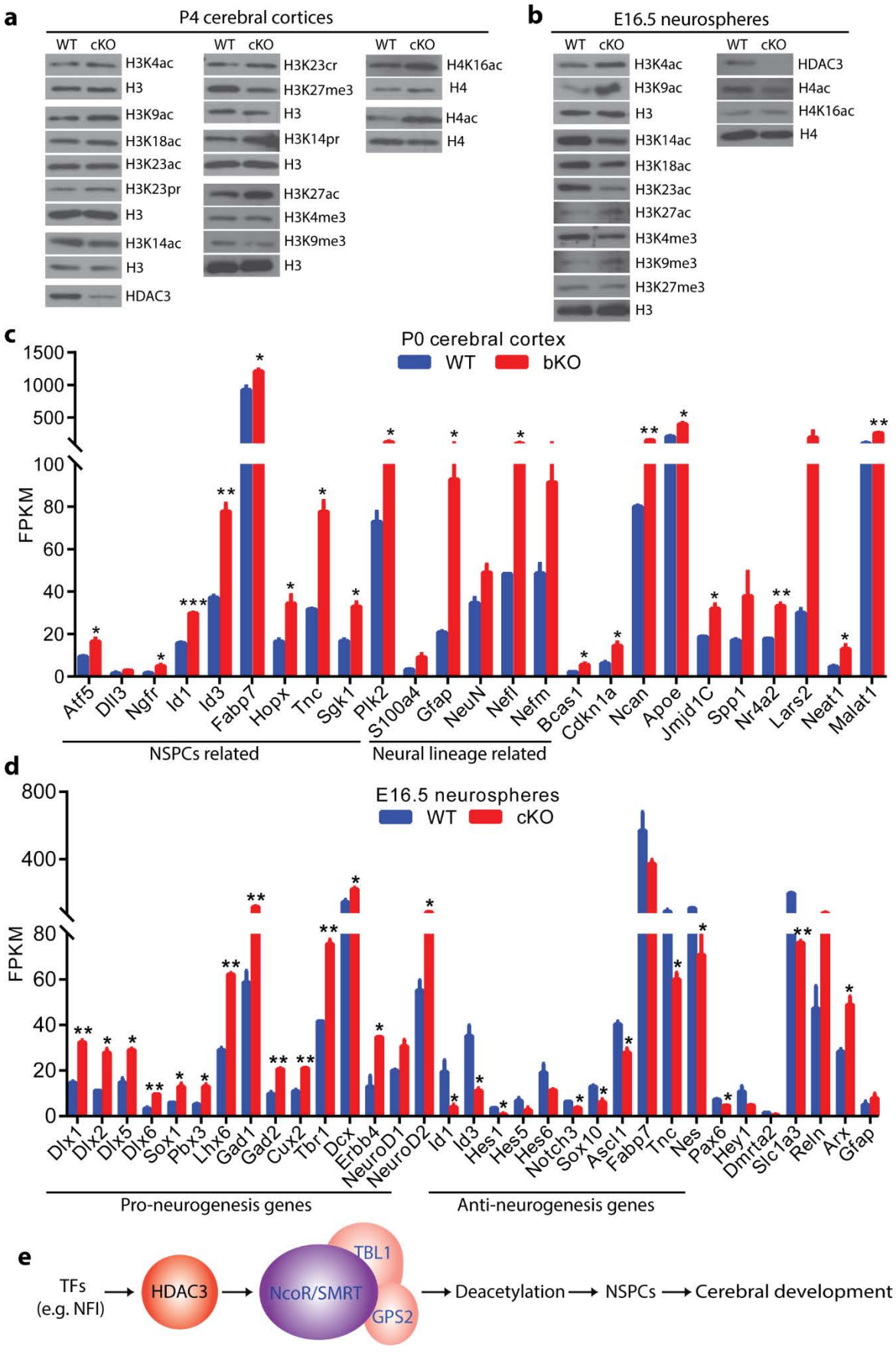
a
P4 cerebral cortices
WT cKO
H3K4ac
H3
H3K9ac
H3K18ac
H3K23ac
H3K23pr
H3
H3K14ac
H3
HDAC3
H3K23cr
H3K27me3
H3
H3K14pr
H3
H3K27ac
H3K4me3
H3K9me3
H3
H4K16ac
H4
H4ac
H4
b
E16.5 neurospheres
H3K4ac
H3K9ac
H3
H3K14ac
H3K18ac
H3K23ac
H3K27ac
H3K4me3
H3K9me3
H3K27me3
H3
HDAC3
H4ac
H4K16ac
H4
c
P0 cerebral cortex
WT
bKO
FPKM
Atf5
Dll3
Ngfr
Id1
Id3
Fabp7
Hopx
Tnc
Sgk1
Plk2
S100a4
Gfap
NeuN
Nefl
Nefm
Bcas1
Cdkn1a
Ncan
Apoe
Jmjd1C
Spp1
Nr4a2
Lars2
Neat1
Malat1
NSPCs related
Neural lineage related
d
E16.5 neurospheres
WT
cKO
FPKM
Dlx1
Dlx2
Dlx5
Dlx6
Sox1
Pbx3
Lhx6
Gad1
Gad2
Cux2
Tbr1
Dcx
Erbb4
NeuroD1
NeuroD2
Id1
Id3
Hes1
Hes5
Hes6
Notch3
Sox10
Ascl1
Fabp7
Tnc
Nes
Pax6
Hey1
Dmrta2
Slc1a3
Reln
Arx
Gfap
Pro-neurogenesis genes
Anti-neurogenesis genes
e
TFs
(e.g. NFI)
HDAC3
NcoR/SMRT
TBL1
GPS2
Deacetylation
NSPCs
Cerebral development

Figure 3.6. *Hdac3* deletion alters epigenetic marks differently in the cerebral cortex and neurospheres.

(**a**) Western blotting analysis of proteins extracts from cerebral cortices of the control and mutant pups at P4. Modification-specific antibodies were used to detect changes of histone acetylation and methylation. As shown in Fig. 3.1e, HDAC3 was efficiently deleted (compare the two panels at the bottom left here). Notably, the deletion led to histone hyperacetylation and hypomethylation at multiple sites. (**b**) Same as (**a**) except that proteins extracts from neurospheres cultured from the control and mutant cerebral cortices of embryos at E16.5. (**c**) *Hdac3* deletion altered transcription of multiple genes related to NSPC and lineage cell development in neonatal (P0) cerebral cortex. Illustrated are FPKM values of genes related to NPSC and lineage cell development, and other potential genes in brain development. The values were from RNA-Seq analysis of the wild-type and mutant neonatal cerebral cortices. (**d**) *Hdac3* loss deregulated transcription of multiple genes related to neurogenesis in neurospheres. Illustrated are FPKM values of pro- and anti-neurogenesis genes, and some other genes related to NSCs function. The values were from RNA-Seq analyses of neurospheres cultured for 4 days *in vitro* from the wild-type and mutant embryos at E16.5. (**e**) A model explaining how multiple DNA-binding transcription factors recruit HDAC3 and its associated subunits for genomic loci-specific deacetylation during NSPC and cerebral development. TF, DNA-binding transcription factor.

SUPPLEMENTAL FIGURES AND LEGE

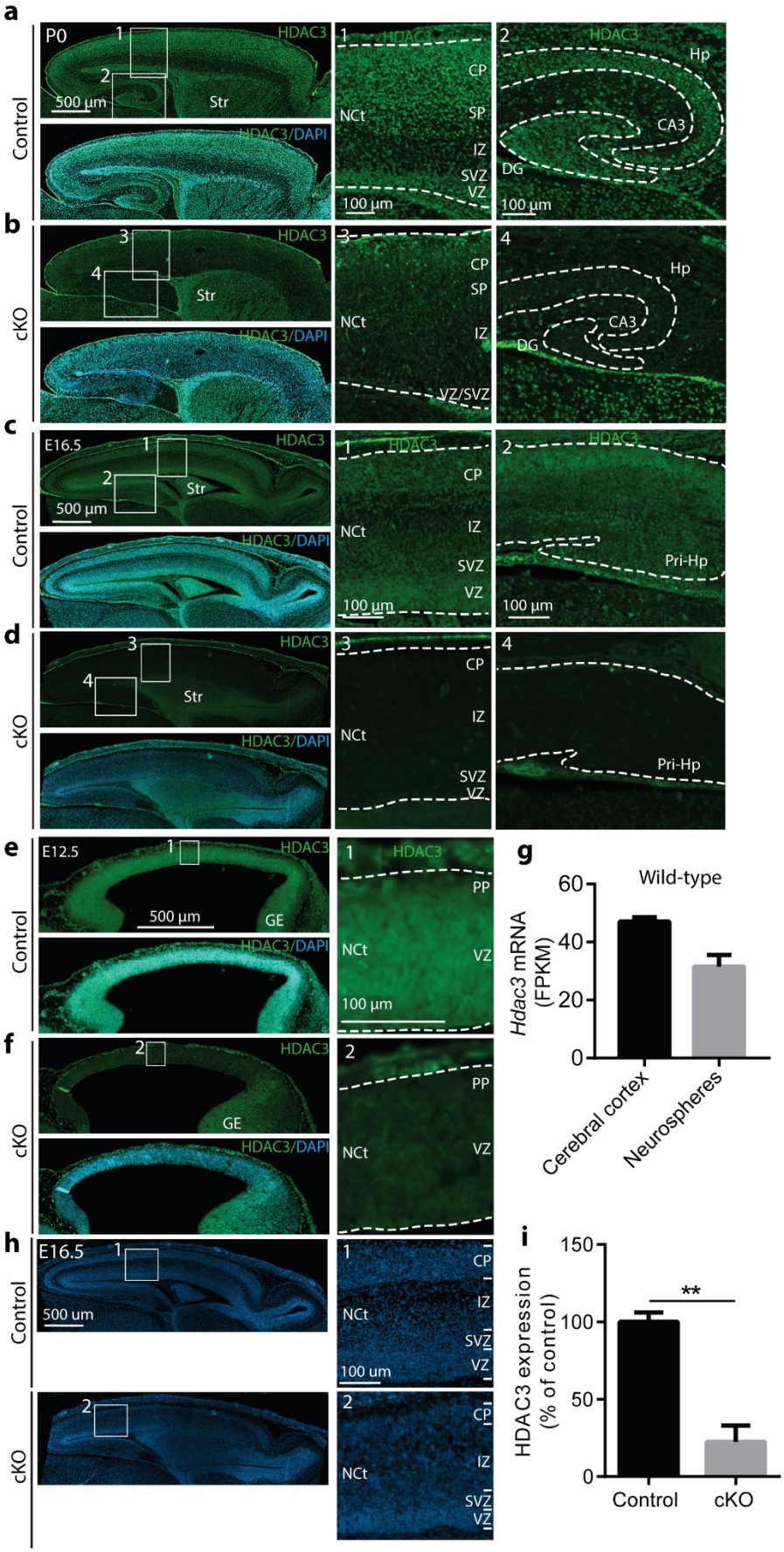

Figure S3.1. High-level expression of *Hdac3* in the developing cerebrum and efficient inactivation of the gene in the mutant embryos and mice.

(a,b) Immunostaining with an anti-HDAC3 antibody in the wild-type (**a**) and mutant (**b**) neonatal brain sections. Enlarged images of the neocortices and hippocampi are shown at the right. Scale bars, 500 μm for the left panel, and 100 μm for the middle and right panels. **(c,d)** Immunostaining for HDAC3 in the wild-type (**c**) and mutant (**d**) brain sections from E16.5 embryos. Enlarged images of the neocortices and hippocampi are shown at the right. Scale bar, 500 μm for the left panel and 100 μm for the middle and right panels. (**e,f)** Immunostaining to detect HDAC3 in the wild-type (**c**) and mutant (**d**) E12.5 embryonic sections. Enlarged images of the neuroepithelia are shown at the right. Scale bars, 500 μm for the left panel and 100 μm for the right panels. **(g)** FPKM values for *Hdac3* mRNA in the wild-type cerebral cortex at P0 and the wild-type NSPCs cultured from E16.5 embryos. (**h**) DAPI staining of E16.5 embryonic sections uncovered compression of VZ/SVZ and disorganization of the cerebral cortex in the mutant. Scale bars, 500 μm for the left panel and 100 μm for the right panels. (**i**) Quantification of the HDAC3 levels in the wild-type and mutant cerebral cortices. The immunoblotting results shown in Fig. 3.1e were subject to quantification by imaging analysis, and the average values are shown here. Abbreviations are listed in the legend to Fig. 3.1.

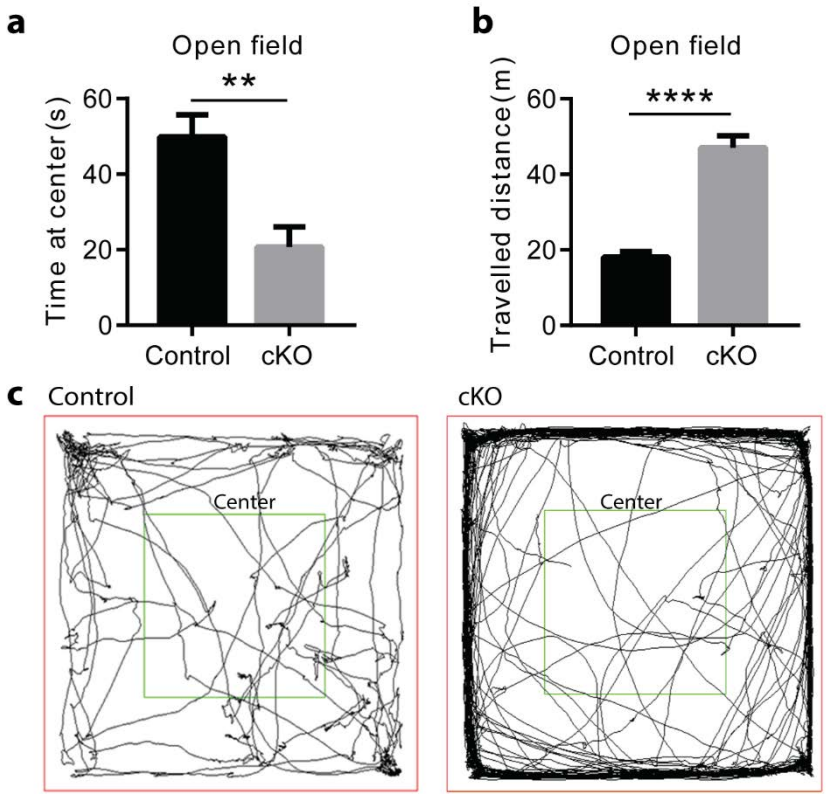

Figure S3.2. Anxiety and hyperactivity in cerebrum-specific *Hdac3* knockouts revealed by open field tests.

(**a**) Time spent at the center of the test arena was significantly reduced in the mutant mice (n=6 for both the wild-type and mutant). (**b**) Total distance that the mutant mice travelled during the open field tests was significantly increased. (**c**) Representative trajectory maps for the control and cKO mice at P22. Red boxes indicate open field arenas (40 cm x 40 cm), and the green boxes denote centers of the arenas (20 cm x 20 cm).

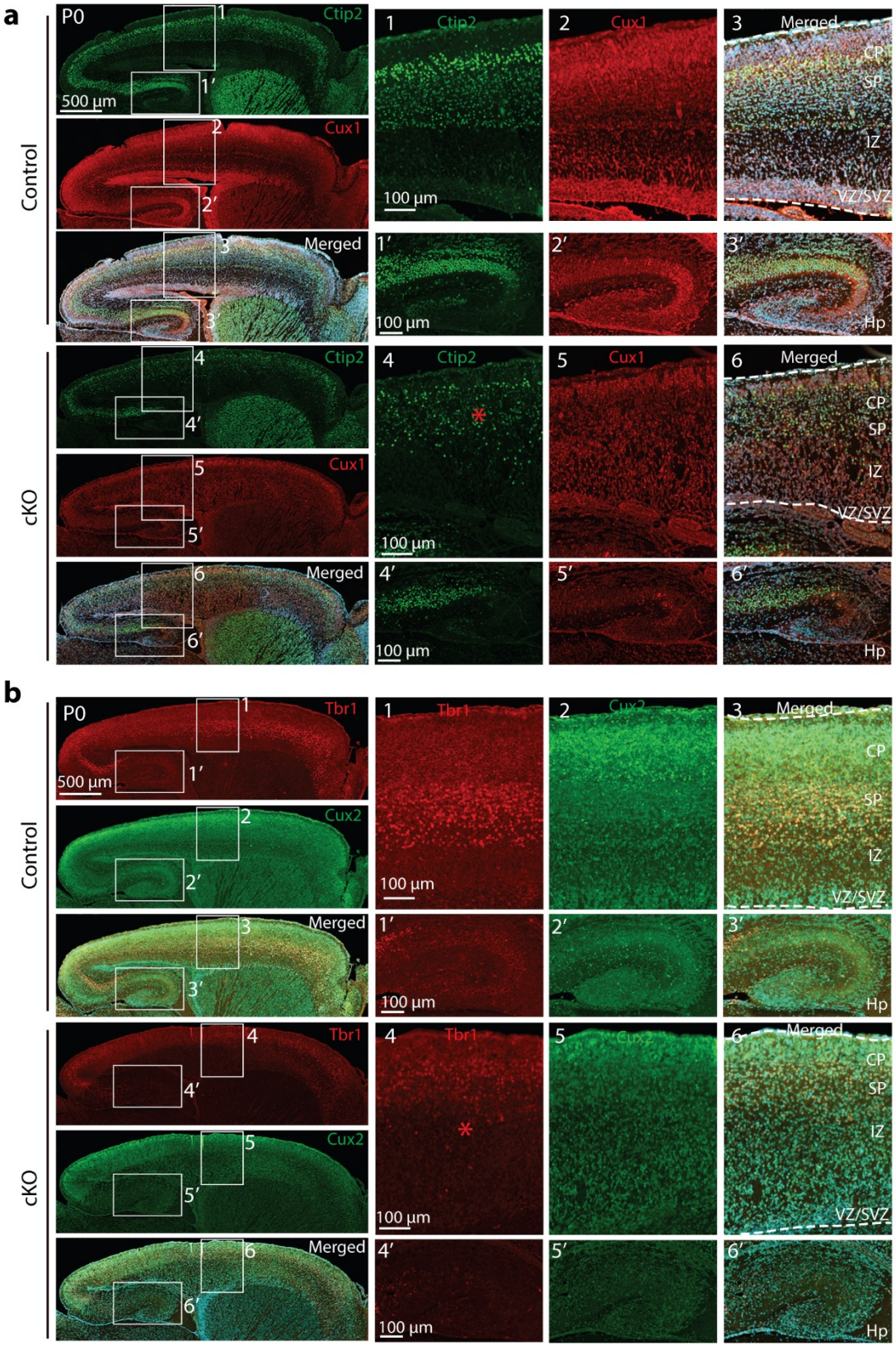
a
Control
cKO
P0
Ctip2
Cux1
Merged
500 μm
100 μm
CP
SP
IZ
VZ/SVZ
Hp
b
Tbr1
Cux2

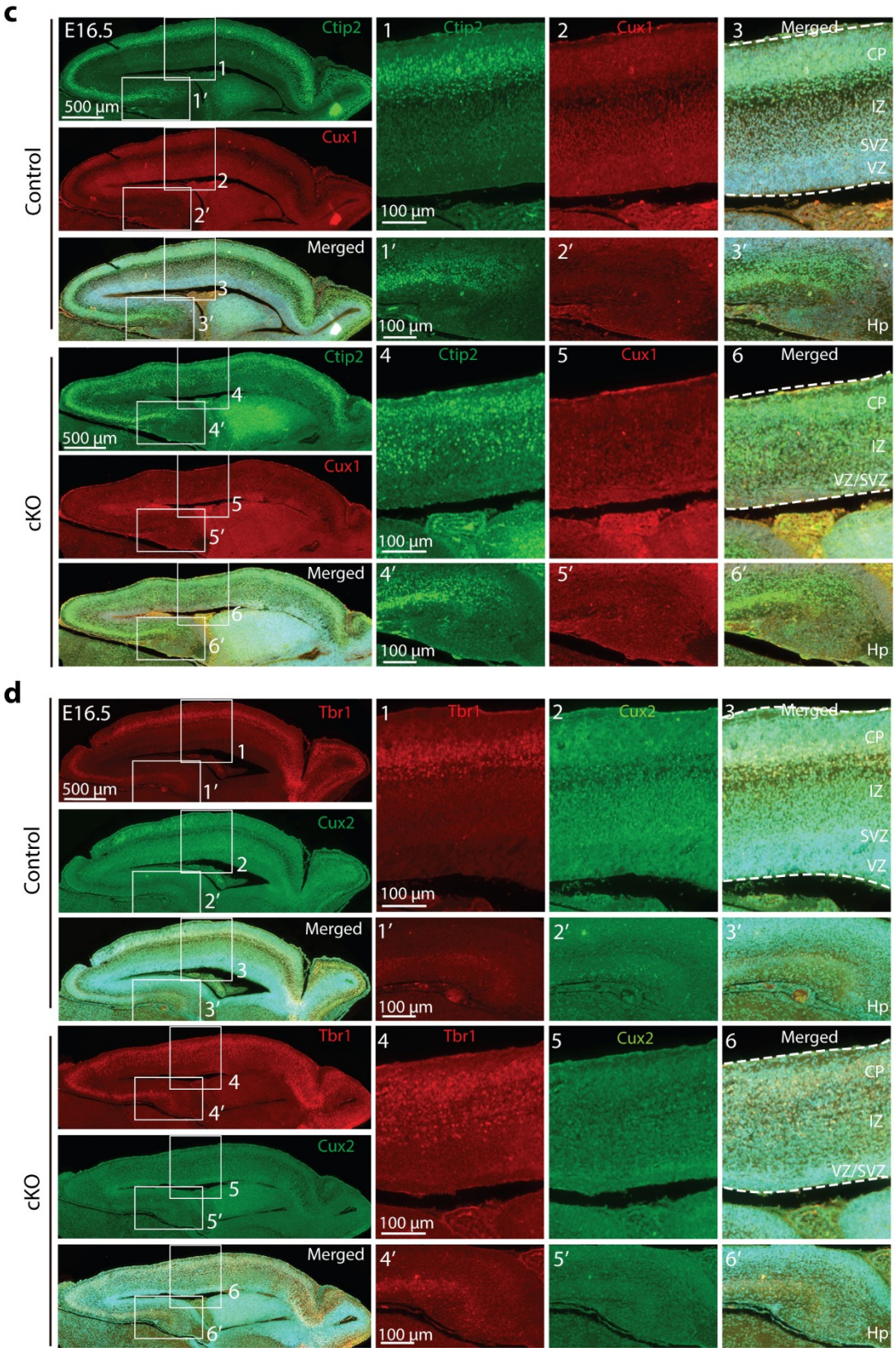
c
Control
cKO
E16.5
Ctip2
Cux1
Merged
500 μm
100 μm
CP
IZ
SVZ
VZ
VZ/SVZ
Hp
d
Tbr1
Cux2

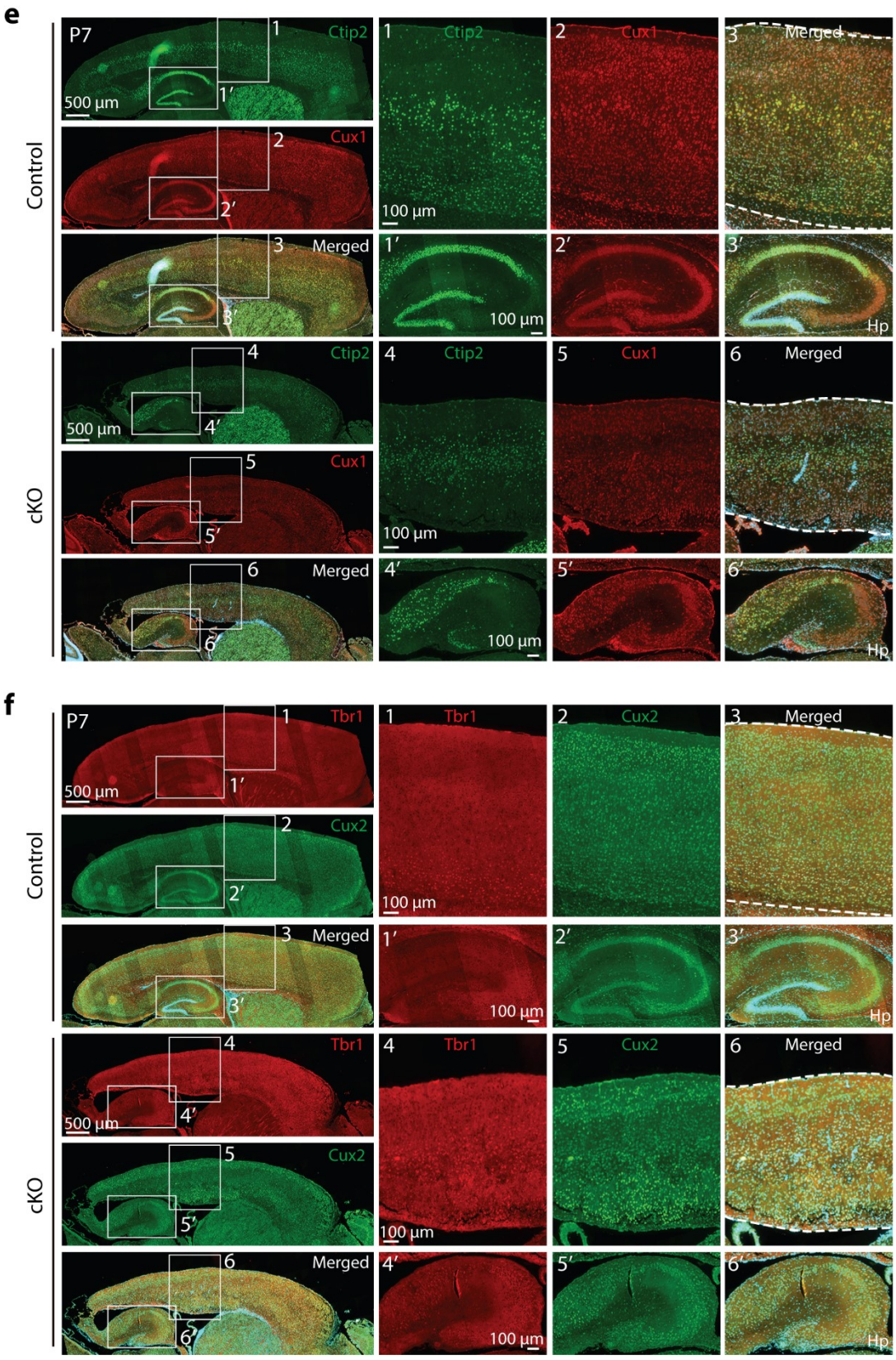
e
Control
cKO
P7
Ctip2
Cux1
Merged
500 µm
100 µm
Hp
f
Control
cKO
P7
Tbr1
Cux2
Merged
500 µm
100 µm
Hp

Figure S3.3. Defective neocortical lamination and hippocampal development in the *Hdac3*-deficient brain.

(**a**) Co-immunostaining of wild-type and mutant neonatal brain sections with anti-Cux1 and -Ctip2 antibodies. In the neonatal neocortex, the antibodies label the $Cux1^+$ (labels SVZ and layers II-IV of adult neocortex (411)) and $Ctip2^+$ (labels layers V-VI of adult neocortex (412)) layers. A red asterisk denotes a disorganized $Ctip2^+$ layer in the mutant. (**b**) Co-immunostaining of wild-type and mutant neonatal brain sections with anti-Tbr1 and -Cux2 antibodies. In the neonatal neocortex, the antibodies label the $Tbr1^+$ (labels layer VI in adult neocortex (413)) and $Cux2^+$ (labels layers II-IV of adult neocortex (411)) layers. A red asterisk denotes the ectopic distribution of $Tbr1^+$ cells. Scale bar, 500 μm for left panels, 100 μm for the rest panels. (**c,d**) Same as (**a,b**) except E16.5 wild-type and mutant embryonic sections were compared. (**e,f**) Same as (**a,b**) except P7 wild-type and mutant brain sections were compared. Abbreviations are listed in the legend to Fig. 3.1.

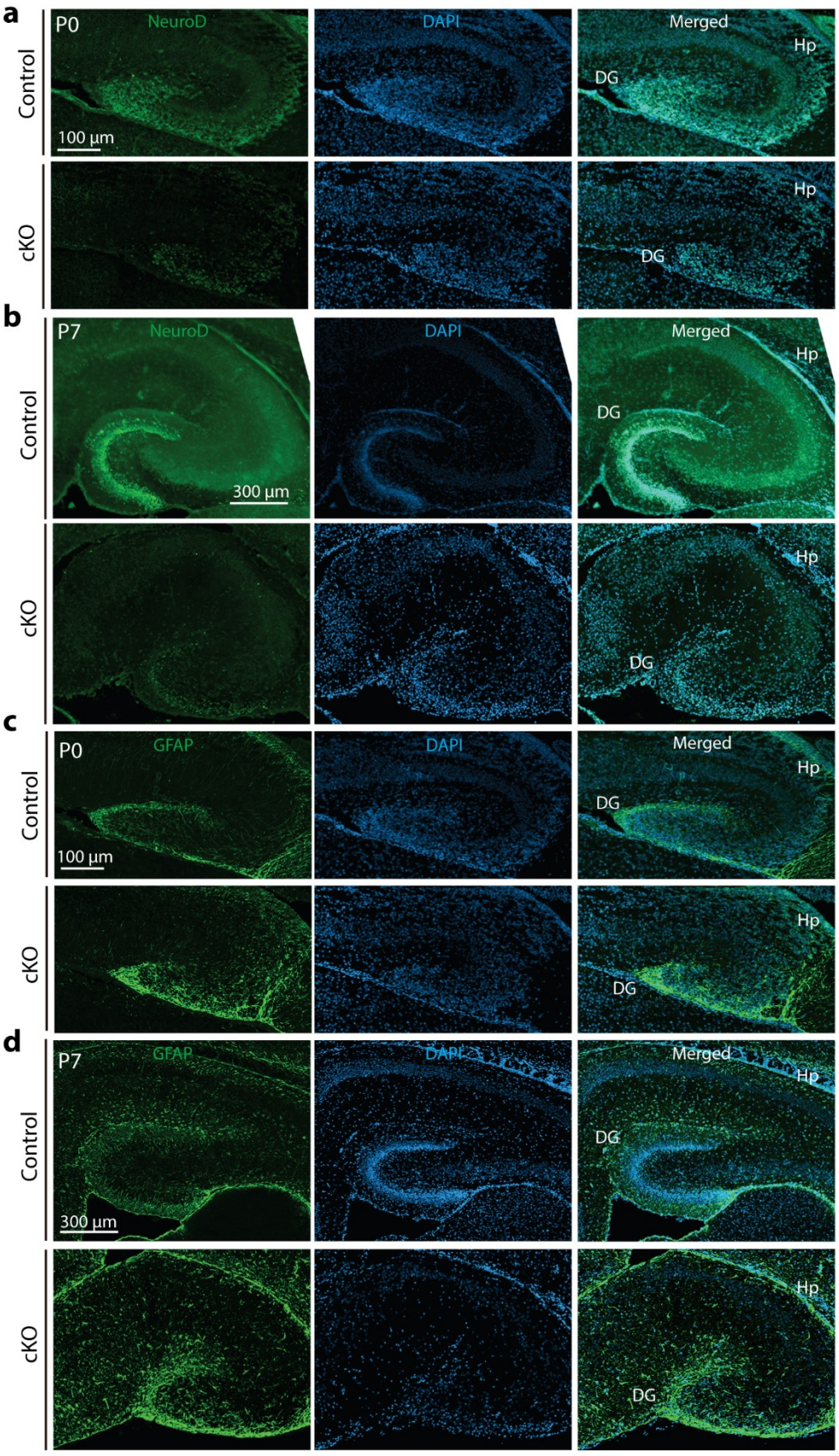
a
P0
NeuroD
DAPI
Merged
Hp
DG
Control
100 µm
cKO
b
P7
NeuroD
DAPI
Merged
Hp
DG
Control
300 µm
cKO
c
P0
GFAP
DAPI
Merged
Hp
DG
Control
100 µm
cKO
d
P7
GFAP
DAPI
Merged
Hp
DG
Control
300 µm
cKO

Figure S3.4. Immunostaining to detect NeuroD and GFAP in wild-type and mutant hippocampi.

(**a**) Immunofluorescence microscopic analysis of neonatal brain sections with an anti-NeuroD antibody. For the analysis, brains sections were prepared from one-week old wild-type and mutant pups. Only the hippocampal areas are shown here. The images illustrate disorganization of $NeuroD^{+}$ neurons in the mutant hippocampus and low expression of NeuroD in these neurons. (**b**) Same as (**a**) except that P7 brain sections were analyzed. (**c**,**d**) Same as (**a,b**) except that an anti-GFAP antibody was used. Scale bar, 300 μm for a and c; 100 μm for b and d. Abbreviations are listed in the legend to Fig. 3.1.

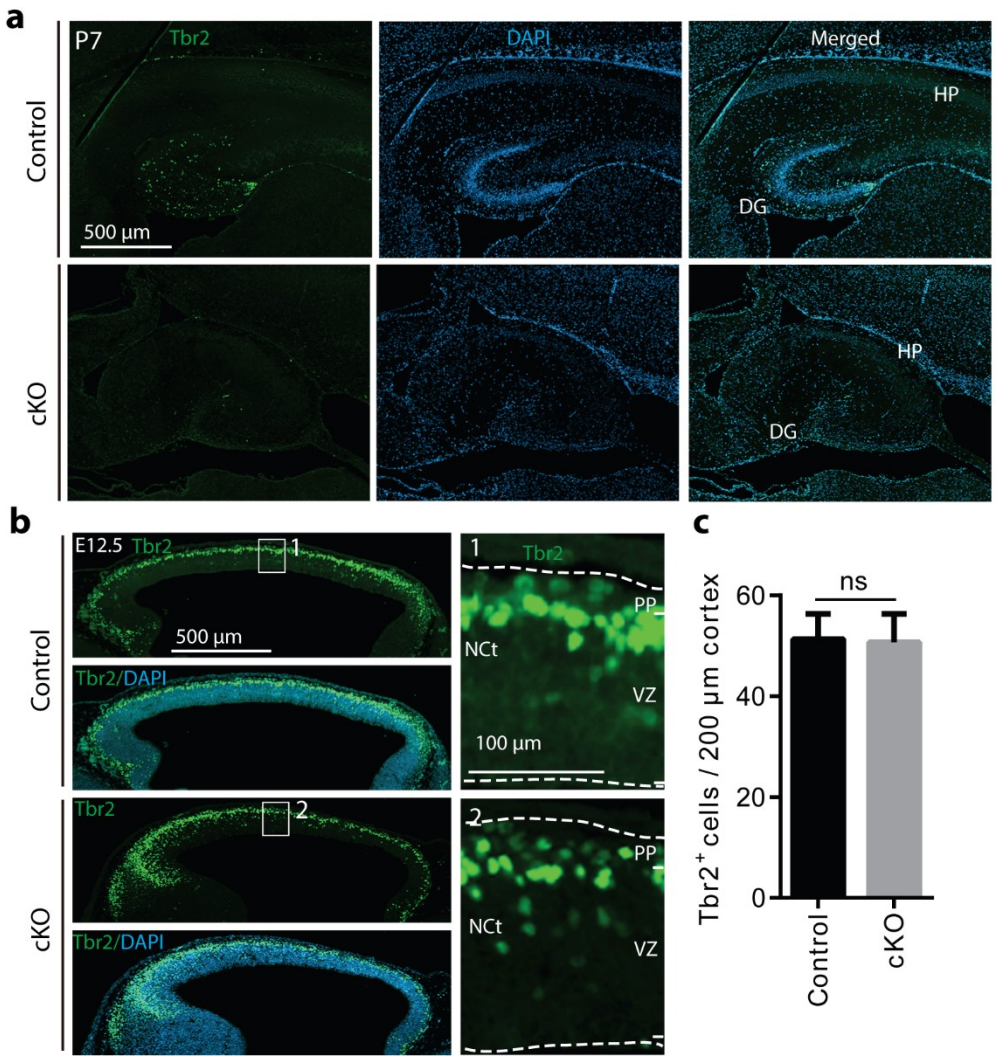

Figure S3.5. Detection of Tbr2$^+$ progenitor populations in one-week pups and E12.5 embryos.

(**a**) Immunostaining of brain sections with an anti-Tbr2 antibody. Brains sections were prepared from E12.5 wild-type and mutant embryos. Scale bars: 500 µm for the left panels and 100 µm for the middle or right panels. Dotted lines mark boundaries of the neuroepithelia. (**b**) Quantification of Tbr2$^+$ progenitors. n=3; ns, not statistically significant. (**c**) same as (**a**) except that P7 brain sections were analyzed. Only the hippocampal areas are shown here. The images illustrate few Tbr2$^+$ progenitors in the mutant hippocampus. Scale bar, 500 µm.

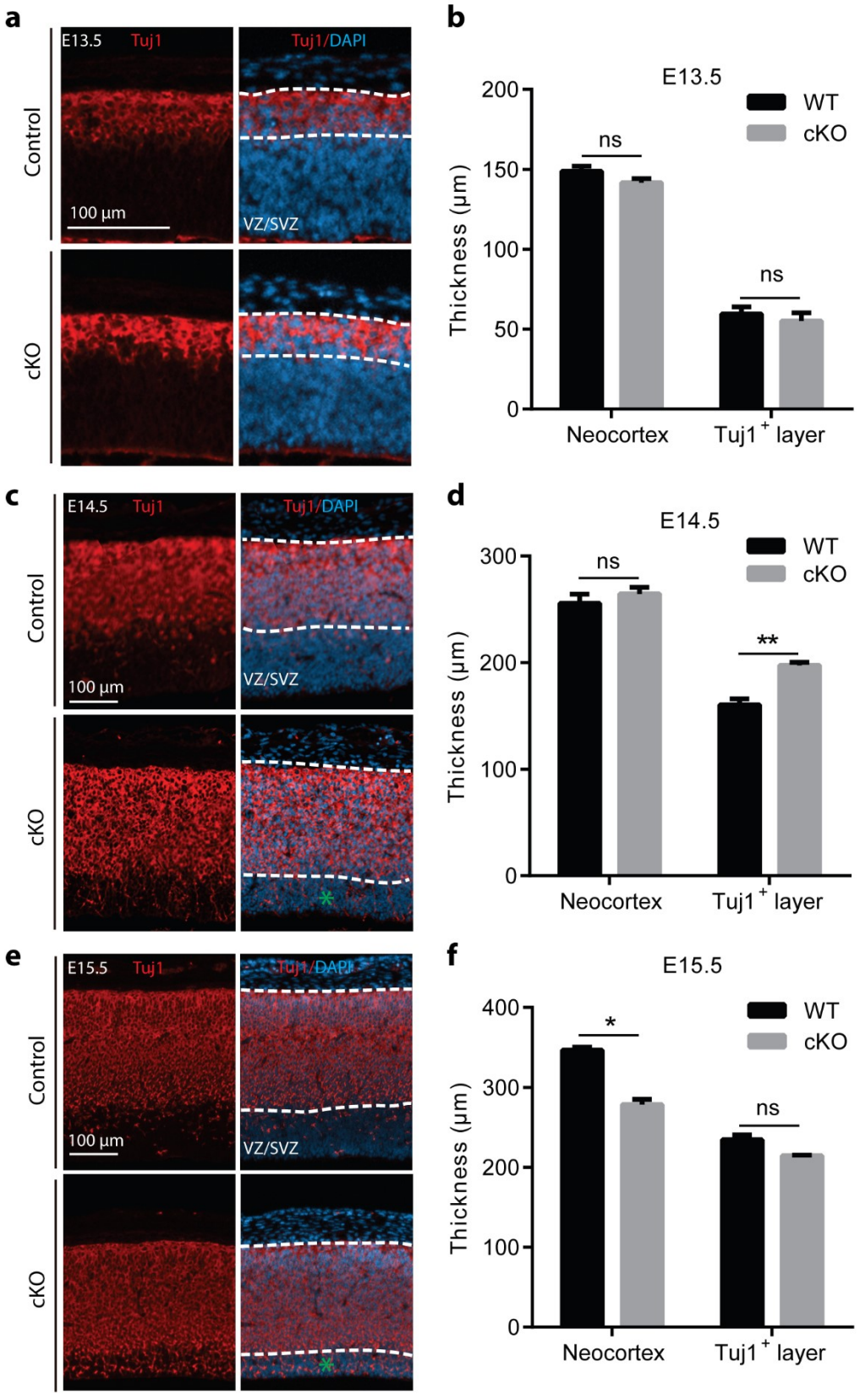
a
E13.5
Tuj1
Tuj1/DAPI
Control
cKO
100 µm
VZ/SVZ
b
E13.5
WT
cKO
Thickness (µm)
200
150
100
50
0
ns
ns
Neocortex
Tuj1+ layer
c
E14.5
Tuj1
Tuj1/DAPI
Control
cKO
100 µm
VZ/SVZ
d
E14.5
WT
cKO
Thickness (µm)
300
200
100
0
ns
**
Neocortex
Tuj1+ layer
e
E15.5
Tuj1
Tuj1/DAPI
Control
cKO
100 µm
VZ/SVZ
f
E15.5
WT
cKO
Thickness (µm)
400
300
200
100
0
*
ns
Neocortex
Tuj1+ layer

Figure S3.6. *Hdac3* deletion triggers premature neurogenesis in the developing neocortex. (**a**) Immunostaining of wild-type and mutant embryonic sections with an anti-Tuj1 antibody. Embryos were collected at E13.5. Only an enlarged area of the neuroepithelium is shown here for the wild-type or mutant embryonic section. Dotted lines mark boundaries of the $Tuj1^+$ layer. (**b**) Quantification of thickness of entire neocortex and $Tuj1^+$ layer on sections as shown in (**a**). (**c**,**d**) same as (**a**,**b**) except that E15.5 embryonic sections were analyzed. (**e**,**f**) same as (**a**,**b**) except that E14.5 embryonic sections were analyzed. Green asterisks denote ectopic distribution of $Tuj1^+$ cells and compression of the ventricular/subventricular zone. Scale bars, 100 μm; n=3; ns, not statistically significant; *, $p<0.05$; **, $p<0.01$.

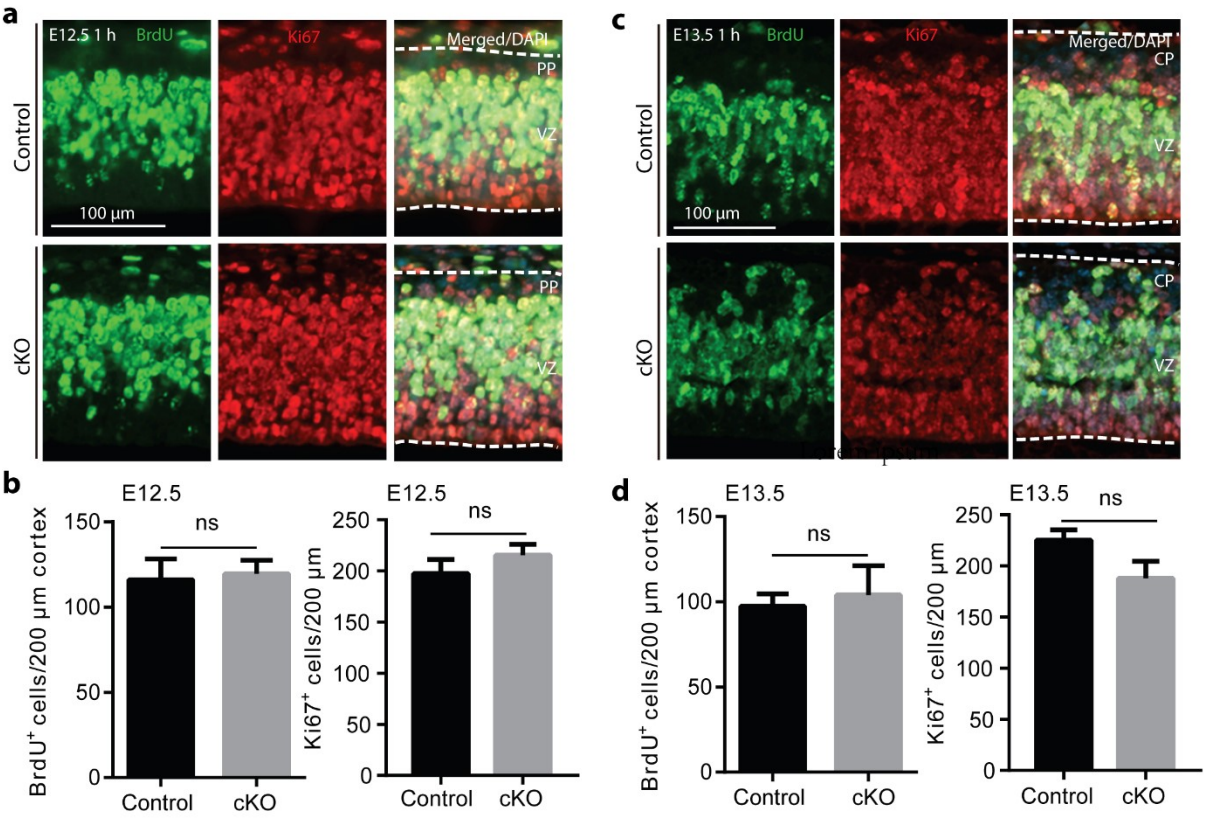

Figure S3.7. Normal proliferation in the *Hdac3*-deficient neocortex.

(a) BrdU was injected into pregnant mice at E12.5 for embryo retrieval 1 h later. Embryonic sections were double- stained with anti-BrdU and -Ki67 antibodies. Only an enlarged area of the neocortex is shown here for the wild-type or mutant embryonic section. Scale bar, 100 µm. **(b)** Quantification of $BrdU^+$ or $Ki67^+$ cells on embryonic sections prepared as in (**a**). n=3 for the wild-type or mutant embryo. ns, not statistically significant. (**c,d**) Same as (**a,b**) except BrdU was injected into pregnant mice at E13.5.

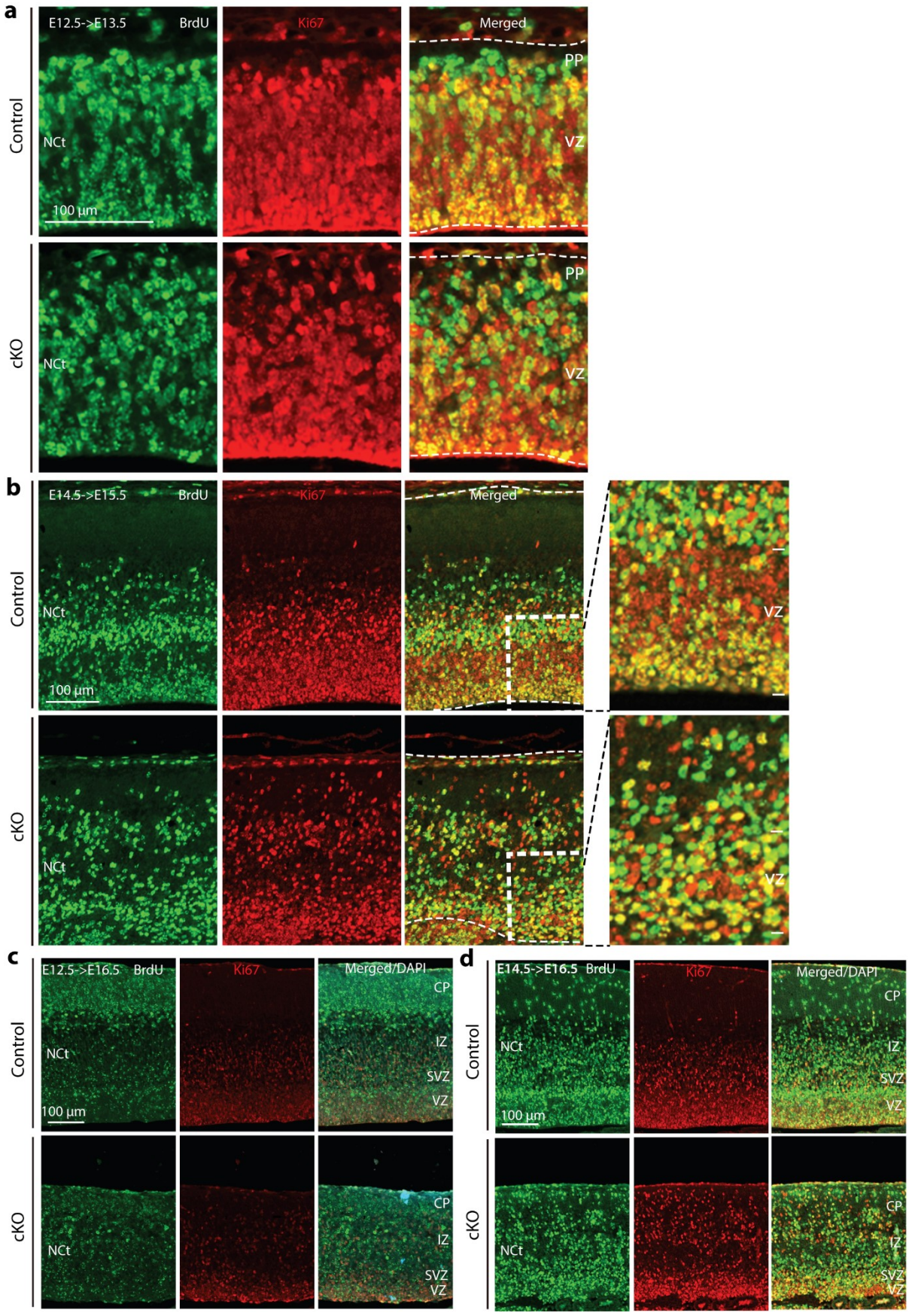
a
E12.5->E13.5
BrdU
Ki67
Merged
Control
NCt
100 µm
PP
VZ
cKO
NCt
PP
VZ
b
E14.5->E15.5
BrdU
Ki67
Merged
Control
NCt
100 µm
VZ
cKO
NCt
VZ
c
E12.5->E16.5
BrdU
Ki67
Merged/DAPI
Control
NCt
100 µm
CP
IZ
SVZ
VZ
cKO
NCt
CP
IZ
SVZ
VZ
d
E14.5->E16.5
BrdU
Ki67
Merged/DAPI
Control
NCt
100 µm
CP
IZ
SVZ
VZ
cKO
NCt
CP
IZ
SVZ
VZ

Figure S3.8. *Hdac3* deletion alters neuronal migration and induces premature cell cycle exit.

(a,b) BrdU was injected into E12.5 (**a**) or E14.5 (**b**) pregnant mice for embryo retrieval 24 h later. Embryonic sections were double stained with anti-BrdU and -Ki67 antibodies. Only an enlarged area of the neocortex is shown here for the wild-type or mutant embryonic section. $BrdU^{+}Ki67^{-}$ cells indicate cells that already exit from the cell cycle. There are significantly more $BrdU^{+}Ki67^{-}$ cells in the mutant ventricular zone at E13.5 (**a**) and E15.5 (**b**). Scale bar, 100 μm. (**c,d**) BrdU was injected into E12.5 and E14.5 pregnant mice for embryos collection and brain dissection at E16.5. The brain sections were double stained with anti-BrdU and -Ki67 antibodies. Only an enlarged area of the developing neocortex is shown here for the wild-type or mutant brain section. Scale bar, 100 μm.

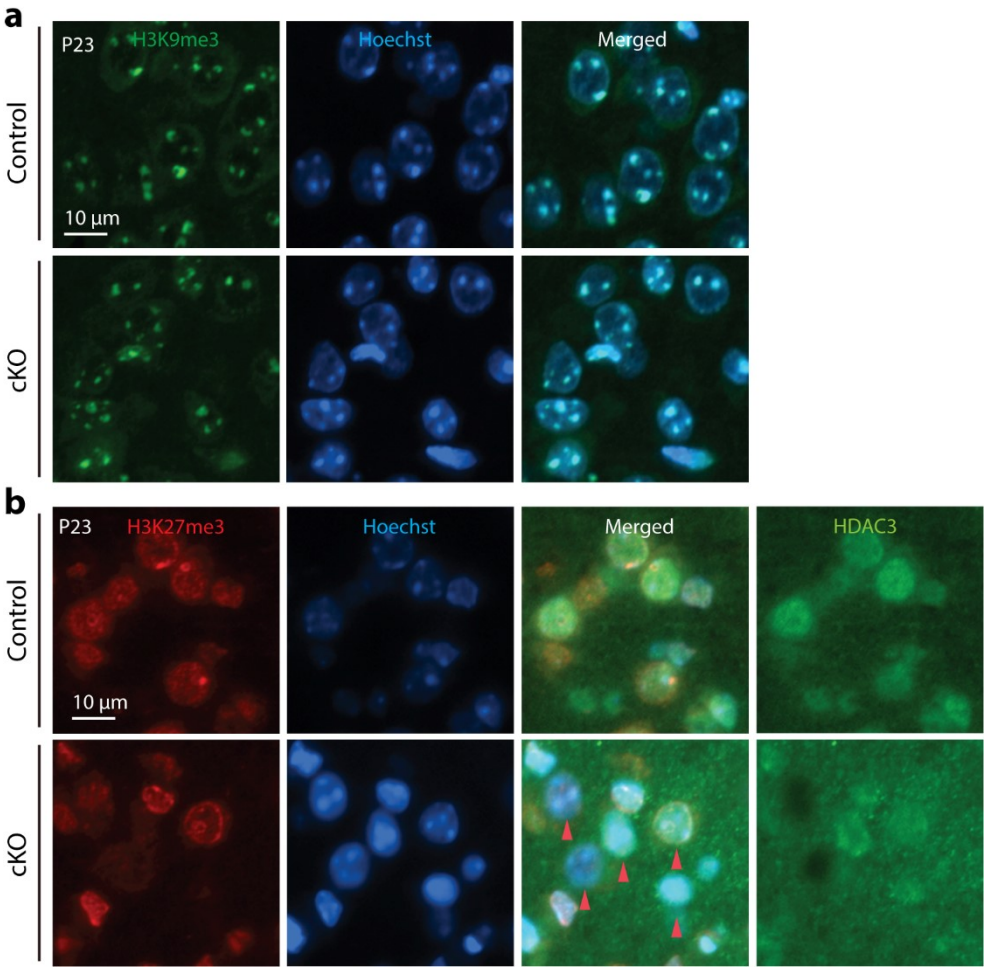

Figure S3.9. Global histone modifications in the mutant cerebral cortex.

(**a**) Immunostaining of wild-type and mutant brain sections with an anti-H3K9me3 antibody. The sections were prepared from pups at P23. The enlarged area shown was taken from the cortical plate. The H3K9me3 levels was similar between the wild-type and mutant cerebral cortices. (**b**) Same as (**a**) except that double immunostaining with both anti-HDAC3 and -H3K27me3 antibodies was carried out. The enlarged area shown was taken from the cortical plate. The H3K27me3 level decreased in the mutant cerebral cortex. Red arrowheads denote weak H3K27me3 signals in the mutant cerebral cortex. Scale bar, 10 µm.

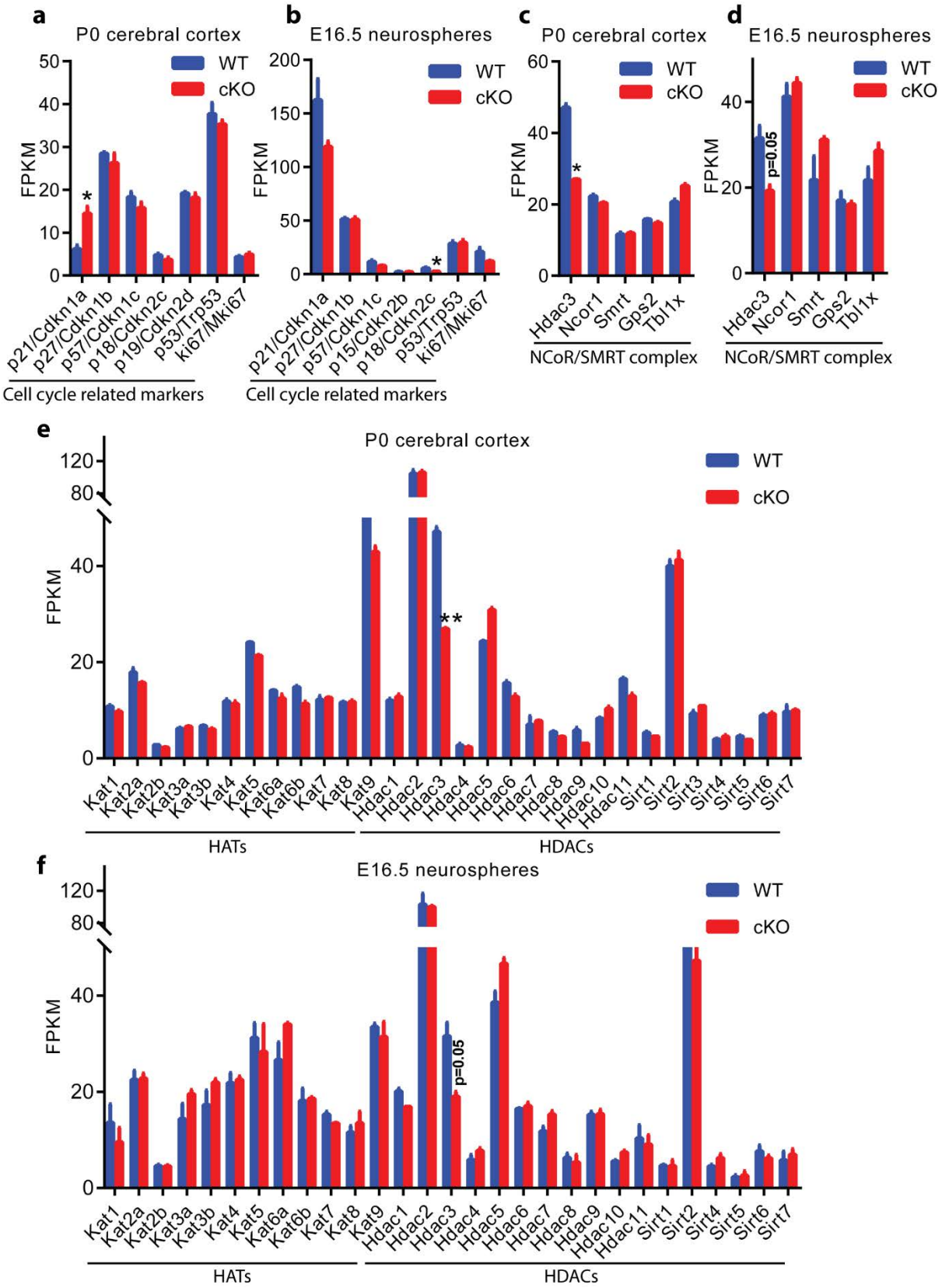
a
P0 cerebral cortex
WT
cKO
FPKM
p21/Cdkn1a
p27/Cdkn1b
p57/Cdkn1c
p18/Cdkn2c
p19/Cdkn2d
p53/Trp53
ki67/Mki67
Cell cycle related markers
b
E16.5 neurospheres
p15/Cdkn2b
c
P0 cerebral cortex
Hdac3
Ncor1
Smrt
Gps2
Tbl1x
NCoR/SMRT complex
d
E16.5 neurospheres
p=0.05
e
P0 cerebral cortex
Kat1
Kat2a
Kat2b
Kat3a
Kat3b
Kat4
Kat5
Kat6a
Kat6b
Kat7
Kat8
Kat9
Hdac1
Hdac2
Hdac3
Hdac4
Hdac5
Hdac6
Hdac7
Hdac8
Hdac9
Hdac10
Hdac11
Sirt1
Sirt2
Sirt3
Sirt4
Sirt5
Sirt6
Sirt7
HATs
HDACs
f
E16.5 neurospheres

Figure S3.10. Altered transcription of multiple genes in the mutant cerebrum and neurospheres.

(**a,b**) FPKM values for cell cycle inhibitors and related genes in the wild-type and *Hdac3*-deficient neonatal cerebral cortex and neurospheres. (**c,d**) FPKM values for *Ncor*, *Smrt*, *Gps2*, and *Tbl1x* in the wild-type and *Hdac3*-deficient neonatal cerebral cortex and neurospheres. (**e,f**) FPKM values for genes for different lysine acetyltransferases (KATs) and HDACs in the *Hdac3*-deficient neonatal cerebral cortex and neurospheres. The FPKM values for *Hdac3* transcripts were significantly (**e**) or almost significantly (**f**) reduced (p=0.05), but the values for the excised two exons in the mutant was much more dramatically reduced in the mutant from RNA-Seq analysis (data not shown). In agreement with this, RT-PCR with primers to these two exons confirmed *Hdac3* is efficiently deleted in the mutant (Fig. S3.1i). Moreover, Western blotting (Fig. 3.1e) and immunostaining using the anti-HDAC3 antibody (Fig. S3.1a-e) indicated that *Hdac3* is efficiently deleted in the mutant starting at E12.5.

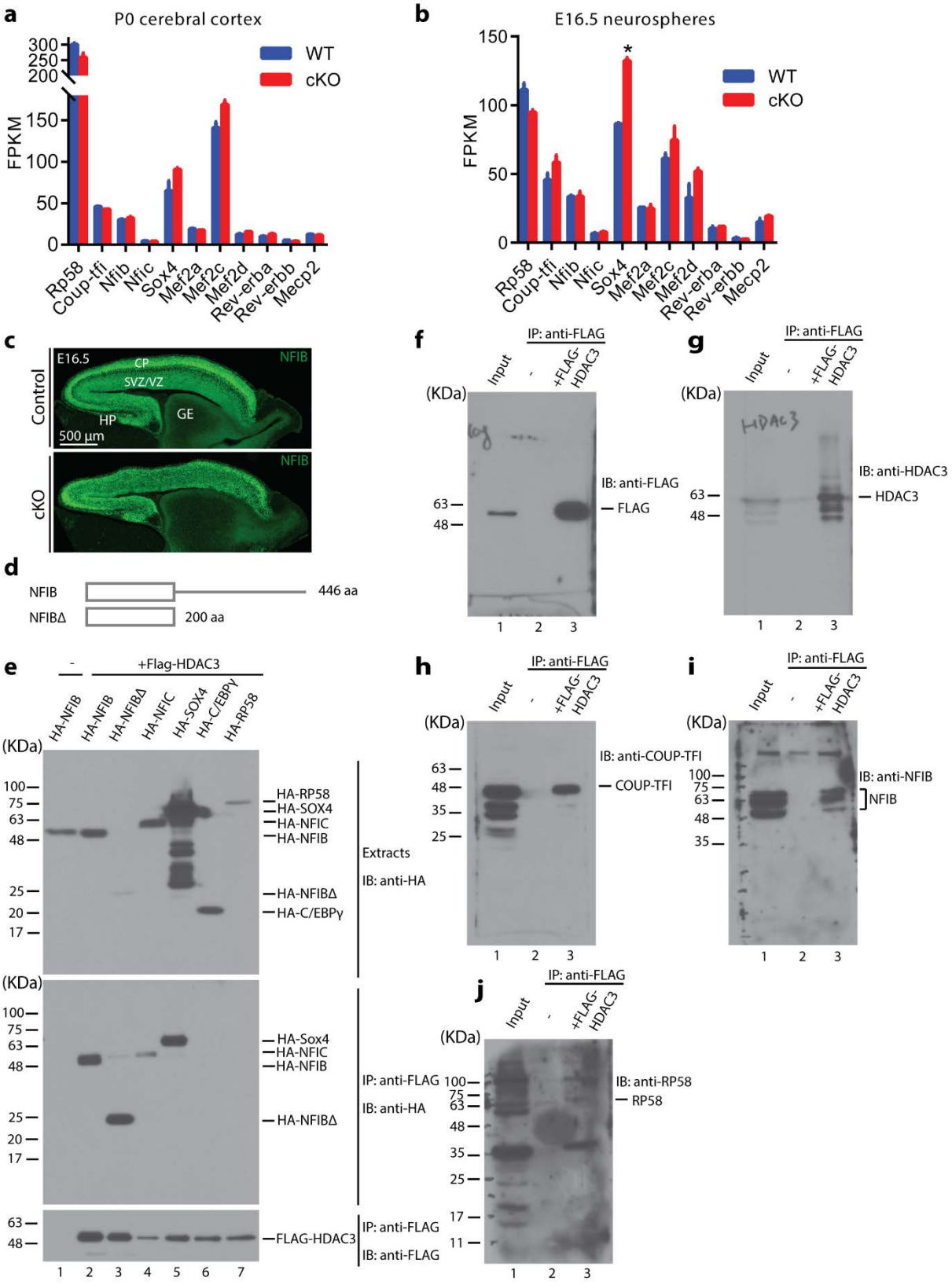
a
P0 cerebral cortex
WT
cKO
FPKM
Rp58
Coup-tfi
Nfib
Nfic
Sox4
Mef2a
Mef2c
Mef2d
Rev-erba
Rev-erbb
Mecp2
b
E16.5 neurospheres
c
E16.5
CP
SVZ/VZ
HP
GE
500 μm
NFIB
Control
cKO
d
NFIB
446 aa
NFIBΔ
200 aa
e
-
+Flag-HDAC3
HA-NFIB
HA-NFIBΔ
HA-NFIC
HA-SOX4
HA-C/EBPγ
HA-RP58
(KDa)
HA-RP58
HA-SOX4
HA-NFIC
HA-NFIB
HA-NFIBΔ
HA-C/EBPγ
Extracts
IB: anti-HA
HA-Sox4
FLAG-HDAC3
IP: anti-FLAG
IB: anti-FLAG
f
IP: anti-FLAG
Input
+FLAG-HDAC3
IB: anti-FLAG
FLAG
g
IB: anti-HDAC3
HDAC3
h
IB: anti-COUP-TFI
COUP-TFI
i
IB: anti-NFIB
NFIB
j
IB: anti-RP58
RP58

Figure S3.11. Interaction of HDAC3 with multiple DNA-binding transcription factors highly expressed in the developing brain.

(**a,b**) FPKM values of *Rp58*, *Coup-tfi*, *Nfib*, *Nfic*, *Sox4*, *Mef2a*, *Mef2c*, *Mef2d*, *Rev-erba*, *Rev-erbb* and *Mecp2* in the wild-type or *Hdac3*-deficient neonatal cerebral cortex or E16.5 neurospheres. (**c**) Immunostaining of E16.5 wild-type and mutant embryonic brain sections with an anti-NFIB antibody. The results indicate that NFIB is highly expressed in the cerebrum at E16.5 and *Hdac3* deletion does not affect NFIB expression. Abbreviations: CP, cortical plate; HP, hippocampus; GE, ganglionic eminence; SVZ/VZ, subventricular zone/ventricular zone. (**d**) Schematic illustration of NFIB and its truncation mutant. NFIB has a conserved DNA-binding domain in the N-terminal part. The truncation mutant contains this domain, which is conserved among different members of the NFI family of transcription factors. (**e**) Co-immunoprecipitation to assess the interaction of HDAC3 with NFIB, its N-terminal fragment (NFIBΔ), NFIC, SOX4, C/EBPγ and RP58. HDAC3 was transiently expressed a FLAG-tagged fusion protein whereas the potential partners were expressed as HA-tagged fusion proteins in HEK293 cells. Soluble extracts were prepared for co-immunoprecipitation on agarose conjugated with an anti-FLAG monoclonal antibody and after extensive washing, bound proteins were eluted with the FLAG peptide for immunoblotting with anti-FLAG and -HA antibodies as specified. Lane 1 is a negative control, for which HA-tagged NFIB was expressed without FLAG-HDAC3. (**f-j**) HDAC3 was transiently expressed as the FLAG fusion protein in HEK293 cells for co-immunoprecipitation with endogenous proteins of COUP-TFI, NFIB, and RP58, detected by their respective antibodies. Lanes 2 were negative controls, for which an empty expression vector was transfected into HEK293 cells.

Bridging Text between Chapters III and IV

In the previous chapter, we showed that HDAC3 regulates mouse cerebral development, so we then asked how the gene might be related to human brain development and whether the gene is mutated in neurodevelopmental disorders. By collaborating with clinical doctors, we identified 4 patients, who carry heterozygous *de novo HDAC3* mutations and display developmental delay, microcephaly, intellectual disability, and epilepsy. Based on these results and also those in Chapter III, we propose that the patient-derived mutations affect the human brain development by impairing the enzymatic activity of HDAC3. Thus, in Chapter IV, I will describe results of *in vitro* assays to investigate whether and how these mutations affect HDAC3 properties.

CHAPTER IV: Heterozygous *HDAC3* mutations cause epilepsy and brain anomalies

Lin Li[1,2,#], Justine Rousseau[3,4,#], …, Philippe Campeau[3,4,*], and Xiang-Jiao Yang[1,2,5,6,*]

[1]Rosalind & Morris Goodman Cancer Research Center and [2]Department of Medicine, McGill University, Montreal, QC H3A 1A3, Canada

[3]CHUSJ Research Center, CHU Sainte-Justine, Montreal, QC H3T 1J4, Canada

[4]Department of Pediatrics, Sainte-Justine Hospital and University of Montreal, QC H3T 1J4, Canada

[5]Department of Biochemistry, McGill University and [6]McGill University Health Center, Montreal, QC, H3A 1A3, Canada

[#] Authors of equal contribution

[*]Correspondence: p.campeau@umontreal.ca (P.M.C); xiang-jiao.yang@mcgill.ca (X.-J.Y.)

Running Title: HDAC3 variation leads to brain disorders

Keywords: HDAC3; mutations; epilepsy; brain development

4.1 ABSTRACT

HDAC3 is a histone deacetylase important for cellular functions as well as tissue development. Molecularly, HDAC3 forms tetrameric complexes with NCoR/SMRT, GPS2 and TBL1 to repress transcription. In the previous chapter, we have shown that mouse HDAC3 is essential for early brain development via regulation of neural stem and progenitor cells, but the role of HDAC3 in human developmental disease is unknown. Here, we report 4 clinical cases of heterozygous *de novo HDAC3* mutations that link the deacetylase to a new neurodevelopmental disorder. These patients show developmental delay, epilepsy, microcephaly and intellectual disability. Using patient-derived *HDAC3* mutations, we demonstrate that the complex formation of HDAC3 with SMRT, GPS2 and TABL1Y is not affected. However, the enzymatic activity of HDAC3 variants with such mutations is compromised. These results indicate that the 4 mutations inactivate HDAC3, thus shedding light on the pathology of the new neurodevelopmental disorder.

4.2 INTRODUCTION

Developmental delay and brain disorders constitute a large proportion of defects in newborns (414). Most of these brain developmental disorders are genetic diseases due to gene variations that either are inherited from parents or arise during early stage of gestation (415). As unprecedented progress is made in the genome editing technology, correcting these diseases-causing mutations has become possible. Several cases have already been carried out in correcting mutations in the oocytes or sperms of humans (416). Identification of rare mutations in developmental diseases is accelerated due to great advances in the next-generation sequencing techniques. For individuals with developmental diseases, exome sequencing provides a cheap and efficient way to identify the possible disease-causing genes.

We have shown that mouse HDAC3 is important in regulating cerebral cortex development through neural stem cells (see Chapter III). However, the role of HDAC3 in human brains is unclear, with only one report showing a patient with neonatal epileptic encephalopathy bearing an *HDAC3* mutation (417). To identify a possible role of HDAC3 in the human developmental disorders, we collaborated with clinical doctors who through exome sequencing have identified 4 cases of *HDAC3* mutations linked to a new brain developmental

disorder. The patients show developmental delay, microcephaly, epilepsy and intellectual disability.

We used *in vitro* assays to investigate whether and how these patient-derived mutations affect HDAC3 properties. For this, we constructed FLAG-tagged HDAC3 expression plasmids carrying these mutations, as well as HA-tagged SMRT, GPS2 and TBL1Y expression plasmids, for expression and affinity purification of the wild-type and mutant HDAC3 complexes. I*n vitro* reconstitution assays showed that the patient-derived *HDAC3* mutations do not affect the SMRT tetrameric complex formation, while HDAC activity assays revealed that such mutations compromise the enzymatic activity of HDAC3. This study provides the first evidence to link *HDAC3* mutations to a new brain developmental disorder and thus sheds light on the pathogenicity of these mutations.

4.3 RESULTS

Identification of 4 *HDAC3* mutations linked to a new brain developmental disorder

Through exome-sequencing, 4 heterozygous *HDAC3* mutations were identified in 4 patients showing developmental delay, intellectual disability, microcephaly and epilepsy. These *HDAC3* mutations were in the deacetylase domain of HDAC3 (Fig. 4.1), which is essential not only for the enzymatic activity of HDAC3 but also for binding to the SANT domain of SMRT/NCoR (418, 419). We thus hypothesized that these mutations either affect the SMRT complex formation and/or affect the enzymatic activity of HDAC3.

Patient-derived *HDAC3* mutations do not affect the SMRT complex formation *in vitro*, but compromise the enzymatic activity of HDAC3 toward H3K14ac

To test how these *HDAC3* mutations might affect HDAC3 properties, we investigated how the NCoR/SMRT complex might be affected. For this, we constructed FLAG-tagged plasmids expressing either wild-type *HDAC3* or *HDAC3* bearing patient-derived mutations, and HA-tagged plasmids expressing *SMRT*, *GPS2* and *TBL1Y*. The plasmids were transfected into HEK293 cells, and the cells were collected 48 h later and lysed with a lysis buffer, followed by immunoprecipitation with M2 beads. Western blotting demonstrated that the complex

formation was not affected (Fig. 4.2), indicating these patient-derived *HDAC3* mutations do not have an significant impact on the SMRT tetrameric complex formation.

Since the 4 identified mutations are in the HDAC domain, which is essential for HDAC3 activity. We asked whether the enzymatic activity of these HDAC3 variants is affected. To confirm this, we carried out HDAC activity assay using the purified tetrameric complexes which contain either wild-type or mutated HDAC3 (the 4th patient was identified later and thus not included in our assay yet). Compared with wild-type HDAC3, which shows strong enzymatic activity toward H3K14ac (Fig. 4.3, lane 2), patient 1 (p.Arg359His) and patient 3 (p.Arg301Gln) almost totally lose their HDAC3 enzymatic activity toward H3K14ac (Fig. 4.3, lanes 3 and 5) as compared with the negative control (Fig. 4.3, lane 1). Patient 2 (p.Leu266Ser) partially loses its HDAC3 enzymatic activity (Fig. 4.3 lane 3) compared with wild-type HDAC3 (Fig. 4.3, lane 2). In contrast, we didn't detect any enzymatic activity of HDAC3 toward H3K23ac, indicating HDAC3 do not have enzymatic activity toward this site *in vitro*. Note that we use a small amount of purified SMRT tetrameric complexes for HDAC activity assay, and thus during our detection of HA-tagged proteins, the HA-SMRT (marked by * in Fig. 4.3) is not detected due to its big molecular mass (275kDa). However, HA-SMRT is detected when using more total proteins and transferred for longer time during western blotting (Fig. 4.2).

4.4 DISCUSSION

HDAC3 mutations link HDAC3 to a new brain developmental disorder

Many neurodevelopmental disorders, including developmental delay, epilepsy, autism, intellectual disability, microcephaly, ADHD (attention deficient hyperactivity disorder) *etc*. could find their origin in the gene mutations. Many genes relate to neural developmental and other brain disorders. Until recently, ~30 chromatin modifiers have been associated with human diseases, a lot of which show symptoms such as neurodevelopmental delay, microcephaly and intellectual disability. For KATs alone, CREBBP, EP300, KAT6A, KAT6B and ESCO2 have been identified in those disorders so far (77-85). For KDACs, only HDAC4 and HDAC8 are implicated in human diseases directly (86, 87). Previously, one potential *HDAC3* mutation (c.902G>A (p.R301Q)) was identified in one patient showing neonatal epileptic

encephalopathy (417). However, this case is not conclusive as there is another *LPHN1* mutation found in this patient as well. Moreover, the pathogenicity of either *HDAC3* or *LPHN1* mutation was not analyzed in the previous study (417). Thus, whether HDAC3 mutations relate to brain developmental disorders and other brain disorders remains unclear until the current analysis presented herein.

Here we have analyzed this mutation and identified 3 additional *HDAC3* mutations (Fig. 4.1) that link HDAC3 to a new brain developmental disorder including symptoms of developmental delay, microcephaly, intellectual disability and epilepsy or seizures (the clinical features of these patients will be included when the paper is submitted for publication). We further demonstrated that enzymatic activity of HDAC3 with such mutations is compromised toward H3K14ac (Fig. 4.3) while the SMRT complex formation is unaffected (Fig. 4.2).

H3K14ac is important for cell cycle progression (420, 421), and protein recruitment to the chromatin (422). In the mice, we have shown that inhibition of HDAC3 enzymatic activity by a selective inhibitor impairs neurosphere formation, indicating an important role for HDAC3 enzymatic activity in neural stem cell development. The compromised enzymatic activity of HDAC3 toward H3K14ac in these patients may be responsible their disease initiation and progression.

We have demonstrated that loss of mouse *Hdac3* in the cerebral cortex leads to hypoplasia in the neocortex, hippocampus and corpus callosum (Fig. 3.1 with hyperactivity and anxiety (Fig. S3.8). We also observed the mutant mice are more prone to irritation (data not shown). The 4 patients with *HDAC3* mutations show symptoms of epilepsy or seizures, microcephaly and developmental delay. Patients with epilepsy frequently show behavioral disturbance including hyperactivity and irritability (423), and have a strong correlation with attention deficit hyperactivity disorder (ADHD). These common features between *Hdac3*-deficient mice and *HDAC3*-muated human patients imply that HDAC3 have an important role in regulating both mouse and human brain development and brain functions.

The study reports the first characterization of *HDAC3* mutations present in 4 clinical cases with a new brain developmental disorder and determined the pathogenicity. The study complements the analysis of *Hdac3* cerebrum-specific knockout mice and sheds light on how

HDAC3 mutations might cause human brain disorders including epilepsy, developmental delay and microcephaly.

4.5 SUBJECTS AND METHODS

Human subjects

Families gave consent for studies approved by the CHU Sainte-Justine Institutional Review Board or by the institutional review boards of the DDD (Decipher Developmental Disorder) Study, or the CAUSES (Clinical Assessment of the Utility of Sequencing and Evaluation as a Service) Study. Written informed consent was obtained for all four individuals.

Exome sequencing

Clinical exome sequencing for the patients were carried out by clinicians (this part will be filled when the paper is ready for publication).

Plasmids construction

The plasmids used were as following: Flag-HDAC3 (NM_003883.3), HA-SMRT (AF125672.1), HA-GPS2 (NM_004489.4), HA-TBL1Y (NM_033284.1). All these plasmids are based pcDNA3.1(+) or pcDNA3.1(-) vectors.

Western blotting and immunoprecipitation

An expression plasmid for Flag-tagged HDAC3 (either wild-type or bearing patient-derived mutations) was transfected into HEK293 cells, together with expression plasmids for HA-tagged SMRT, GPS2 and TBL1Y. Transfected HEK293 cells were further cultured for 48 hours before the cells were washed twice with PBS and soluble protein extracts were collected. Affinity purification with anti-FLAG M2 beads were carried out as described somewhere else (424). The FLAG-peptide was used for elution of bound proteins on the M2 beads. Immunoblotting was carried out with anti-FLAG and -HA antibodies. Band of FLAG-HDAC3 on films was adjusted to same level to compare whether binding of HDAC3 with the other components is affected.

HDAC3 deacetylase activity assay

The eluted proteins were used for histone deacetylation reactions. After deacetylation reactions, immunoblotting was carried out to detect histone H3 and its site-specific acetylation using anti-histone H3 (Abcam, ab1791), anti-H3K14ac (EMD Millipore, 07-353) and anti-H3K23ac (EMD Millipore, 07-355) antibodies.

Acknowledgement

Those patients and their families are greatly appreciated for their participation in this study. This work was supported by grants from Canadian Institutes of Health Research, Natural Sciences and Engineering Research Council of Canada, and the Canadian Cancer Society (to X.-J.Y.). Lin Li is financially supported by the China Scholarship Council, the Clifford C.F. Wong Fellowship, the studentship from the CIHR/FRSQ training grant in cancer research FRN53888 of the McGill Integrated Cancer Research Training Program, and the Canderel studentship.

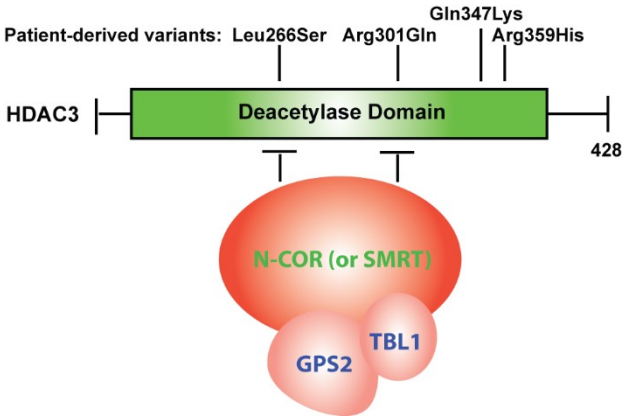

Figure 4.1. Four *HDAC3* variants identified in 4 patients showing a novel neurodevelopmental disorder.

These 4 mutations are in the deacetylase domain (i.e. residues 3-383) of HDAC3 and may thus affect HDAC3 enzymatic activity through binding with the SANT domain of NCoR/SMRT. GPS2 and TBL1 (which could also be its paralog TBL1X or TBL1Y) interact with HDAC3 through NCoR or SMRT.

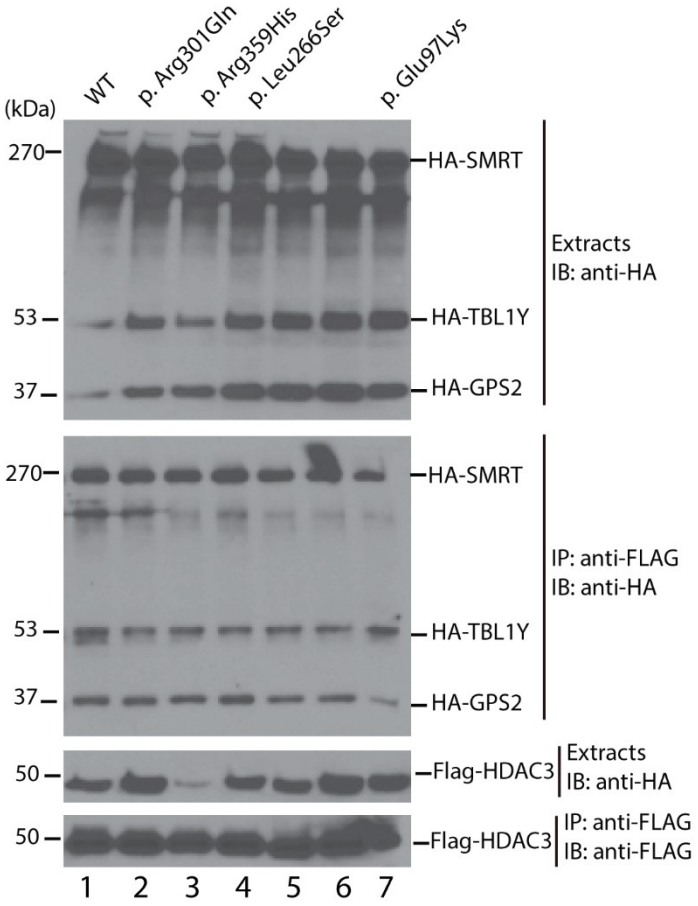

Figure 4.2. Patient-derived *HDAC3* mutations do not affect complex formation of HDAC3 with SMRT, GPS2 and TBL1Y.

FLAG-tagged HDAC3, either wild-type or bearing patient-derived mutations (p.Arg301Gln, p.Arg359His and p.Leu266Ser; the fourth patient was identified a few weeks ago and the mutation has not been included in the assay yet) was expressed together with HA-tagged SMRT, GPS2 and TBL1Y in HEK293 cells. The tetrameric complex was affinity-purified on anti-FLAG M2 agarose beads. The levels of Flag-HDAC3, HA-SMRT, -TBL1Y and -GPS2 are comparable between wild-type and HDAC3 mutations, indicating that the complex formation is not affected. Note that lanes 5 and 6 are from other HDAC3 variants not related to the patients. Lane 7 represents a GPS2 variant (p.Glu97Lys) carried by one patient with neurodevelopmental abnormalities.

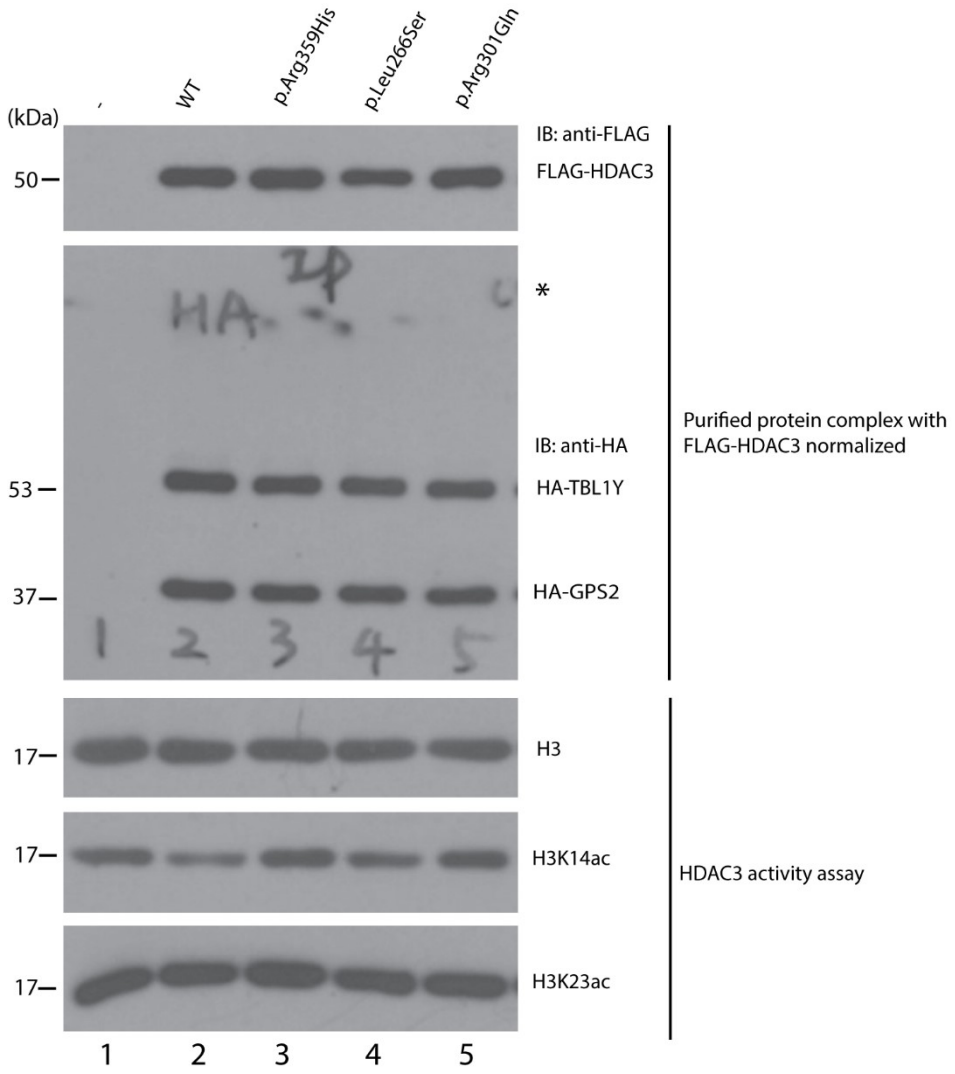

Figure 4.3. Patient-derived *HDAC3* mutations compromise HDAC3 enzymatic activity toward H3K14ac.

The affinity-purified HDAC3 complexes were used for HDAC activity assay. Briefly, purified HDAC3 complexes were incubated with histones for 2 h in a reaction buffer at 37°C, followed by Western blotting detecting H3, H3K14ac, and H3K23ac. H3K14ac levels were markedly reduced for wild-type HDAC3 (lane 2) compared with negative control (lane 1). However, HDAC3 mutations derived from patient 1 (p.Arg359His) and patient 3 (p.Arg301Gln) led to total loss of enzymatic activity as the H3K14ac levels were not altered (lanes 3 and 5) compared with the negative control (lane 1). HDAC3 mutations derived from patient 2 (p.Leu266Ser) show partially loss of enzymatic activity (lane 4) as the H3K14ac level was lower than the negative control (lane 1) but higher than wild-type HDAC3 (lane 2). As a comparison, HDAC3 does not have enzymatic activity toward H3K23ac *in vitro* (bottom panel).

CHAPTER V: Conclusion, general discussion and future direction

5.1 Lysine acetylation and responsible enzymes in normal and abnormal brain development

Lysine acetylation is important for regulating transcriptional programs as well as many other nuclear processes. Here, we present evidence that disturbance of tubulin acetylation and histone acetylation leads to abnormal brain development and functions.

In Chapter II, we concluded that loss of mouse *Atat1* and tubulin acetylation leads to hypoplasia in the striatum and septum, which causes a mild defect in motor coordination. We analyzed multiple cellular processes such as proliferation, apoptosis and autophagy in both the mutant brain and MEFs, and found no major abnormalities in these processes. With BrdU tracing analysis, we found there were fewer $BrdU^{+}$ cells in the mutant striatum and septum but not in the neocortex, implying defects in neuronal migration into the striatum and septum. We also established that *Atat1* is not essential for hematopoiesis and has a minor role on MEF proliferation. We found that MEFs lacking *Atat1* failed to induce tubulin hyperacetylation in response to cellular stress. Further, we noticed residual tubulin acetylation in the cilia of trachea and oviduct in absence of *Atat1*, indicating the existence of another tubulin acetyltransferase in the trachea and oviduct.

In Chapter III, we established that loss of *Hdac3* impairs embryonic neocortical and hippocampal development, along with anxiety and hyperactivity in the resulting pups. Further analyses revealed that the developmental defects are due to abnormal development of neural stem and progenitor cells (NSPCs). *In vitro* culture showed that the NSPCs in the *Hdac3*-deficient embryonic cortex can form intact neurospheres initially but subsequently the neurospheres showed altered morphology and could not be maintained in the culture medium. Consistent with this, an HDAC3-selective inhibitor (RGFP966) impaired formation of neurospheres from the wild-type embryonic cerebral cortex. We further showed that histone marks at multiple sites are perturbed in $Hdac3^{-/-}$ cortices and neurospheres. In agreement with this, we uncovered transcriptional deregulation of multiple genes that are related to neural stem cell functions. Specifically relate to neurogenesis, we observed increased transcription of multiple neurogenesis-promoting genes (such as *Dlx1*, *Dlx2*, *Dlx5*, *Dlx6*, *Sox1*, *Pbx3*, *Lhx6*,

Gad1, *Gad2*, *Cux2*, *Tbr1*, *Dcx*, *Erbb4*, *NeuroD1* and *NeuroD2*) and decreased transcription of multiple neurogenesis-inhibiting genes (such as *Id1*, *Id3*, *Hes1*, *Hes5*, *Hes6*, *Notch3*, *Sox10*, *Ascl1*, *Fabp7*, *Tnc* and *Nes*) in the *Hdac3*-deficient neurospheres. Further, we identified 4 novel HDAC3-interacting transcription factors (NFIB, COUP-TFI, RP58 and SOX4) that are highly expressed in the wild-type cerebral cortex and NSPCs, implying that HDAC3 and its complexes might be recruited by these transcription factors during prenatal cerebral development.

In Chapter IV, we identified 4 *HDAC3* mutations that link HDAC3 to a new neurodevelopmental disorder, of which the symptoms include developmental delay, microcephaly, intellectual disability, and epilepsy. With *in vitro* assays, we concluded that patient-derived *HDAC3* mutations compromise HDAC3 enzymatic activity toward H3K14ac while the ability to form a protein complex with SMRT, GPS2 and TBL1Y is normal. Thus, we identified and linked the *HDAC3* mutations to a novel genetic disease that affects brain development and functions.

5.2 HDAC3 regulates NSPC development through a unique transcriptional program

In Chapter III, we presented evidence showing how HDAC3 regulates transcriptional programs in NSPCs at a transcriptome level. We identified a unique transcriptional program in which loss of *Hdac3* leads to a marked increase in transcriptional expression of genes such as *Dlx* family genes, with decreased expression of genes such as *Id* and *Hes* family genes. This regulation pattern (i.e., increased transcription for *Dlx* family genes and decreased transcription for *Id* and *Hes* family genes) is unique to NSPCs and has not been reported in any previous transcriptome studies using *Hdac3*-deficient cells or tissues.

Dlx, *Id* and *Hes* family genes are well established transcription factors in regulating neural stem cell development. Transcription of these family genes are significantly altered in *Hdac3*-deficient neurospheres. Transcription of *Dlx1*, *-2*, *-5* and *-6* are significantly increased (2.2, 2.5, 2.0, 2.8 folds for *Dlx1*, *-2*, *-5* and *-6* respectively) in our *Hdac3*-deficient neurospheres (Chapter III). The other two *Dlx* genes, *Dlx3* and *Dlx4* are not expressed in both wild-type and *Hdac3*-deficient neurospheres. *Dlx* family genes are essential in NSPC development by promoting differentiation. Overexpression of *Dlx2* can rescue neurogenesis defect in *Mll1*-deficient neural

stem cells which remain undifferentiated (425). In the loss of *Dlx*5, neural stem cells have a severely reduced capacity in generating neurons, while forced expression of *Dlx5* in *Dlx5*-deficient NSCs fully restored their neurogenic potential (426), indicating an essential role for DLX5 in promoting neurogenesis.

In *Hdac3*-deficient neurospheres, we observed a 4.9-fold decrease of transcription in *Id1*, and a 3.1-fold decrease in *Id3*, while the rest *Id* genes are either comparable in transcription (1.1-fold decrease for *Id2*) or not expressed (*Id4*) in the NSPCs (Chapter III). Inhibitor of differentiation (ID) proteins are well known for their roles in inhibiting differentiation. Double knockout of *Id1* and *Id3* in the mice leads to premature neurogenesis (427), consistent with our *Hdac3*-deficient cerebral cortices which show enhanced neurogenesis in the early embryonic stage.

In *Hdac3*-deficient neurospheres, transcription of *Hes1*, *-5*, and *-6* decreased by 4.0, 2.7, 1.6 folds respectively, while the other *Hes* genes (*Hes2*, *-3*, *-4*, and *-7*) are not expressed in the NSPCs (Chapter III). Hairy and enhancer of split (HES) proteins are essential for NSC niche maintenance. Previous studies show that overexpression of *Hes1* and *Hes5* inhibits neuronal differentiation, whereas NSCs absent of *Hes1* and *Hes5* display premature neurogenesis (428-432), consistent with our *Hdac3*-deificient embryonic cerebral cortex showing premature neurogenesis.

In addition to these three clusters of family genes (*Dlx*, *Id* and *Hes*), transcription of the other pro-neurogenesis genes (such as *Sox1*, *Pbx*, *Lhx6*, *Gad1*, *Gad2*, *Cux2*, *Tbr1*, *Dcx*, *Erbb4*, *NeuroD1* and *NeuroD2*) are significantly increased, while anti-neurogenesis genes (such as *Notch3*, *Sox10*, *Ascl1*, *Fabp7, Tnc and Nes*) are significantly decreased in our *Hdac3*-deficient neurospheres as well (Chapter III). The alteration in multiple neurogenesis-related genes reflects how loss of HDAC3 promotes neuronal differentiation in the NSPCs at the protein level.

This unique transcriptional program regulated by HDAC3 indicates that there might be transcription factors for recruiting HDAC3 to specific genetic loci in the NSPCs. Indeed, we reported here for the first time that several transcription factors, including NFIB, COUP-TFI, RP58, and SOX4, are highly expressed in the mouse NSPCs and have a strong binding affinity for HDAC3 (Chapter III). The N-terminal conserved part of NFIB (1-200 aa, which contains a

MH1 domain) has a very strong binding affinity for HDAC3 as well (Chapter III). NFIC, another family member of NFI proteins, is also interacting with HDAC3, though the binding affinity is weaker compared with NFIB.

These HDAC3-interacting transcription factors have well-known roles in neurogenesis and in the embryonic brain development. NFI/B (nuclear factor one isoform B) proteins are master regulators of cell differentiation (402). NFIB is strongly expressed in the radial glial cells, and loss of *Nfib* in the brain leads to failed generation of outer radial glia and a loss of late basal progenitors (433). Neuronal differentiation related genes are misexpressed in the *Nfib*$^{-/-}$ brains shown by RNA-sequencing (433). *Coup-tfI* and *II* are transiently co-expressed in the ventricular zone of embryonic cerebral cortex. The double knockout of *Coup-tfI/II* in either NSPCs or developing mouse forebrain causes sustained neurogenesis and prolonged generation of early-born neurons (403). RP58 controls neuron and astrocyte differentiation by downregulating the expression of *Id1-4* genes in the developing cortex (434), and favors neuronal differentiation and brain growth by coherently repressing multiple proneurogenic genes such as *Ngn2* and *NeuroD1* (435). These 2 studies correlate well with our study showing that knockout of HDAC3 in the cerebral cortex significantly downregulates the expression of *Id1*, *-3* and increases the expression of both *Neurod1*, *-2* (*Ngn2* expression in our neurospheres is very low with a FPKM ~1), indicating that RP58 might recruit HDAC3 into promotors to regulate *Id1*, *Id3*, *Neurod1* and *Neurod2* expression. SOX4 is also related to cerebral cortex development that knockout of *Sox4* in the mice leads to an almost total loss of hippocampus (436). All these lines of evidence show HDAC3 probably regulates transcription in the neural stem and progenitor cells through these transcription factors.

HDAC3 functions within the NCoR/SMRT complexes (270, 437, 438). Germline deletion of *Ncor* or *Smrt* shows that both NCoR and SMRT are essential for embryonic brain development (311). In our *Hdac3*-deficient neurospheres, we show the expression of *Ncor*, *Smrt*, *Gps2* or *Tbl1x* (*Tbl1y* is expressed only in humans but not in mice) is unaffected (Fig. S3.10c,d). Thus, loss of *Hdac3* affects neural stem and progenitor cell development through transcription factors, rather than altering the expression of *Ncor*, *Smrt*, *Gps2* or *Tbl1x*.

5.3 HDAC3 in cerebral development and neurodevelopmental disorders

In Chapter III, we demonstrated for the first time that mouse HDAC3 is critical for regulating embryonic cerebral cortex as well as hippocampus development. Previously, by using *Nes-Cre*, it was shown that loss of *Hdac3* leads to defective lamination in the neonatal neocortex (312). However, the cellular as well as molecular mechanisms were not investigated. We showed that in early embryonic stage that HDAC3 affects cerebral cortex development through regulation of neural stem cells and uncovered the possible molecular mechanism. Especially, this is the first line of evidence showing that loss of *Hdac3* disrupts hippocampus formation. The hippocampus is associated mainly with learning and memory, especially long-term memory (439). Several previous studies showed that HDAC3 associates with memory or long-term memory (440-442). Our observation implies that loss of *Hdac3* perhaps affects memory through regulating pre- and postnatal hippocampus development, at least to some extent.

Many developmental abnormalities, including developmental delay, epilepsy, autism, intellectual disability, and microcephaly could find their origin in genetic mutations. Previously, in a large cohort screen in patients with epilepsy and seizures, one *HDAC3* mutation [c.902G>A(p.R301Q)] was identified in a patient with neonatal epileptic encephalopathy. However, this case is not conclusive as there is another *LPHN1* mutation found in this patient. Also, the pathogenicity of either *HDAC3* or *LPHN1* mutation was not analyzed. In Chapter IV we analyzed this and three other *HDAC3* mutations that link HDAC3 to a new neurodevelopmental disorder, and further demonstrated that (only the first 3 patients included, as the fourth patient was only identified a few weeks ago and has not been included in our assay yet) enzymatic activity of HDAC3 toward H3K14ac with such mutations is compromised, while the SMRT complex formation is unaffected.

Interestingly, loss of *Hdac3* in the cerebral cortex leads to hyperactivity and anxiety in the mice (Chapter III). We also observed the mutant mice are more prone to irritation. Several cases of the patients with *HDAC3* mutations also show symptoms of epilepsy or seizures. Patients with epilepsy frequently show behavioral disturbance, including hyperactivity and irritability (423) and have a strong correlation with attention deficit hyperactivity disorder (ADHD). The *in vivo* study in the mice and *in vitro* study using patient-derived HDAC3 mutations thus shed light on how *HDAC3* mutations might cause epilepsy, developmental delay and microcephaly.

5.4 Future directions

In Chapter II, we have shown that MEFs lacking *Atat1* fail to respond to cellular stress to induce tubulin hyperacetylation, implying that tubulin acetylation may have a role under stress or pathological conditions. The function of ATAT1 and tubulin acetylation is rarely studied in mice that is maintained other than non-stressful conditions. Thus, dissecting role of ATAT1 and tubulin acetylation under special conditions, such as exposure to high salt and challenging with lipopolysaccharides, might shed light on the role of tubulin acetylation under stressful conditions. Also, it will be important to investigate whether the *ATAT1* gene is mutated in human diseases. Our results on the mutant mice will serve as guides for identification and analysis of such mutations.

In Chapter III, we have identified a unique transcriptional program regulated by HDAC3 in the neurospheres which contains neural stem and progenitor cells, and further identified 4 new transcription factors that might mediate the regulation of this transcriptional program by HDAC3. The following three questions are worth further investigation. 1) Of our identified transcription factors, which is the main one responsible for recruiting HDAC3? For this, we can perform ChIP-qPCR with the anti-HDAC3 antibody using cultured primary neurospheres, to further determine which is the principal transcription factor. Alternatively, we will carry out ATAC-seq to gain further insights into how HDAC3 is recruited to specific promotors and alters chromatin accessibility. 2) Whether does HDAC3 regulate neural stem cells (NSCs) and neuronal progenitor cells (NPCs) differently? For this, reprogrammed neural stem and progenitor cells, or primary NSCs and NPCs sorted out by FACS, could be subject to RNA-seq or ChIP-seq, to gain further insights into how HDAC3 regulates transcriptional programs differently in NSCs and NPCs. 3) How does HDAC3 interact with the other components of NCoR/SMRT complex in neural stem and/or progenitor cells? For this, one approach is to utilize conditional knockout mouse lines for NCoR, SMRT and GPS2, to dissect their roles in the embryonic cerebral cortex and NSPCs.

In Chapter IV, we have shown that *HDAC3* mutations affect enzymatic activity of HDAC3 in *vitro*. To analyze how heterozygous HDAC3 mutations affect the human cells *in vivo*, we

will need to use patient-derived lymphoblastoid cell lines to check how histone acetylation (by Western blotting) and the transcriptome (by RNA-seq) are affected.

REFERENCES

1. Zhang ZH, Tan MJ, Xie ZY, Dai LZ, Chen Y, and Zhao YM. Identification of lysine succinylation as a new post-translational modification. *Nat Chem Biol.* 2011;7(1):58-63.
2. Driessen HPC, Dejong WW, Tesser GI, and Bloemendal H. The Mechanism of N-Terminal Acetylation of Proteins. *Crit Rev Biochem Mol.* 1985;18(4):281-325.
3. Van Damme P, Hole K, Pimenta-Marques A, Helsens K, Vandekerckhove J, Martinho RG, Gevaert K, and Arnesen T. NatF Contributes to an Evolutionary Shift in Protein N-Terminal Acetylation and Is Important for Normal Chromosome Segregation. *Plos Genet.* 2011;7(7).
4. Drazic A, Myklebust LM, Ree R, and Arnesen T. The world of protein acetylation. *Bba-Proteins Proteom.* 2016;1864(10):1372-401.
5. Arnesen T. Towards a Functional Understanding of Protein N-Terminal Acetylation. *Plos Biol.* 2011;9(5).
6. Shogren-Knaak M, Ishii H, Sun JM, Pazin MJ, Davie JR, and Peterson CL. Histone H4-K16 acetylation controls chromatin structure and protein interactions. *Science.* 2006;311(5762):844-7.
7. Li L, and Yang XJ. Tubulin acetylation: responsible enzymes, biological functions and human diseases. *Cell Mol Life Sci.* 2015;72(22):4237-55.
8. Glozak MA, Sengupta N, Zhang XH, and Seto E. Acetylation and deacetylation of non-histone proteins. *Gene.* 2005;363(15-23.
9. Spange S, Wagner T, Heinzel T, and Kramer OH. Acetylation of non-histone proteins modulates cellular signalling at multiple levels. *Int J Biochem Cell B.* 2009;41(1):185-98.
10. Kovacs JJ, Murphy PJM, Gaillard S, Zhao XA, Wu JT, Nicchitta CV, Yoshida M, Toft DO, Pratt WB, and Yao TP. HDAC6 regulates Hsp90 acetylation and chaperone-dependent activation of glucocorticoid receptor. *Mol Cell.* 2005;18(5):601-7.
11. Cao WS, Bao C, Padalko E, and Lowenstein CJ. Acetylation of mitogen-activated protein kinase phosphatase-1 inhibits Toll-like receptor signaling. *J Exp Med.* 2008;205(6):1491-503.
12. Choudhary C, Kumar C, Gnad F, Nielsen ML, Rehman M, Walther TC, Olsen JV, and Mann M. Lysine Acetylation Targets Protein Complexes and Co-Regulates Major Cellular Functions. *Science.* 2009;325(5942):834-40.
13. Jenuwein T, and Allis CD. Translating the histone code. *Science.* 2001;293(5532):1074-80.
14. Bannister AJ, and Kouzarides T. Regulation of chromatin by histone modifications. *Cell Research.* 2011;21(3):381-95.
15. Zentner GE, and Henikoff S. Regulation of nucleosome dynamics by histone modifications. *Nat Struct Mol Biol.* 2013;20(3):259-66.
16. Strahl BD, and Allis CD. The language of covalent histone modifications. *Nature.* 2000;403(6765):41-5.
17. Marmorstein R, and Zhou MM. Writers and Readers of Histone Acetylation: Structure, Mechanism, and Inhibition. *Csh Perspect Biol.* 2014;6(7).
18. Gong FD, Chiu LY, and Miller KM. Acetylation Reader Proteins: Linking Acetylation Signaling to Genome Maintenance and Cancer. *Plos Genet.* 2016;12(9).
19. Yang XJ. Lysine acetylation and the bromodomain: a new partnership for signaling. *Bioessays.* 2004;26(10):1076-87.
20. Zeng L, Zhang Q, Li S, Plotnikov AN, Walsh MJ, and Zhou MM. Mechanism and regulation of acetylated histone binding by the tandem PHD finger of DPF3b. *Nature.* 2010;466(7303):258-U138.
21. Li HT, Ilin S, Wang WK, Duncan EM, Wysocka J, Allis CD, and Patel DJ. Molecular basis for site-specific read-out of histone H3K4me3 by the BPTF PHD finger of NURF. *Nature.* 2006;442(7098):91-

5.
22. Taverna SD, Ilin S, Rogers RS, Tanny JC, Lavender H, Li HT, Baker L, Boyle J, Blair LP, Chait BT, et al. Yng1 PHD finger binding to H3 trimethylated at K4 promotes NuA3 HAT activity at K14 of H3 and transcription at a subset of targeted ORFs. *Mol Cell.* 2006;24(5):785-96.
23. Schulze JM, Wang AY, and Kobor MS. YEATS domain proteins: a diverse family with many links to chromatin modification and transcription. *Biochem Cell Biol.* 2009;87(1):65-75.
24. Li YY, Sabari BR, Panchenko T, Wen H, Zhao D, Guan HP, Wan LL, Huang H, Tang ZY, Zhao YM, et al. Molecular Coupling of Histone Crotonylation and Active Transcription by AF9 YEATS Domain. *Mol Cell.* 2016;62(2):181-93.
25. Wang L, Xie L, Ramachandran S, Lee Y, Yan Z, Zhou L, Krajewski K, Liu F, Zhu C, Chen DJ, et al. Non-canonical Bromodomain within DNA-PKcs Promotes DNA Damage Response and Radioresistance through Recognizing an IR-Induced Acetyl-Lysine on H2AX. *Chem Biol.* 2015;22(7):849-61.
26. Kouzarides T. Acetylation: a regulatory modification to rival phosphorylation? *Embo J.* 2000;19(6):1176-9.
27. Barlev NA, Liu L, Chehab NH, Mansfield K, Harris KG, Halazonetis TD, and Berger SL. Acetylation of p53 activates transcription through recruitment of coactivators/histone acetyltransferases. *Mol Cell.* 2001;8(6):1243-54.
28. Waluk DP, Sucharski F, Sipos L, Silberring J, and Hunt MC. Reversible Lysine Acetylation Regulates Activity of Human Glycine N-Acyltransferase-like 2 (hGLYATL2) IMPLICATIONS FOR PRODUCTION OF GLYCINE-CONJUGATED SIGNALING MOLECULES. *J Biol Chem.* 2012;287(20):16158-67.
29. Nakayasu ES, Burnet MC, Walukiewicz HE, Wilkins CS, Shukla AK, Brooks S, Plutz MJ, Lee BD, Schilling B, Wolfe AJ, et al. Ancient Regulatory Role of Lysine Acetylation in Central Metabolism. *Mbio.* 2017;8(6).
30. Portran D, Schaedel L, Xu ZJ, Thery M, and Nachury MV. Tubulin acetylation protects long-lived microtubules against mechanical ageing. *Nat Cell Biol.* 2017;19(4):391-+.
31. Xu ZJ, Schaedel L, Portran D, Aguilar A, Gaillard J, Marinkovich MP, Thery M, and Nachury MV. Microtubules acquire resistance from mechanical breakage through intralumenal acetylation. *Science.* 2017;356(6335):328-32.
32. Seo JH, Park JH, Lee EJ, Vo TTL, Choi H, Kim JY, Jang JK, Wee HJ, Lee HS, Jang SH, et al. ARD1-mediated Hsp70 acetylation balances stress-induced protein refolding and degradation. *Nat Commun.* 2016;7(
33. Singh BN, Zhang GH, Hwa YL, Li JP, Dowdy SC, and Jiang SW. Nonhistone protein acetylation as cancer therapy targets. *Expert Rev Anticanc.* 2010;10(6):935-54.
34. Matsuzaki H, Daitoku H, Hatta M, Aoyama H, Yoshimochi K, and Fukamizu A. Acetylation of Foxo1 alters its DNA-binding ability and sensitivity to phosphorylation. *P Natl Acad Sci USA.* 2005;102(32):11278-83.
35. Yang XJ. The diverse superfamily of lysine acetyltransferases and their roles in leukemia and other diseases. *Nucleic Acids Res.* 2004;32(3):959-76.
36. Neuwald AF, and Landsman D. GCN5-related histone N-acetyltransferases belong to a diverse superfamily that includes the yeast SPT10 protein. *Trends Biochem Sci.* 1997;22(5):154-5.
37. Vetting MW, de Carvalho LPS, Yu M, Hegde SS, Magnet S, Roderick SL, and Blanchard JS. Structure and functions of the GNAT superfamily of acetyltransferases. *Arch Biochem Biophys.* 2005;433(1):212-26.

38. Aka JA, Kim GW, and Yang XJ. K-acetylation and its enzymes: overview and new developments. *Handb Exp Pharmacol.* 2011;206(1-12.
39. Verreault A, Kaufman PD, Kobayashi R, and Stillman B. Nucleosomal DNA regulates the core-histone-binding subunit of the human Hat1 acetyltransferase. *Current Biology.* 1998;8(2):96-108.
40. McCullough CE, and Marmorstein R. Molecular Basis for Histone Acetyltransferase Regulation by Binding Partners, Associated Domains, and Autoacetylation. *Acs Chem Biol.* 2016;11(3):632-42.
41. Sapountzi V, and Cote J. MYST-family histone acetyltransferases: beyond chromatin. *Cellular and Molecular Life Sciences.* 2011;68(7):1147-56.
42. Yang XJ. MOZ and MORF acetyltransferases: Molecular interaction, animal development and human disease. *Bba-Mol Cell Res.* 2015;1853(8):1818-26.
43. Torchia J, Glass C, and Rosenfeld MG. Co-activators and co-repressors in the integration of transcriptional responses. *Curr Opin Cell Biol.* 1998;10(3):373-83.
44. Ullah M, Pelletier N, Xiao L, Zhao SP, Wang K, Degerny C, Tahmasebi S, Cayrou C, Doyon Y, Goh SL, et al. Molecular Architecture of Quartet MOZ/MORF Histone Acetyltransferase Complexes. *Mol Cell Biol.* 2008;28(22):6828-43.
45. Yun MY, Wu J, Workman JL, and Li B. Readers of histone modifications. *Cell Research.* 2011;21(4):564-78.
46. Hecht A, Vleminckx K, Stemmler MP, van Roy F, and Kemler R. The p300/CBP acetyltransferases function as transcriptional coactivators of beta-catenin in vertebrates. *Embo J.* 2000;19(8):1839-50.
47. Shida T, Cueva JG, Xu ZJ, Goodman MB, and Nachury MV. The major alpha-tubulin K40 acetyltransferase alpha TAT1 promotes rapid ciliogenesis and efficient mechanosensation. *P Natl Acad Sci USA.* 2010;107(50):21517-22.
48. Ivanov D, Schleiffer A, Eisenhaber F, Mechtler K, Haering CH, and Nasmyth K. Eco1 is a novel acetyltransferase that can acetylate proteins involved in cohesion. *Current Biology.* 2002;12(4):323-8.
49. Hou FJ, and Zou H. Two human orthologues of Eco1/Ctf7 acetyltransferases are both required for proper sister-chromatid cohesion. *Mol Biol Cell.* 2005;16(8):3908-18.
50. Williams BC, Garrett-Engele CM, Li ZX, Williams EV, Rosenman ED, and Goldberg ML. Two putative acetyltransferases, San and deco, are required for establishing sister chromatid cohesion in drosophila. *Current Biology.* 2003;13(23):2025-36.
51. Cohen TJ, Friedmann D, Hwang AW, Marmorstein R, and Lee VMY. The microtubule-associated tau protein has intrinsic acetyltransferase activity. *Nat Struct Mol Biol.* 2013;20(6):756-+.
52. Yang XJ, and Seto E. The Rpd3/Hda1 family of lysine deacetylases: from bacteria and yeast to mice and men. *Nat Rev Mol Cell Bio.* 2008;9(3):206-18.
53. Kelly RDW, and Cowley SM. The physiological roles of histone deacetylase (HDAC) 1 and 2: complex co-stars with multiple leading parts. *Biochem Soc T.* 2013;41(741-9.
54. Ooi L, and Wood IC. Chromatin crosstalk in development and disease: lessons from REST. *Nature Reviews Genetics.* 2007;8(7):544-54.
55. Lai AY, and Wade PA. Cancer biology and NuRD: a multifaceted chromatin remodelling complex. *Nat Rev Cancer.* 2011;11(8):588-96.
56. Segre CV, and Chiocca S. Regulating the Regulators: The Post-Translational Code of Class I HDAC1 and HDAC2. *J Biomed Biotechnol.* 2011.
57. Bantscheff M, Hopf C, Savitski MM, Dittmann A, Grandi P, Michon AM, Schlegl J, Abraham Y, Becher I, Bergamini G, et al. Chemoproteomics profiling of HDAC inhibitors reveals selective targeting of HDAC complexes. *Nat Biotechnol.* 2011;29(3):255-U124.

58. Liang J, Wan M, Zhang Y, Gu PL, Xin HW, Jung SY, Qin J, Wong JM, Cooney AJ, Liu D, et al. Nanog and Oct4 associate with unique transcriptional repression complexes in embryonic stem cells. *Nature Cell Biology.* 2008;10(6):731-9.
59. Reichert N, Choukrallah MA, and Matthias P. Multiple roles of class I HDACs in proliferation, differentiation, and development. *Cellular and Molecular Life Sciences.* 2012;69(13):2173-87.
60. Millard CJ, Watson PJ, Fairall L, and Schwabe JWR. Targeting Class I Histone Deacetylases in a "Complex" Environment. *Trends Pharmacol Sci.* 2017;38(4):363-77.
61. Perissi V, Jepsen K, Glass CK, and Rosenfeld MG. Deconstructing repression: evolving models of co-repressor action. *Nature Reviews Genetics.* 2010;11(2):109-23.
62. Hassig CA, Tong JK, Fleischer TC, Owa T, Grable PG, Ayer DE, and Schreiber SL. A role for histone deacetylase activity in HDAC1-mediated transcriptional repression. *P Natl Acad Sci USA.* 1998;95(7):3519-24.
63. Jensen ED, Schroeder TM, Bailey J, Gopalakrishnan R, and Westendorf JJ. Histone deacetylase 7 associates with Runx2 and represses its activity during osteoblast maturation in a deacetylation-independent manner. *J Bone Miner Res.* 2008;23(3):361-72.
64. Khan O, and La Thangue NB. HDAC inhibitors in cancer biology: emerging mechanisms and clinical applications. *Immunology and cell biology.* 2012;90(1):85-94.
65. Hubbert C, Guardiola A, Shao R, Kawaguchi Y, Ito A, Nixon A, Yoshida M, Wang XF, and Yao TP. HDAC6 is a microtubule-associated deacetylase. *Nature.* 2002;417(6887):455-8.
66. Stiles J, and Jernigan TL. The Basics of Brain Development. *Neuropsychol Rev.* 2010;20(4):327-48.
67. Martynoga B, Drechsel D, and Guillemot F. Molecular Control of Neurogenesis: A View from the Mammalian Cerebral Cortex. *Csh Perspect Biol.* 2012;4(10).
68. Miller FD, and Gauthier AS. Timing is everything: Making neurons versus glia in the developing cortex. *Neuron.* 2007;54(3):357-69.
69. Urban N, and Guillemot F. Neurogenesis in the embryonic and adult brain: same regulators, different roles (vol 8, 396, 2014). *Front Cell Neurosci.* 2015;9(
70. Pereira JD, Sansom SN, Smith J, Dobenecker MW, Tarakhovsky A, and Livesey FJ. Ezh2, the histone methyltransferase of PRC2, regulates the balance between self-renewal and differentiation in the cerebral cortex. *P Natl Acad Sci USA.* 2010;107(36):15957-62.
71. Viosca J, Lopez-Atalaya JP, Olivares R, Eckner R, and Barco A. Syndromic features and mild cognitive impairment in mice with genetic reduction on p300 activity: Differential contribution of p300 and CBP to Rubinstein-Taybi syndrome etiology. *Neurobiol Dis.* 2010;37(1):186-94.
72. Yao TP, Oh SP, Fuchs M, Zhou ND, Ch'ng LE, Newsome D, Bronson RT, Li E, Livingston DM, and Eckner R. Gene dosage-dependent embryonic development and proliferation defects in mice lacking the transcriptional integrator p300. *Cell.* 1998;93(3):361-72.
73. Montgomery RL, Hsieh J, Barbosa AC, Richardson JA, and Olson EN. Histone deacetylases 1 and 2 control the progression of neural precursors to neurons during brain development. *P Natl Acad Sci USA.* 2009;106(19):7876-81.
74. Cunliffe VT. Eloquent silence: developmental functions of Class I histone deacetylases. *Curr Opin Genet Dev.* 2008;18(5):404-10.
75. Shah RR, and Bird AP. MeCP2 mutations: progress towards understanding and treating Rett syndrome. *Genome Med.* 2017;9(
76. Tapias A, and Wang ZQ. Lysine Acetylation and Deacetylation in Brain Development and Neuropathies. *Genom Proteom Bioinf.* 2017;15(1):19-36.

77. Berdasco M, and Esteller M. Genetic syndromes caused by mutations in epigenetic genes. *Hum Genet.* 2013;132(4):359-83.
78. Kraft M, Cirstea IC, Voss AK, Thomas T, Goehring I, Sheikh BN, Gordon L, Scott H, Smyth GK, Ahmadian MR, et al. Disruption of the histone acetyltransferase MYST4 leads to a Noonan syndrome-like phenotype and hyperactivated MAPK signaling in humans and mice. *Journal of Clinical Investigation.* 2011;121(9):3479-91.
79. Clayton-Smith J, O'Sullivan J, Daly S, Bhaskar S, Day R, Anderson B, Voss AK, Thomas T, Biesecker LG, Smith P, et al. Whole-Exome-Sequencing Identifies Mutations in Histone Acetyltransferase Gene KAT6B in Individuals with the Say-Barber-Biesecker Variant of Ohdo Syndrome. *Am J Hum Genet.* 2011;89(5):675-81.
80. Simpson MA, Deshpande C, Dafou D, Vissers LELM, Woollard WJ, Holder SE, Gillessen-Kaesbach G, Derks R, White SM, Cohen-Snuijf R, et al. De Novo Mutations of the Gene Encoding the Histone Acetyltransferase KAT6B Cause Genitopatellar Syndrome. *Am J Hum Genet.* 2012;90(2):290-4.
81. Campeau PM, Kim JC, Lu JT, Schwartzentruber JA, Abdul-Rahman OA, Schlaubitz S, Murdock DM, Jiang MM, Lammer EJ, Enns GM, et al. Mutations in KAT6B, Encoding a Histone Acetyltransferase, Cause Genitopatellar Syndrome. *Am J Hum Genet.* 2012;90(2):282-9.
82. Yu HC, Geiger EA, Medne L, Zackai EH, and Shaikh TH. An Individual With Blepharophimosis-PtosisEpicanthus Inversus Syndrome (BPES) and Additional Features Expands the Phenotype Associated With Mutations in KAT6B. *Am J Med Genet A.* 2014;164(4):950-7.
83. Arboleda VA, Lee H, Dorrani N, Zadeh N, Willis M, Macmurdo CF, Manning MA, Kwan A, Hudgins L, Barthelemy F, et al. De Novo Nonsense Mutations in KAT6A, a Lysine Acetyl-Transferase Gene, Cause a Syndrome Including Microcephaly and Global Developmental Delay. *Am J Hum Genet.* 2015;96(3):498-506.
84. Tham E, Lindstrand A, Santani A, Malmgren H, Nesbitt A, Dubbs HA, Zackai EH, Parker MJ, Millan F, Rosenbaum K, et al. Dominant Mutations in KAT6A Cause Intellectual Disability with Recognizable Syndromic Features. *Am J Hum Genet.* 2015;96(3):507-13.
85. Vega H, Waisfisz Q, Gordillo M, Sakai N, Yanagihara I, Yamada M, van Gosliga D, Kayserili H, Xu CZ, Ozono K, et al. Roberts syndrome is caused by mutations in ESCO2, a human homolog of yeast ECO1 that is essential for the establishment of sister chromatid cohesion. *Nat Genet.* 2005;37(5):468-70.
86. Williams SR, Aldred MA, Kaloustian VMD, Halal F, Gowans G, McLeod DR, Zondag S, Toriello HV, Magenis RE, and Elsea SH. Haploinsufficiency of HDAC4 Causes Brachydactyly Mental Retardation Syndrome, with Brachydactyly Type E, Developmental Delays, and Behavioral Problems. *Am J Hum Genet.* 2010;87(2):219-28.
87. Deardorff MA, Bando M, Nakato R, Watrin E, Itoh T, Minamino M, Saitoh K, Komata M, Katou Y, Clark D, et al. HDAC8 mutations in Cornelia de Lange syndrome affect the cohesin acetylation cycle. *Nature.* 2012;489(7415):313-+.
88. Yan KZ, Rousseau J, Littlejohn RO, Kiss C, Lehman A, Rosenfeld JA, Stumpel CTR, Stegmann APA, Robak L, Scaglia F, et al. Mutations in the Chromatin Regulator Gene BRPF1 Cause Syndromic Intellectual Disability and Deficient Histone Acetylation. *Am J Hum Genet.* 2017;100(1):91-104.
89. Chiu CT, Wang ZF, Hunsberger JG, and Chuang DM. Therapeutic Potential of Mood Stabilizers Lithium and Valproic Acid: Beyond Bipolar Disorder. *Pharmacol Rev.* 2013;65(1):105-42.
90. McIntyre RS, Mancini DA, McCann S, Srinivasan J, and Kennedy SH. Valproate, bipolar disorder and polycystic ovarian syndrome. *Bipolar Disord.* 2003;5(1):28-35.
91. Mckeithan TW, and Rosenbaum JL. Multiple Forms of Tubulin in the Cytoskeletal and Flagellar

Microtubules of Polytomella. *Journal of Cell Biology.* 1981;91(2):352-60.

92. Mckeithan TW, Lefebvre PA, Silflow CD, and Rosenbaum JL. Multiple Forms of Tubulin in Polytomella and Chlamydomonas - Evidence for a Precursor of Flagellar Alpha-Tubulin. *Journal of Cell Biology.* 1983;96(4):1056-63.
93. Lhernault SW, and Rosenbaum JL. Chlamydomonas Alpha-Tubulin Is Posttranslationally Modified in the Flagella during Flagellar Assembly. *Journal of Cell Biology.* 1983;97(1):258-63.
94. Lhernault SW, and Rosenbaum JL. Chlamydomonas Alpha-Tubulin Is Posttranslationally Modified by Acetylation on the Epsilon-Amino Group of a Lysine. *Biochemistry-Us.* 1985;24(2):473-8.
95. Ledizet M, and Piperno G. Identification of an Acetylation Site of Chlamydomonas Alpha-Tubulin. *P Natl Acad Sci USA.* 1987;84(16):5720-4.
96. Piperno G, and Fuller MT. Monoclonal-Antibodies Specific for an Acetylated Form of Alpha-Tubulin Recognize the Antigen in Cilia and Flagella from a Variety of Organisms. *J Cell Biol.* 1985;101(6):2085-94.
97. Piperno G, Ledizet M, and Chang XJ. Microtubules Containing Acetylated Alpha-Tubulin in Mammalian-Cells in Culture. *J Cell Biol.* 1987;104(2):289-302.
98. Nakagawa U, Suzuki D, Ishikawa M, Sato H, Kamemura K, and Imamura A. Acetylation of alpha-Tubulin on Lys(40) Is a Widespread Post-Translational Modification in Angiosperms. *Biosci Biotech Bioch.* 2013;77(7):1602-5.
99. Yang XJ, and Grégoire S. Class II histone deacetylases: From sequence to function, regulation and clinical implication. *Mol Cell Biol.* 2005;25(2873-84.
100. Choudhary C, Kumar C, Gnad F, Nielsen ML, Rehman M, Walther TC, Olsen JV, and Mann M. Lysine acetylation targets protein complexes and co-regulates major cellular functions. *Science.* 2009;325(5942):834-40.
101. Chu CW, Hou FJ, Zhang JM, Phu L, Loktev AV, Kirkpatrick DS, Jackson PK, Zhao YM, and Zou H. A novel acetylation of beta-tubulin by San modulates microtubule polymerization via down-regulating tubulin incorporation. *Mol Biol Cell.* 2011;22(4):448-56.
102. Greer K, Maruta H, L'Hernault SW, and Rosenbaum JL. Alpha-tubulin acetylase activity in isolated Chlamydomonas flagella. *J Cell Biol.* 1985;101(6):2081-4.
103. Creppe C, Malinouskaya L, Volvert ML, Gillard M, Close P, Malaise O, Laguesse S, Cornez I, Rahmouni S, Ormenese S, et al. Elongator controls the migration and differentiation of cortical neurons through acetylation of alpha-tubulin. *Cell.* 2009;136(3):551-64.
104. Solinger JA, Paolinelli R, Kloss H, Scorza FB, Marchesi S, Sauder U, Mitsushima D, Capuani F, Sturzenbaum SR, and Cassata G. The Caenorhabditis elegans Elongator Complex Regulates Neuronal alpha-tubulin Acetylation. *Plos Genet.* 2010;6(1).
105. Ohkawa N, Sugisaki S, Tokunaga E, Fujitani K, Hayasaka T, Setou M, and Inokuchi K. N-acetyltransferase ARD1-NAT1 regulates neuronal dendritic development. *Genes Cells.* 2008;13(11):1171-83.
106. Conacci-Sorrell M, Ngouenet C, and Eisenman RN. Myc-nick: a cytoplasmic cleavage product of Myc that promotes alpha-tubulin acetylation and cell differentiation. *Cell.* 2010;142(3):480-93.
107. Zhang Y, Ma C, Delohery T, Nasipak B, Foat BC, Bounoutas A, Bussemaker HJ, Kim SK, and Chalfie M. Identification of genes expressed in C. elegans touch receptor neurons. *Nature.* 2002;418(6895):331-5.
108. Chalfie M. Neurosensory mechanotransduction. *Nat Rev Mol Cell Biol.* 2009;10(1):44-52.
109. Steczkiewicz K, Kinch L, Grishin NV, Rychlewski L, and Ginalski K. Eukaryotic domain of unknown

function DUF738 belongs to Gcn5-related N-acetyltransferase superfamily. *Cell Cycle.* 2006;5(24):2927-30.

110. Akella JS, Wloga D, Kim J, Starostina NG, Lyons-Abbott S, Morrissette NS, Dougan ST, Kipreos ET, and Gaertig J. MEC-17 is an alpha-tubulin acetyltransferase. *Nature.* 2010;467(7312):218-22.
111. Kim GW, Li L, Gorbani M, You L, and Yang XJ. Mice lacking alpha-tubulin acetyltransferase 1 are viable but display alpha-tubulin acetylation deficiency and dentate gyrus distortion. *J Biol Chem.* 2013;288(28):20334-50.
112. Kalebic N, Sorrentino S, Perlas E, Bolasco G, Martinez C, and Heppenstall PA. alpha TAT1 is the major alpha-tubulin acetyltransferase in mice. *Nat Commun.* 2013;4(
113. Aguilar A, Becker L, Tedeschi T, Heller S, Iomini C, and Nachury MV. alpha-Tubulin K40 acetylation is required for contact inhibition of proliferation and cell-substrate adhesion. *Mol Biol Cell.* 2014;25(12):1854-66.
114. Kormendi V, Szyk A, Piszczek G, and Roll-Mecak A. Crystal Structures of Tubulin Acetyltransferase Reveal a Conserved Catalytic Core and the Plasticity of the Essential N Terminus. *J Biol Chem.* 2012;287(50):41569-75.
115. Taschner M, Vetter M, and Lorentzen E. Atomic resolution structure of human alpha-tubulin acetyltransferase bound to acetyl-CoA. *Proc Natl Acad Sci U S A.* 2012;109(48):19649-54.
116. Friedmann DR, Aguilar A, Fan J, Nachury MV, and Marmorstein R. Structure of the alpha-tubulin acetyltransferase, alphaTAT1, and implications for tubulin-specific acetylation. *Proc Natl Acad Sci U S A.* 2012;109(48):19655-60.
117. Davenport AM, Collins LN, Chiu H, Minor PJ, Sternberg PW, and Hoelz A. Structural and Functional Characterization of the alpha-Tubulin Acetyltransferase MEC-17. *J Mol Biol.* 2014;426(14):2605-16.
118. Yuzawa S, Kamakura S, Hayase J, and Sumimoto H. Structural basis of cofactor-mediated stabilization and substrate recognition of the alpha-tubulin acetyltransferase alphaTAT1. *The Biochemical journal.* 2015;467(1):103-13.
119. Westermann S, and Weber K. Post-translational modifications regulate microtubule function. *Nat Rev Mol Cell Bio.* 2003;4(12):938-47.
120. Wloga D, and Gaertig J. Post-translational modifications of microtubules. *J Cell Sci.* 2010;123(20):3447-55.
121. Janke C, and Bulinski JC. Post-translational regulation of the microtubule cytoskeleton: mechanisms and functions. *Nat Rev Mol Cell Bio.* 2011;12(12):773-86.
122. Janke C. The tubulin code: molecular components, readout mechanisms, and functions. *J Cell Biol.* 2014;206(4):461-72.
123. Odde D. Diffusion inside microtubules. *Eur Biophys J Biophy.* 1998;27(5):514-20.
124. Maruta H, Greer K, and Rosenbaum JL. The Acetylation of Alpha-Tubulin and Its Relationship to the Assembly and Disassembly of Microtubules. *Journal of Cell Biology.* 1986;103(2):571-9.
125. Szyk A, Deaconescu AM, Spector J, Goodman B, Valenstein ML, Ziolkowska NE, Kormendi V, Grigorieff N, and Roll-Mecak A. Molecular basis for age-dependent microtubule acetylation by tubulin acetyltransferase. *Cell.* 2014;157(6):1405-15.
126. Zhang Y, Li N, Caron C, Matthias G, Hess D, Khochbin S, and Matthias P. HDAC-6 interacts with and deacetylates tubulin and microtubules in vivo. *Embo J.* 2003;22(5):1168-79.
127. Matsuyama A, Shimazu T, Sumida Y, Saito A, Yoshimatsu Y, Seigneurin-Berny D, Osada H, Komatsu Y, Nishino N, Khochbin S, et al. In vivo destabilization of dynamic microtubules by HDAC6-mediated deacetylation. *Embo J.* 2002;21(24):6820-31.

128. North BJ, Marshall BL, Borra MT, Denu JM, and Verdin E. The human Sir2 ortholog, SIRT2, is an NAD(+)-dependent tubulin deacetylase. *Mol Cell.* 2003;11(2):437-44.
129. Bobrowska A, Donmez G, Weiss A, Guarente L, and Bates G. SIRT2 Ablation Has No Effect on Tubulin Acetylation in Brain, Cholesterol Biosynthesis or the Progression of Huntington's Disease Phenotypes In Vivo. *Plos One.* 2012;7(4).
130. Taes I, Timmers M, Hersmus N, Bento-Abreu A, Van den Bosch L, Van Damme P, Auwerx J, and Robberecht W. Hdac6 deletion delays disease progression in the SOD1(G93A) mouse model of ALS. *Hum Mol Genet.* 2013;22(9):1783-90.
131. Zhang Y, Kwon S, Yamaguchi T, Cubizolles F, Rousseaux S, Kneissel M, Cao C, Li N, Cheng HL, Chua K, et al. Mice lacking histone deacetylase 6 have hyperacetylated tubulin but are viable and develop normally. *Mol Cell Biol.* 2008;28(5):1688-701.
132. Nagai T, Ikeda M, Chiba S, Kanno S, and Mizuno K. Furry promotes acetylation of microtubules in the mitotic spindle by inhibition of SIRT2 tubulin deacetylase. *J Cell Sci.* 2013;126(19):4369-80.
133. Misawa T, Takahama M, Kozaki T, Lee H, Zou J, Saitoh T, and Akira S. Microtubule-driven spatial arrangement of mitochondria promotes activation of the NLRP3 inflammasome. *Nat Immunol.* 2013;14(5):454-60.
134. Cho Y, and Cavalli V. HDAC5 is a novel injury-regulated tubulin deacetylase controlling axon regeneration. *Embo J.* 2012;31(14):3063-78.
135. Bertos NR, Gilquin B, Chan GK, Yen TJ, Khochbin S, and Yang XJ. Role of the tetradecapeptide repeat domain of human histone deacetylase 6 in cytoplasmic retention. *J Biol Chem.* 2004;279(46):48246-54.
136. Liu YJ, Peng LR, Seto E, Huang SM, and Qiu Y. Modulation of Histone Deacetylase 6 (HDAC6) Nuclear Import and Tubulin Deacetylase Activity through Acetylation. *J Biol Chem.* 2012;287(34):29168-74.
137. Zhang M, Xiang S, Joo HY, Wang L, Williams KA, Liu W, Hu C, Tong D, Haakenson J, Wang C, et al. HDAC6 deacetylates and ubiquitinates MSH2 to maintain proper levels of MutSalpha. *Mol Cell.* 2014;55(1):31-46.
138. Verdel A, Curtet S, Brocard MP, Rousseaux S, Lemercier C, Yoshida M, and Khochbin S. Active maintenance of mHDA2/mHDAC6 histone-deacetylase in the cytoplasm. *Curr Biol.* 2000;10(747-9.
139. Cook C, Gendron TF, Scheffel K, Carlomagno Y, Dunmore J, DeTure M, and Petrucelli L. Loss of HDAC6, a novel CHIP substrate, alleviates abnormal tau accumulation. *Hum Mol Genet.* 2012;21(13):2936-45.
140. Fusco C, Micale L, Augello B, Mandriani B, Pellico MT, De Nittis P, Calcagni A, Monti M, Cozzolino F, Pucci P, et al. HDAC6 mediates the acetylation of TRIM50. *Cell Signal.* 2014;26(2):363-9.
141. Zhang XH, Yuan ZG, Zhang YT, Yong S, Salas-Burgos A, Koomen J, Olashaw N, Parsons JT, Yang XJ, Dent SR, et al. HDAC6 modulates cell motility by altering the acetylation level of cortactin. *Mol Cell.* 2007;27(2):197-213.
142. Boyault C, Zhang Y, Fritah S, Caron C, Gilquin B, Kwon SH, Garrido C, Yao TP, Vourc'h C, Matthias P, et al. HDAC6 controls major cell response pathways to cytotoxic accumulation of protein aggregates. *Gene Dev.* 2007;21(17):2172-81.
143. Kawaguchi Y, Kovacs JJ, McLaurin A, Vance JM, Ito A, and Yao TP. The deacetylase HDAC6 regulates aggresome formation and cell viability in response to misfolded protein stress. *Cell.* 2003;115(6):727-38.
144. Palijan A, Fernandes I, Bastien Y, Tang LQ, Verway M, Kourelis M, Tavera-Mendoza LE, Li Z, Bourdeau V, Mader S, et al. Function of Histone Deacetylase 6 as a Cofactor of Nuclear Receptor Coregulator LCoR. *J Biol Chem.* 2009;284(44):30264-74.

145. Chen SG, Owens GC, Makarenkova H, and Edelman DB. HDAC6 Regulates Mitochondrial Transport in Hippocampal Neurons. *Plos One.* 2010;5(5).
146. Pandey UB, Nie ZP, Batlevi Y, McCray BA, Ritson GP, Nedelsky NB, Schwartz SL, DiProspero NA, Knight MA, Schuldiner O, et al. HDAC6 rescues neurodegeneration and provides an essential link between autophagy and the UPS. *Nature.* 2007;447(7146):859-63.
147. Fukada M, Hanai A, Nakayama A, Suzuki T, Miyata N, Rodriguiz RM, Wetsel WC, Yao TP, and Kawaguchi Y. Loss of Deacetylation Activity of Hdac6 Affects Emotional Behavior in Mice. *Plos One.* 2012;7(2).
148. Sadoul K, Wang J, Diagouraga B, Vitte AL, Buchou T, Rossini T, Polack B, Xi XD, Matthias P, and Khochbin S. HDAC6 controls the kinetics of platelet activation. *Blood.* 2012;120(20):4215-8.
149. Wang B, Rao YH, Inoue M, Hao R, Lai CH, Chen D, McDonald SL, Choi MC, Wang Q, Shinohara ML, et al. Microtubule acetylation amplifies p38 kinase signalling and anti-inflammatory IL-10 production. *Nat Commun.* 2014;5(3479.
150. Ledizet M, and Piperno G. Cytoplasmic Microtubules Containing Acetylated Alpha-Tubulin in Chlamydomonas-Reinhardtii - Spatial Arrangement and Properties. *Journal of Cell Biology.* 1986;103(1):13-22.
151. Cambray-Deakin MA, and Burgoyne RD. Acetylated and detyrosinated alpha-tubulins are co-localized in stable microtubules in rat meningeal fibroblasts. *Cell motility and the cytoskeleton.* 1987;8(3):284-91.
152. Webster DR, and Borisy GG. Microtubules Are Acetylated in Domains That Turn over Slowly. *J Cell Sci.* 1989;92(57-65.
153. Robson SJ, and Burgoyne RD. Differential Localization of Tyrosinated, Detyrosinated, and Acetylated Alpha-Tubulins in Neurites and Growth Cones of Dorsal-Root Ganglion Neurons. *Cell motility and the cytoskeleton.* 1989;12(4):273-82.
154. Sale WS, Besharse JC, and Piperno G. Distribution of acetylated alpha-tubulin in retina and in vitro-assembled microtubules. *Cell motility and the cytoskeleton.* 1988;9(3):243-53.
155. Cambraydeakin MA, and Burgoyne RD. Posttranslational Modifications of Alpha-Tubulin - Acetylated and Detyrosinated Forms in Axons of Rat Cerebellum. *Journal of Cell Biology.* 1987;104(6):1569-74.
156. Cambraydeakin MA, and Burgoyne RD. Acetylated and Detyrosinated Alpha-Tubulins Are Co-Localized in Stable Microtubules in Rat Meningeal Fibroblasts. *Cell motility and the cytoskeleton.* 1987;8(3):284-91.
157. Wehland J, and Weber K. Turnover of the Carboxy-Terminal Tyrosine of Alpha-Tubulin and Means of Reaching Elevated Levels of Detyrosination in Living Cells. *J Cell Sci.* 1987;88(185-203.
158. Bre MH, Kreis TE, and Karsenti E. Control of Microtubule Nucleation and Stability in Madin-Darby Canine Kidney-Cells - the Occurrence of Noncentrosomal, Stable Detyrosinated Microtubules. *Journal of Cell Biology.* 1987;105(3):1283-96.
159. Khawaja S, Gundersen GG, and Bulinski JC. Enhanced Stability of Microtubules Enriched in Detyrosinated Tubulin Is Not a Direct Function of Detyrosination Level. *Journal of Cell Biology.* 1988;106(1):141-9.
160. Palazzo A, Ackerman B, and Gundersen GG. Cell biology - Tubulin acetylation and cell motility. *Nature.* 2003;421(6920):230-.
161. Howes SC, Alushin GM, Shida T, Nachury MV, and Nogales E. Effects of tubulin acetylation and tubulin acetyltransferase binding on microtubule structure. *Mol Biol Cell.* 2014;25(2):257-66.
162. Barisic M, Silva ESR, Tripathy SK, Magiera MM, Zaytsev AV, Pereira AL, Janke C, Grishchuk EL, and Maiato H. Microtubule detyrosination guides chromosomes during mitosis. *Science.* 2015:epub.

163. Zilberman Y, Ballestrem C, Carramusa L, Mazitschek R, Khochbin S, and Bershadsky A. Regulation of microtubule dynamics by inhibition of the tubulin deacetylase HDAC6. *J Cell Sci.* 2009;122(19):3531-41.
164. Neumann B, and Hilliard MA. Loss of MEC-17 Leads to Microtubule Instability and Axonal Degeneration. *Cell Rep.* 2014;6(1):93-103.
165. Tilney LG, Bryan J, Bush DJ, Fujiwara K, Mooseker MS, Murphy DB, and Snyder DH. Microtubules: evidence for 13 protofilaments. *J Cell Biol.* 1973;59(2 Pt 1):267-75.
166. Burton PR, Hinkley RE, and Pierson GB. Tannic acid-stained microtubules with 12, 13, and 15 protofilaments. *J Cell Biol.* 1975;65(1):227-33.
167. Saito K, and Hama K. Structural diversity of microtubules in the supporting cells of the sensory epithelium of guinea pig organ of Corti. *J Electron Microsc (Tokyo).* 1982;31(3):278-81.
168. Nagano T, and Suzuki F. Microtubules with 15 subunits in cockroach epidermal cells. *J Cell Biol.* 1975;64(1):242-5.
169. Chalfie M, and Thomson JN. Organization of neuronal microtubules in the nematode Caenorhabditis elegans. *J Cell Biol.* 1979;82(1):278-89.
170. Pierson GB, Burton PR, and Himes RH. Wall substructure of microtubules polymerized in vitro from tubulin of crayfish nerve cord and fixed with tannic acid. *J Cell Sci.* 1979;39(89-99.
171. Aamodt EJ, and Culotti JG. Microtubules and microtubule-associated proteins from the nematode Caenorhabditis elegans: periodic cross-links connect microtubules in vitro. *J Cell Biol.* 1986;103(1):23-31.
172. Andreu JM, Bordas J, Diaz JF, Garcia de Ancos J, Gil R, Medrano FJ, Nogales E, Pantos E, and Towns-Andrews E. Low resolution structure of microtubules in solution. Synchrotron X-ray scattering and electron microscopy of taxol-induced microtubules assembled from purified tubulin in comparison with glycerol and MAP-induced microtubules. *J Mol Biol.* 1992;226(1):169-84.
173. Moores CA, Perderiset M, Francis F, Chelly J, Houdusse A, and Milligan RA. Mechanism of microtubule stabilization by doublecortin. *Mol Cell.* 2004;14(6):833-9.
174. Bechstedt S, and Brouhard GJ. Doublecortin recognizes the 13-protofilament microtubule cooperatively and tracks microtubule ends. *Dev Cell.* 2012;23(1):181-92.
175. White JG, Southgate E, Thomson JN, and Brenner S. The structure of the nervous system of the nematode Caenorhabditis elegans. *Philos Trans R Soc Lond B Biol Sci.* 1986;314(1165):1-340.
176. Cueva JG, Mulholland A, and Goodman MB. Nanoscale organization of the MEC-4 DEG/ENaC sensory mechanotransduction channel in Caenorhabditis elegans touch receptor neurons. *J Neurosci.* 2007;27(51):14089-98.
177. Topalidou I, Keller C, Kalebic N, Nguyen KCQ, Somhegyi H, Politi KA, Heppenstall P, Hall DH, and Chalfie M. Genetically Separable Functions of the MEC-17 Tubulin Acetyltransferase Affect Microtubule Organization. *Curr Biol.* 2012;22(12):1057-65.
178. Siddiqui SS, Aamodt E, Rastinejad F, and Culotti J. Anti-tubulin monoclonal antibodies that bind to specific neurons in Caenorhabditis elegans. *J Neurosci.* 1989;9(8):2963-72.
179. Fukushige T, Siddiqui ZK, Chou M, Culotti JG, Gogonea CB, Siddiqui SS, and Hamelin M. MEC-12, an alpha-tubulin required for touch sensitivity in C. elegans. *J Cell Sci.* 1999;112 (Pt 3)(395-403.
180. Cueva JG, Hsin J, Huang KC, and Goodman MB. Posttranslational Acetylation of alpha-Tubulin Constrains Protofilament Number in Native Microtubules. *Curr Biol.* 2012;22(12):1066-74.
181. Tolomeo JA, and Holley MC. Mechanics of microtubule bundles in pillar cells from the inner ear. *Biophys J.* 1997;73(4):2241-7.

182. Tannenbaum J, and Slepecky NB. Localization of microtubules containing posttranslationally modified tubulin in cochlear epithelial cells during development. *Cell motility and the cytoskeleton.* 1997;38(2):146-62.
183. Reed NA, Cai DW, Blasius TL, Jih GT, Meyhofer E, Gaertig J, and Verhey KJ. Microtubule acetylation promotes kinesin-1 binding and transport. *Curr Biol.* 2006;16(21):2166-72.
184. Cai DW, McEwen DP, Martens JR, Meyhofer E, and Verhey KJ. Single Molecule Imaging Reveals Differences in Microtubule Track Selection Between Kinesin Motors. *Plos Biol.* 2009;7(10).
185. Bhuwania R, Castro-Castro A, and Linder S. Microtubule acetylation regulates dynamics of KIF1C-powered vesicles and contact of microtubule plus ends with podosomes. *European journal of cell biology.* 2014.
186. Dompierre JP, Godin JD, Charrin BC, Cordelieres FP, King SJ, Humbert S, and Saudou F. Histone deacetylase 6 inhibition compensates for the transport deficit in Huntington's disease by increasing tubulin acetylation. *J Neurosci.* 2007;27(13):3571-83.
187. Kaul N, Soppina V, and Verhey KJ. Effects of alpha-tubulin K40 acetylation and detyrosination on kinesin-1 motility in a purified system. *Biophys J.* 2014;106(12):2636-43.
188. Hammond JW, Huang CF, Kaech S, Jacobson C, Banker G, and Verhey KJ. Posttranslational Modifications of Tubulin and the Polarized Transport of Kinesin-1 in Neurons. *Mol Biol Cell.* 2010;21(4):572-83.
189. Witte H, Neukirchen D, and Bradke F. Microtubule stabilization specifies initial neuronal polarization. *Journal of Cell Biology.* 2008;180(3):619-32.
190. Birdsey GM, Dryden NH, Shah AV, Hannah R, Hall MD, Haskard DO, Parsons M, Mason JC, Zvelebil M, Gottgens B, et al. The transcription factor Erg regulates expression of histone deacetylase 6 and multiple pathways involved in endothelial cell migration and angiogenesis. *Blood.* 2012;119(3):894-903.
191. Li L, Wei D, Wang Q, Pan J, Liu R, Zhang X, and Bao L. MEC-17 Deficiency Leads to Reduced alpha-Tubulin Acetylation and Impaired Migration of Cortical Neurons. *J Neurosci.* 2012;32(37):12673-83.
192. Selvadurai K, Wang P, Seimetz J, and Huang RH. Archaeal Elp3 catalyzes tRNA wobble uridine modification at C5 via a radical mechanism. *Nat Chem Biol.* 2014;10(10):810-2.
193. Deakin NO, and Turner CE. Paxillin inhibits HDAC6 to regulate microtubule acetylation, Golgi structure, and polarized migration. *J Cell Biol.* 2014;206(3):395-413.
194. Montagnac G, Meas-Yedid V, Irondelle M, Castro-Castro A, Franco M, Shida T, Nachury MV, Benmerah A, Olivo-Marin JC, and Chavrier P. alphaTAT1 catalyses microtubule acetylation at clathrin-coated pits. *Nature.* 2013;502(7472):567-70.
195. Tran ADA, Marmo TP, Salam AA, Che S, Finkelstein E, Kabarriti R, Xenias HS, Mazitschek R, Hubbert C, Kawaguchi Y, et al. HDAC6 deacetylation of tubulin modulates dynamics of cellular adhesions. *J Cell Sci.* 2007;120(8):1469-79.
196. Castro-Castro A, Janke C, Montagnac G, Paul-Gilloteaux P, and Chavrier P. ATAT1/MEC-17 acetyltransferase and HDAC6 deacetylase control a balance of acetylation of alpha-tubulin and cortactin and regulate MT1-MMP trafficking and breast tumor cell invasion. *European journal of cell biology.* 2012;91(11-12):950-60.
197. Wu Y, Song SW, Sun JY, Bruner JM, Fuller GN, and Zhang W. IIp45 Inhibits Cell Migration through Inhibition of HDAC6. *J Biol Chem.* 2010;285(6):3554-60.
198. Penela P, Lafarga V, Tapia O, Rivas V, Nogues L, Lucas E, Vila-Bedmar R, Murga C, and Mayor F. Roles of GRK2 in Cell Signaling Beyond GPCR Desensitization: GRK2-HDAC6 Interaction Modulates Cell Spreading and Motility. *Sci Signal.* 2012;5(224).

199. Chang JF, Baloh RH, and Milbrandt J. The NIMA-family kinase Nek3 regulates microtubule acetylation in neurons. *J Cell Sci.* 2009;122(13):2274-82.
200. Pugacheva EN, Jablonski SA, Hartman TR, Henske EP, and Golemis EA. HEF1-dependent Aurora A activation induces disassembly of the primary cilium. *Cell.* 2007;129(7):1351-63.
201. Bangs FK, Schrode N, Hadjantonakis AK, and Anderson KV. Lineage specificity of primary cilia in the mouse embryo. *Nat Cell Biol.* 2015;17(2):113-22.
202. Nakakura T, Asano-Hoshino A, Suzuki T, Arisawa K, Tanaka H, Sekino Y, Kiuchi Y, Kawai K, and Hagiwara H. The elongation of primary cilia via the acetylation of alpha-tubulin by the treatment with lithium chloride in human fibroblast KD cells. *Medical molecular morphology.* 2014.
203. Loktev AV, Zhang Q, Beck JS, Searby CC, Scheetz TE, Bazan JF, Slusarski DC, Sheffield VC, Jackson PK, and Nachury MV. A BBSome subunit links ciliogenesis, microtubule stability, and acetylation. *Dev Cell.* 2008;15(6):854-65.
204. He Q, Wang G, Wakade S, Dasgupta S, Dinkins M, Kong JN, Spassieva SD, and Bieberich E. Primary cilia in stem cells and neural progenitors are regulated by neutral sphingomyelinase 2 and ceramide. *Mol Biol Cell.* 2014;25(11):1715-29.
205. Wickstrom SA, Masoumi KC, Khochbin S, Fassler R, and Massoumi R. CYLD negatively regulates cell-cycle progression by inactivating HDAC6 and increasing the levels of acetylated tubulin. *Embo J.* 2010;29(1):131-44.
206. Eguether T, Ermolaeva MA, Zhao Y, Bonnet MC, Jain A, Pasparakis M, Courtois G, and Tassin AM. The deubiquitinating enzyme CYLD controls apical docking of basal bodies in ciliated epithelial cells. *Nat Commun.* 2014;5(4585.
207. Yang Y, Ran J, Liu M, Li D, Li Y, Shi X, Meng D, Pan J, Ou G, Aneja R, et al. CYLD mediates ciliogenesis in multiple organs by deubiquitinating Cep70 and inactivating HDAC6. *Cell Res.* 2014;24(11):1342-53.
208. Oh EC, and Katsanis N. Cilia in vertebrate development and disease. *Development.* 2012;139(3):443-8.
209. Goetz SC, and Anderson KV. The primary cilium: a signalling centre during vertebrate development. *Nat Rev Genet.* 2010;11(5):331-44.
210. de Zoeten EF, Wang L, Butler K, Beier UH, Akimova T, Sai H, Bradner JE, Mazitschek R, Kozikowski AP, Matthias P, et al. Histone deacetylase 6 and heat shock protein 90 control the functions of Foxp3(+) T-regulatory cells. *Mol Cell Biol.* 2011;31(10):2066-78.
211. Hanania R, Sun HS, Xu K, Pustylnik S, Jeganathan S, and Harrison RE. Classically activated macrophages use stable microtubules for matrix metalloproteinase-9 (MMP-9) secretion. *J Biol Chem.* 2012;287(11):8468-83.
212. Schroder K, and Tschopp J. The inflammasomes. *Cell.* 2010;140(6):821-32.
213. Misawa T, Takahama M, Kozaki T, Park S, Saitoh T, and Akira S. Resveratrol inhibits the acetylated alpha-tubulin-mediated assembly of the NLRP3-inflammasome. *Int Immunol.* 2015.
214. Kratzer E, Tian Y, Sarich N, Wu T, Meliton A, Leff A, and Birukova AA. Oxidative stress contributes to lung injury and barrier dysfunction via microtubule destabilization. *Am J Respir Cell Mol Biol.* 2012;47(5):688-97.
215. Ishiguro K, Ando T, Maeda O, Watanabe O, and Goto H. Cutting edge: tubulin alpha functions as an adaptor in NFAT-importin beta interaction. *J Immunol.* 2011;186(5):2710-3.
216. Ishiguro K, Ando T, Maeda O, Watanabe O, and Goto H. Suppressive action of acetate on interleukin-8 production via tubulin-alpha acetylation. *Immunology and cell biology.* 2014.
217. Sabo Y, Walsh D, Barry DS, Tinaztepe S, de Los Santos K, Goff SP, Gundersen GG, and Naghavi MH.

HIV-1 induces the formation of stable microtubules to enhance early infection. *Cell Host Microbe.* 2013;14(5):535-46.

218. Valenzuela-Fernandez A, Alvarez S, Gordon-Alonso M, Barrero M, Ursa A, Cabrero JR, Fernandez G, Naranjo-Suarez S, Yanez-Mo M, Serrador JM, et al. Histone deacetylase 6 regulates human immunodeficiency virus type 1 infection. *Mol Biol Cell.* 2005;16(11):5445-54.
219. Husain M, and Harrod KS. Enhanced acetylation of alpha-tubulin in influenza A virus infected epithelial cells. *FEBS Lett.* 2011;585(1):128-32.
220. Husain M, and Cheung CY. Histone deacetylase 6 inhibits influenza A virus release by downregulating the trafficking of viral components to the plasma membrane via its substrate, acetylated microtubules. *J Virol.* 2014;88(19):11229-39.
221. Naranatt PP, Krishnan HH, Smith MS, and Chandran B. Kaposi's sarcoma-associated herpesvirus modulates microtubule dynamics via RhoA-GTP-diaphanous 2 signaling and utilizes the dynein motors to deliver its DNA to the nucleus. *J Virol.* 2005;79(2):1191-206.
222. Zhong M, Zheng K, Chen M, Xiang Y, Jin F, Ma K, Qiu X, Wang Q, Peng T, Kitazato K, et al. Heat-shock protein 90 promotes nuclear transport of herpes simplex virus 1 capsid protein by interacting with acetylated tubulin. *Plos One.* 2014;9(6):e99425.
223. Li W, Zhao YZ, and Chou IN. Nickel (Ni2+) enhancement of alpha-tubulin acetylation in cultured 3T3 cells. *Toxicol Appl Pharm.* 1996;140(2):461-70.
224. Mackeh R, Lorin S, Ratier A, Mejdoubi-Charef N, Baillet A, Bruneel A, Hamai A, Codogno P, Pous C, and Perdiz D. Reactive Oxygen Species, AMP-activated Protein Kinase, and the Transcription Cofactor p300 Regulate alpha- Tubulin Acetyltransferase-1 (alpha TAT-1/MEC-17)- dependent Microtubule Hyperacetylation during Cell Stress. *J Biol Chem.* 2014;289(17):11816-28.
225. Pandey K, and Sharma SK. Activity-Dependent Acetylation of Alpha Tubulin in the Hippocampus. *J Mol Neurosci.* 2011;45(1):1-4.
226. Takemura R, Okabe S, Umeyama T, Kanai Y, Cowan NJ, and Hirokawa N. Increased Microtubule Stability and Alpha-Tubulin Acetylation in Cells Transfected with Microtubule-Associated Proteins Map1b, Map2 or Tau. *J Cell Sci.* 1992;103(953-64.
227. Erdozain AM, Morentin B, Bedford L, King E, Tooth D, Brewer C, Wayne D, Johnson L, Gerdes HK, Wigmore P, et al. Alcohol-related brain damage in humans. *Plos One.* 2014;9(4):e93586.
228. Sudo H, and Baas PW. Acetylation of Microtubules Influences Their Sensitivity to Severing by Katanin in Neurons and Fibroblasts. *Journal of Neuroscience.* 2010;30(21):7215-26.
229. Casale CH, Previtali G, and Barra HS. Involvement of acetylated tubulin in the regulation of Na+,K+ -ATPase activity in cultured astrocytes. *FEBS Lett.* 2003;534(1-3):115-8.
230. Santander VS, Bisig CG, Purro SA, Casale CH, Arce CA, and Barra HS. Tubulin must be acetylated in order to form a complex with membrane Na+,K+-ATPase and to inhibit its enzyme activity. *Mol Cell Biochem.* 2006;291(1-2):167-74.
231. Casale CH, Previtali G, Serafino JJ, Arce CA, and Barra HS. Regulation of acetylated tubulin/Na+ K+-ATPase interaction by L-glutamate in non-neural cells: involvement of microtubules. *Bba-Gen Subjects.* 2005;1721(1-3):185-92.
232. Casale CH, Alonso AD, and Barra HS. Brain plasmamembrane NA(+),K+-ATPase is inhibited by acetylated tubulin. *Mol Cell Biochem.* 2001;216(1-2):85-92.
233. Arce CA, Casale CH, and Barra HS. Submembraneous microtubule cytoskeleton: regulation of ATPases by interaction with acetylated tubulin. *Febs J.* 2008;275(19):4664-74.
234. Yang WL, Guo XX, Thein S, Xu F, Sugii S, Baas PW, Radda GK, and Han WP. Regulation of

adipogenesis by cytoskeleton remodelling is facilitated by acetyltransferase MEC-17-dependent acetylation of alpha-tubulin. *Biochemical Journal.* 2013;449(605-12.

235. Xie R, Nguyen S, McKeehan WL, and Liu LY. Acetylated microtubules are required for fusion of autophagosomes with lysosomes. *Bmc Cell Biol.* 2010;11(

236. Geeraert C, Ratier A, Pfisterer SG, Perdiz D, Cantaloube I, Rouault A, Pattingre S, Proikas-Cezanne T, Codogno P, and Pous C. Starvation-induced Hyperacetylation of Tubulin Is Required for the Stimulation of Autophagy by Nutrient Deprivation. *J Biol Chem.* 2010;285(31):24184-94.

237. d'Ydewalle C, Krishnan J, Chiheb DM, Van Damme P, Irobi J, Kozikowski AP, Vanden Berghe P, Timmerman V, Robberecht W, and Van Den Bosch L. HDAC6 inhibitors reverse axonal loss in a mouse model of mutant HSPB1-induced Charcot-Marie-Tooth disease. *Nat Med.* 2011;17(8):968-74.

238. Dafinger C, Liebau MC, Elsayed SM, Hellenbroich Y, Boltshauser E, Korenke GC, Fabretti F, Janecke AR, Ebermann I, Nurnberg G, et al. Mutations in KIF7 link Joubert syndrome with Sonic Hedgehog signaling and microtubule dynamics. *J Clin Invest.* 2011;121(7):2662-7.

239. Gilks WP, Abou-Sleiman PM, Gandhi S, Jain S, Singleton A, Lees AJ, Shaw K, Bhatia KP, Bonifati V, Quinn NP, et al. A common LRRK2 mutation in idiopathic Parkinson's disease. *Lancet.* 2005;365(9457):415-6.

240. Law BM, Spain VA, Leinster VH, Chia R, Beilina A, Cho HJ, Taymans JM, Urban MK, Sancho RM, Blanca Ramirez M, et al. A direct interaction between leucine-rich repeat kinase 2 and specific beta-tubulin isoforms regulates tubulin acetylation. *J Biol Chem.* 2014;289(2):895-908.

241. Godena VK, Brookes-Hocking N, Moller A, Shaw G, Oswald M, Sancho RM, Miller CC, Whitworth AJ, and De Vos KJ. Increasing microtubule acetylation rescues axonal transport and locomotor deficits caused by LRRK2 Roc-COR domain mutations. *Nat Commun.* 2014;5(5245.

242. Govindarajan N, Rao P, Burkhardt S, Sananbenesi F, Schluter OM, Bradke F, Lu J, and Fischer A. Reducing HDAC6 ameliorates cognitive deficits in a mouse model for Alzheimer's disease. *EMBO molecular medicine.* 2013;5(1):52-63.

243. Selenica ML, Benner L, Housley SB, Manchec B, Lee DC, Nash KR, Kalin J, Bergman JA, Kozikowski A, Gordon MN, et al. Histone deacetylase 6 inhibition improves memory and reduces total tau levels in a mouse model of tau deposition. *Alzheimer's research & therapy.* 2014;6(1):12.

244. Yu CW, Chang PT, Hsin LW, and Chern JW. Quinazolin-4-one derivatives as selective histone deacetylase-6 inhibitors for the treatment of Alzheimer's disease. *J Med Chem.* 2013;56(17):6775-91.

245. Zhang L, Liu C, Wu J, Tao JJ, Sui XL, Yao ZG, Xu YF, Huang L, Zhu H, Sheng SL, et al. Tubastatin A/ACY-1215 Improves Cognition in Alzheimer's Disease Transgenic Mice. *Journal of Alzheimer's disease : JAD.* 2014.

246. Saba NF, Magliocca KR, Kim S, Muller S, Chen Z, Owonikoko TK, Sarlis NJ, Eggers C, Phelan V, Grist WJ, et al. Acetylated tubulin (AT) as a prognostic marker in squamous cell carcinoma of the head and neck. *Head and neck pathology.* 2014;8(1):66-72.

247. Boggs AE, Vitolo MI, Whipple RA, Charpentier MS, Goloubeva OG, Ioffe OB, Tuttle KC, Slovic J, Lu Y, Mills GB, et al. alpha-Tubulin acetylation elevated in metastatic and basal-like breast cancer cells promotes microtentacle formation, adhesion, and invasive migration. *Cancer Res.* 2015;75(1):203-15.

248. Bailey JM, Alsina J, Rasheed ZA, McAllister FM, Fu YY, Plentz R, Zhang H, Pasricha PJ, Bardeesy N, Matsui W, et al. DCLK1 marks a morphologically distinct subpopulation of cells with stem cell properties in preinvasive pancreatic cancer. *Gastroenterology.* 2014;146(1):245-56.

249. Santo L, Hideshima T, Kung AL, Tseng JC, Tamang D, Yang M, Jarpe M, van Duzer JH, Mazitschek R, Ogier WC, et al. Preclinical activity, pharmacodynamic, and pharmacokinetic properties of a selective

HDAC6 inhibitor, ACY-1215, in combination with bortezomib in multiple myeloma. *Blood.* 2012;119(11):2579-89.

250. McLendon PM, Ferguson BS, Osinska H, Bhuiyan MS, James J, McKinsey TA, and Robbins J. Tubulin hyperacetylation is adaptive in cardiac proteotoxicity by promoting autophagy. *Proc Natl Acad Sci U S A.* 2014;111(48):E5178-86.
251. Zhang D, Wu CT, Qi X, Meijering RA, Hoogstra-Berends F, Tadevosyan A, Cubukcuoglu Deniz G, Durdu S, Akar AR, Sibon OC, et al. Activation of histone deacetylase-6 induces contractile dysfunction through derailment of alpha-tubulin proteostasis in experimental and human atrial fibrillation. *Circulation.* 2014;129(3):346-58.
252. Lam HC, Cloonan SM, Bhashyam AR, Haspel JA, Singh A, Sathirapongsasuti JF, Cervo M, Yao H, Chung AL, Mizumura K, et al. Histone deacetylase 6-mediated selective autophagy regulates COPD-associated cilia dysfunction. *J Clin Invest.* 2013;123(12):5212-30.
253. Nam HJ, Kang JK, Kim SK, Ahn KJ, Seok H, Park SJ, Chang JS, Pothoulakis C, Lamont JT, and Kim H. Clostridium difficile toxin A decreases acetylation of tubulin, leading to microtubule depolymerization through activation of histone deacetylase 6, and this mediates acute inflammation. *J Biol Chem.* 2010;285(43):32888-96.
254. Li L, and Yang XJ. Tubulin acetylation: responsible enzymes, biological functions and human diseases. *Cellular and Molecular Life Sciences.* 2015;72(22):4237-55.
255. Kim GW, Li L, Gorbani M, You LY, and Yang XJ. Mice Lacking alpha-Tubulin Acetyltransferase 1 Are Viable but Display alpha-Tubulin Acetylation Deficiency and Dentate Gyrus Distortion. *J Biol Chem.* 2013;288(28):20334-50.
256. Aiken J, Sept D, Costanzo M, Boone C, Cooper JA, and Moore JK. Genome-wide analysis reveals novel and discrete functions for tubulin carboxy-terminal tails. *Curr Biol.* 2014;24(12):1295-303.
257. Sirajuddin M, Rice LM, and Vale RD. Regulation of microtubule motors by tubulin isotypes and post-translational modifications. *Nat Cell Biol.* 2014;16(4):335-44.
258. Roll-Mecak A. Intrinsically disordered tubulin tails: complex tuners of microtubule functions? *Semin Cell Dev Biol.* 2015;37(11-9.
259. Song Y, and Brady ST. Post-translational modifications of tubulin: pathways to functional diversity of microtubules. *Trends Cell Biol.* 2015;25(3):125-36.
260. Yang XJ, and Seto E. Lysine acetylation: codified crosstalk with other posttranslational modifications. *Mol Cell.* 2008;31(4):449-61.
261. Butler KV, Kalin J, Brochier C, Vistoli G, Langley B, and Kozikowski AP. Rational design and simple chemistry yield a superior, neuroprotective HDAC6 inhibitor, tubastatin A. *J Am Chem Soc.* 2010;132(31):10842-6.
262. Emiliani S, Fischle W, Van Lint C, Al-Abed Y, and Verdin E. Characterization of a human RPD3 ortholog, HDAC3. *P Natl Acad Sci USA.* 1998;95(6):2795-800.
263. Yang WM, Yao YL, Sun JM, Davie JR, and Seto E. Isolation and characterization of cDNAs corresponding to an additional member of the human histone deacetylase gene family. *J Biol Chem.* 1997;272(44):28001-7.
264. Zhu CC, Bornemann DJ, Zhitomirsky D, Miller EL, O'Connor MB, and Simon JA. Drosophila histone deacetylase-3 controls imaginal disc size through suppression of apoptosis. *Plos Genet.* 2008;4(2).
265. Yang WM, Tsai SC, Wen YD, Fejer G, and Seto E. Functional domains of histone deacetylase-3. *J Biol Chem.* 2002;277(11):9447-54.
266. Longworth MS, and Laimins LA. Histone deacetylase 3 localizes to the plasma membrane and is a

substrate of Src. *Oncogene.* 2006;25(32):4495-500.

267. Guenther MG, Lane WS, Fischle W, Verdin E, Lazar MA, and Shiekhattar R. A core SMRT corepressor complex containing HDAC3 and TBL1, a WD40-repeat protein linked to deafness. *Gene Dev.* 2000;14(9):1048-57.
268. Wen YD, Perissi V, Staszewski LM, Yang WM, Krones A, Glass CK, Rosenfeld MG, and Seto E. The histone deacetylase-3 complex contains nuclear receptor corepressors. *P Natl Acad Sci USA.* 2000;97(13):7202-7.
269. Li JW, Wang J, Wang JX, Nawaz Z, Liu JM, Qin J, and Wong JM. Both corepressor proteins SMRT and N-CoR exist in large protein complexes containing HDAC3. *Embo J.* 2000;19(16):4342-50.
270. Zhang JS, Kalkum M, Chait BT, and Roeder RG. The N-CoR-HDAC3 nuclear receptor corepressor complex inhibits the JNK pathway through the integral subunit GPS2. *Mol Cell.* 2002;9(3):611-23.
271. Mottis A, Mouchiroud L, and Auwerx J. Emerging roles of the corepressors NCoR1 and SMRT in homeostasis. *Gene Dev.* 2013;27(8):819-35.
272. Watson PJ, Fairall L, Santos GM, and Schwabe JWR. Structure of HDAC3 bound to co-repressor and inositol tetraphosphate. *Nature.* 2012;481(7381):335-U114.
273. Lan XJ, Atanassov BS, Li WQ, Zhang Y, Florens L, Mohan RD, Galardy PJ, Washburn MP, Workman JL, and Dent SYR. USP44 Is an Integral Component of N-CoR that Contributes to Gene Repression by Deubiquitinating Histone H2B. *Cell Rep.* 2016;17(9):2382-93.
274. Gregoire S, Xiao L, Nie JY, Zhang XH, Xu MH, Li JR, Wong JM, Seto E, and Yang XJ. Histone deacetylase 3 interacts with and deacetylates myocyte enhancer factor 2. *Mol Cell Biol.* 2007;27(4):1280-95.
275. Schroeder TM, Kahler RA, Li XD, and Westendorf JJ. Histone deacetylase 3 interacts with Runx2 to repress the osteocalcin promoter and regulate osteoblast differentiation. *J Biol Chem.* 2004;279(40):41998-2007.
276. Ozawa Y, Towatari M, Tsuzuki S, Hayakawa F, Maeda T, Miyata Y, Tanimoto M, and Saito H. Histone deacetylase 3 associates with and represses the transcription factor GATA-2. *Blood.* 2001;98(7):2116-23.
277. Grozinger CM, and Schreiber SL. Regulation of histone deacetylase 4 and 5 and transcriptional activity by 14-3-3-dependent cellular localization. *P Natl Acad Sci USA.* 2000;97(14):7835-40.
278. Sankar N, Baluchamy S, Kadeppagari RK, Singhal G, Weitzman S, and Thimmapaya B. p300 provides a corepressor function by cooperating with YY1 and HDAC3 to repress c-Myc. *Oncogene.* 2008;27(43):5717-28.
279. Seto E, and Yoshida M. Erasers of Histone Acetylation: The Histone Deacetylase Enzymes. *Csh Perspect Biol.* 2014;6(4).
280. Wang L, Rajan H, Pitman JL, McKeown M, and Tsai CC. Histone deacetylase-associating Atrophin proteins are nuclear receptor corepressors. *Gene Dev.* 2006;20(5):525-30.
281. You SH, Lim HW, Sun Z, Broache M, Won KJ, and Lazar MA. Nuclear receptor co-repressors are required for the histone-deacetylase activity of HDAC3 in vivo. *Nat Struct Mol Biol.* 2013;20(2):182-7.
282. Zhang XH, Ozawa Y, Lee H, Wen YD, Tan TH, Wadzinski BE, and Seto E. Histone deacetylase 3 (HDAC3) activity is regulated by interaction with protein serine/threonine phosphatase 4. *Gene Dev.* 2005;19(7):827-39.
283. Hong SH, and Privalsky ML. The SMRT corepressor is regulated by a MEK-1 kinase pathway: Inhibition of corepressor function is associated with SMRT phosphorylation and nuclear export. *Mol Cell Biol.* 2000;20(17):6612-25.
284. Chini CCS, Escande C, Nin V, and Chini EN. HDAC3 Is Negatively Regulated by the Nuclear Protein

DBC1. *J Biol Chem.* 2010;285(52):40830-7.

285. Gao ZG, He Q, Peng BL, Chiao PJ, and Ye JP. Regulation of nuclear translocation of HDAC3 by I kappa B alpha is required for tumor necrosis factor inhibition of peroxisome proliferator-activated receptor gamma function. *J Biol Chem.* 2006;281(7):4540-7.
286. Thevenet L, Mejean C, Moniot B, Bonneaud N, Galeotti N, Aldrian-Herrada G, Poulat F, Berta P, Benkirane M, and Boizet-Bonhoure B. Regulation of human SRY subcellular distribution by its acetylation/deacetylation. *Embo J.* 2004;23(16):3336-45.
287. Dai Y, Rahmani M, Dent P, and Grant S. Blockade of histone deacetylase inhibitor-induced RelA/p65 acetylation and NF-kappa B activation potentiates apoptosis in leukemia cells through a process mediated by oxidative damage, XIAP downregulation, and c-jun n-terminal kinase 1 activation. *Mol Cell Biol.* 2005;25(13):5429-44.
288. Delcuve GP, Khan DH, and Davie JR. Targeting class I histone deacetylases in cancer therapy. *Expert Opin Ther Tar.* 2013;17(1):29-41.
289. Choi E, Han C, Park I, Lee B, Jin S, Choi H, Kim DH, Park ZY, Eddy EM, and Cho C. A Novel Germ Cell-specific Protein, SHIP1, Forms a Complex with Chromatin Remodeling Activity during Spermatogenesis. *J Biol Chem.* 2008;283(50):35283-94.
290. Ye F, Chen Y, Hoang T, Montgomery RL, Zhao XH, Bu H, Hu T, Taketo MM, van Es JH, Clevers H, et al. HDAC1 and HDAC2 regulate oligodendrocyte differentiation by disrupting the beta-catenin-TCF interaction. *Nat Neurosci.* 2009;12(7):829-U35.
291. Castelo-Branco G, Lilja T, Wallenborg K, Falcao AM, Marques SC, Gracias A, Solum D, Paap R, Walfridsson J, Teixeira AI, et al. Neural Stem Cell Differentiation Is Dictated by Distinct Actions of Nuclear Receptor Corepressors and Histone Deacetylases. *Stem Cell Rep.* 2014;3(3):502-15.
292. Dovey OM, Foster CT, Conte N, Edwards SA, Edwards JM, Singh R, Vassiliou G, Bradley A, and Cowley SM. Histone deacetylase 1 and 2 are essential for normal T-cell development and genomic stability in mice. *Blood.* 2013;121(8):1335-44.
293. Winter M, Moser MA, Meunier D, Fischer C, Machat G, Mattes K, Lichtenberger BM, Brunmeir R, Weissmann S, Murko C, et al. Divergent roles of HDAC1 and HDAC2 in the regulation of epidermal development and tumorigenesis. *Embo J.* 2013;32(24):3176-91.
294. Montgomery RL, Davis CA, Potthoff MJ, Haberland M, Fielitz J, Qi XX, Hill JA, Richardson JA, and Olson EN. Histone deacetylases 1 and 2 redundantly regulate cardiac morphogenesis, growth, and contractility. *Gene Dev.* 2007;21(14):1790-802.
295. Haberland M, Mokalled MH, Montgomery RL, and Olson EN. Epigenetic control of skull morphogenesis by histone deacetylase 8. *Gene Dev.* 2009;23(14):1625-30.
296. Bhaskara S, Knutson SK, Jiang GC, Chandrasekharan MB, Wilson AJ, Zheng SY, Yenamandra A, Locke K, Yuan JL, Bonine-Summers AR, et al. Hdac3 Is Essential for the Maintenance of Chromatin Structure and Genome Stability. *Cancer Cell.* 2010;18(5):436-47.
297. Bhaskara S, Chyla BJ, Amann JM, Knutson SK, Cortez D, Sun ZW, and Hiebert SW. Deletion of histone deacetylase 3 reveals critical roles in S phase progression and DNA damage control. *Mol Cell.* 2008;30(1):61-72.
298. Jepsen K, and Rosenfeld MG. Biological roles and mechanistic actions of co-repressor complexes. *J Cell Sci.* 2002;115(4):689-98.
299. Montgomery RL, Potthoff MJ, Haberland M, Qi XX, Matsuzaki S, Humphries KM, Richardson JA, Bassel-Duby R, and Olson EN. Maintenance of cardiac energy by histone deacetylase 3 metabolism in mice. *Journal of Clinical Investigation.* 2008;118(11):3588-97.

300. Knutson SK, Chyla BJ, Amann JM, Bhaskara S, Huppert SS, and Hiebert SW. Liver-specific deletion of histone deacetylase 3 disrupts metabolic transcriptional networks. *Embo J.* 2008;27(7):1017-28.
301. Feng D, Liu T, Sun Z, Bugge A, Mullican SE, Alenghat T, Liu XS, and Lazar MA. A Circadian Rhythm Orchestrated by Histone Deacetylase 3 Controls Hepatic Lipid Metabolism. *Science.* 2011;331(6022):1315-9.
302. Lewandowski SL, Janardhan HP, Smee KM, Bachman M, Sun Z, Lazar MA, and Trivedi CM. Histone deacetylase 3 modulates Tbx5 activity to regulate early cardiogenesis. *Hum Mol Genet.* 2014;23(14):3801-9.
303. Lewandowski SL, Janardhan HP, and Trivedi CM. Histone Deacetylase 3 Coordinates Deacetylase-independent Epigenetic Silencing of Transforming Growth Factor-beta 1 (TGF-beta 1) to Orchestrate Second Heart Field Development. *J Biol Chem.* 2015;290(45):27067-89.
304. Alenghat T, Osborne LC, Saenz SA, Kobuley D, Ziegler CGK, Mullican SE, Choi I, Grunberg S, Sinha R, Wynosky-Dolfi M, et al. Histone deacetylase 3 coordinates commensal-bacteria-dependent intestinal homeostasis. *Nature.* 2013;504(7478):153-+.
305. Summers AR, Fischer MA, Stengel KR, Zhao Y, Kaiser JF, Wells CE, Hunt A, Bhaskara S, Luzwick JW, Sampathi S, et al. HDAC3 is essential for DNA replication in hematopoietic progenitor cells. *Journal of Clinical Investigation.* 2013;123(7):3112-23.
306. Jepsen K, Hermanson O, Onami TM, Gleiberman AS, Lunyak V, McEvilly RJ, Kurokawa R, Kumar V, Liu F, Seto E, et al. Combinatorial roles of the nuclear receptor corepressor in transcription and development. *Cell.* 2000;102(6):753-63.
307. Glozak MA, and Seto E. Histone deacetylases and cancer. *Oncogene.* 2007;26(37):5420-32.
308. Barneda-Zahonero B, and Parra M. Histone deacetylases and cancer. *Mol Oncol.* 2012;6(6):579-89.
309. Moskowitz AJ, and Horwitz SM. Targeting histone deacetylases in T-cell lymphoma. *Leukemia Lymphoma.* 2017;58(6):1306-19.
310. Loscher W. Basic pharmacology of valproate - A review after 35 years of clinical use for the treatment of epilepsy. *Cns Drugs.* 2002;16(10):669-94.
311. Jepsen K, Solum D, Zhou TY, McEvilly RJ, Kim HJ, Glass CK, Hermanson O, and Rosenfeld MG. SMRT-mediated repression of an H3K27 demethylase in progression from neural stem cell to neuron. *Nature.* 2007;450(7168):415-U8.
312. Norwood J, Franklin JM, Sharma D, and D'Mello SR. Histone Deacetylase 3 Is Necessary for Proper Brain Development. *J Biol Chem.* 2014;289(50):34569-82.
313. Nott A, Cheng J, Gao F, Lin YT, Gjoneska E, Ko T, Minhas P, Zamudio AV, Meng J, Zhang FR, et al. Histone deacetylase 3 associates with MeCP2 to regulate FOXO and social behavior. *Nat Neurosci.* 2016;19(11):1497-505.
314. Collins CM, Ellis JA, and Holaska JM. MAPK signaling pathways and HDAC3 activity are disrupted during differentiation of emerin-null myogenic progenitor cells. *Dis Model Mech.* 2017;10(4):385-97.
315. Spurling CC, Godman CA, Noonan EJ, Rasmussen TP, Rosenberg DW, and Giardina C. HDAC3 overexpression and colon cancer cell proliferation and differentiation. *Mol Carcinogen.* 2008;47(2):137-47.
316. Sun Z, Singh N, Mullican SE, Everett LJ, Li L, Yuan LJ, Liu X, Epstein JA, and Lazar MA. Diet-induced Lethality Due to Deletion of the Hdac3 Gene in Heart and Skeletal Muscle. *J Biol Chem.* 2011;286(38):33301-9.
317. Sun Z, Miller RA, Patel RT, Chen J, Dhir R, Wang H, Zhang DY, Graham MJ, Unterman TG, Shulman GI, et al. Hepatic Hdac3 promotes gluconeogenesis by repressing lipid synthesis and sequestration.

Nature Medicine. 2012;18(6):934-+.

318. Hong SG, Zhou WJ, Fang B, Lu WY, Loro E, Damle M, Ding GL, Jager J, Zhang SS, Zhang YX, et al. Dissociation of muscle insulin sensitivity from exercise endurance in mice by HDAC3 depletion. *Nature Medicine.* 2017;23(2):223-34.
319. Emmett MJ, Lim HW, Jager J, Richter HJ, Adlanmerini M, Peed LC, Briggs ER, Steger DJ, Ma T, Sims CA, et al. Histone deacetylase 3 prepares brown adipose tissue for acute thermogenic challenge. *Nature.* 2017;546(7659):544-+.
320. Boggs AE, Vitolo MI, Whipple RA, Charpentier MS, Goloubeva OG, Ioffe OB, Tuttle KC, Slovic J, Lu YL, Mills GB, et al. alpha-Tubulin Acetylation Elevated in Metastatic and Basal-like Breast Cancer Cells Promotes Microtentacle Formation, Adhesion, and Invasive Migration. *Cancer Res.* 2015;75(1):203-15.
321. Lin X, Liu BH, Yang XS, Yue XJ, Diao LX, Wang J, and Chang J. Genetic deletion of Rnd3 results in aqueductal stenosis leading to hydrocephalus through up-regulation of Notch signaling. *P Natl Acad Sci USA.* 2013;110(20):8236-41.
322. Banizs B, Pike MM, Millican CL, Ferguson WB, Komlosi P, Sheetz J, Bell PD, Schwiebert EM, and Yoder BK. Dysfunctional cilia lead to altered ependyma and choroid plexus function, and result in the formation of hydrocephalus. *Development.* 2005;132(23):5329-39.
323. Kalebic N, Sorrentino S, Perlas E, Bolasco G, Martinez C, and Heppenstall PA. alphaTAT1 is the major alpha-tubulin acetyltransferase in mice. *Nat Commun.* 2013;4(1962.
324. McLendon PM, Ferguson BS, Osinska H, Bhuiyan MS, James J, McKinsey TA, and Robbins J. Tubulin hyperacetylation is adaptive in cardiac proteotoxicity by promoting autophagy. *P Natl Acad Sci USA.* 2014;111(48):E5178-E86.
325. Watt AJ, Cuntz H, Mori M, Nusser Z, Sjostrom PJ, and Hausser M. Traveling waves in developing cerebellar cortex mediated by asymmetrical Purkinje cell connectivity. *Nat Neurosci.* 2009;12(4):463-73.
326. Prodromou NV, Thompson CL, Osborn DPS, Cogger KF, Ashworth R, Knight MM, Beales PL, and Chapple JP. Heat shock induces rapid resorption of primary cilia. *J Cell Sci.* 2012;125(18):4297-305.
327. Banreti A, Sass M, and Graba Y. The emerging role of acetylation in the regulation of autophagy. *Autophagy.* 2013;9(6):819-29.
328. He Q, Wang GH, Wakade S, Dasgupta S, Dinkins M, Kong JN, Spassieva SD, and Bieberich E. Primary cilia in stem cells and neural progenitors are regulated by neutral sphingomyelinase 2 and ceramide. *Mol Biol Cell.* 2014;25(11):1715-29.
329. Kreitzer AC, and Malenka RC. Striatal plasticity and basal ganglia circuit function. *Neuron.* 2008;60(4):543-54.
330. Ma Q, Yang JM, Li T, Milner TA, and Hempstead BL. Selective reduction of striatal mature BDNF without induction of proBDNF in the zQ175 mouse model of Huntington's disease. *Neurobiol Dis.* 2015;82(466-77.
331. Iwata A, Riley BE, Johnston JA, and Kopito RR. HDAC6 and microtubules are required for autophagic degradation of aggregated Huntingtin. *J Biol Chem.* 2005;280(48):40282-92.
332. Guedes-Dias P, de Proenca J, Soares TR, Leitao-Rocha A, Pinho BR, Duchen MR, and Oliveira JMA. HDAC6 inhibition induces mitochondrial fusion, autophagic flux and reduces diffuse mutant huntingtin in striatal neurons. *Bba-Mol Basis Dis.* 2015;1852(11):2484-93.
333. Simoes-Pires C, Zwick V, Nurisso A, Schenker E, Carrupt PA, and Cuendet M. HDAC6 as a target for neurodegenerative diseases: what makes it different from the other HDACs? *Mol Neurodegener.* 2013;8(
334. Bobrowska A, Paganetti P, Matthias P, and Bates GP. Hdac6 Knock-Out Increases Tubulin Acetylation but Does Not Modify Disease Progression in the R6/2 Mouse Model of Huntington's Disease. *Plos One.*

2011;6(6).
335. Messaoudi K, Ali A, Ishaq R, Palazzo A, Sliwa D, Bluteau O, Souquere S, Muller D, Diop KM, Rameau P, et al. Critical role of the HDAC6-cortactin axis in human megakaryocyte maturation leading to a proplatelet-formation defect. *Nat Commun.* 2017;8(1):1786.
336. Wang N, and Tall AR. Cholesterol in platelet biogenesis and activation. *Blood.* 2016;127(16):1949-53.
337. Krishnegowda M, and Rajashekaraiah V. Platelet disorders: an overview. *Blood Coagul Fibrinolysis.* 2015;26(5):479-91.
338. Li L, Wei D, Wang Q, Pan J, Liu R, Zhang X, and Bao L. MEC-17 deficiency leads to reduced alpha-tubulin acetylation and impaired migration of cortical neurons. *J Neurosci.* 2012;32(37):12673-83.
339. Morley SJ, Qi YM, Iovino L, Andolfi L, Guo D, Kalebic N, Castaldi L, Tischer C, Portulano C, Bolasco G, et al. Acetylated tubulin is essential for touch sensation in mice. *Elife.* 2016;5(
340. Shah N, Kumar S, Zaman N, Pan CC, Bloodworth JC, Lei W, Streicher JM, Hempel N, Mythreye K, and Lee NY. TAK1 activation of alpha-TAT1 and microtubule hyperacetylation control AKT signaling and cell growth. *Nat Commun.* 2018;9(
341. Oh S, You E, Ko P, Jeong J, Keum S, and Rhee S. Genetic disruption of tubulin acetyltransferase, alpha TAT1, inhibits proliferation and invasion of colon cancer cells through decreases in Wnt1/beta-catenin signaling. *Biochem Bioph Res Co.* 2017;482(1):8-14.
342. Wang B, Rao YH, Inoue M, Hao R, Lai CH, Chen D, McDonald SL, Choi MC, Wang Q, Shinohara ML, et al. Microtubule acetylation amplifies p38 kinase signalling and anti-inflammatory IL-10 production. *Nat Commun.* 2014;5(
343. You L, Yan K, Zou J, Zhao H, Bertos NR, Park M, Wang E, and Yang XJ. The lysine acetyltransferase activator Brpf1 governs dentate gyrus development through neural stem cells and progenitors. *Plos Genet.* 2015;11(e1005034.
344. You L, Zou J, Zhao H, Bertos NR, Park M, Wang E, and Yang XJ. Deficiency of the chromatin regulator Brpf1 causes abnormal brain development. *J Biol Chem.* 2015;290(7114-29.
345. Sansregret L, Vadnais C, Livingstone J, Kwiatkowski N, Awan A, Cadieux C, Leduy L, Hallett MT, and Nepveu A. Cut homeobox 1 causes chromosomal instability by promoting bipolar division after cytokinesis failure. *Proc Natl Acad Sci U S A.* 2011;108(5):1949-54.
346. Gingras H, Cases O, Krasilnikova M, Berube G, and Nepveu A. Biochemical characterization of the mammalian Cux2 protein. *Gene.* 2005;344(273-85.
347. You L, Zou J, Zhao H, Bertos NR, Park M, Wang E, and Yang XJ. Deficiency of the chromatin regulator BRPF1 causes abnormal brain development. *J Biol Chem.* 2015;290(11):7114-29.
348. Heinsbroek RPW, Vanhaaren F, and Vandepoll NE. Sex-Differences in Passive-Avoidance Behavior of Rats - Sex-Dependent Susceptibility to Shock-Induced Behavioral Depression. *Physiol Behav.* 1988;43(2):201-6.
349. Yan K, You L, Degerny C, Ghorbani M, Liu X, Chen L, Li L, Miao D, and Yang XJ. The chromatin regulator BRPF3 preferentially activates the HBO1 acetyltransferase but is dispensable for mouse development and survival. *J Biol Chem.* 2016;291(2647-63.
350. You L, Li L, Yan K, Zou J, Belle J, Nijnik A, Wang E, and Yang XJ. BRPF1 is essential for development of fetal hematopoietic stem cells. *J Clin Invest.* 2016;126(9):3247-62.
351. You LY, Li L, Zou JF, Yan KZ, Belle J, Nijnik A, Wang E, and Yang XJ. BRPF1 is essential for development of fetal hematopoietic stem cells. *Journal of Clinical Investigation.* 2016;126(9):3247-62.
352. Kouzarides T. Chromatin modifications and their function. *Cell.* 2007;128(693-705.
353. Kim GW, and Yang XJ. Comprehensive lysine acetylomes emerging from bacteria to humans. *Trends*

Biochem Sci. 2011;36(4):211-20.

354. Yang XJ, and Seto E. The Rpd3/Hda1 family of lysine deacetylases: from bacteria and yeast to mice and men. *Nat Rev Mol Cell Biol.* 2008;9(206-18.
355. Haberland M, Montgomery RL, and Olson EN. The many roles of histone deacetylases in development and physiology: implications for disease and therapy. *Nat Rev Genet.* 2009;10(1):32-42.
356. Karagianni P, and Wong J. HDAC3: taking the SMRT-N-CoRrect road to repression. *Oncogene.* 2007;26(5439-49.
357. Oberoi J, Fairall L, Watson PJ, Yang JC, Czimmerer Z, Kampmann T, Goult BT, Greenwood JA, Gooch JT, Kallenberger BC, et al. Structural basis for the assembly of the SMRT/NCoR core transcriptional repression machinery. *Nat Struct Mol Biol.* 2011;18(2):177-84.
358. Codina A, Love JD, Li Y, Lazar MA, Neuhaus D, and Schwabe JW. Structural insights into the interaction and activation of histone deacetylase 3 by nuclear receptor corepressors. *Proc Natl Acad Sci USA.* 2005;102(17):6009-14.
359. Guenther MG, Lane WS, Fischle W, Verdin E, Lazar MA, and Shiekhattar R. A core SMRT corepressor complex containing HDAC3 and TBL1, a WD40-repeat protein linked to deafness. *Genes Dev.* 2000;14(9):1048-57.
360. Guenther MG, Barak O, and Lazar MA. The SMRT and N-CoR corepressors are activating cofactors for histone deacetylase 3. *Mol Cell Biol.* 2001;21(6091-101.
361. Lu XF, Cao XY, Zhu YJ, Wu ZR, Zhuang X, Shao MY, Xu Q, Zhou YJ, Ji HJ, Lu QR, et al. Histone deacetylase 3 promotes liver regeneration and liver cancer cells proliferation through signal transducer and activator of transcription 3 signaling pathway. *Cell Death Dis.* 2018;9(
362. Farooq M, Sulochana KN, Pan XF, To JW, Sheng D, Gong ZY, and Ge RW. Histone deacetylase 3 (hdac3) is specifically required for liver development in zebrafish. *Dev Biol.* 2008;317(1):336-53.
363. Knutson SK, Chyla BJ, Amann JM, Bhaskara S, Huppert SS, and Hiebert SW. Liver-specific deletion of histone deacetylase 3 disrupts metabolic transcriptional networks. *EMBO J.* 2008;27(7):1017-28.
364. Montgomery RL, Potthoff MJ, Haberland M, Qi X, Matsuzaki S, Humphries KM, Richardson JA, Bassel-Duby R, and Olson EN. Maintenance of cardiac energy metabolism by histone deacetylase 3 in mice. *J Clin Invest.* 2008;118(11):3588-97.
365. Alenghat T, Osborne LC, Saenz SA, Kobuley D, Ziegler CG, Mullican SE, Choi I, Grunberg S, Sinha R, Wynosky-Dolfi M, et al. Histone deacetylase 3 coordinates commensal-bacteria-dependent intestinal homeostasis. *Nature.* 2013;504(7478):153-7.
366. Emmett MJ, Lim HW, Jager J, Richter HJ, Adlanmerini M, Peed LC, Briggs ER, Steger DJ, Ma T, Sims CA, et al. Histone deacetylase 3 prepares brown adipose tissue for acute thermogenic challenge. *Nature.* 2017;546(7659):544-8.
367. Norwood J, Franklin JM, Sharma D, and D'Mello SR. Histone deacetylase 3 is necessary for proper brain development. *J Biol Chem.* 2014;289(50):34569-82.
368. Helbig KL, Farwell Hagman KD, Shinde DN, Mroske C, Powis Z, Li S, Tang S, and Helbig I. Diagnostic exome sequencing provides a molecular diagnosis for a significant proportion of patients with epilepsy. *Genet Med.* 2016;18(9):898-905.
369. Saitsu H, Tohyama J, Walsh T, Kato M, Kobayashi Y, Lee M, Tsurusaki Y, Miyake N, Goto Y, Nishino I, et al. A girl with West syndrome and autistic features harboring a de novo TBL1XR1 mutation. *J Hum Genet.* 2014;59(10):581-3.
370. Heinen CA, Jongejan A, Watson PJ, Redeker B, Boelen A, Boudzovitch-Surovtseva O, Forzano F, Hordijk R, Kelley R, Olney AH, et al. A specific mutation in TBL1XR1 causes Pierpont syndrome. *J*

Med Genet. 2016;53(5):330-7.

371. Laskowski RA, Tyagi N, Johnson D, Joss S, Kinning E, McWilliam C, Splitt M, Thornton JM, Firth HV, Study DDD, et al. Integrating population variation and protein structural analysis to improve clinical interpretation of missense variation: application to the WD40 domain. *Hum Mol Genet.* 2016;25(5):927-35.
372. Gorski JA, Talley T, Qiu MS, Puelles L, Rubenstein JLR, and Jones KR. Cortical excitatory neurons and glia, but not GABAergic neurons, are produced in the Emx1-expressing lineage. *Journal of Neuroscience.* 2002;22(15):6309-14.
373. Chou SJ, Perez-Garcia CG, Kroll TT, and O'Leary DDM. Lhx2 specifies regional fate in Emx1 lineage of telencephalic progenitors generating cerebral cortex. *Nat Neurosci.* 2009;12(11):1381-9.
374. Gould TD, Dao DT, and Kovacsics CE. The Open Field Test. *Neuromethods.* 2009;42(1-20.
375. Sestakova N, Puzserova A, Kluknavsky M, and Bernatova I. Determination of motor activity and anxiety-related behaviour in rodents: methodological aspects and role of nitric oxide. *Interdiscip Toxicol.* 2013;6(3):126-35.
376. Marin O, and Rubenstein JL. A long, remarkable journey: tangential migration in the telencephalon. *Nat Rev Neurosci.* 2001;2(11):780-90.
377. Noctor SC, Flint AC, Weissman TA, Dammerman RS, and Kriegstein AR. Neurons derived from radial glial cells establish radial units in neocortex. *Nature.* 2001;409(6821):714-20.
378. Ellis P, Fagan BM, Magness ST, Hutton S, Taranova O, Hayashi S, McMahon A, Rao M, and Pevny L. SOX2, a persistent marker for multipotential neural stem cells derived from embryonic stem cells, the embryo or the adult. *Dev Neurosci.* 2004;26(2-4):148-65.
379. Hodge RD, Nelson BR, Kahoud RJ, Yang R, Mussar KE, Reiner SL, and Hevner RF. Tbr2 Is Essential for Hippocampal Lineage Progression from Neural Stem Cells to Intermediate Progenitors and Neurons. *Journal of Neuroscience.* 2012;32(18):6275-87.
380. Arnold SJ, Huang GJ, Cheung AFP, Era T, Nishikawa SI, Bikoff EK, Molnar Z, Robertson EJ, and Groszer M. The T-box transcription factor Eomes/Tbr2 regulates neurogenesis in the cortical subventricular zone. *Gene Dev.* 2008;22(18):2479-84.
381. Urban N, and Guillemot F. Neurogenesis in the embryonic and adult brain: same regulators, different roles. *Front Cell Neurosci.* 2014;8(
382. Cattaneo E, and McKay R. Proliferation and differentiation of neuronal stem cells regulated by nerve growth factor. *Nature.* 1990;347(6295):762-5.
383. Singec I, Knoth R, Meyer RP, Maciaczyk J, Volk B, Nikkhah G, Frotscher M, and Snyder EY. Defining the actual sensitivity and specificity of the neurosphere assay in stem cell biology. *Nat Methods.* 2006;3(10):801-6.
384. Emiliani S, Fischle W, Van Lint C, Al-Abed Y, and Verdin E. Characterization of a human RPD3 ortholog, HDAC3. *Proc Natl Acad Sci U S A.* 1998;95(6):2795-800.
385. Malvaez M, McQuown SC, Rogge GA, Astarabadi M, Jacques V, Carreiro S, Rusche JR, and Wood MA. HDAC3-selective inhibitor enhances extinction of cocaine-seeking behavior in a persistent manner. *Proc Natl Acad Sci U S A.* 2013;110(7):2647-52.
386. Yoon HG, Chan DW, Huang ZQ, Li JW, Fondell JD, Qin J, and Wong JM. Purification and functional characterization of the human N-CoR complex: the roles of HDAC3, TBL1 and TBLR1. *Embo J.* 2003;22(6):1336-46.
387. Remsberg JR, Ediger BN, Ho WY, Damle M, Li ZH, Teng C, Lanzillotta C, Stoffers DA, and Lazar MA. Deletion of histone deacetylase 3 in adult beta cells improves glucose tolerance via increased insulin

secretion. *Mol Metab.* 2017;6(1):30-7.

388. Nanou A, Toumpeki C, Lavigne MD, Lazou V, Demmers J, Paparountas T, Thanos D, and Katsantoni E. The dual role of LSD1 and HDAC3 in STAT5-dependent transcription is determined by protein interactions, binding affinities, motifs and genomic positions. *Nucleic Acids Res.* 2017;45(1):142-54.
389. Armour SM, Remsberg JR, Damle M, Sidoli S, Ho WY, Li ZH, Garcia BA, and Lazar MA. An HDAC3-PROX1 corepressor module acts on HNF4 alpha to control hepatic triglycerides. *Nat Commun.* 2017;8(
390. He XL, Zhang LG, Queme LF, Liu XZ, Lu A, Waclaw RR, Dong XR, Zhou WH, Kidd G, Yoon SO, et al. A histone deacetylase 3-dependent pathway delimits peripheral myelin growth and functional regeneration. *Nature Medicine.* 2018;24(3):338-+.
391. Heng JI, Qu Z, Ohtaka-Maruyama C, Okado H, Kasai M, Castro D, Guillemot F, and Tan SS. The zinc finger transcription factor RP58 negatively regulates Rnd2 for the control of neuronal migration during cerebral cortical development. *Cereb Cortex.* 2015;25(3):806-16.
392. Ohtaka-Maruyama C, Hirai S, Miwa A, Heng JI, Shitara H, Ishii R, Taya C, Kawano H, Kasai M, Nakajima K, et al. RP58 regulates the multipolar-bipolar transition of newborn neurons in the developing cerebral cortex. *Cell Rep.* 2013;3(2):458-71.
393. Huynh KD, and Bardwell VJ. The BCL-6 POZ domain and other POZ domains interact with the co-repressors N-CoR and SMRT. *Oncogene.* 1998;17(19):2473-84.
394. Caviness VS, Bhide PG, and Nowakowski RS. Histogenetic processes leading to the laminated neocortex: Migration is only a part of the story. *Dev Neurosci-Basel.* 2008;30(1-3):82-95.
395. Liang H, Hippenmeyer S, and Ghashghaei HT. A Nestin-cre transgenic mouse is insufficient for recombination in early embryonic neural progenitors. *Biol Open.* 2012;1(12):1200-3.
396. Liang H, Xiao G, Yin H, Hippenmeyer S, Horowitz JM, and Ghashghaei HT. Neural development is dependent on the function of specificity protein 2 in cell cycle progression. *Development.* 2013;140(3):552-61.
397. Gorski JA, Talley T, Qiu M, Puelles L, Rubenstein JL, and Jones KR. Cortical excitatory neurons and glia, but not GABAergic neurons, are produced in the Emx1-expressing lineage. *J Neurosci.* 2002;22(15):6309-14.
398. McQuown SC, Barrett RM, Matheos DP, Post RJ, Rogge GA, Alenghat T, Mullican SE, Jones S, Rusche JR, Lazar MA, et al. HDAC3 is a critical negative regulator of long-term memory formation. *J Neurosci.* 2011;31(2):764-74.
399. Rogge GA, Singh H, Dang R, and Wood MA. HDAC3 is a negative regulator of cocaine-context-associated memory formation. *J Neurosci.* 2013;33(15):6623-32.
400. He X, Zhang L, Queme LF, Liu X, Lu A, Waclaw RR, Dong X, Zhou W, Kidd G, Yoon SO, et al. A histone deacetylase 3-dependent pathway delimits peripheral myelin growth and functional regeneration. *Nat Med.* 2018;24(3):338-51.
401. Hermanson O, Jepsen K, and Rosenfeld MG. N-CoR controls differentiation of neural stem cells into astrocytes. *Nature.* 2002;419(6910):934-9.
402. Becker-Santos DD, Lonergan KM, Gronostajski RM, and Lam WL. Nuclear Factor I/B: A Master Regulator of Cell Differentiation with Paradoxical Roles in Cancer. *Ebiomedicine.* 2017;22(2-9.
403. Naka H, Nakamura S, Shimazaki T, and Okano H. Requirement for COUP-TFI and II in the temporal specification of neural stem cells in CNS development. *Nat Neurosci.* 2008;11(9):1014-23.
404. Yamaguchi H, Zhou C, Lin SC, Durand B, Tsai SY, and Tsai MJ. The nuclear orphan receptor COUP-TFI is important for differentiation of oligodendrocytes. *Dev Biol.* 2004;266(2):238-51.
405. Arai Y, Funatsu N, Numayama-Tsuruta K, Nomura T, Nakamura S, and Osumi N. Role of Fabp7, a

downstream gene of Pax6, in the maintenance of neuroepithelial cells during early embryonic development of the rat cortex. *Journal of Neuroscience.* 2005;25(42):9752-61.

406. Kruusvee V, Lyst MJ, Taylor C, Tarnauskaite Z, Bird AP, and Cook AG. Structure of the MeCP2-TBLR1 complex reveals a molecular basis for Rett syndrome and related disorders. *Proc Natl Acad Sci U S A.* 2017;114(16):E3243-E50.
407. Guy J, Hendrich B, Holmes M, Martin JE, and Bird A. A mouse Mecp2-null mutation causes neurological symptoms that mimic Rett syndrome. *Nat Genet.* 2001;27(3):322-6.
408. Chen RZ, Akbarian S, Tudor M, and Jaenisch R. Deficiency of methyl-CpG binding protein-2 in CNS neurons results in a Rett-like phenotype in mice. *Nat Genet.* 2001;27(3):327-31.
409. Bugge A, Feng D, Everett LJ, Briggs ER, Mullican SE, Wang F, Jager J, and Lazar MA. Rev-erbalpha and Rev-erbbeta coordinately protect the circadian clock and normal metabolic function. *Genes Dev.* 2012;26(7):657-67.
410. Malvaez M, McQuown SC, Rogge GA, Astarabadi M, Jacques V, Carreiro S, Rusche JR, and Wood MA. HDAC3-selective inhibitor enhances extinction of cocaine-seeking behavior in a persistent manner. *P Natl Acad Sci USA.* 2013;110(7):2647-52.
411. Nieto M, Monuki ES, Tang H, Imitola J, Haubst N, Khoury SJ, Cunningham J, Gotz M, and Walsh CA. Expression of Cux-1 and Cux-2 in the subventricular zone and upper layers II-IV of the cerebral cortex. *J Comp Neurol.* 2004;479(2):168-80.
412. Lai T, Jabaudon D, Molyneaux BJ, Azim E, Arlotta P, Menezes JR, and Macklis JD. SOX5 controls the sequential generation of distinct corticofugal neuron subtypes. *Neuron.* 2008;57(2):232-47.
413. Hevner RF, Shi L, Justice N, Hsueh Y, Sheng M, Smiga S, Bulfone A, Goffinet AM, Campagnoni AT, and Rubenstein JL. Tbr1 regulates differentiation of the preplate and layer 6. *Neuron.* 2001;29(2):353-66.
414. Kirby RS, Brewster MA, Canino CU, and Pavin M. Early-Childhood Surveillance of Developmental Disorders by a Birth-Defects Surveillance System - Methods, Prevalence Comparisons, and Mortality Patterns. *J Dev Behav Pediatr.* 1995;16(5):318-26.
415. Gonzalez-Mantilla AJ, Moreno-De-Luca A, Ledbetter DH, and Martin CL. A Cross-Disorder Method to Identify Novel Candidate Genes for Developmental Brain Disorders. *Jama Psychiat.* 2016;73(3):275-83.
416. Liang PP, Ding CH, Sun HW, Xie XW, Xu YW, Zhang XY, Sun Y, Xiong YY, Ma WB, Liu YX, et al. Correction of beta-thalassemia mutant by base editor in human embryos. *Protein Cell.* 2017;8(11):811-22.
417. Helbig KL, Hagman KDF, Shinde DN, Mroske C, Powis Z, Li SW, Tang S, and Helbig I. Diagnostic exome sequencing provides a molecular diagnosis for a significant proportion of patients with epilepsy. *Genet Med.* 2016;18(9):898-905.
418. Yu JJ, Li Y, Ishizuka T, Guenther MG, and Lazar MA. A SANT motif in the SMRT corepressor interprets the histone code and promotes histone deacetylation. *Embo J.* 2003;22(13):3403-10.
419. Boyer LA, Latek RR, and Peterson CL. The SANT domain: a unique histone-tail-binding module? *Nat Rev Mol Cell Bio.* 2004;5(2):158-63.
420. Howe L, Auston D, Grant P, John S, Cook RG, Workman JL, and Pillus L. Histone H3 specific acetyltransferases are essential for cell cycle progression. *Gene Dev.* 2001;15(23):3144-54.
421. Maltby VE, Martin BJE, Brind'Amour J, Chruscicki AT, McBurney KL, Schulze JM, Johnson IJ, Hills M, Hentrich T, Kobor MS, et al. Histone H3K4 demethylation is negatively regulated by histone H3 acetylation in Saccharomyces cerevisiae. *P Natl Acad Sci USA.* 2012;109(45):18505-10.
422. Qiu Y, Liu L, Zhao C, Han CC, Li FD, Zhang JH, Wang Y, Li GH, Mei YD, Wu MA, et al. Combinatorial

readout of unmodified H3R2 and acetylated H3K14 by the tandem PHD finger of MOZ reveals a regulatory mechanism for HOXA9 transcription. *Gene Dev.* 2012;26(12):1376-91.

423. Schubert R. Attention deficit disorder and epilepsy. *Pediatr Neurol.* 2005;32(1):1-10.

424. Yan KZ, You LY, Degerny C, Ghorbani M, Liu X, Chen LL, Li L, Miao DS, and Yang XJ. The Chromatin Regulator BRPF3 Preferentially Activates the HBO1 Acetyltransferase but Is Dispensable for Mouse Development and Survival. *J Biol Chem.* 2016;291(6):2647-63.

425. Lim DA, Huang YC, Swigut T, Mirick AL, Garcia-Verdugo JM, Wysocka J, Ernst P, and Alvarez-Buylla A. Chromatin remodelling factor Mll1 is essential for neurogenesis from postnatal neural stem cells. *Nature.* 2009;458(7237):529-U9.

426. Perera M, Merlo GR, Verardo S, Paleari L, Corte G, and Levi G. Defective neuronogenesis in the absence of Dlx5. *Mol Cell Neurosci.* 2004;25(1):153-61.

427. Lyden D, Young AZ, Zagzag D, Yan W, Gerald W, O'Reilly R, Bader BL, Hynes RO, Zhuang Y, Manova K, et al. Id1 and Id3 are required for neurogenesis, angiogenesis and vascularization of tumour xenografts. *Nature.* 1999;401(6754):670-7.

428. Nakamura Y, Sakakibara S, Miyata T, Ogawa M, Shimazaki T, Weiss S, Kageyama R, and Okano H. The bHLH gene Hes1 as a repressor of the neuronal commitment of CNS stem cells. *Journal of Neuroscience.* 2000;20(1):283-93.

429. Ishibashi M, Ang SL, Shiota K, Nakanishi S, Kageyama R, and Guillemot F. Targeted disruption of mammalian hairy and Enhancer of split homolog-1 (HES-1) leads to up-regulation of neural helix-loop-helix factors, premature neurogenesis, and severe neural tube defects. *Gene Dev.* 1995;9(24):3136-48.

430. Hirata H, Ohtsuka T, Bessho Y, and Kageyama R. Generation of structurally and functionally distinct factors from the basic helix-loop-helix gene Hes3 by alternative first exons. *J Biol Chem.* 2000;275(25):19083-9.

431. Ohtsuka T, Ishibashi M, Gradwohl G, Nakanishi S, Guillemot F, and Kageyama R. Hes1 and Hes5 as Notch effectors in mammalian neuronal differentiation. *Embo J.* 1999;18(8):2196-207.

432. Ishibashi M, Moriyoshi K, Sasai Y, Shiota K, Nakanishi S, and Kageyama R. Persistent Expression of Helix-Loop-Helix Factor Hes-1 Prevents Mammalian Neural Differentiation in the Central-Nervous-System. *Embo J.* 1994;13(8):1799-805.

433. Betancourt J, Katzman S, and Chen B. Nuclear Factor One B Regulates Neural Stem Cell Differentiation and Axonal Projection of Corticofugal Neurons. *J Comp Neurol.* 2014;522(1):6-35.

434. Hirai S, Miwa A, Ohtaka-Maruyama C, Kasai M, Okabe S, Hata Y, and Okado H. RP58 controls neuron and astrocyte differentiation by downregulating the expression of Id1-4 genes in the developing cortex. *Embo J.* 2012;31(5):1190-202.

435. Xiang C, Baubet V, Pal S, Holderbaum L, Tatard V, Jiang P, Davuluri RV, and Dahmane N. RP58/ZNF238 directly modulates proneurogenic gene levels and is required for neuronal differentiation and brain expansion. *Cell Death Differ.* 2012;19(4):692-702.

436. Miller JA, Nathanson J, Franjic D, Shim S, Dalley RA, Shapouri S, Smith KA, Sunkin SM, Bernard A, Bennett JL, et al. Conserved molecular signatures of neurogenesis in the hippocampal subgranular zone of rodents and primates. *Development.* 2013;140(22):4633-44.

437. Jayne S, Zwartjes CGM, van Schaik FMA, and Timmers HTM. Involvement of the SMRT/NCoR-HDAC3 complex in transcriptional repression by the CNOT2 subunit of the human Ccr4-Not complex. *Biochemical Journal.* 2006;398(461-7.

438. Guenther MG, Barak O, and Lazar MA. The SMRT and N-CoR corepressors are activating cofactors for histone deacetylase 3. *Mol Cell Biol.* 2001;21(18):6091-101.

439. Bliss TVP, and Collingridge GL. A Synaptic Model of Memory - Long-Term Potentiation in the Hippocampus. *Nature.* 1993;361(6407):31-9.
440. McQuown SC, Barrett RM, Matheos DP, Post RJ, Rogge GA, Alenghat T, Mullican SE, Jones S, Rusche JR, Lazar MA, et al. HDAC3 Is a Critical Negative Regulator of Long-Term Memory Formation. *Journal of Neuroscience.* 2011;31(2):764-74.
441. Shu GH, Kramar EA, Lopez AJ, Huynh G, Wood MA, and Kwapis JL. Deleting HDAC3 rescues long-term memory impairments induced by disruption of the neuron-specific chromatin remodeling subunit BAF53b. *Learn Memory.* 2018;25(3):109-14.
442. Zhu XL, Wang SL, Yu LJ, Jin JL, Ye X, Liu Y, and Xu Y. HDAC3 negatively regulates spatial memory in a mouse model of Alzheimer's disease. *Aging Cell.* 2017;16(5):1073-82.

APPENDICES A and B

APPENDIX A: Mice lacking α-tubulin acetyltransferase 1 are viable but displays dentate gyrus distortion (reprint).

Kim, G.W., Li, L., Ghorbani, M., You, L., and Yang, X.-J. (2013) **J. Biol. Chem**. *288,* 20334-50.

APPENDIX B: BRPF1 is essential for development of fetal hematopoietic stem cells (reprint).

You, L.*, Li, L.*, Zou, J., Yan, K., Belle, J., Nijnik, A., Wang, E., and Yang, X.-J. (2016) **J. Clin. Invest.** *126*, 3247–3262 (* co-1st authors).

THE JOURNAL OF BIOLOGICAL CHEMISTRY VOL. 288, NO. 28, pp. 20334–20350, July 12, 2013

Mice Lacking α-Tubulin Acetyltransferase 1 Are Viable but Display α-Tubulin Acetylation Deficiency and Dentate Gyrus Distortion*

Received for publication, February 25, 2013, and in revised form, May 27, 2013 Published, JBC Papers in Press, May 28, 2013, DOI 10.1074/jbc.M113.464792

Go-Woon Kim[‡§], Lin Li[‡¶], Mohammad Gorbani[‡¶], Linya You[‡¶], and Xiang-Jiao Yang[‡§¶‖1]**

*From [‡]The Rosalind and Morris Goodman Cancer Research Center, Departments of [§]Anatomy and Cell Biology, [¶]Medicine, and [‖]Biochemistry, McGill University and the **McGill University Health Center, Montréal, Québec H3A 1A3, Canada*

Background: Biological functions of mammalian Atat1 and its contribution to α-tubulin acetylation *in vivo* remain elusive.
Results: Atat1-null mice are viable but possess deficient α-tubulin acetylation and a bulge in the dentate gyrus.
Conclusion: Mouse Atat1 is a predominant α-tubulin acetyltransferase *in vivo* and fine-tunes hippocampus development.
Significance: Mammalian Atat1 is not required for survival and development but may regulate more advanced functions.

α-Tubulin acetylation at Lys-40, located on the luminal side of microtubules, has been widely studied and used as a marker for stable microtubules in the cilia and other subcellular structures, but the functional consequences remain perplexing. Recent studies have shown that Mec-17 and its paralog are responsible for α-tubulin acetylation in *Caenorhabditis elegans*. There is one such protein known as Atat1 (α-tubulin acetyltransferase 1) per higher organism. Zebrafish Atat1 appears to govern embryo development, raising the intriguing possibility that Atat1 is also critical for development in mammals. In addition to Atat1, three other mammalian acetyltransferases, ARD1-NAT1, ELP3, and GCN5, have been shown to acetylate α-tubulin *in vitro*, so an important question is how these four enzymes contribute to the acetylation *in vivo*. We demonstrate here that Atat1 is a major α-tubulin acetyltransferase in mice. It is widely expressed in mouse embryos and tissues. Although Atat1-null animals display no overt phenotypes, α-tubulin acetylation is lost in sperm flagella and the dentate gyrus is slightly deformed. Furthermore, human ATAT1 colocalizes on bundled microtubules with doublecortin. These results thus suggest that mouse Atat1 may regulate advanced functions such as learning and memory, thereby shedding novel light on the physiological roles of α-tubulin acetylation in mammals.

Along with the recent proteomic analyses by mass spectrometry, numerous molecular and cell-based studies in the past 17 years have convincingly established lysine acetylation as an important post-translational modification likely to occur in all living species and to rival other well known modifications such as phosphorylation and ubiquitination (1–3). First discovered with histones in the early 1960s (4), the importance of lysine acetylation was initially recognized for its relation to chromatin organization and its impact on chromatin-templated nuclear processes (5–8). However, it is now clear that the spectrum of lysine acetylation is much broader than initially anticipated, comprising thousands of eukaryotic proteins that are not only involved in various nuclear events but also in a diversity of cytoplasmic processes (9–12). In addition, this modification is abundant in prokaryotic cells (13, 14). Unlike N-terminal acetylation, lysine acetylation is an N^{ϵ}-modification and is reversible and highly dynamic, governed by two groups of enzymes called lysine acetyltransferases and deacetylases (15–17). Based on sequence similarity, mammalian lysine acetyltransferases are grouped into three major families (15–17), and the deacetylases are divided into two large families composed of four classes (18–22). Therefore, lysine acetylation is an abundant covalent modification with its level actively maintained by acetyltransferases and deacetylases.

As one of two key components of microtubules (23, 24), α-tubulin is the first N^{ϵ}-acetylated non-histone protein discovered in the mid-1980s (25–28). The acetylated residue was identified as Lys-40 (25). This modification is conserved in a wide variety of species ranging from unicellular organisms, such as the green algae *Chlamydomonas* and the protist *Tetrahymena,* to mammals (25–28). Unlike many other tubulin modifications, the acetylation occurs on the luminal side of microtubules (23, 24, 29). Because of the early successful development of monoclonal antibodies (such as the 6-11b-1 clone) specific to Lys-40 acetylation (26), this modification has been used as a routine marker for stable microtubules in cilia, flagella, axons, midbodies, and other subcellular structures (23, 24, 29). However, it still remains debatable whether Lys-40 acetylation plays a causal role in regulating microtubule stability and dynamics (30–33). The acetylation has been linked to microtubule-mediated transport of proteins and organelles (31, 34–38), but it is enigmatic how a luminal modification affects transport processes occurring on the external surface of microtubules (29).

Substitution of Lys-40 in lower organisms such as *Tetrahymena* and *Chlamydomonas* exerts little impact on their survival (39, 40). Lys-40 of Mec-12 (mechanosensory-defective 12), the sole acetylatable α-tubulin, is not essential for nematodes (41). Moreover, substitution of Lys-40 with arginine exerts little effects on the function of a plant α-tubulin (42). Recent studies

* This work was supported by research grants from the Canadian Institutes of Health Research, the Canadian Cancer Society, the Canada Foundation for Innovation, and the Ministère du Développement Économique, Innovation, et Exportation du Québec (to X. J. Y.).
[1] To whom correspondence should be addressed. Tel.: 514-398-5883; Fax: 514-398-6769; E-mail: xiang-jiao.yang@mcgill.ca.

indicate that Lys-40 acetylation is important for mammalian neuron migration (36, 43, 44). Further knock-in analyses in genetically amendable mammalian models such as mice should substantiate how important Lys-40 acetylation is *in vivo*. Insights into the physiological function of α-tubulin acetylation can also be gained from studies of the responsible enzymes.

HDAC6 was discovered to be an α-tubulin deacetylase over 10 years ago (45–47). Global hyperacetylation of α-tubulin was subsequently found in *Hdac6*$^{-/-}$ mouse tissues and embryonic fibroblasts (48). SIRT2 was reported to be another α-tubulin deacetylase (49), but genetic deletion of mouse *Sirt2* does not affect α-tubulin acetylation significantly (48, 50). Thus, HDAC6 is now considered to be the predominant α-tubulin deacetylase *in vivo*. Despite this unique and crucial function in α-tubulin deacetylation, *Hdac6*$^{-/-}$ mice are viable and fertile (48), only displaying minor phenotypes, including moderate immune responses (48), anti-depressant-like symptoms (51), and slow platelet activation (52). This unexpected outcome suggests a potential role of HDAC6 and perhaps also α-tubulin acetylation in advanced biological functions.

Multiple acetyltransferases have been shown to acetylate α-tubulin *in vitro*, including the ARD1-NAT1 N^{α}-acetyltransferase complex (53), the transcriptional elongator complex subunit ELP3 (43, 54), and the well known acetyltransferase GCN5 (55). The ARD1-NAT1 complex was the first reported to acetylate α-tubulin *in vitro* (53). ELP3 was then found to acetylate α-tubulin and to regulate the migration of cortical neurons in the developing mouse brain (43). GCN5 was recently described to acetylate α-tubulin upon recruitment to microtubules by Myc-nick, a cytoplasmic isoform of Myc (55). More recent biochemical and genetic studies have demonstrated that a new member of the GNAT family (56), Mec-17 (mechanosensory-defective 17), is an α-tubulin acetyltransferase in *Tetrahymena* and *Caenorhabditis elegans* (32, 57). As a result, Mec-17 was renamed Atat1 (α-tubulin *N*-acetyltransferase 1). Atat1 is conserved from *C. elegans* to humans, although in *C. elegans* there are two Atat proteins and only one such ortholog exists in a higher organism (32, 57). Survey of 50 genomes of evolutionarily diverse organisms revealed that the presence of an Atat1 ortholog correlates perfectly with the possession of a cilium or flagellum (32). For example, an Atat1-like protein is encoded in the green algae *Chlamydomonas* (32), where α-tubulin acetylation was initially discovered (25–28). Moreover, mammalian Atat1 efficiently acetylates α-tubulin both in enzymatic assays with purified proteins and in cultured cells (32, 57). Recent structural analyses have provided elegant insights into how Atat1 targets and acetylates Lys-40 of α-tubulin (58–60). These studies all support that Atat1 is a *bona fide* α-tubulin acetyltransferase.

Morpholino analysis revealed an essential role of Atat1 in zebrafish development (57), raising the exciting possibility that Atat1 is also important for mammalian development. This is in agreement with a recent study (32) showing that Atat1 regulates assembly of the primary cilium, a unique organelle important for cellular signaling and animal development (61). However, it remains to be formally investigated whether Atat1 indeed plays a critical role in mammalian development. It is also unclear how mammalian Atat1 and the other aforementioned acetyltransferases contribute to α-tubulin acetylation *in vivo*.

Through analyzing *Atat1*$^{-/-}$ mutant mice generated by gene targeting, we demonstrate herein that mouse Atat1 is the predominant α-tubulin acetyltransferase in embryonic fibroblasts and various adult tissues. We also show that Atat1 is widely expressed, most highly in the brain, testis, renal pelvis, and gastrointestinal tract. Unexpectedly, *Atat1*$^{-/-}$ mutant embryos and mice are viable and display no overt phenotypes. Fluorescence microscopy and histological analyses revealed that Atat1 is required for α-tubulin acetylation in sperm flagella and that the dentate gyrus is slightly deformed. These results suggest that although not important for basic functions such as animal survival and development, mouse Atat1 may regulate more advanced functions, thereby shedding novel light on roles of mammalian α-tubulin acetylation *in vivo*.

MATERIALS AND METHODS

Animals—Three *Atat1*$^{tm1(KOMP)Vlcg}$ heterozygous C57BL6 male mice were obtained from the knock-out mouse project (KOMP) repository affiliated with University of California at Davis. Crossing them with wild-type C57BL6 mice produced heterozygous female mutant mice. Interbreeding between heterozygous male and female mice was then carried out to obtain homozygous knock-out embryos and mice. The mice used were housed in barrier cages, with 1–5 animals per cage. The animals were provided with food and water *ad libitum*. The experimental procedures performed on mice were carried out according to standard operating procedures created by the Veterinary Care Subcommittee, and the use of the mice for this project received approval by the McGill University Animal Care Committee.

Mouse Genotyping—Mice were genotyped by PCR with genomic DNA extracted from tissues from ear punch typically used for mouse identification. After ear punching, each tissue piece (round, roughly 2 mm in the diameter) was carefully collected and immersed in 200 μl of 50 mM NaOH and incubated at 95 °C for 10 min. After addition of 20 μl of 1 M Tris-HCl, pH 6.8, the mixture was vortexed for 7 s and centrifuged in a benchtop centrifuge at ~20,000 × *g* for 6 min. 2 μl of the supernatant was used for PCR. The primers used were as follows: Atat-F1 (5′-ACTGA AGGAC ACCTC AGCCC GA-3′), Atat-R1 (5′-TACCT CATTG TGAGC CTCCC GG-3′), LacInF (5′-GGTAA ACTGG CTCGG ATTAG GG-3′), and LacInR (5′-TTGAC TGTAG CGGCT GATGT TG-3′). A 10-μl PCR was set up with 5 μl of 2× GoTaq Green Master Mix (Promega, PRM5122), 2 μl of genomic DNA, 0.25 μl for each of two primers (10 pmol/μl), and 2.5 μl of sterile nuclease-free water. Cycling conditions were as follows: 95 °C for 3 min, 30 PCR cycles (95 °C for 30 s, 50 °C for 30 s, and 72 °C for 30 s per cycle) and 72 °C for 2 min. The reaction was kept at 4 or −20 °C until further analysis by agarose gel electrophoresis.

RT-PCR—Fresh mouse tissues were collected and then rinsed in ice-cold PBS, which was pretreated with 0.1% diethyl pyrocarbonate (DEPC,[2] Sigma) to inactivate RNases and then

[2] The abbreviations used are: DEPC, diethyl pyrocarbonate; MEF, mouse embryonic fibroblast; PFA, paraformaldehyde; DCX, doublecortin; RFP, red fluorescent protein.

autoclaved to remove residual DEPC. The rinsed mouse tissues were transferred to 1.5-ml microtubes. After addition of 200 μl of PBS pretreated with 0.1% DEPC, tissues were crushed in 1.5-ml Eppendorf tubes and mixed with 1 ml of the TRIzol reagent (Invitrogen, 16520-100). After vortexing, the suspension was then incubated at room temperature for 5 min and centrifuged at ~20,000 × *g* and 4 °C for 10 min. The supernatant was carefully transferred to a new microtube and mixed with 200 μl of chloroform. After vigorous vortexing, the suspension was centrifuged at ~20,000 × *g* for 2 min. The upper aqueous phase was then pipetted out and transferred to a new microtube for mixing with 500 μl of isopropyl alcohol and subsequent centrifugation at ~20,000 × *g* and 4 °C for 15 min. The supernatant was carefully decanted, and the pellet was washed with 750 μl of 75% cold ethanol prepared with sterile DEPC-treated Nano-pure water. The pellet was then air-dried and dissolved in an appropriate amount of sterile DEPC-treated Nanopure water. After quantification of the RNA concentration with a NanoDrop 2000 spectrophotometer (Thermo Scientific), cDNA was synthesized by use of a QuantiTect reverse transcription kit (Qiagen, 205313) according to the manufacturer's instructions. PCR was performed with the synthesized cDNA as the template. PCR conditions were identical to that used for genotyping, but the reaction volume was adjusted to 25 μl. The primers for Atat1 and LacZ were also the same as the ones used for genotyping. The primers for Gapdh were mGAPDH-RT01 (5′-GCACA GTCAA GGCCG AGAAT-3′) and mGAPDH-RT02 (5′-GCCTT CTCCA TGGTG GTGAA-3′).

Tissue Extract Preparation and Western Blotting—All these procedures were carried out at 4 °C or on ice. Tissues were weighted and homogenized with a small plastic pestle in 3 volumes of the RIPA buffer (25 mM Tris-HCl, pH 7.6, 150 mM NaCl, 1% Nonidet P-40, 1% sodium deoxycholate, 0.1% SDS, and a mixture of protease inhibitors). After additional homogenization by sonication with a Virsonic 100 sonicator (Virtis, Inc.) at setting 5, the suspension was centrifuged at ~20,000 × *g* for 10 min at 4 °C, and the supernatant was collected as the soluble extract, snap-frozen on dry ice, and stored at −80 °C. Protein concentration was measured by use of the Bradford assay reagent (Bio-Rad).

Tissue extracts were diluted in a 3× reduced SDS-PAGE sample buffer and denatured by boiling for 5 min. After electrophoresis, proteins were transferred onto nitrocellulose membranes, which were blocked for 1 h in the blocking solution (PBS containing 0.15% Tween 20 (Sigma) and 5% nonfat milk powder (Carnation)). Anti-α-tubulin antibody (Sigma, T5168, diluted at 1:2500) or the 6-11b-1 monoclonal antibody (specific to acetyl-Lys-40 of α-tubulin; Sigma, T7451, diluted at 1:10,000) was then added to the blocking solution for incubation overnight at 4 °C, with agitation. Blots were washed with PBS containing 0.15% Tween 20 five times (8 min each) and incubated with the horseradish peroxidase-conjugated sheep anti-mouse IgG secondary antibody (GE Healthcare, NA931V; diluted at 1:5000) for 1–3 h. After extensive washing, the Supersignal chemiluminescence solution (Pierce) was used to develop the signals.

Whole-mount β-Gal Staining of Embryos and Adult Tissues—Mice were anesthetized and transcardially perfused first with PBS and then with PBS containing 2% PFA. After perfusion was completed, embryos or tissues were collected and fixed at 4 °C for 2–3 h (up to 1 h for embryos) in PBS containing 2% PFA, 0.2% glutaraldehyde, 0.02% Nonidet P-40, and 0.2 mM $MgCl_2$. The fixative solution was changed to the detergent rinse (0.1 M phosphate buffer, pH 7.3, 2 mM $MgCl_2$, 0.01% sodium deoxycholate, and 0.02% Nonidet P-40). After incubation in the detergent rinse (changed 3–5 times) for 2–16 h, tissues or embryos were incubated in the β-galactosidase staining solution composed of 5 mM $K_3(Fe(CN)_6)/K_4(Fe(CN)_6)$ and 1 mg/ml X-Gal (62) until the desired intensity of blue color was developed.

Stained embryos were examined and analyzed under a Lumar V12 SteREO dissecting microscope (Zeiss), linked to an Axiocam HRc color camera, and controlled by Axiovision Re 4.8. Images were exported to Adobe Photoshop for processing and then imported to Adobe Illustrator for final presentation.

Frozen Section Preparation—Mice were anesthetized and sacrificed by cervical dislocation. Tissues were fixed overnight in PBS, 4% PFA at 4 °C and equilibrated first with PBS, 15% sucrose at 4 °C for ~8 h and then overnight with PBS, 30% sucrose. After that, tissues were found to be at the bottom of the tubes and were further equilibrated with the optimal cutting temperature (OCT) compound (Tissue-Tek) for 30 min at 4 °C, with gentle agitation. Tissues were then carefully oriented prior to snap-freezing on dry ice. Tissue blocks were transferred to −80 °C for storage. 30 min prior to sectioning, tissues blocks were transferred to dry ice. The blocks were sectioned on a cryotome electronic cryostat (Thermo Shandon, A77210167), and 10–30-μm sections were collected onto glass slides (Fisher Scientific, 12-550-19). The sections were then air-dried and stored at −80 °C.

β-Gal Staining of Frozen Sections—Sections were post-fixed in a fixative (0.2% PFA in 0.1 M PIPES, pH 6.9, 2 mM $MgCl_2$, and 5 mM EGTA) on ice for 10 min and rinsed with PBS containing 2 mM $MgCl_2$, followed by washing in the same solution for 10 min. Sections were permeabilized by incubation in the detergent rinse on ice for 10 min. The detergent rinse was changed to the β-galactosidase staining solution for incubation at 37 °C in the dark until the desired blue color was reached (1 h to overnight). The slides were then washed three times in PBS containing 2 mM $MgCl_2$ at room temperature for 5 min, followed by washing in distilled water. Counterstaining was carried out in the Nuclear Fast-Red solution (Sigma), with sequential dehydration by incubation with 50, 70, and 100% methanol (5 min each). Sections were cleared twice in Histoclear (Diamed, HS-200) for 5 min and mounted onto glass slides with a mounting medium (American Master Tech, MMC0126).

Paraffin Section Preparation—Mice were anesthetized for transcardial perfusion first with PBS and then with PBS containing 4% PFA. After perfusion was completed, major tissues were collected and fixed in PBS containing 4% PFA. In addition, Bouin's solution (saturated picric acid (Sigma), 40% formaldehyde, and 5% glacial acetic acid mixed at the 15:5:1 ratio) was also used for fixation of testes. The tissues were kept in PBS containing 4% PFA or in Bouin's solution overnight at 4 °C for subsequent paraffin embedding. The resulting paraffin blocks were sectioned on a Leica Rotary Microtome (Leica RM2125

RTS), and 5-μm sections were collected onto glass slides (Fisher Scientific, 12-550-19). The tissue section-containing slides were baked overnight in a 37 °C incubator and stored at 4 °C.

Nissl Staining of Brain Sections—Paraffin sections were deparaffinized in xylene twice for 5 min each, then rehydrated in 100% alcohol twice (5 min each), followed by 95 and 70% alcohol (3 min each), and subsequently rinsed in tap water and distilled water. The sections were then placed in 0.1% cresyl violet (Sigma) containing 0.3% glacial acetic acid for 7 min and rinsed quickly in distilled water. The sections were subsequently dehydrated in 70 and 95% alcohol for 3 min each, 100% alcohol twice for 5 min each, and cleared in xylene twice (5 min each). The sections were finally mounted with glass coverslips (Fisher Scientific) in the ClearMount mounting solution (Invitrogen). The slides were either examined under a regular light microscope or scanned with a digital slide scanner (ScanScope XT, Aperio ePathology). For the latter, the Spectrum software (Aperio ePathology) was then used to analyze the digitized images, and the ruler tool was employed to measure the size and dimensions of various structures in the sections.

Indirect Immunofluorescence Microscopy—Paraffin-embedded testis sections were fixed in Bouin's solution and prepared as above. The sections were deparaffinized and rehydrated the same as the brain sections mentioned above. Then heat-induced epitope retrieval was performed with the sections by boiling the slides in 10 mM citrate, pH 6.0, for 20 min. After cooling down for 20 min, the sections were circled with a PAP pen (Invitrogen, 00-8877) and rinsed with PBS three times for 5 min each. The remaining fluorescence microscopic analysis was similar to that used for cultured cells (63). After permeabilization with a few drops of the immunofluorescence (IF) buffer (PBS, 0.2% Triton X-100, and 0.05% Tween 20) for 30 min, the sections were incubated with drops of the IF blocking solution (IF buffer containing 2% bovine serum albumin) for 1 h. Then the anti-α-tubulin antibody (diluted at 1:500) or the anti-acetylated α-tubulin antibody (the 6-11b-1 clone, diluted to 1:1000) was added, and the incubation was carried out at room temperature for 3 h or overnight at 4 °C, with gentle agitation. After washing with the IF buffer three times (5 min each), the sections were incubated with Alexa Fluor-labeled anti-mouse IgG (Invitrogen, A11031) for 1 h, followed by three washes with the IF buffer. After incubation with PBS containing DAPI (0.5 ng/ml) for 5 min and subsequently washing twice with water (5 min each), the sections were mounted with coverslips in the ImmuMount mounting medium (Thermo Shandon, 9990402).

Preparation of Mouse Embryonic Fibroblasts (MEFs)—MEFs were derived from E13.5 embryos as described previously (64, 65).

Fluorescence-activated Cell Sorting (FACS) Analysis of MEFs—*Atat1*$^{+/-}$ and *Atat1*$^{-/-}$ MEFs were seeded in 10-cm dishes and cultured in MEF medium, composed of DMEM, 10% FBS, nonessential amino acids (1×, diluted from 100× stocks, Invitrogen), sodium pyruvate (1×, diluted from 100× stocks, Invitrogen) and were incubated in a low oxygen incubator (3% O_2) for 4 days. Cells were then trypsinized before reaching confluency and washed with PBS. Collected cells were fixed in 75% ethanol at −20 °C for 2–3 h. Cells were incubated with the staining solution (300 μl of PBS, 1 μl of DAPI, and 7 μl of RNase A (10 μg/ml)) for 15 min. Then the stained cells were analyzed on a FACS analyzer.

Live Green/Red Fluorescence Microscopy—The microscopic analysis was performed as described previously (66). Briefly, HEK293 cells were plated onto 12-well plates at 4×10^4 per well. 16–24 h later, the cells were transfected with expression plasmids for eGFP-ATAT1, eGFP-α-tubulin, and RFP-DCX as indicated. The eGFP-ATAT1 construct was prepared from a human cDNA clone from Open Biosystems, whereas the ones for eGFP-α-tubulin and RFP-DCX were obtained from Addgene (plasmids 30387 and 32851, respectively). The transfections were performed with 1.5 μl of Lipofectamine 2000 (Invitrogen). 16–18 h post-transfection, green and red fluorescence signals in the cells were analyzed, without any further processing, under an Axiovert 200 inverted microscope (Zeiss), linked to an Axiocam HRm camera and controlled by Axiovision Re 4.8. Fluorescence images were taken and further processed with CS5 Adobe Photoshop and Illustrator.

RESULTS

Targeted Deletion of Mouse Atat1—To determine the necessity of *Atat1* in mice and to investigate what roles Atat1 plays at the physiological level, we analyzed mutant mice in which *Atat1* is inactivated by homologous recombination. These mice were generated by gene targeting through a BacVec-derived targeting vector (KOMP affiliated with the University of California at Davis). In the resulting mutant allele (Fig. 1*A*), a 9.2-kb genomic fragment spanning all coding exons of Atat1 was replaced with a promoterless *lacZ* knock-in cassette and a selection marker flanked by a splice acceptor and a polyadenylation site. The *lacZ* coding sequence is under the control of the 5′ promoter of *Atat1* and thereby provides a convenient and sensitive reporter system for assessment of *Atat1* transcription by detecting β-galactosidase activities in whole-mount embryos and tissues or in thin sections at the single cell level.

Three male heterozygous mice were obtained from the KOMP repository and mated with wild-type female mice to obtain male and female heterozygous knock-out mice. Interbreeding was then carried out to yield wild-type, heterozygous, and homozygous littermates for subsequent experimental analyses. Genotyping by PCR with two specific primer pairs confirmed the expected genotypes (Fig. 1*B*). Mating between *Atat1*$^{+/-}$ mice yielded offspring with the three genotypes at the expected Mendelian ratio.

Atat1$^{-/-}$ mice were viable and did not yield obvious phenotypes (Fig. 1*C* and data not shown). Both male and female *Atat1*$^{-/-}$ mice were indistinguishable from their wild-type or *Atat1*$^{+/-}$ littermates by gross examination. Genetic deletion of *Atat1* did not affect the size and the overall growth (data not shown), and both *Atat1*$^{+/-}$ and *Atat1*$^{-/-}$ mice were fertile. In addition, compared with the wild-type counterparts, the mutant mice showed no obvious differences in pup retrieval and nest building (data not shown). Overall, no overt phenotypes were observed.

Next, we sought to validate the knock-out strategy by analyzing the expected mRNA transcripts. For this, RNA from different tissues in wild-type and *Atat1*$^{-/-}$ mice was extracted for

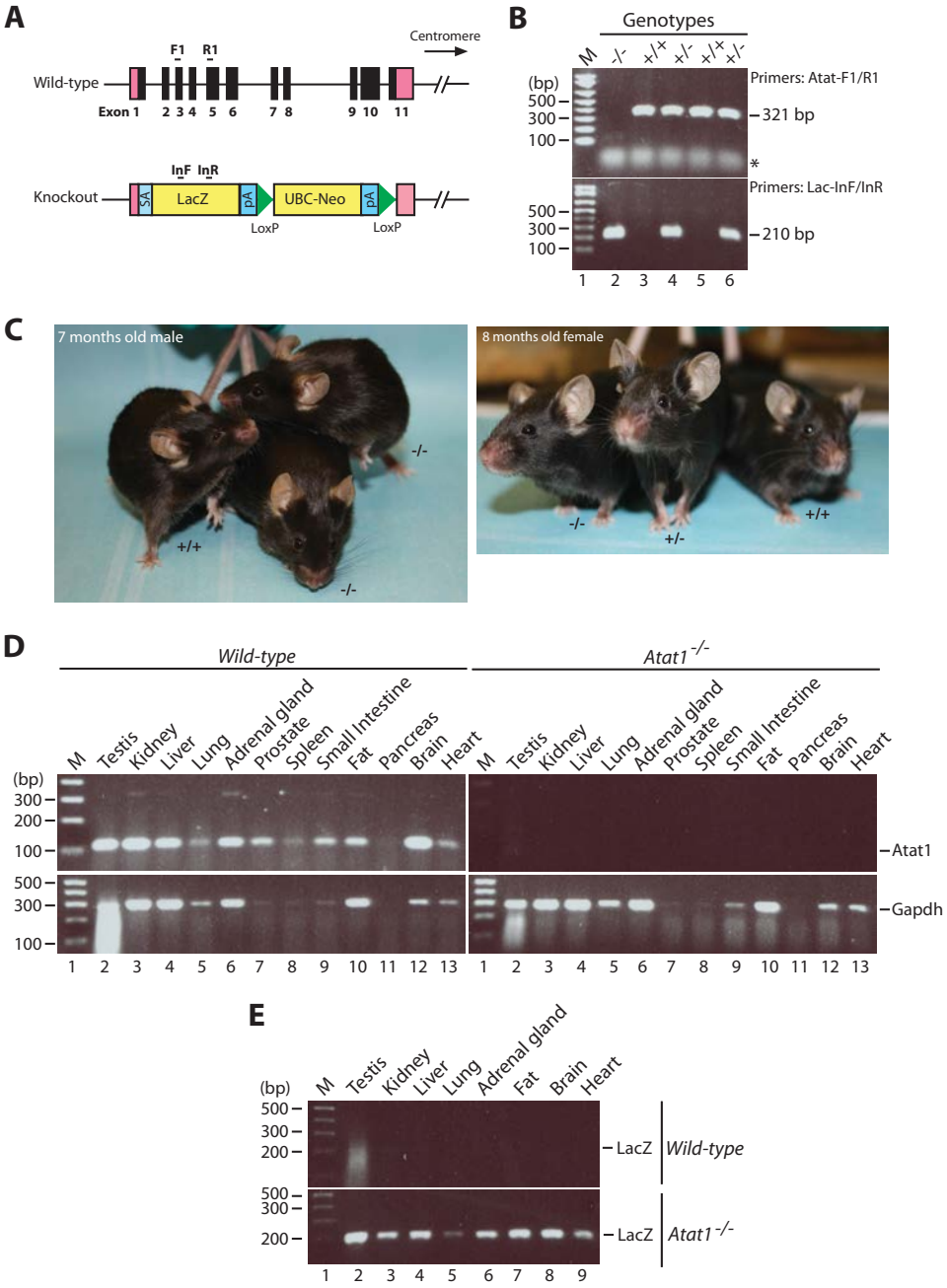

FIGURE 1. **Analysis of mouse *Atat1* by gene targeting.** *A*, strategy for generation of the *Atat1*-null allele. *Pink boxes* denote the 5′- and 3′-untranslated sequences, and *solid boxes* indicate exons of the *Atat1* gene located at the mouse chromosome 17qB1 (UCSC Genome Browser). A Bac targeting vector was utilized to replace the 9.2-kb genomic sequence of *Atat1*, spanning the entire coding region, with the promoterless *lacZ* coding sequence and a ubiquitin C (*UBC*) promoter-neomycin selection cassette flanked by two LoxP sites. *SA,* splicing acceptor; *pA,* polyadenylation signal. Rough positions of the PCR genotyping primers are indicated with *tiny bars*; *F1* and *R1* are for amplifying a 321-bp fragment from wild-type allele, and *InF* and *InR* are used to amplify a 210-bp fragment from the knock-out allele. *B*, PCR genotyping with the indicated primer pairs. The *asterisk* denotes nonspecific bands. *M* indicates the 100-bp DNA ladder as the molecular size marker (*lane 1*). *C*, adult *Atat1*$^{-/-}$ mice are indistinguishable from wild-type littermates by gross examination. *D*, RT-PCR analysis of *Atat1* expression in tissues from the wild-type and homozygous knock-out mice. *Atat1* mRNA was detected in the indicated tissues from the wild-type but not *Atat1*$^{-/-}$ mouse. *Gapdh*, internal control. *E*, RT-PCR analysis of *lacZ* mRNA in various tissues from the wild-type and knock-out mice. The cDNA templates were the same as those used in *D*, with PCR primers Lac-InF/-InR (*A*). *M,* 100-bp DNA ladder (*lane 1*).

RT-PCR, to compare the levels of mRNA species transcribed from endogenous *Atat1* and the exogenously inserted *lacZ* reporter gene. As shown in Fig. 1*D*, the *Atat1* transcript was widely expressed in the wild-type mice but was absent in the *Atat1*$^{-/-}$ mice. Conversely, the exogenous *lacZ* reporter was expressed in the *Atat1*$^{-/-}$ but not wild-type mice (Fig. 1*E*). These results confirm the knock-out accuracy and efficiency.

Atat1 as the Predominant α-Tubulin Acetyltransferase in Mice—To substantiate genetic ablation of *Atat1* at the functional level, we extracted soluble proteins from wild-type and *Atat1*$^{-/-}$ mice and performed Western blotting using antibodies specific to regular and acetylated α-tubulin. For acetylated α-tubulin, we employed the widely used monoclonal antibody 6-11b-1. As shown in Fig. 2*A*, α-tubulin acetylation was totally

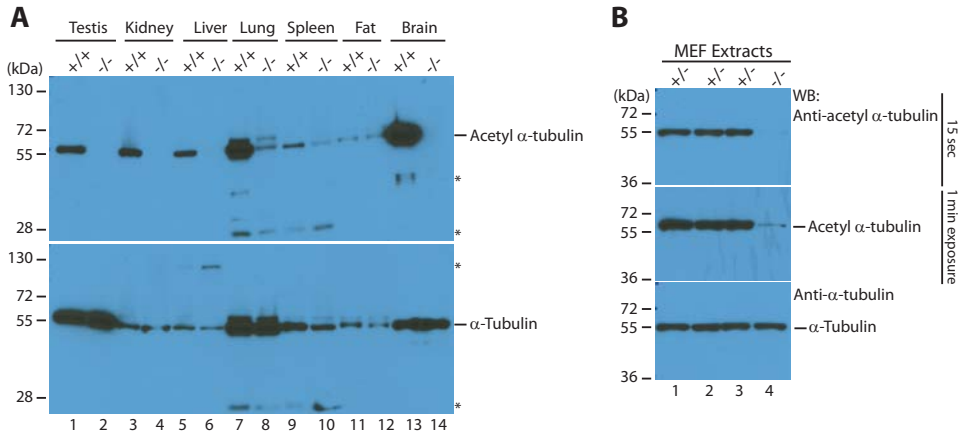

FIGURE 2. **Mouse Atat1 is the predominant α-tubulin acetyltransferase *in vivo*.** *A*, protein extracts were prepared from various tissues of wild-type and *Atat1*$^{-/-}$ young male mice for Western blotting (*WB*) using the monoclonal antibody recognizing α-tubulin acetylated at Lys-40 (*top panel*) or the anti-α-tubulin antibody (*bottom panel*). *B*, same as *A* except that protein extracts were prepared from fibroblasts prepared from E13.5 embryos with the indicated genotypes. Yolk sacs were initially used to determine the genotypes as shown in Fig. 1*B*, and the genotypes were subsequently confirmed by PCR with genomic DNA directly isolated from the expanded MEFs. To illustrate the residual acetylation signal detected in *Atat1*$^{-/-}$ MEF extracts, two exposures for the same blot are shown (*top two blots*).

ablated in major organs such as the testis (*lanes 1* and *2*), kidney (*lanes 3* and *4*), liver (*lanes 5* and *6*), and brain (*lanes 13* and *14*) of the *Atat1*$^{-/-}$ mice. It is interesting to note that the acetylation was the highest in the brain (Fig. 2*A*). Although α-tubulin acetylation was still detectable in the lung (Fig. 2*A, lanes 7* and *8*) and spleen (*lanes 9* and *10*), the levels dramatically or significantly decreased. In the white fat tissue, the acetylation was only minimally affected (Fig. 2*A, lanes 11* and *12*). These results demonstrate that *Atat1*$^{-/-}$ mice exhibit complete or dramatic loss of α-tubulin acetylation in major tissues, including the testis, kidney, liver, lung, and brain, indicating that Atat1 is the predominant α-tubulin acetyltransferase *in vivo*. The retained acetylation in the mutant lung, spleen, and fat tissues may be due to other α-tubulin acetyltransferases. The candidates include Ard1-Nat1, ELP3, and GCN5, which are known to acetylate α-tubulin *in vitro* (43, 53, 55). Further genetic analyses are needed to investigate whether any of them are responsible for the remaining α-tubulin acetylation detected in the mutant lung, spleen, and fat.

In addition to tissue analysis, we also examined extracts prepared from MEFs, which were isolated from heterozygous and homozygous mutant embryos dissected out at gestation day E13.5. Embryonic days were calculated according to the convention that E0.5 corresponds to the noon after the morning when the copulation plug was found if the mating was assumed to occur at the preceding midnight. Compared with that in the heterozygous fibroblasts, α-tubulin acetylation in the homozygous MEFs decreased dramatically to a minimal level (Fig. 2*B*), supporting that Atat1 is also a major α-tubulin acetyltransferase in mouse embryos. As discussed above for adult tissues, the residual level of acetylation (Fig. 2*B, lane 4, middle panel*) could be due to the existence of additional α-tubulin acetyltransferases.

Broad Expression of Atat1 in Mouse Embryos—Taking advantage of the *lacZ* knock-in cassette in the mutant allele (Fig. 1*A*), we then determined the expression pattern of mouse Atat1 during embryonic development. For this, embryos at E10.75 and E13.5 were used for whole-mount β-galactosidase staining. Gross morphological examination of the resulting wild-type and homozygous knock-out embryos did not reveal any obvious defects during the embryonic period (Fig. 3). This is expected in light of grossly normal *Atat1*$^{-/-}$ mice (Fig. 1*C* and data not shown). At both E10.75 and E13.5, Atat1 was highly expressed throughout the embryos (Fig. 3), with the spinal cord being the most intensely stained in the E13.5 mutant embryo (data not shown). These results indicate that mouse Atat1 is not required for embryonic development and is widely expressed. Therefore, Atat1 does not appear to play a major role in either embryonic or postnatal development.

Wide Atat1 Expression in Adult Mouse Tissues—We next set out to determine the global expression pattern of Atat1 in adult mice. For this, we collected a variety of tissues from wild-type and *Atat1*$^{-/-}$ mice for whole-mount β-galactosidase staining. By gross examination of the appearance, no signs of obvious pathogenicity were found in the tissues from the *Atat1*$^{-/-}$ mice, and the size of the tissues was also similar between the wild-type and *Atat1*$^{-/-}$ mice. As shown in Fig. 4, the expression of Atat1 varied among different tissues, with the testis, the renal pelvis, the gastrointestinal tract (stomach, small intestine and rectum), and the brain having the most intense β-galactosidase staining (Fig. 4, *A, B, H–J,* and *L–N,* respectively). In addition, high β-galactosidase activities were detected in the habenula, as well as in islands of Calleja located within the olfactory tubercle, of the mutant mouse brain (data not shown).

However, no strong signals were observed in the spleen and heart (Fig. 4, *E* and *F,* respectively). These results suggest that Atat1 is highly expressed in many but not all tissues. Robust Atat1 expressions in the testis and brain (Fig. 4, *A* and *L–N*) are consistent with high levels of α-tubulin acetylation detected in these tissue extracts (Fig. 2*A*). Related to this, it has been reported that α-tubulin acetylation is associated with stable, long-lived microtubules found in the basal bodies and axonemes of sperm flagella (26, 67) and in axons of neurons (68–70). In contrast to the robust expression of Atat1 in the testis, renal pelvis, gastrointestinal tract, and brain, gross examination revealed no overt defects in these tissues of *Atat1*$^{-/-}$ embryos

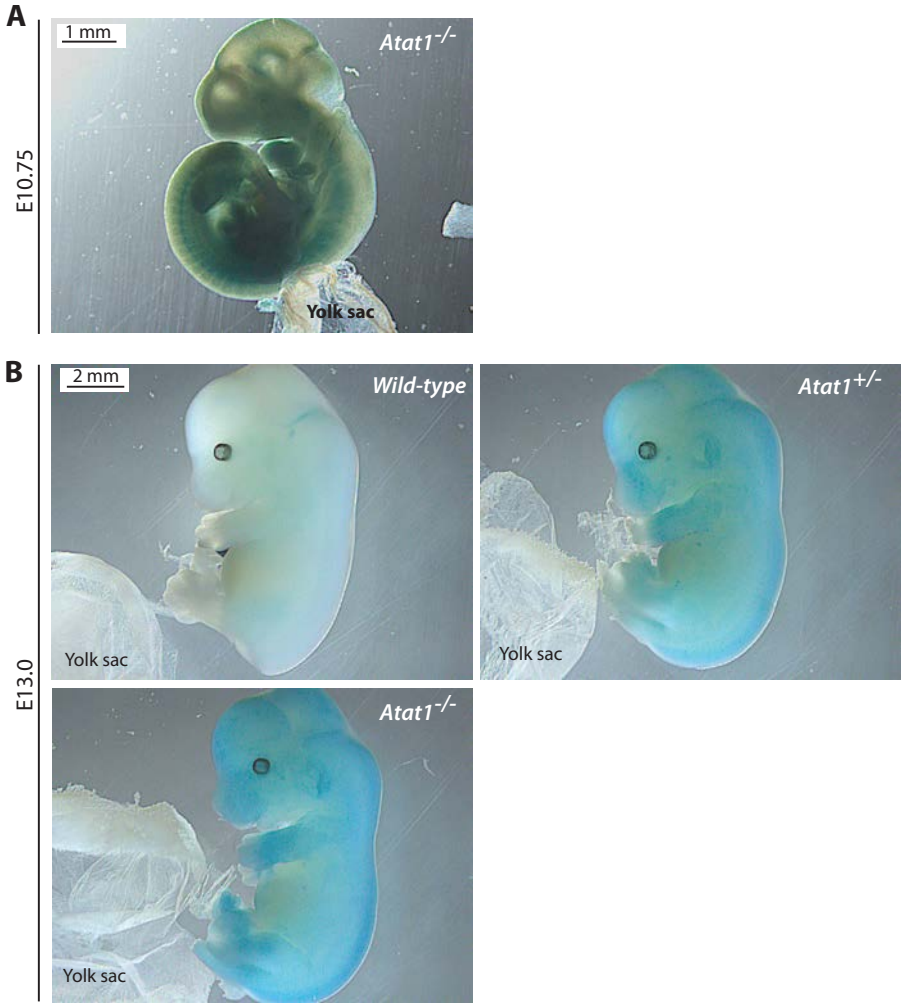

FIGURE 3. **Whole-mount β-galactosidase staining of wild-type and *Atat1*$^{-/-}$ embryos.** At both E10.75 (*A*) and E13.5 (*B*), LacZ expression was wide in the *Atat1*$^{-/-}$ but not wild-type embryo (data not shown for the wild-type E10.75 embryo, which displayed no staining). No morphological defects were found in the mutant embryos at these two and other embryonic stages (data not shown), indicating that Atat1 is not required for normal embryonic development. Yolk sacs were used to determine the genotypes as shown in Fig. 1*B*.

and mice (Fig. 4 and data not shown). To determine whether there were minor defects, we carried out more thorough and careful analyses of the testis and brain, two tissues that have high α-tubulin acetylation and Atat1 expression (see below).

Requirement of Atat1 for α-Tubulin Acetylation on Sperm Flagella—To gain further insights about Atat1 functions at the histological level, we examined β-galactosidase staining in thin tissue sections prepared from the mouse testes in light of the high expression in this organ (Fig. 4*A*). For this, frozen tissue blocks were prepared from testes and sectioned to 10–30 μm on a cryostat. Hematoxylin and eosin (H&E) and β-galactosidase stainings were then performed to gain information on tissue morphology and Atat1 expression, as well as on the potential impact of *Atat1* deletion.

Specific Atat1 expression was observed in internal cell layers of the mutant seminiferous tubules, where spermatids and spermatocytes reside (Fig. 5*A*). By indirect immunofluorescence microscopy, we detected α-tubulin in all cells within wild-type and mutant seminiferous tubules, with the signals localized exclusively to the cytoplasm (Fig. 6, *A* and *B, top rows of images*). In addition, strong signals were detected at the luminal centers of seminiferous tubules (Fig. 6, *A* and *B, top rows of images*). The central regions, which were devoid of DAPI staining and lack of nuclei (Fig. 6, *A* and *B, top rows of images*), correspond to structures formed by sperm flagella. Under the regular light microscope, there were no obvious differences on the sperm flagella of the wild-type and mutant seminiferous tubules. Consistent with this, H&E staining revealed the presence of sperm flagella at the luminal centers of both wild-type and *Atat1*$^{-/-}$ seminiferous tubules (Fig. 6*C*).

Interestingly, acetylated α-tubulin was highly abundant at the luminal centers of the wild-type seminiferous tubules (Fig. 6*B*, *bottom three images*). Importantly, the α-tubulin acetylation signals were absent at the central regions of the mutant seminiferous tubules (Fig. 6*B*, *bottom three images*). These results indicate that Atat1 is required for α-tubulin acetylation of sperm flagella at the luminal centers of seminiferous tubules.

Histological Analysis of Atat1 Expression in the Brain—As the β-galactosidase activity resulting from the knock-in *lacZ* gene (Fig. 1*A*) was very high in the whole-mount brain (Fig. 4, *L–N*), we performed β-galactosidase staining in thin brain sec-

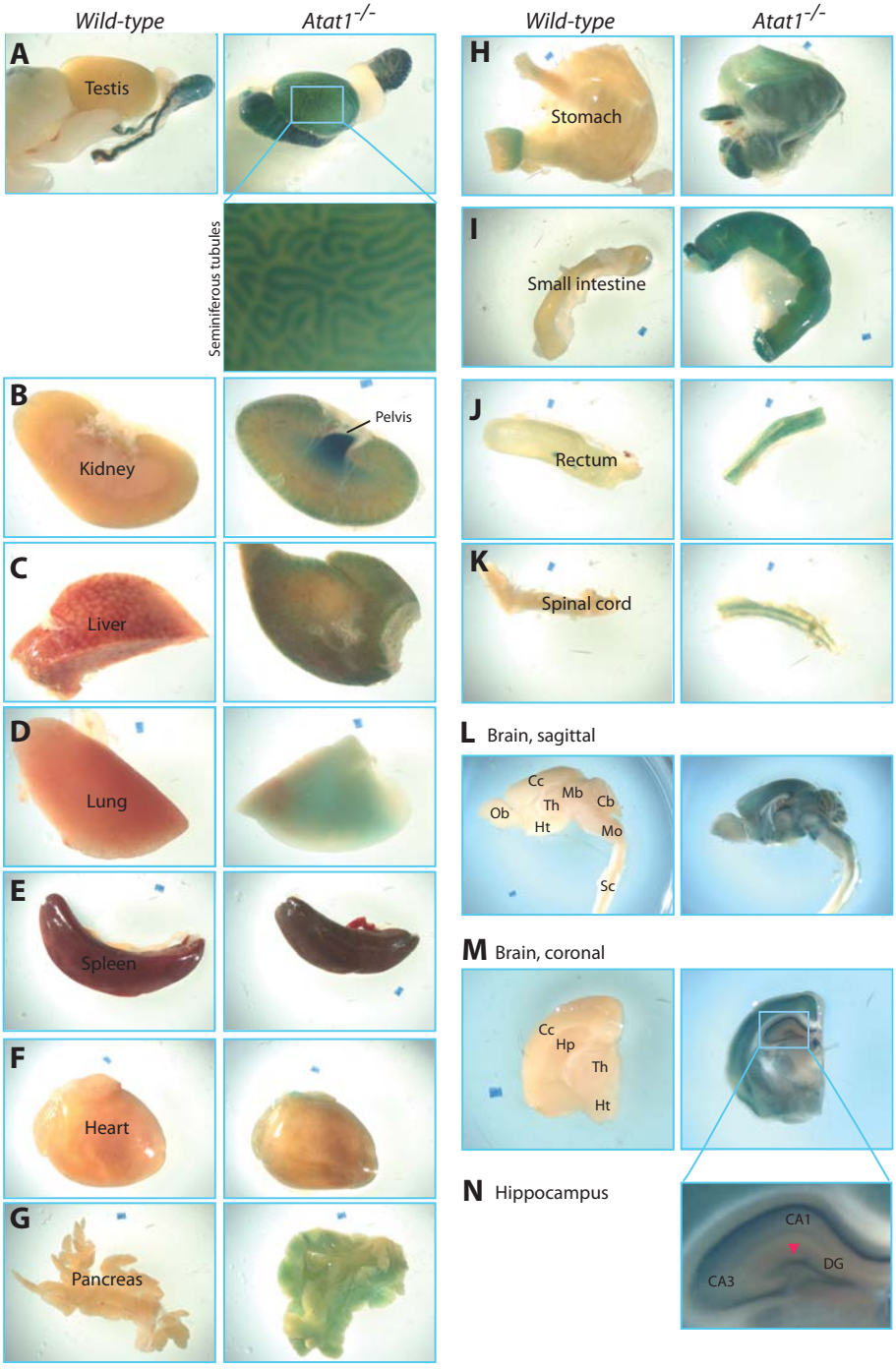

FIGURE 4. **Whole-mount β-galactosidase staining of adult mouse organs.** *A–N*, strong expression was observed in the testis, renal pelvis, gastrointestinal tract, and brain of the *Atat1*$^{-/-}$ but not wild-type mouse. For the testis (*A*) and brain (*M* and *N*), two *boxed* regions are shown at higher magnifications to illustrate β-galactosidase activities detected in seminiferous tubules and the hippocampus of *Atat1*$^{-/-}$ mice. Although not clear from *L*, *M*, and *N*, high β-galactosidase activities were detected in the habenula as well as in islands of Calleja located within the olfactory tubercle. Different structures in the brain were labeled according to published atlases (71, 72). Abbreviations for regions marked in *L*, *M*, and *N* are as follows: *CA1* and *CA3*, cornu ammonis areas 1 and 3 of the hippocampus, respectively; *DG,* dentate gyrus; *Cc*, cerebral cortex; *Cb,* cerebellum; *Mb,* midbrain; *Mo,* medulla oblongata; *Hp,* hippocampus; *Ht,* hypothalamus; *Ob,* olfactory bulb; *Sc,* spinal cord; *Th,* thalamus.

tions to gain information on Atat1 expression at the histological level. The staining revealed that the β-galactosidase activity was wide in the mutant brain, including the cerebral cortex and cerebellum (Fig. 5, *B* and *C*). Moreover, consistent with the results from whole-mount staining (Fig. 4, *M* and *N*), specific and strong β-galactosidase staining was also detected in different regions of the mutant hippocampus, including the pyramidal layers in CA1 and CA3, as well as the granular cell layers in the lateral blade (suprapyramidal portion) and the medial blade (infrapyramidal portion) of the dentate gyrus (Fig. 5*D*). The wide β-galactosidase staining in the brain is consistent with the result that α-tubulin acetylation is the highest in this organ (Fig. 2*A*). Wide expression of Atat1 in different regions of the brain suggests a potential physiological role of Atat1 in this important organ.

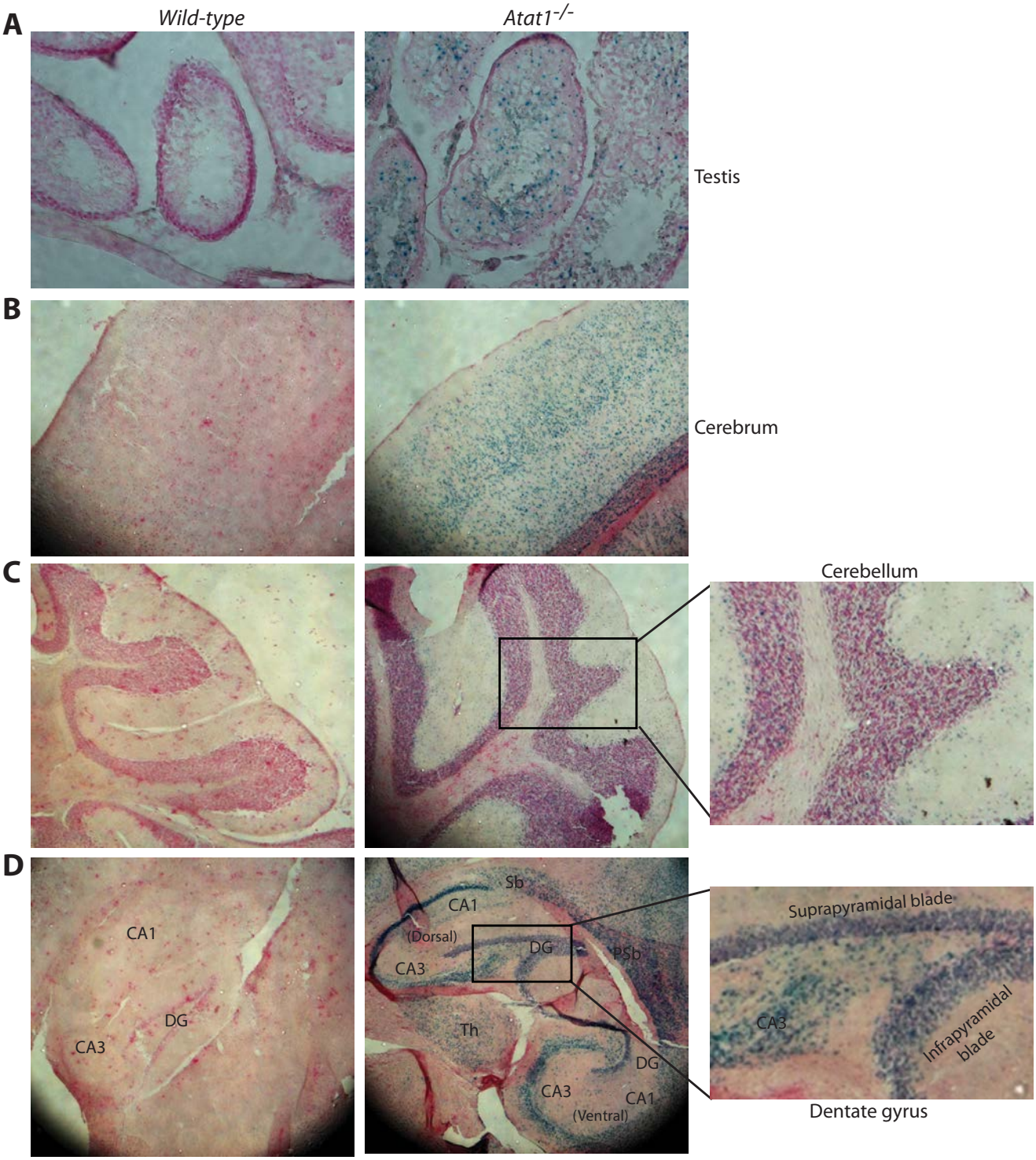

FIGURE 5. **β-Galactosidase expression in testis and brain sections.** *A*, β-galactosidase activity detection in frozen sections of wild-type and *Atat1*$^{-/-}$ testes. β-Galactosidase staining showed that Atat1 was mainly expressed in the internal cell layers of seminiferous tubules, where spermatocytes and spermatids are located. *B–D*, β-galactosidase staining of frozen wild-type and *Atat1*$^{-/-}$ brain sections. High level β-galactosidase expression was detected in the cerebral cortex (*B*), cerebellum (*C*), and hippocampus (*D*). This is consistent with results from whole-mount staining of the corresponding tissues (Fig. 4, *L–N*). At the mutant sagittal plane in *D*, the dentate gyrus did not display a bulge (refer to Figs. 7 and 8). See Fig. 4 for abbreviations of different structures in the hippocampus; Sb, subiculum; PSb, parasubiculum.

Dentate Gyrus Distortion in Mutant Mice—During analysis of Atat1 expression in the brain, we noticed a bulge in the suprapyramidal blade (Fig. 4*N*, marked by *red arrowhead*). H&E staining confirmed that this bulge was more prominent in the mutant dentate gyrus than the wild-type counterpart (data not shown). Cresyl violet is frequently used to stain Nissl bodies (corresponding to rough endoplasmic reticulum) in neurons for histological analysis of various structures in the brain, so we performed Nissl staining. As shown in Fig. 7, compared with the wild-type counterpart, the

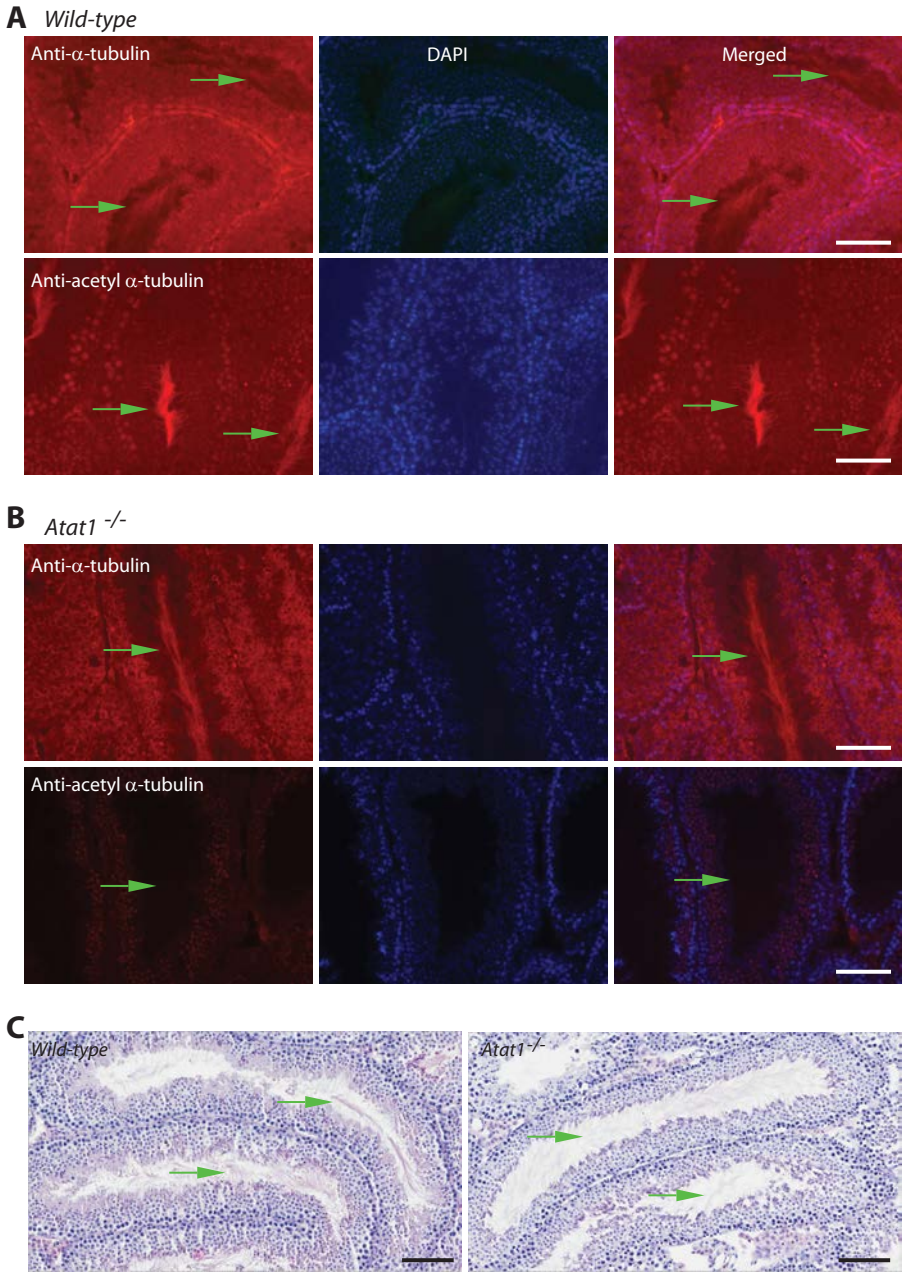

FIGURE 6. **Comparison of testis sections from wild-type and *Atat1*$^{-/-}$ mice.** *A* and *B*, immunofluorescence microscopic analysis with antibodies recognizing regular (*A*) and acetylated (*B*) α-tubulin. Probing with the anti-α-tubulin antibody detected α-tubulin in almost every cell within seminiferous tubules of wild-type and *Atat1*$^{-/-}$ testis sections. In addition, strong signals were present at the luminal centers of the tubules (denoted with *green arrows*; *A* and *B*, *top rows of images*). The centers correspond to the areas where sperm flagella reside. Staining with the antibody against acetylated α-tubulin revealed the presence of α-tubulin acetylation at the central regions of seminiferous tubules in the wild-type testis section (*A*, *bottom three images*). Importantly, this signal was no longer observed in the testis section of the *Atat1*$^{-/-}$ mouse (*B*, *bottom three images*). *Scale bar,* 40 μm. *C*, H&E staining of testis sections. The sections were fixed in Bouin's solution and subjected to H&E staining. *Green arrows* denote sperm flagella. *Scale bar,* 100 μm.

mutant dentate gyrus was slightly deformed, especially for the possession of a prominent bulge in the lateral blade of the granular cell layers. In addition to this difference, the lateral ventricle appeared to be dilated, which is currently under investigation. Although more thorough and careful analyses are needed, other regions of the brain appeared to be normal.

Anatomically, the size and morphology of the mouse hippocampus vary at different sagittal planes (71, 72). To determine alteration of the dentate gyrus at different section planes, we systematically performed Nissl staining with sagittal brain sections from the wild-type and mutant mice. Shown in Fig. 8, *A–C* and *E,* are hippocampal images taken from four pairs of representative sagittal brain sections at the medial-to-lateral direction. Comparison of the wild-type and mutant dentate gyri confirmed the difference in the lateral blade of granular cell layers in the dorsal hippocampus (Fig. 8, *A–C* and *E*), whereas the dentate gyrus in the ventral hippocampus was not affected (Fig. 8*D*). The results presented in Fig. 8 were taken from one pair of the wild-type and mutant mice, and two other pairs of mice displayed similar differences in the dentate gyrus (data not shown).

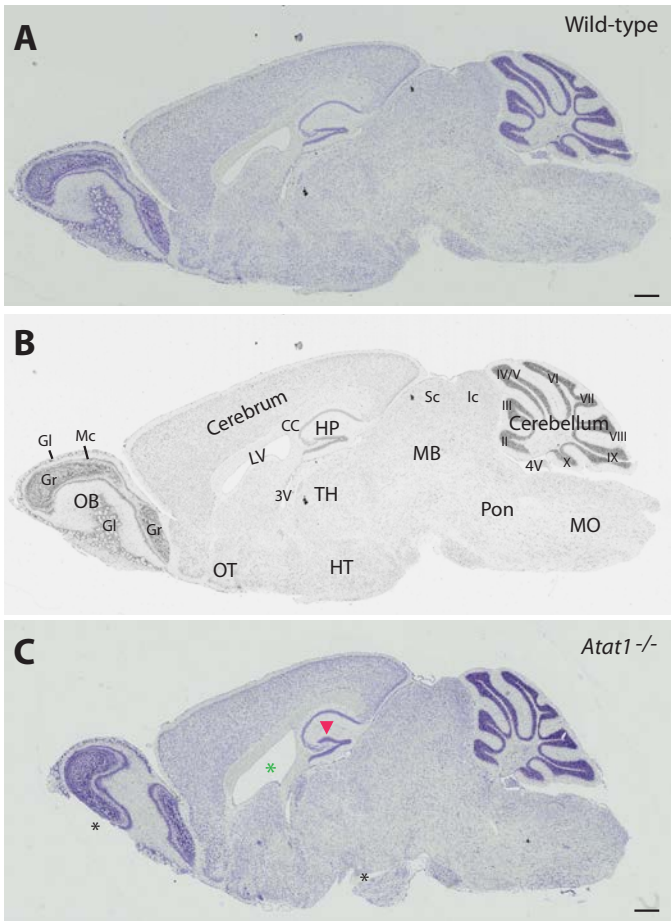

FIGURE 7. **Histological analysis of wild-type and *Atat1*$^{-/-}$ brain sections.** *A*, Nissl staining of a sagittal section from the wild-type mouse brain. *B*, *black/white* copy of the color image shown in *A*, with different brain regions annotated. Structures of the brain were labeled according to published atlases (71, 72). Abbreviations used are as follows: *3V,* third ventricle; *4V,* 4th ventricle; *II–X,* nine lobes of the cerebellum, with lobe I missing in the section; *CC,* corpus callosum; *Gr,* granular cell layers in the olfactory bulb; *Gl,* glomerulus of the olfactory bulb; *LV,* lateral ventricle; *MB,* midbrain; *Mc,* mitral cell layer of the olfactory bulb; *MO,* medulla oblongata; *HP,* hippocampus; *HT,* hypothalamus; *Ic,* inferior colliculus; *OB,* olfactory bulb; *OT,* olfactory tubercle; *Sc,* superior colliculus; *TH,* thalamus. *C*, Nissl staining of a sagittal section from the *Atat1*$^{-/-}$ mouse brain. The position of this section corresponds roughly to that shown in *A*. The *red arrowhead* in *C* marks a bulge in the lateral or suprapyramidal blade of the mutant dentate gyrus. The *green asterisk* denotes the dilated lateral ventricle, and *dark asterisks* indicate two broken areas due to section processing. *Scale bar,* 500 μm.

Normally, the wild-type mouse dorsal dentate gyrus is V-shaped in the granular cell layer and possesses one crest (Fig. 8), whereas the human counterpart is wavy and has multiple bulges or crests. In light of the peculiar bulge in the *Atat1*$^{-/-}$ dentate gyrus, we exhaustively searched the literature for mutant mouse strains with similar distortion in the dentate gyrus. This search uncovered two early studies showing that mice lacking the Src-related tyrosine kinase Fyn display two similar bulges in the lateral blade of the dentate gyrus (73, 74). Strikingly, one of the bulges is located at a position close to that in the *Atat1*$^{-/-}$ dentate gyrus. Fyn is required for learning and memory (73, 74), but how the two bulges are developed remains to be elucidated.

To gain mechanistic insights into how the bulge in the *Atat1*$^{-/-}$ dentate gyrus is formed, we analyzed the structure at the cellular level. For this, we analyzed the digitized images of Nissl-stained brain sections using the ruler tool of the Spectrum software to measure the size and dimensions of different structures in the hippocampus. This analysis revealed two major differences. First, the space between the two blades was wider in the mutant dentate gyrus, especially in the bulged region (Fig. 8*C*). Of relevance, the peak width of the bulge was 136 μm in the mutant dentate gyrus, as compared with 79 μm in the corresponding region of the wild-type dentate gyrus (Fig. 8*D*). Second, in the bulge, there were more granular cells. According to the ruler tool of the Spectrum software, the diameter of the round granular cell soma remained the same in the mutant (10–12 μm). There were 6–7 layers of tightly packed granular cells in the wild type, whereas there were 11–13 cell layers in the bulge of the mutant dentate gyrus (Fig. 8*D*). Although to a different extent at various sagittal planes (*e.g.* Fig. 8*F*), cell hyperplasia was apparent in the bulge of the mutant dentate gyrus. Therefore, Atat1 deletion caused hyperplasia in a specific region of the dentate gyrus, subsequently leading to bulge formation there.

Colocalization of Atat1 with Doublecortin in Cultured Cells—To gain further mechanistic insights into the overgrowth in the lateral blade of the *Atat1*$^{-/-}$ dentate gyrus, we first asked whether Atat1 plays a role in regulating cell cycle progression. For this, we performed FACS analysis of wild-type and mutant MEFs. The analysis revealed that *Atat1* deletion did not affect cell proliferation (G_0-G_1/S/G_2-M, 51.6:10.1:38.3% and 48.5:11.0:39.9% for *Atat1*$^{+/-}$ and *Atat1*$^{-/-}$ MEFs, respectively). However, when coexpressed in HEK293 cells, human ATAT1 colocalized nicely with nuclear mitotic apparatus antigen in mitotic spindles (data not shown), which is consistent with a recent report that ATAT1 associates with the mitotic spindle in CHO cells (75). Thus, it is still possible that ATAT1 fine-tunes mitotic programs under certain conditions.

From Nissl staining, we noticed a darkly stained cell population in the subgranular zone of the dentate gyrus (Fig. 8, *D* and *F*). This population appeared to be expanded in the bulge of the mutant dentate gyrus (Fig. 8, *D* and *F*). The subgranular zones of mouse and human dentate gyri contain adult neural stem cells (76). These stem cells are positive for doublecortin (DCX), a microtubule-associated protein (77–79). DCX is important for neurogenesis, and its gene is mutated in two genetic disorders, X-linked lissencephaly (smooth brain) and double cortex, both of which are characterized with structural abnormalities in the brain (80, 81). Mechanistically, DCX binds selectively to and stabilizes 13-protofilament microtubules (82). Intriguingly, Mec-17 in *C. elegans* is required for formation of predominantly 15-protofilament microtubules in touch receptor neurons (83, 84). In light of this exciting analogy between human DCX and *C. elegans* Mec-17, we wondered whether human ATAT1 interacts with DCX.

Immunoprecipitation revealed no detectable interaction in soluble protein extracts (data not shown). Because DCX induces microtubule bundling (77, 78), we investigated whether Atat1 associates with DCX in cells. To avoid complication from potential fixation artifacts, live fluorescence microscopy was performed. When expressed alone, GFP-α-tubulin distributed evenly in the cytoplasm, whereas RFP-DCX associated with

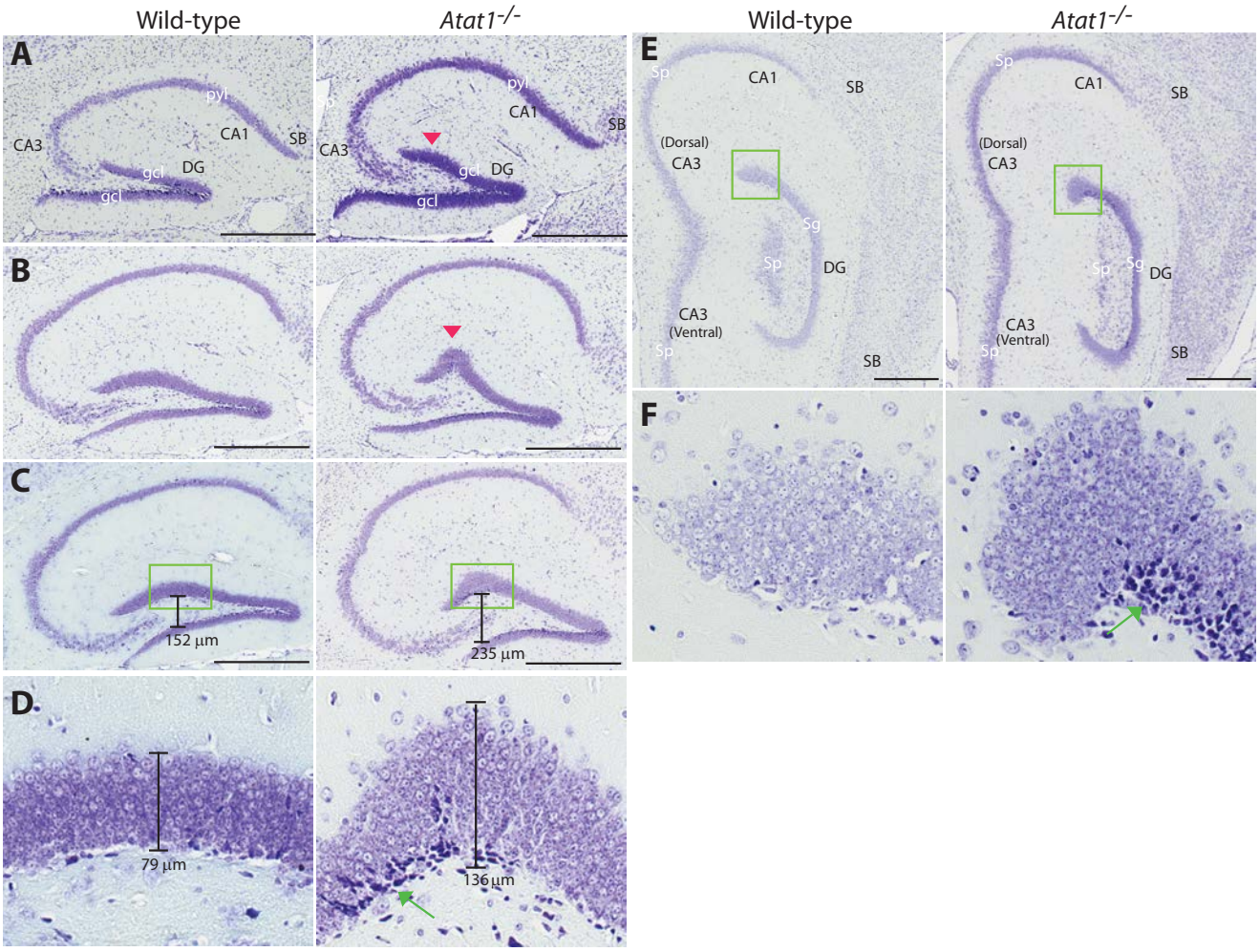

FIGURE 8. **Histological analysis of wild-type and *Atat1*$^{-/-}$ hippocampi.** *A–C* and *E*, representative hippocampal images taken from serial sections on four different sagittal planes in the medial-to-lateral direction. Nissl staining was performed as in Fig. 7, the two sections of which correspond to a sagittal position between those in *A* and *B* shown here. *Red arrowheads* in *A* and *B* mark the bulge in the lateral or suprapyramidal blade of the mutant dentate gyrus. Note that at the sagittal plane corresponding to that shown in Fig. 5*D* (*middle* and *right*), no bulge was found. *D* and *F*, high resolution images of the *boxed areas* in *C* and *E*, respectively. *Green arrows* denote darkly stained cell populations within the subgranular zone of the mutant dentate gyrus. *D*, the peak width of the granular cell layer is shown; the width was measured with the ruler tool of the Spectrum software used to analyze images digitized by the ScanScope. Abbreviations used are as follows: *CA1* and *CA3*, cornu ammonis areas 1 and 3 of the hippocampus, respectively; *DG*, dentate gyrus; *gcl*, granular cell layer of the dentate gyrus; *pyl*, pyramidal layer of CA1 or CA3; *SB*, subiculum. *Scale bar*, 500 μm.

bundled microtubules (Fig. 9*A*, *left* and *middle panels*) (77, 78). As reported (77, 78), when coexpressed, GFP-α-tubulin colocalized with RFP-DCX in bundled microtubules (Fig. 9*B*). When expressed alone, GFP-tagged and mCherry-tagged human ATAT1 proteins were pan-cellular or slightly enriched in the cytoplasm (Fig. 9*A*, *right panel*, and data not shown). Strikingly, when coexpressed, GFP-ATAT1 colocalized with RFP-DCX on bundled microtubules (Fig. 9*C*). Similar colocalization was also found between mCherry-ATAT1 and GFP-DCX (data not shown). These results suggest a potential mechanism through which ATAT1 associates with DCX and regulates neuronal properties *in vivo*.

DISCUSSION

Mouse Atat1 Is the Predominant α-Tubulin Acetyltransferase in Vivo—In this study, we have taken a genetic approach and demonstrated that *Atat1*$^{-/-}$ mice exhibited dramatic loss of α-tubulin acetylation in a majority of adult tissues, including the testis, kidney, liver, and brain, as well as in embryonic fibroblasts (Fig. 2 and data not shown). In the mutant lung, there was only a minimal level of α-tubulin acetylation (<5%; Fig. 2*A*, *lanes 7* and *8*). Thus, although they acetylate α-tubulin acetylation *in vitro*, the acetyltransferases ARD1-NAT1 (53), ELP3 (43, 54), and GCN5 (55) may not contribute significantly to α-tubulin acetylation in these tissues and cells *in vivo*. However, the acetylation was not so much affected in the spleen and fat of *Atat1*$^{-/-}$ mice (Fig. 2*A*). There was a residual level of α-tubulin acetylation in the lung (Fig. 2). ARD1-NAT1 (53), ELP3 (43, 54), and GCN5 (55) may be responsible for the retained acetylation in these organs of the mutant mice.

This is the first knock-out analysis of mouse *Atat1* and provides direct evidence that Atat1 is the predominant α-tubulin acetyltransferase in mouse embryos and different adult organs. By RNAi, it has been shown that Atat1 contributes significantly to α-tubulin acetylation in HeLa and immortalized retinal pigment epithelial cells (32, 57). Our knock-out analysis provides unequivocal genetic support for the knockdown studies based on cultured cells. This knock-out analysis also yields the first

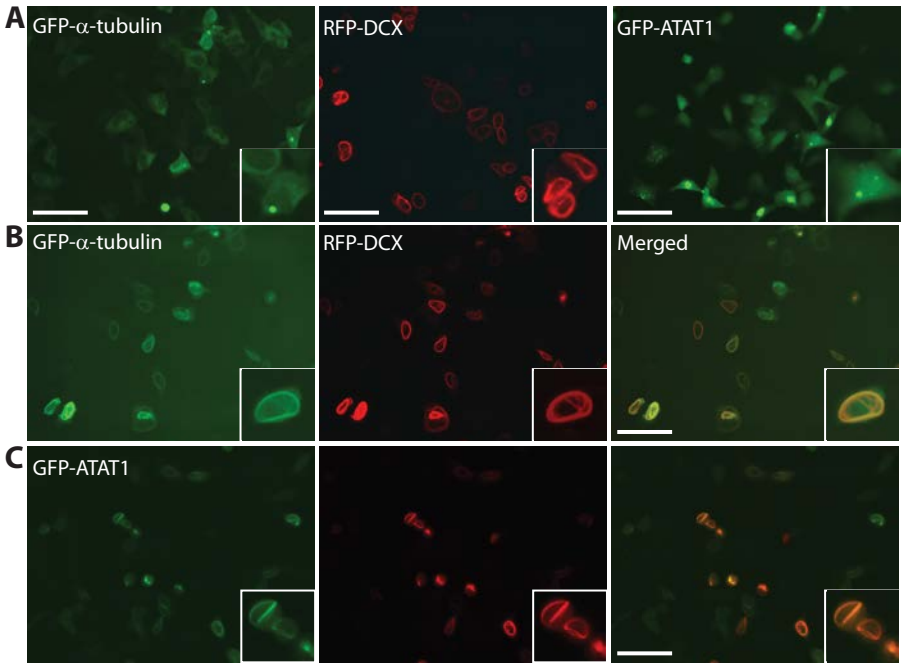

FIGURE 9. **Human ATAT1 colocalizes with doublecortin-bundled microtubules.** *A*, HEK293 cells were transfected with an expression plasmid for GFP-α-tubulin, RFP-DCX, or GFP-ATAT1 for live *green* or *red* fluorescence microscopy. *B*, HEK293 cells were cotransfected with the expression plasmids for GFP-α-tubulin and RFP-DCX for live *green* and *red* fluorescence microscopy. Cross-talk between different channels was none or minimal (data not shown). *C*, same as *B* except that GFP-ATAT1 was expressed instead of GFP-α-tubulin. Similar results were obtained with mCherry-ATAT1 and GFP-DCX, although mCherry-ATAT1 was more enriched in the cytoplasm than GFP-ATAT1 (data not shown). *Scale bar,* 40 μm.

unexpected picture about the functional impact of mouse *Atat1* deletion at the organismal level.

Roles of Atat1 in Regulating Advanced Functions of the Brain, Testis, and Other Organs—Surprisingly, *Atat1*$^{-/-}$ mice exhibited no overt phenotypes: viable, fertile, and healthy as their wild-type littermates (Fig. 1*A* and data not shown). The viability and fertility of mutant mice are really unexpected in light of the reported importance of Atat1 in zebrafish development and mammalian cilium assembly (32, 57). The primary cilium is a unique organelle important for cellular signaling and animal development (61). However, our results are consistent with the findings that Atat1 homologs play nonessential roles in *Tetrahymena* and *C. elegans* (32, 57). Related to this, Lys-40 is not required for survival of *Chlamydomonas*, *Tetrahymena,* and *C. elegans* (39–41), and arginine substitution exerts little effect on the function of a plant α-tubulin (42). Our results are also in agreement with the report that *Hdac6*-null mice are viable and develop rather normally (48). Our findings indicate that mouse Atat1 is not required for animal survival, thereby shedding light on functions of α-tubulin acetylation *in vivo*.

Expression analysis using the knock-in *lacZ* reporter revealed high expression of Atat1 in the brain, testis, and gastrointestinal tract (Fig. 4). The high expression in the brain is consistent with the highest level of α-tubulin acetylation in this organ (Fig. 2*A*). In line with our results, recent *in situ* hybridization studies revealed high and dynamic expression of Atat1 in the mouse and rat brains (44, 75). Based on the high Atat1 expression in the mouse brain, testis, and gastrointestinal tract, it is tempting to speculate that Atat1 and perhaps α-tubulin acetylation may fine-tune microtubule-dependent processes in the brain, testis, and gastrointestinal tract. Because of dramatic loss of α-tubulin acetylation (Fig. 2 and data not shown) and the presence of the knock-in *lacZ* reporter (Fig. 1*A*), *Atat1*$^{-/-}$ mice are invaluable for investigating whether this is indeed the case.

To detect subtle changes in the organs where Atat1 is highly expressed, we performed histological analyses, which revealed that Atat1 was highly and specifically expressed in the cerebral cortex and the hippocampus (Fig. 5, *B* and *D*). Related to the hippocampus, the mutant dentate gyrus was deformed, displaying a bulge in the lateral blade of granular cell layers (Figs. 7 and 8). Of relevance, the dorsal dentate gyrus of the wild-type mouse is normally V-shaped in the granular cell layer and possesses one crest (Fig. 8) (71, 72), whereas the human counterpart is wavy and has multiple bulges or crests. In terms of morphology, the bulged dentate gyrus in the mutant mouse is more similar to the rat dentate gyrus. Intriguingly, mice lacking the Src-related tyrosine kinase Fyn display two similar bulges in the lateral blade of the dentate gyrus, with one of them located at a position close to that in the *Atat1*$^{-/-}$ dentate gyrus (73, 74). How the bulges are developed in the *Fyn*$^{-/-}$ dentate gyrus remains to be determined. Analysis of the *Atat1*$^{-/-}$ dentate gyrus revealed that *Atat1* deletion caused cell hyperplasia in the specific region of the dentate gyrus, subsequently leading to bulge formation (Fig. 8, *D* and *F*). Although no morphologic differences have been found in other regions of the hippocampus and within the cerebral cortex, it will be important to carry out more thorough and systematic analyses by using different molecular markers. This is particularly important in light of recent studies showing that α-tubulin acetylation and Atat1 regulate neuronal migration (43, 44). The hippocampus is crucial for learning and memory, so it will be exciting to analyze

Atat1$^{-/-}$ mice by various behavioral tests, such as navigation in the Morris water maze, to gain insights into how advanced functions like learning and memory are affected by *Atat1* deletion.

Lateral ventricles of the mutant brain seemed to be dilated (Fig. 7), so it will be important to systematically analyze this dilation, which may be related to potential ciliary defects (32, 57). Of relevance, a survey of 50 genomes of evolutionarily diverse organisms revealed that the presence of Mec-17 orthologs correlates perfectly with the possession of cilia or flagella (32), suggesting the importance of such proteins in cilia or flagella. This is also related to defective α-tubulin acetylation on *Atat1*$^{-/-}$ sperm flagella (see Fig. 6 and below).

In the mouse testis, Atat1 expression was detected in the internal cell layers of seminiferous tubules (Fig. 5). Indirect immunofluorescence microscopy revealed high α-tubulin acetylation at the luminal centers of the wild-type but not mutant seminiferous tubules (Fig. 6, *A* and *B*). Related to this, Western blotting (Fig. 2) identified Atat1 as the sole α-tubulin acetyltransferase in the testis. The luminal centers of seminiferous tubules are devoid of nuclei but contain sperm flagella. Thus, Atat1 is required for α-tubulin acetylation of sperm flagella. As for the functional impact, it will be necessary to systematically analyze sperm development and maturation. Even though the mutant male mice are fertile, it is still possible that they have subtle defects. It is noteworthy that the lumens of seminiferous tubules appeared to be dilated when compared with the wild-type counterparts (Fig. 6*C*), so it will be important to carry out systematic analysis to verify this.

In addition to the brain and testis, it will be important to systematically analyze other organs where cilia and related structures are important. The oldest *Atat1*$^{-/-}$ mutant mice that we have examined are about 18 months old, so it still remains possible that Atat1 has important roles at later stages of life. Moreover, Atat1 may play a role under special conditions. Treatment for spinal cord injury depends on axon regeneration and appropriate synapse formation. Several reports implicate microtubule stabilization in facilitating axon regeneration (85, 86). Our results showed that Atat1 is the sole α-tubulin acetyltransferase in the brain (Fig. 2) and is highly expressed in the spinal cord (Fig. 4*K*). It has been recently reported that Atat1 and α-tubulin acetylation regulate microtubule structure in *C. elegans* (83, 84). Thus, it will be important to investigate how Atat1 may play a role in axon regeneration. Furthermore, α-tubulin acetylation decreases in response to intestinal inflammation induced by the bacterium *Clostridium difficile*, suggesting a need to investigate how Atat1 and α-tubulin acetylation may be involved in this and related pathogenic conditions (87).

Regulation of Microtubule Architecture and Function by Atat1—α-Tubulin acetylation at Lys-40 has been used as a routine marker for stable microtubules in cilia, flagella, axons, midbodies, and other subcellular structures (23, 24, 29). It still remains debatable whether the acetylation is causal in microtubule stabilization (30–33). The acetylation has also been linked to microtubule-mediated transport of proteins and organelles (31, 34–38), but it is mysterious how a luminal modification affects transport processes that occur on the external surface of microtubules (29). Further analysis of cell and tissues from *Atat1*$^{-/-}$ mice will shed light on the precise role of α-tubulin acetylation in these processes.

In *C. elegans*, Mec-17 was recently discovered to be important for maintaining unique microtubule architecture (83, 84). In this organism, the touch receptor neurons have mainly 15-protofilament microtubules, whereas the other cells possess 11-protofilament microtubules (84). In the touch receptor neurons lacking *Mec-17*, there are fewer and shorter microtubules, containing 11–15 protofilaments as compared with the predominantly 15 protofilaments in microtubules from the wild type (83, 84). Mec-17 increases cohesion between tubulin subunits in the microtubule lattice and constrains the protofilament number by acetylating Lys-40 of α-tubulin. This modification promotes formation of inter-protofilament salt bridges, which then stabilize lateral interactions between protofilaments and constrain quinary structure to produce stable and structurally uniform 15-protofilament microtubules in the wild-type touch receptor neurons (83).

An important question is how to translate these intriguing findings to microtubules in mammals. It will be interesting to investigate how the microtubule architecture is affected in tissues and cells from *Atat1*$^{-/-}$ mice. Notably, different from *C. elegans*, most microtubules in other organisms (including mammals) have 13 protofilaments (84); to compensate for this difference, Atat1 in other organisms may need to have roles distinct from that of Mec-17 in *C. elegans*. Of relevance, the mammalian neural stem cell marker DCX binds selectively to and stabilizes 13-protofilament microtubules (82). Importantly, when coexpressed, DCX colocalized with ATAT1 in bundled microtubules (Fig. 9), suggesting that these two proteins may cooperate with each other in regulating microtubule structure and function. One exception to the general 13-protofilament rule is that like touch receptor neurons in *C. elegans*, mammalian pillar cells also have 15-protofilament microtubules (84). It will be particularly interesting to analyze how the microtubule architecture is affected in such cells from *Atat1*$^{-/-}$ mice. Thus, these mice should be useful for analyzing microtubule structure, function, and regulation in various cells and tissues *in vivo*.

Conclusion—The genetic and molecular analyses presented herein provide direct evidence that Atat1 is the predominant α-tubulin acetyltransferase in mouse embryos and tissues. This is the first demonstration that mammalian Atat1 acts as a *bona fide* α-tubulin acetyltransferase *in vivo*. The viability and grossly normal development of *Atat1*$^{-/-}$ embryos and mice indicate that Atat1 is not essential for basic functions such as animal survival and development, but it may be important for more advanced functions, including learning and memory. It is highly expressed in the brain, testis, renal pelvis, and gastrointestinal tract, so further studies should focus on how mammalian Atat1 fine-tunes advanced functions in the organs under various physiological and pathological conditions. The mutant mice should also be valuable for studying how mammalian α-tubulin acetylation regulates microtubule structure and function *in vivo*.

REFERENCES

1. Kouzarides, T. (2000) Acetylation: a regulatory modification to rival phosphorylation? *EMBO J.* **19,** 1176–1179
2. Yang, X. J., and Seto, E. (2008) Lysine acetylation: codified crosstalk with other posttranslational modifications. *Mol. Cell* **31,** 449–461
3. Beltrao, P., Albanèse, V., Kenner, L. R., Swaney, D. L., Burlingame, A., Villén, J., Lim, W. A., Fraser, J. S., Frydman, J., and Krogan, N. J. (2012) Systematic functional prioritization of protein posttranslational modifications. *Cell* **150,** 413–425
4. Allfrey, V., Faulkner, R. M., and Mirsky, A. E. (1964) Acetylation and methylation of histones and their possible role in the regulation of RNA synthesis. *Proc. Natl. Acad. Sci. U.S.A.* **51,** 786–794
5. Strahl, B. D., and Allis, C. D. (2000) The language of covalent histone modifications. *Nature* **403,** 41–45
6. Kouzarides, T. (2007) Chromatin modifications and their function. *Cell* **128,** 693–705
7. Berger, S. L. (2007) The complex language of chromatin regulation during transcription. *Nature* **447,** 407–412
8. Latham, J. A., and Dent, S. Y. (2007) Cross-regulation of histone modifications. *Nat. Struct. Mol. Biol.* **14,** 1017–1024
9. Kim, S. C., Sprung, R., Chen, Y., Xu, Y., Ball, H., Pei, J., Cheng, T., Kho, Y., Xiao, H., Xiao, L., Grishin, N. V., White, M., Yang, X. J., and Zhao, Y. (2006) Substrate and functional diversity of lysine acetylation revealed by a proteomics survey. *Mol. Cell* **23,** 607–618
10. Choudhary, C., Kumar, C., Gnad, F., Nielsen, M. L., Rehman, M., Walther, T. C., Olsen, J. V., and Mann, M. (2009) Lysine acetylation targets protein complexes and co-regulates major cellular functions. *Science* **325,** 834–840
11. Zhao, S., Xu, W., Jiang, W., Yu, W., Lin, Y., Zhang, T., Yao, J., Zhou, L., Zeng, Y., Li, H., Li, Y., Shi, J., An, W., Hancock, S. M., He, F., Qin, L., Chin, J., Yang, P., Chen, X., Lei, Q., Xiong, Y., and Guan, K. L. (2010) Regulation of cellular metabolism by protein lysine acetylation. *Science* **327,** 1000–1004
12. Kaluarachchi Duffy, S., Friesen, H., Baryshnikova, A., Lambert, J. P., Chong, Y. T., Figeys, D., and Andrews, B. (2012) Exploring the yeast acetylome using functional genomics. *Cell* **149,** 936–948
13. Zhang, J., Sprung, R., Pei, J., Tan, X., Kim, S., Zhu, H., Liu, C. F., Grishin, N. V., and Zhao, Y. (2009) Lysine acetylation is a highly abundant and evolutionarily conserved modification in *Escherichia coli*. *Mol. Cell. Proteomics* **8,** 215–225
14. Wang, Q., Zhang, Y., Yang, C., Xiong, H., Lin, Y., Yao, J., Li, H., Xie, L., Zhao, W., Yao, Y., Ning, Z. B., Zeng, R., Xiong, Y., Guan, K. L., Zhao, S., and Zhao, G. P. (2010) Acetylation of metabolic enzymes coordinates carbon source utilization and metabolic flux. *Science* **327,** 1004–1007
15. Yang, X. J., and Seto, E. (2007) HATs and HDACs: from structure, function, and regulation to novel strategies for therapy and prevention. *Oncogene* **26,** 5310–5318
16. Allis, C. D., Berger, S. L., Cote, J., Dent, S., Jenuwien, T., Kouzarides, T., Pillus, L., Reinberg, D., Shi, Y., Shiekhattar, R., Shilatifard, A., Workman, J., and Zhang, Y. (2007) New nomenclature for chromatin-modifying enzymes. *Cell* **131,** 633–636
17. Lee, K. K., and Workman, J. L. (2007) Histone acetyltransferase complexes: one size doesn't fit all. *Nat. Rev. Mol. Cell Biol.* **8,** 284–295
18. Khochbin, S., Verdel, A., Lemercier, C., and Seigneurin-Berny, D. (2001) Functional significance of histone deacetylase diversity. *Curr. Opin. Genet. Dev.* **11,** 162–166
19. Grozinger, C. M., and Schreiber, S. L. (2002) Deacetylase enzymes: biological functions and the use of small-molecule inhibitors. *Chem. Biol.* **9,** 3–16
20. Verdin, E., Dequiedt, F., and Kasler, H. G. (2003) Class II histone deacetylases: versatile regulators. *Trends Genet.* **19,** 286–293
21. Yang, X. J., and Seto, E. (2008) The Rpd3/Hda1 family of lysine deacetylases: from bacteria and yeast to mice and men. *Nat. Rev. Mol. Cell Biol.* **9,** 206–218
22. Haberland, M., Montgomery, R. L., and Olson, E. N. (2009) The many roles of histone deacetylases in development and physiology: implications for disease and therapy. *Nat. Rev. Genet.* **10,** 32–42
23. Westermann, S., and Weber, K. (2003) Post-translational modifications regulate microtubule function. *Nat. Rev. Mol. Cell Biol.* **4,** 938–947
24. Janke, C., and Bulinski, J. C. (2011) Post-translational regulation of the microtubule cytoskeleton: mechanisms and functions. *Nat. Rev. Mol. Cell Biol.* **12,** 773–786
25. L'Hernault, S. W., and Rosenbaum, J. L. (1985) *Chlamydomonas* α-tubulin is posttranslationally modified by acetylation on the ϵ-amino group of a lysine. *Biochemistry* **24,** 473–478
26. Piperno, G., and Fuller, M. T. (1985) Monoclonal antibodies specific for an acetylated form of α-tubulin recognize the antigen in cilia and flagella from a variety of organisms. *J. Cell Biol.* **101,** 2085–2094
27. Piperno, G., LeDizet, M., and Chang, X. J. (1987) Microtubules containing acetylated α-tubulin in mammalian cells in culture. *J. Cell Biol.* **104,** 289–302
28. LeDizet, M., and Piperno, G. (1987) Identification of an acetylation site of *Chlamydomonas* α-tubulin. *Proc. Natl. Acad. Sci. U.S.A.* **84,** 5720–5724
29. Soppina, V., Herbstman, J. F., Skiniotis, G., and Verhey, K. J. (2012) Luminal localization of α-tubulin K40 acetylation by cryo-EM analysis of Fab-labeled microtubules. *PLoS One* **7,** e48204
30. Palazzo, A., Ackerman, B., and Gundersen, G. G. (2003) Cell biology: tubulin acetylation and cell motility. *Nature* **421,** 230
31. Zilberman, Y., Ballestrem, C., Carramusa, L., Mazitschek, R., Khochbin, S., and Bershadsky, A. (2009) Regulation of microtubule dynamics by inhibition of the tubulin deacetylase HDAC6. *J. Cell Sci.* **122,** 3531–3541
32. Shida, T., Cueva, J. G., Xu, Z., Goodman, M. B., and Nachury, M. V. (2010) The major α-tubulin K40 acetyltransferase αTAT1 promotes rapid ciliogenesis and efficient mechanosensation. *Proc. Natl. Acad. Sci. U.S.A.* **107,** 21517–21522
33. Sudo, H., and Baas, P. W. (2010) Acetylation of microtubules influences their sensitivity to severing by katanin in neurons and fibroblasts. *J. Neurosci.* **30,** 7215–7226
34. Reed, N. A., Cai, D., Blasius, T. L., Jih, G. T., Meyhofer, E., Gaertig, J., and Verhey, K. J. (2006) Microtubule acetylation promotes kinesin-1 binding and transport. *Curr. Biol.* **16,** 2166–2172
35. Dompierre, J. P., Godin, J. D., Charrin, B. C., Cordelières, F. P., King, S. J., Humbert, S., and Saudou, F. (2007) Histone deacetylase 6 inhibition compensates for the transport deficit in Huntington's disease by increasing tubulin acetylation. *J. Neurosci.* **27,** 3571–3583
36. Witte, H., Neukirchen, D., and Bradke, F. (2008) Microtubule stabilization specifies initial neuronal polarization. *J. Cell Biol.* **180,** 619–632
37. Friedman, J. R., Webster, B. M., Mastronarde, D. N., Verhey, K. J., and Voeltz, G. K. (2010) ER sliding dynamics and ER-mitochondrial contacts occur on acetylated microtubules. *J. Cell Biol.* **190,** 363–375
38. Hammond, J. W., Huang, C. F., Kaech, S., Jacobson, C., Banker, G., and Verhey, K. J. (2010) Posttranslational modifications of tubulin and the polarized transport of kinesin-1 in neurons. *Mol. Biol. Cell* **21,** 572–583
39. Gaertig, J., Cruz, M. A., Bowen, J., Gu, L., Pennock, D. G., and Gorovsky, M. A. (1995) Acetylation of lysine 40 in α-tubulin is not essential in *Tetrahymena thermophila*. *J. Cell Biol.* **129,** 1301–1310
40. Kozminski, K. G., Diener, D. R., and Rosenbaum, J. L. (1993) High level expression of nonacetylatable α-tubulin in *Chlamydomonas reinhardtii*. *Cell Motil. Cytoskeleton* **25,** 158–170
41. Fukushige, T., Siddiqui, Z. K., Chou, M., Culotti, J. G., Gogonea, C. B., Siddiqui, S. S., and Hamelin, M. (1999) MEC-12, an α-tubulin required for touch sensitivity in *C. elegans*. *J. Cell Sci.* **112,** 395–403
42. Xiong, X., Xu, D., Yang, Z., Huang, H., and Cui, X. (2013) A single amino-acid substitution at lysine 40 of an *Arabidopsis thaliana* α-tubulin causes extensive cell proliferation and expansion defects. *J. Integr. Plant Biol.* **55,** 209–220
43. Creppe, C., Malinouskaya, L., Volvert, M. L., Gillard, M., Close, P., Malaise, O., Laguesse, S., Cornez, I., Rahmouni, S., Ormenese, S., Belachew, S., Malgrange, B., Chapelle, J. P., Siebenlist, U., Moonen, G., Chariot, A., and Nguyen, L. (2009) Elongator controls the migration and differentiation of cortical neurons through acetylation of α-tubulin. *Cell* **136,** 551–564
44. Li, L., Wei, D., Wang, Q., Pan, J., Liu, R., Zhang, X., and Bao, L. (2012) MEC-17 deficiency leads to reduced α-tubulin acetylation and impaired migration of cortical neurons. *J. Neurosci.* **32,** 12673–12683
45. Hubbert, C., Guardiola, A., Shao, R., Kawaguchi, Y., Ito, A., Nixon, A.,

Yoshida, M., Wang, X. F., and Yao, T. P. (2002) HDAC6 is a microtubule-associated deacetylase. *Nature* **417,** 455–458
46. Matsuyama, A., Shimazu, T., Sumida, Y., Saito, A., Yoshimatsu, Y., Seigneurin-Berny, D., Osada, H., Komatsu, Y., Nishino, N., Khochbin, S., Horinouchi, S., and Yoshida, M. (2002) *In vivo* destabilization of dynamic microtubules by HDAC6-mediated deacetylation. *EMBO J.* **21,** 6820–6831
47. Zhang, Y., Li, N., Caron, C., Matthias, G., Hess, D., Khochbin, S., and Matthias, P. (2003) HDAC-6 interacts with and deacetylates tubulin and microtubules *in vivo*. *EMBO J.* **22,** 1168–1179
48. Zhang, Y., Kwon, S., Yamaguchi, T., Cubizolles, F., Rousseaux, S., Kneissel, M., Cao, C., Li, N., Cheng, H. L., Chua, K., Lombard, D., Mizeracki, A., Matthias, G., Alt, F. W., Khochbin, S., and Matthias, P. (2008) Mice lacking histone deacetylase 6 have hyperacetylated tubulin but are viable and develop normally. *Mol. Cell. Biol.* **28,** 1688–1701
49. North, B. J., Marshall, B. L., Borra, M. T., Denu, J. M., and Verdin, E. (2003) The human Sir2 ortholog, SIRT2, is an NAD^+-dependent tubulin deacetylase. *Mol. Cell* **11,** 437–444
50. Bobrowska, A., Donmez, G., Weiss, A., Guarente, L., and Bates, G. (2012) SIRT2 ablation has no effect on tubulin acetylation in brain, cholesterol biosynthesis, or the progression of Huntington's disease phenotypes *in vivo*. *PLoS One* **7,** e34805
51. Fukada, M., Hanai, A., Nakayama, A., Suzuki, T., Miyata, N., Rodriguiz, R. M., Wetsel, W. C., Yao, T. P., and Kawaguchi, Y. (2012) Loss of deacetylation activity of Hdac6 affects emotional behavior in mice. *PLoS One* **7,** e30924
52. Sadoul, K., Wang, J., Diagouraga, B., Vitte, A. L., Buchou, T., Rossini, T., Polack, B., Xi, X., Matthias, P., and Khochbin, S. (2012) HDAC6 controls the kinetics of platelet activation. *Blood* **120,** 4215–4218
53. Ohkawa, N., Sugisaki, S., Tokunaga, E., Fujitani, K., Hayasaka, T., Setou, M., and Inokuchi, K. (2008) *N*-Acetyltransferase ARD1-NAT1 regulates neuronal dendritic development. *Genes Cells* **13,** 1171–1183
54. Solinger, J. A., Paolinelli, R., Klöss, H., Scorza, F. B., Marchesi, S., Sauder, U., Mitsushima, D., Capuani, F., Stürzenbaum, S. R., and Cassata, G. (2010) The *Caenorhabditis elegans* elongator complex regulates neuronal α-tubulin acetylation. *PLoS Genet* **6,** e1000820
55. Conacci-Sorrell, M., Ngouenet, C., and Eisenman, R. N. (2010) Myc-nick: a cytoplasmic cleavage product of Myc that promotes α-tubulin acetylation and cell differentiation. *Cell* **142,** 480–493
56. Steczkiewicz, K., Kinch, L., Grishin, N. V., Rychlewski, L., and Ginalski, K. (2006) Eukaryotic domain of unknown function DUF738 belongs to Gcn5-related *N*-acetyltransferase superfamily. *Cell Cycle* **5,** 2927–2930
57. Akella, J. S., Wloga, D., Kim, J., Starostina, N. G., Lyons-Abbott, S., Morrissette, N. S., Dougan, S. T., Kipreos, E. T., and Gaertig, J. (2010) MEC-17 is an α-tubulin acetyltransferase. *Nature* **467,** 218–222
58. Kormendi, V., Szyk, A., Piszczek, G., and Roll-Mecak, A. (2012) Crystal structures of tubulin acetyltransferase reveal a conserved catalytic core and the plasticity of the essential N terminus. *J. Biol. Chem.* **287,** 41569–41575
59. Taschner, M., Vetter, M., and Lorentzen, E. (2012) Atomic resolution structure of human α-tubulin acetyltransferase bound to acetyl-CoA. *Proc. Natl. Acad. Sci. U.S.A.* **109,** 19649–19654
60. Friedmann, D. R., Aguilar, A., Fan, J., Nachury, M. V., and Marmorstein, R. (2012) Structure of the α-tubulin acetyltransferase, αTAT1, and implications for tubulin-specific acetylation. *Proc. Natl. Acad. Sci. U.S.A.* **109,** 19655–19660
61. Goetz, S. C., and Anderson, K. V. (2010) The primary cilium: a signalling centre during vertebrate development. *Nat. Rev. Genet.* **11,** 331–344
62. Nagy, A., Gertsenstein, M., Vintersten, K., and Behringer, R. (2003) *Manipulating the Mouse Embryo*, 3rd Ed., Cold Spring Harbor Laboratory Press, Cold Spring Harbor, NY
63. Walkinshaw, D. R., Weist, R., Xiao, L., Yan, K., Kim, G. W., and Yang, X. J. (2013) Dephosphorylation at a conserved SP motif governs cAMP sensitivity and nuclear localization of class IIa histone deacetylases. *J. Biol. Chem.* **288,** 5591–5605
64. Takahashi, K., Okita, K., Nakagawa, M., and Yamanaka, S. (2007) Induction of pluripotent stem cells from fibroblast cultures. *Nat. Protoc.* **2,** 3081–3089
65. Tahmasebi, S., Ghorbani, M., Savage, P., Yan, K., Gocevski, G., Xiao, L., You, L., and Yang, X. J. (2013) Sumoylation of Kruppel-like factor 4 inhibits its pluripotency induction but promotes adipocyte differentiation. *J. Biol. Chem.* **288,** 12791–12804
66. Walkinshaw, D. R., Weist, R., Kim, G. W., You, L., Xiao, L., Nie, J., Li, C. S., Zhao, S., Xu, M., and Yang, X. J. (2013) The tumor suppressor kinase LKB1 activates the downstream kinases SIK2 and SIK3 to stimulate nuclear export of class IIa histone deacetylases. *J. Biol. Chem.* **288,** 9345–9362
67. LeDizet, M., and Piperno, G. (1986) Cytoplasmic microtubules containing acetylated α-tubulin in *Chlamydomonas reinhardtii*: spatial arrangement and properties. *J. Cell Biol.* **103,** 13–22
68. Baas, P. W., and Black, M. M. (1990) Individual microtubules in the axon consist of domains that differ in both composition and stability. *J. Cell Biol.* **111,** 495–509
69. Smith, C. L. (1994) The initiation of neurite outgrowth by sympathetic neurons grown *in vitro* does not depend on assembly of microtubules. *J. Cell Biol.* **127,** 1407–1418
70. Fukushima, N., Furuta, D., Hidaka, Y., Moriyama, R., and Tsujiuchi, T. (2009) Post-translational modifications of tubulin in the nervous system. *J. Neurochem.* **109,** 683–693
71. Dong, H. W. (2008) *Allen Reference Atlas, A Digital Brain Atlas of the C57BL/6J Male Mouse*, John Wiley & Sons, Inc, Hoboken, NJ
72. Paxinos, G., and Franklin, K. B. (2008) *The Mouse Brain in Stereotaxic Coordinates*, 3rd Ed., Academic Press, New York
73. Grant, S. G., O'Dell, T. J., Karl, K. A., Stein, P. L., Soriano, P., and Kandel, E. R. (1992) Impaired long-term potentiation, spatial learning, and hippocampal development in fyn mutant mice. *Science* **258,** 1903–1910
74. Kojima, N., Wang, J., Mansuy, I. M., Grant, S. G., Mayford, M., and Kandel, E. R. (1997) Rescuing impairment of long-term potentiation in fyn-deficient mice by introducing Fyn transgene. *Proc. Natl. Acad. Sci. U.S.A.* **94,** 4761–4765
75. Kalebic, N., Martinez, C., Perlas, E., Hublitz, P., Bilbao-Cortes, D., Fiedorczuk, K., Andolfo, A., and Heppenstall, P. A. (2013) The tubulin acetyltransferase αTAT1 destabilizes microtubules independently of its acetylation activity. *Mol. Cell. Biol.* **33,** 1114–1123
76. Zhao, C., Deng, W., and Gage, F. H. (2008) Mechanisms and functional implications of adult neurogenesis. *Cell* **132,** 645–660
77. Francis, F., Koulakoff, A., Boucher, D., Chafey, P., Schaar, B., Vinet, M. C., Friocourt, G., McDonnell, N., Reiner, O., Kahn, A., McConnell, S. K., Berwald-Netter, Y., Denoulet, P., and Chelly, J. (1999) Doublecortin is a developmentally regulated, microtubule-associated protein expressed in migrating and differentiating neurons. *Neuron* **23,** 247–256
78. Gleeson, J. G., Lin, P. T., Flanagan, L. A., and Walsh, C. A. (1999) Doublecortin is a microtubule-associated protein and is expressed widely by migrating neurons. *Neuron* **23,** 257–271
79. Magavi, S. S., Leavitt, B. R., and Macklis, J. D. (2000) Induction of neurogenesis in the neocortex of adult mice. *Nature* **405,** 951–955
80. des Portes, V., Pinard, J. M., Billuart, P., Vinet, M. C., Koulakoff, A., Carrié, A., Gelot, A., Dupuis, E., Motte, J., Berwald-Netter, Y., Catala, M., Kahn, A., Beldjord, C., and Chelly, J. (1998) A novel CNS gene required for neuronal migration and involved in X-linked subcortical laminar heterotopia and lissencephaly syndrome. *Cell* **92,** 51–61
81. Gleeson, J. G., Allen, K. M., Fox, J. W., Lamperti, E. D., Berkovic, S., Scheffer, I., Cooper, E. C., Dobyns, W. B., Minnerath, S. R., Ross, M. E., and Walsh, C. A. (1998) Doublecortin, a brain-specific gene mutated in human X-linked lissencephaly and double cortex syndrome, encodes a putative signaling protein. *Cell* **92,** 63–72
82. Moores, C. A., Perderiset, M., Francis, F., Chelly, J., Houdusse, A., and Milligan, R. A. (2004) Mechanism of microtubule stabilization by doublecortin. *Mol. Cell* **14,** 833–839
83. Cueva, J. G., Hsin, J., Huang, K. C., and Goodman, M. B. (2012) Posttranslational acetylation of α-tubulin constrains protofilament number in native microtubules. *Curr. Biol.* **22,** 1066–1074
84. Topalidou, I., Keller, C., Kalebic, N., Nguyen, K. C., Somhegyi, H., Politi, K. A., Heppenstall, P., Hall, D. H., and Chalfie, M. (2012) Genetically separable functions of the MEC-17 tubulin acetyltransferase affect microtubule organization. *Curr. Biol.* **22,** 1057–1065
85. Hellal, F., Hurtado, A., Ruschel, J., Flynn, K. C., Laskowski, C. J., Um-

lauf, M., Kapitein, L. C., Strikis, D., Lemmon, V., Bixby, J., Hoogenraad, C. C., and Bradke, F. (2011) Microtubule stabilization reduces scarring and causes axon regeneration after spinal cord injury. *Science* **331,** 928–931

86. Sengottuvel, V., and Fischer, D. (2011) Facilitating axon regeneration in the injured CNS by microtubules stabilization. *Commun. Integr. Biol.* **4,** 391–393
87. Nam, H. J., Kang, J. K., Kim, S. K., Ahn, K. J., Seok, H., Park, S. J., Chang, J. S., Pothoulakis, C., Lamont, J. T., and Kim, H. (2010) Clostridium difficile toxin A decreases acetylation of tubulin, leading to microtubule depolymerization through activation of histone deacetylase 6, and this mediates acute inflammation. *J. Biol. Chem.* **285,** 32888–32896

BRPF1 is essential for development of fetal hematopoietic stem cells

Linya You,[1,2] Lin Li,[1,2] Jinfeng Zou,[3] Kezhi Yan,[1,2] Jad Belle,[4] Anastasia Nijnik,[4] Edwin Wang,[3] and Xiang-Jiao Yang[1,2,5,6]

[1]Rosalind and Morris Goodman Cancer Research Center and [2]Department of Medicine, McGill University, Montreal, Quebec, Canada. [3]National Research Council Canada, Montreal, Quebec, Canada. [4]Department of Physiology and [5]Department of Biochemistry, McGill University, Montreal, Quebec, Canada. [6]McGill University Health Center, Montreal, Quebec, Canada.

Hematopoietic stem cells (HSCs) serve as a life-long reservoir for all blood cell types and are clinically useful for a variety of HSC transplantation-based therapies. Understanding the role of chromatin organization and regulation in HSC homeostasis may provide important insights into HSC development. Bromodomain- and PHD finger–containing protein 1 (BRPF1) is a multivalent chromatin regulator that possesses 4 nucleosome-binding domains and activates 3 lysine acetyltransferases (KAT6A, KAT6B, and KAT7), suggesting that this protein has the potential to stimulate crosstalk between different chromatin modifications. Here, we investigated the function of BRPF1 in hematopoiesis by selectively deleting its gene in murine blood cells. *Brpf1*-deficient pups experienced early lethality due to acute bone marrow failure and aplastic anemia. The mutant bone marrow and fetal liver exhibited severe deficiency in HSCs and hematopoietic progenitors, along with elevated reactive oxygen species, senescence, and apoptosis. BRPF1 deficiency also reduced the expression of multipotency genes, including *Slamf1*, *Mecom*, *Hoxa9*, *Hlf*, *Gfi1*, *Egr*, and *Gata3*. Furthermore, BRPF1 was required for acetylation of histone H3 at lysine 23, a highly abundant but not well-characterized epigenetic mark. These results identify an essential role of the multivalent chromatin regulator BRPF1 in definitive hematopoiesis and illuminate a potentially new avenue for studying epigenetic networks that govern HSC ontogeny.

Introduction

Hematopoietic stem cells (HSCs) lie at the hierarchical apex of definitive hematopoiesis and form a life-long reservoir for all blood cell types in vertebrates (1–4). These stem cells regulate development (5, 6) and undergo important changes during aging (7). Upon transplantation, HSCs hold the promise to treat various diseases, including lysosomal storage disorders (8), immunodeficiency (9–11), neurological disorders (8, 12), hematological malignancies, and other types of cancer (13). Thus, HSCs are of broad research and clinical interest. Mechanistically, specific gene expression programs ensure HSC generation, self-renewal, homing, quiescence, proliferation, and differentiation (1, 14, 15). Identification and characterization of DNA-binding transcription factors and cytoplasmic signaling molecules have yielded insights into regulatory networks important for HSC homeostasis (1, 14–16). Numerous chromatin regulators have been identified in the past 2 decades (17–19). As a key mechanism of chromatin regulation, histone modifications interplay with DNA methylation and demethylation to form signaling platforms that are essential for governing the identity of differentiated cells and stem cells (20–22). Hundreds of chromatin regulators utilize structural modules to interpret signals conferred by chromatin modifications (23–25), so an important question is how such regulators play a role in HSC homeostasis.

Bromodomain- and PHD finger–containing protein 1 (BRPF1) is a multivalent chromatin regulator composed of multiple histone-recognizing modules, including double PHD fingers, a bromodomain, and a PWWP domain (26–28). The PHD fingers recognize the N-terminal tail of histone H3 (28–30), the bromodomain has acetyllysine-binding ability (31), and the PWWP domain forms a specific pocket for trimethylated histone H3 (32, 33). In addition, BRPF1 possesses motifs for interaction with the acetyltransferases MOZ, MORF, and HBO1, which are also known as lysine acetyltransferase 6A (KAT6A), KAT6B, and KAT7, respectively (26–28). As a scaffold, BRPF1 promotes quartet-complex formation of these enzymes with other subunits, stimulates the catalytic activity of these enzymes, and governs their substrate specificity (26–28). Molecular and cell-based findings suggest that BRPF1 has an important role in vivo. Moreover, it remains possible that BRPF1 functions independently of these 3 enzymes in vivo. To delineate its biological functions at the tissue and organismal levels, we have recently taken a genetic approach to disrupt the mouse gene and uncovered that BRPF1 is crucial for embryogenesis and forebrain development (34–37). Here we identify it as a key regulator of fetal HSCs and progenitors, thereby highlighting its importance in definitive hematopoiesis.

Results

Hematopoietic-specific Brpf1 loss results in early lethality and aplastic anemia. Important roles of MOZ and MORF in leukemia (38–42) prompted us to investigate whether BRPF1 has a role in hematopoiesis. As *Brpf1* expression in the bone marrow remains relatively unclear (34), we sorted different populations of hematopoietic cells by fluorescence-activated multicolor flow cytometry (43, 44)

Authorship note: L. You and L. Li are co–first authors. A. Nijnik and E. Wang contributed equally to this work.
Conflict of interest: The authors have declared that no conflict of interest exists.
Submitted: December 29, 2014; **Accepted:** June 16, 2016.
Reference information: *J Clin Invest*. 2016;126(9):3247–3262. doi:10.1172/JCI80711.

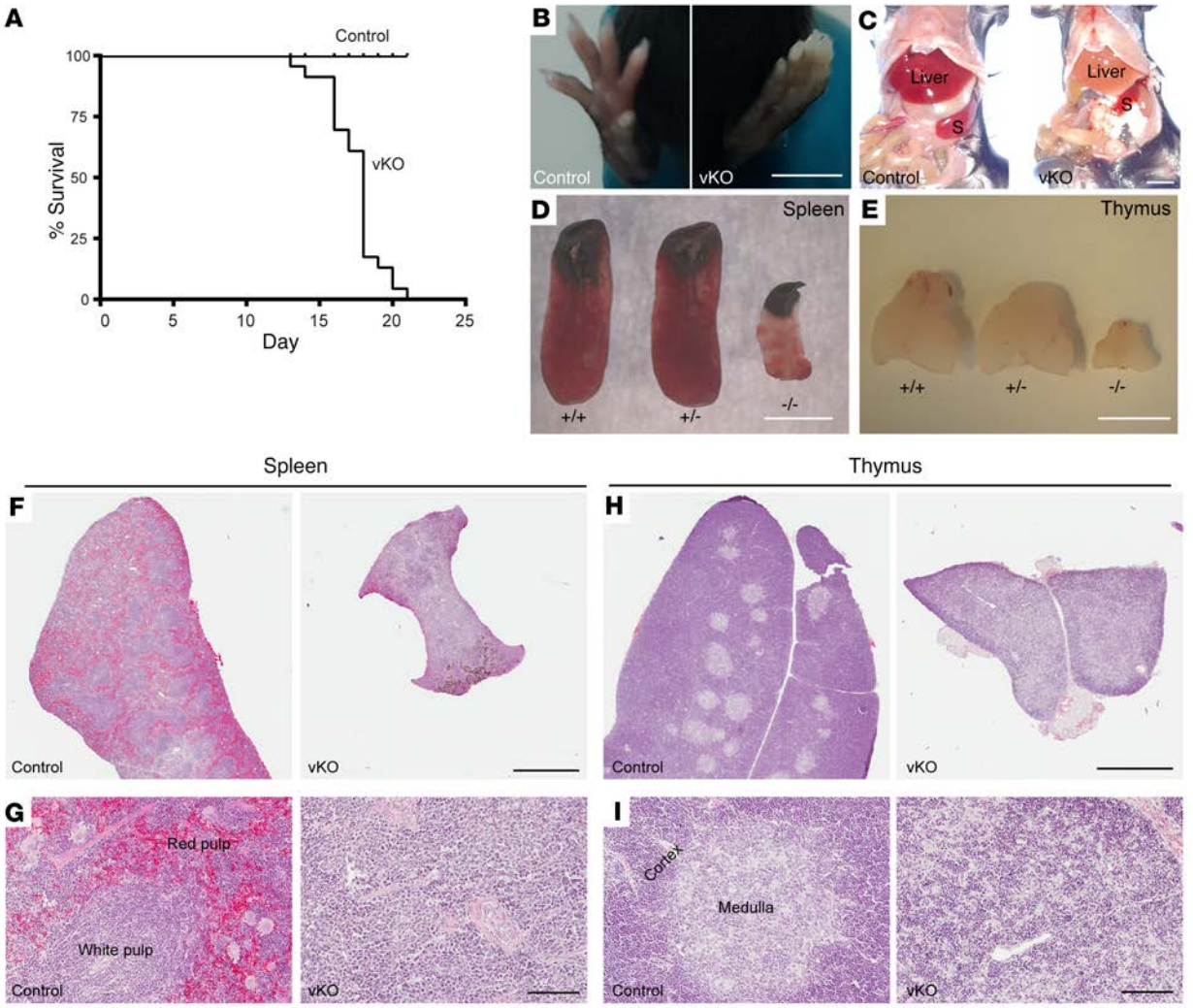

Figure 1. *Brpf1*-deficient mice display postnatal lethality and severe hematopoietic hypoplasia. (**A**) Kaplan-Meier survival curve. Twenty-four pairs of control and *Brpf1*$^{fl/fl}$ *Vav1-iCre* (vKO) mice were monitored for survival. Mutant mice were alive for a maximum of 21 days with median mortality at P18. (**B**–**E**) Unlike the control, mutant mice exhibited pale extremities (**B**) and pale liver (**C**), along with small spleen (**D**) and thymus (**E**) at week 3 after birth. Three pairs were examined and images for 1 representative pair of P19 control and mutant mice are shown. S, spleen. (**F** and **H**) H&E staining of P19 spleen (**F**) and thymus (**H**) paraffin sections. (**G** and **I**) Magnified images taken from **F** and **H**, respectively. Note abnormal histological organizations in mutant sections. Scale bars: **B**–**E**, 5 mm; **F** and **H**, 1 mm; **G** and **I**, 100 μm.

and determined *Brpf1* expression in isolated cell populations by quantitative reverse transcription-PCR (RT-qPCR). As shown in Supplemental Figure 1A (supplemental material available online with this article; doi:10.1172/JCI80711DS1), the transcript was detectable in multiple hematopoietic lineages and Lin$^-$Sca1$^+$cKit$^+$ (LSK) cells from the bone marrow at postnatal day 11 (P11). Similarly, RT-qPCR showed that *Brpf1* mRNA is present in CD34$^-$Flt3$^-$ and CD34$^+$Flt3$^-$ fractions of LSK cells (enriched for long-term and short-term HSCs, respectively), as well as in 3 lineage-committed progenitors in the bone marrow (Supplemental Figure 1B). In addition, we sorted different hematopoietic populations from the fetal liver at embryonic day 12.5 (E12.5). At this stage, *Brpf1* mRNA was detectable in different hematopoietic cell lineages (Supplemental Figure 1C). Interestingly, when compared with other hematopoietic cells, the transcript level was strikingly high in CD48$^-$CD150$^+$ LSK cells (Supplemental Figure 1C). This population is enriched for HSCs (45), so the results suggest a potential role for BRPF1 in HSCs and hematopoiesis.

To investigate this exciting possibility, we generated specific knockouts by mating *Brpf1*$^{fl/fl}$ mice (34) with the *Vav1-iCre* strain, which is known to confer hematopoietic-specific iCre expression (46). To verify the knockout efficiency, we examined *Brpf1* mRNA in control and homozygous mutant pups. Compared with that in the control, *Brpf1* mRNA was low in the mutant spleen, thymus, and bone marrow of *Brpf1*$^{fl/fl}$ *Vav1-iCre* (referred to as vKO hereafter) pups (Supplemental Figure 2, A and B), whereas there were no effects on the *Brpf1* transcript in the mutant testis (Supplemental Figure 2A) and much less effect in the mutant kidney (Supplemental Figure 2B). We also sorted different hematopoietic lineages from wild-type and mutant bone marrows and E12.5 fetal livers. As shown in Supplemental Figure 2, C and D, the knockout efficiency was generally high in different hematopoietic lineages.

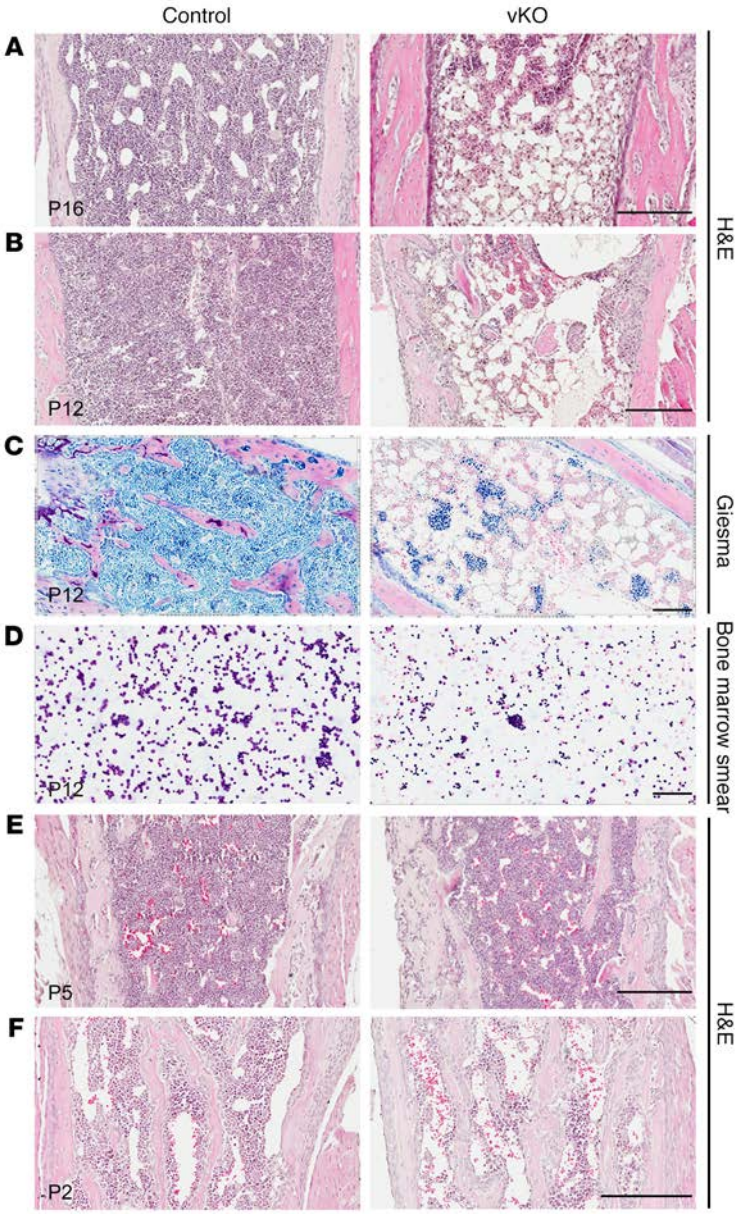

Figure 2. *Brpf1* deletion leads to acute bone marrow failure. (**A** and **B**) H&E staining of long-bone sections from representative control and *Brpf1*$^{fl/fl}$ *Vav1-iCre* (vKO) pups at P16 and P12. (**C** and **D**) Giemsa staining of long-bone sections (**C**) and bone marrow smears (**D**) from P12 control and mutant pups, confirming low cellularity in the mutant. (**E** and **F**) H&E staining of long-bone sections from control and mutant pups at P2 and P5. At each time point, 3 pairs from 3 different litters were examined and images from 1 representative pair are shown here. Scale bars: 200 μm in **A**, **B**, **E**, and **F**; 100 μm in **C** and **D**.

Thus, *Brpf1* disruption was efficient and specific. In terms of survival, *Brpf1*$^{fl/+}$ *Vav1-iCre* mice were indistinguishable from the wild-type, but the homozygous mutant mice exhibited an interesting phenotype (Supplemental Table 1). The vKO newborns were grossly normal, but could not survive beyond the weaning stage (Supplemental Table 1 and Figure 1A). Extensive genotyping of over 400 pups indicated that most of them died in postnatal week 3 (Supplemental Table 1). Therefore, hematopoietic-specific disruption of the *Brpf1* gene causes acute preweaning lethality.

In their last days of life, mutant pups appeared pale in their extremities (Figure 1B), and necropsy revealed pale liver (Figure 1C) and severe hypoplasia in the spleen and thymus (Figure 1, D and E). Histologically, the mutant spleen was pale and lacked clear distinction between red and white pulps (Figure 1, F and G). Similarly, the mutant thymus was poorly organized and lacked a clear medulla (Figure 1, H and I). We noticed that at P17 the peripheral blood from the mutant pups was much lighter than that of the control, so complete blood counts were carried out. The results indicated pancytopenia in the peripheral blood from mutant pups: the 3 lineages (red blood cells, white blood cells, and platelets) were all severely diminished compared to their control counterparts (Supplemental Table 2). Complete blood counts were also performed at P12. As shown in Supplemental Table 3, leukocytes and platelets decreased significantly while erythrocytes were relatively normal in the mutant, indicating that cytopenia occurs progressively from week 2 to 3.

In light of this, we performed histological analysis on paraffin bone sections. H&E staining revealed that at P16, the mutant bone marrow was aplastic and filled with large adipocytes (Figure 2A). A similar difference was observed in the mutant bone marrow at P12 (Figure 2B). Giemsa staining on sections and smear preparations confirmed that aplastic bone marrow occurs as early as P12 (Figure 2, C and D). To trace the developmental origin of the abnormality, we analyzed paraffin sections of long bones from neonates at P2 and P5. As shown in Figure 2, E and F, the mutant and control bone marrow structures were relatively comparable at the histological level. Thus, *Brpf1* deletion in the hematopoietic system leads to bone marrow failure starting at postnatal week 2.

Brpf1 disruption reduces HSC and progenitor populations in the bone marrow. The bone marrow contains stem cells and progenitors for all blood lineages. To identify causes for the bone marrow failure, we investigated how *Brpf1* deletion may affect different cell types. For this, we harvested bone marrow cells from control and mutant neonates for immunophenotyping by multicolor flow cytometry (43, 44). Because a minimal difference between 1-week-old control and mutant bone marrow structures was observed at the histological level (Figure 2, E and F), this age was chosen for flow cytometry to minimize secondary or nonautonomous effects resulting from bone marrow failure. As shown in Supplemental Figure 3A, the total number of nucleated cells decreased in the mutant bone marrow. Cell viability was also reduced (Supplemental Figure 3B). Interestingly, the LSK population disappeared in the mutant bone marrow (Figure 3, A and C), as did the IL-7Rα$^-$ LSK fraction (Figure 3, B and D), which is enriched for HSCs. Moreover, dramatic reduction was observed in myeloid progenitors (MPs; Lin$^-$ Sca1$^-$cKit$^+$) (Figure 3A). This population was further gated into 3 lineage-committed progenitors: common myeloid progenitors (CMPs; Lin$^-$Sca1$^-$cKit$^+$CD34$^+$CD16/32$^-$); granulocyte/macrophage progenitors (GMPs; Lin$^-$Sca1$^-$cKit$^+$CD34$^+$CD16/32$^+$); and mega-

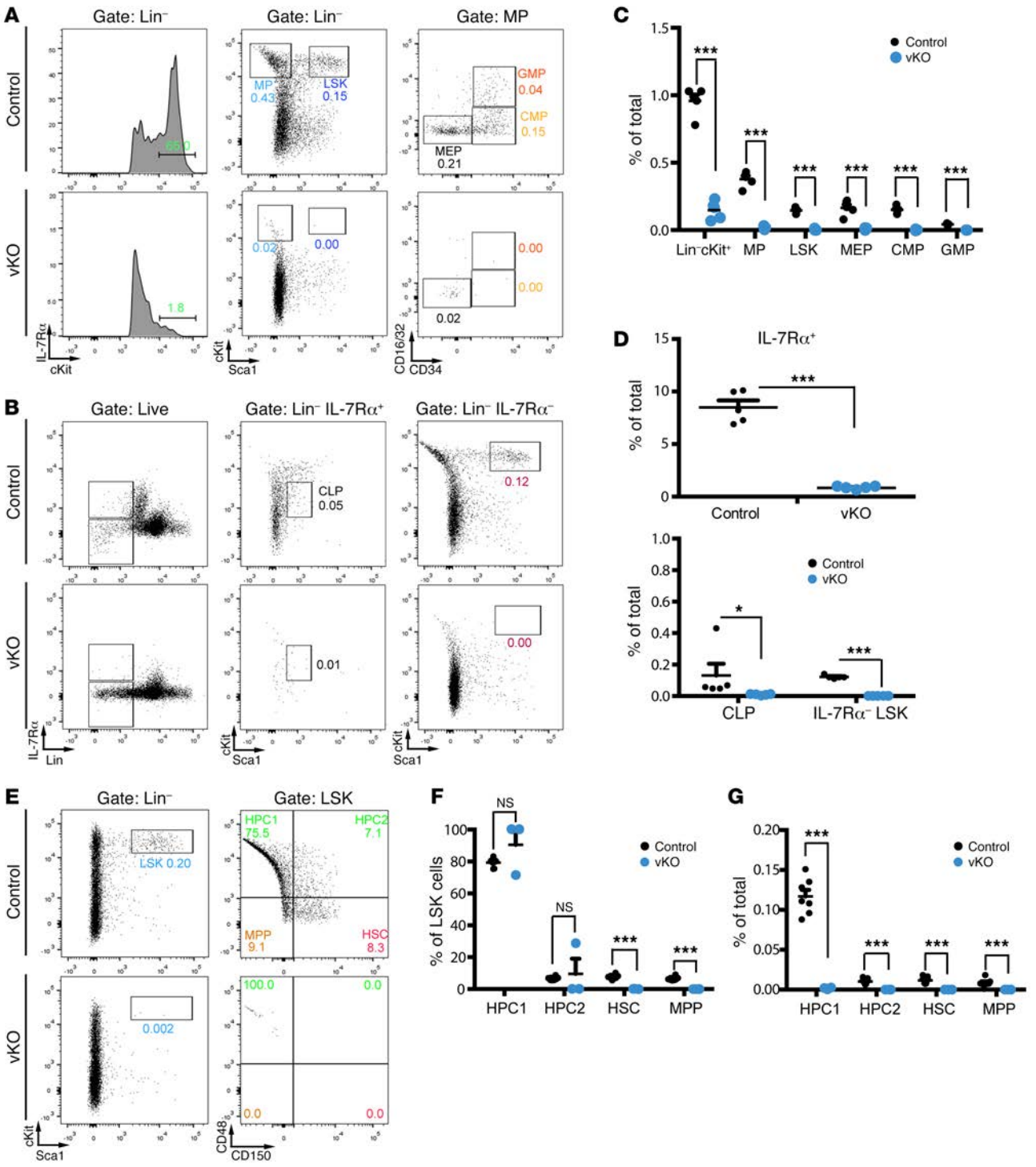

Figure 3. Depleted HSC and hematopoietic progenitor populations in the mutant bone marrow. (**A** and **B**) Representative cytometric analysis of LSK cells, myeloid progenitors, and common lymphoid progenitors in control and *Brpf1*$^{fl/fl}$ *Vav1-iCre* (vKO) bone marrow. P6 bone marrow cells were stained with fluorophore-conjugated monoclonal antibodies for cytometric detection of the following populations of stem cell or progenitor populations: MP (myeloid progenitor), LSK, MEP (megakaryocyte/erythroid progenitor), CMP (common myeloid progenitor), GMP (granulocyte/macrophage progenitor), common lymphoid progenitor (CLP), and IL-7Rα⁻ LSK (enriched for HSCs). (**C** and **D**) Percentage values of different populations detected in **A** and **B**. $n = 5$ for each genotype. (**E**) Representative cytometric analysis of bone marrow HSCs, MPPs (multipotent progenitors), and HPCs (hematopoietic progenitor cells) gated according to expression of the SLAM (signaling lymphocytic activation molecule) cell surface markers CD48 and CD150. (**F** and **G**) Within LSK cells, HPC ratios were not altered in the mutant (**F**). Because the percentage of LSK cells was much lower in the mutant bone marrow (**B**), all 4 populations decreased dramatically in the mutant (**G**). $n = 7$ for wild-type and $n = 3$ for vKO pups. No significant difference was observed between wild-type and heterozygous LSK cell numbers: 0.18% ± 0.01% (wild-type, $n = 4$) vs. 0.22% ± 0.02% (heterozygous, $n = 4$). $^*P < 0.05$, $^{***}P < 0.001$. For statistical analysis, unpaired 2-tailed Student's *t* tests were performed and average values are shown as the mean + SEM in **C**, **D**, **F**, and **G**.

karyocyte/erythroid progenitors (MEPs; $Lin^-Sca1^-cKit^+CD34^-CD16/32^-$). As shown in Figure 3, A and C, reduction was found in all 3 fractions. The IL-7 receptor IL-7Rα also serves as a receptor for thymic stromal lymphopoietin (TSLP), which is important for B and T cell development (47). In the mutant bone marrow, $IL\text{-}7R\alpha^+$ cells were depleted (Figure 3, B and D) and common lymphoid progenitors (CLPs; $Lin^-IL\text{-}7R\alpha^+Sca1^{lo}cKit^{lo}$) disappeared (Figure 3, B and D). We also analyzed different progenitors and stem cells within the LSK population according to expression of 2 signaling lymphocytic activation molecules (SLAMs), CD48 and CD150, as cell-surface markers (45). $CD48^-CD150^+$ LSK cells are relatively enriched for HSCs (45) and will thus be referred to as HSCs hereafter to describe related immunophenotyping results. Within the LSK population, HSCs and multipotent progenitors (MPPs; $CD48^-CD150^-$ LSKs) were depleted in the mutant bone marrow, whereas ratios of hematopoietic progenitor cell (HPC) populations were unaltered (Figure 3, E and F). However, because LSK cells were much lower in the mutant bone marrow (Figure 3C), all 4 populations decreased dramatically in the mutant (Figure 3G). Thus, *Brpf1* is required for proper development and/or maintenance of HSCs and progenitor cells in the bone marrow.

We next assessed how *Brpf1* deletion might affect hematopoietic differentiation, by examining B lymphopoiesis, myelopoiesis, and erythropoiesis in the bone marrow. For this purpose, total bone marrow cells were stained with fluorophore-conjugated monoclonal antibodies against the B lineage marker CD19, the myeloid lineage markers Gr1 and Mac1, and the erythrocyte markers Ter119 and CD71. For B cell lineages, the $CD19^+$ cell population was depleted in the mutant (Supplemental Figure 3, C and D). For myelopoiesis, the mutant contained slightly more $Mac1^+Gr1^-$ and $Mac1^-Gr1^+$ granulocytes but fewer $Mac1^-Gr1^-$ cells than the control (Supplemental Figure 3, E and F). For erythropoiesis, proerythroblasts are $Ter119^-CD71^+$ and maturation proceeds through $Ter119^+CD71^+$ early erythroblasts to $Ter119^+CD71^-$ late-stage erythroblasts. In the mutant, the number of $Ter119^-CD71^+$ proerythroblasts and $Ter119^+CD71^+$ early erythroblasts increased, but the $Ter119^+CD71^-$ late-stage erythroblast population remained normal (Supplemental Figure 3, G and H), indicating that BRPF1 does not dramatically affect erythrocyte maturation. These results indicate that, except for the B cell lineage, the impact on myeloid and erythroid differentiation programs (Supplemental Figure 3) is much less dramatic than that on the stem cell and progenitor compartments (Figure 3). Therefore, BRPF1 appears to be a crucial and specific regulator of HSCs and hematopoietic progenitors in the bone marrow.

BRPF1 regulates spleen and thymus development. In addition to the bone marrow, multiple peripheral organs are important for hematopoiesis. In neonates, the spleen is a major peripheral hematopoietic site. At P6, the control and mutant spleen weights were similar (Supplemental Figure 4A), although there were fewer viable cells in the mutant spleen (Supplemental Figure 4B). Although the proportions of B ($B220^+$) and T ($CD3^+$) lymphocytes in total splenic cells were similar in control and mutant spleens (Supplemental Figure 4B), the LSK and HPC populations were virtually missing in the mutant spleen (Supplemental Figure 4C). These results further support the important role of BRPF1 in HSCs and progenitors. In severe cases at P6, the mutant spleen was smaller (Supplemental Figure 4D) and histologically, the mutant red and white pulps were disorganized (Supplemental Figure 4E), indicating that BRPF1 is also important for development of the spleen per se.

As the mutant thymus was hypoplastic at P19 (Figure 1E), we traced the defect to an earlier time point. At P5, the mutant thymus was smaller than that of control (Supplemental Figure 5A). The total number of thymocytes was significantly reduced (Supplemental Figure 5B). Primitive thymocytes in the thymus do not express CD4 or CD8, and are thus double negative ($CD4^-CD8^-$). As development proceeds, they become double positive ($CD4^+CD8^+$) and then mature into single-positive ($CD4^+CD8^-$ or $CD4^-CD8^+$) thymocytes for release to the peripheral system. As shown in Supplemental Figure 5, C and D, the percentage of $CD4^+CD8^+$ thymocytes was similar between the control and mutant (Supplemental Figure 5, C and D). Also, none of these 4 populations was affected, indicating grossly normal thymocyte differentiation despite a reduced total number of T cells in the mutant thymus (Supplemental Figure 5, C and D). Notably, expression of some cell cycle regulators was altered in the thymus (Supplemental Figure 5E). Thus, BRPF1 is also important for thymus development.

BRPF1 is essential for long-term reconstitution capacity of bone marrow cells. The above immunophenotyping results (Figure 3) suggest that dramatic reduction of HSC and progenitor populations contribute to the bone marrow failure in mutant pups (Figure 2). One remaining question is whether residual HSCs and progenitors are functional. To investigate this possibility, we performed methylcellulose colony formation assays. When cultured in a methylcellulose medium containing IL-6, IL-3, stem cell factor, and erythropoietin (Methocult M3434), the number of colonies formed by mutant bone marrow cells was reduced compared to the control (Figure 4, A and B), indicating that there are fewer functional myeloid and erythroid progenitor cells in the mutant. Moreover, the mutant colonies were smaller, suggesting a proliferative defect. We then examined pre-B progenitors using a methylcellulose medium containing IL-7. As shown in Figure 4C, the number of colonies from mutant bone marrow cells was reduced compared to the control. These results indicate that BRPF1 is essential for hematopoietic progenitor functions in vitro.

To assess the impact of *Brpf1* inactivation on long-term hematopoietic reconstitution capacity in vivo, we performed competitive bone marrow transplantation by injecting $CD45.2^+$ wild-type (or mutant) bone marrow cells, mixed with wild-type $CD45.1^+$ cells, into γ-irradiated $CD45.1^+$ recipient mice. As shown in Figure 4D, at 4 to 16 weeks after transplantation, flow cytometry revealed that the mutant bone marrow cells were unable to repopulate in the recipient peripheral blood, whereas the control bone marrow cells succeeded in contributing about 60%–80% cells to the recipient blood. At week 16, virtually no contribution of the mutant bone marrow cells to multiple lineages in the peripheral blood of the recipients was found (Figure 4, E and F). Furthermore, no contribution to stem/progenitors cells and differentiated lineages in the recipients' bone marrow was detected (Figure 4F). These results indicate that BRPF1 is required for short-term and long-term repopulating activities of bone marrow cells.

Upon transplantation, HSCs and progenitors migrate to recipients' bone marrow and subsequently home to proper niches. The failure of the mutant bone marrow cells to reconstitute the recipi-

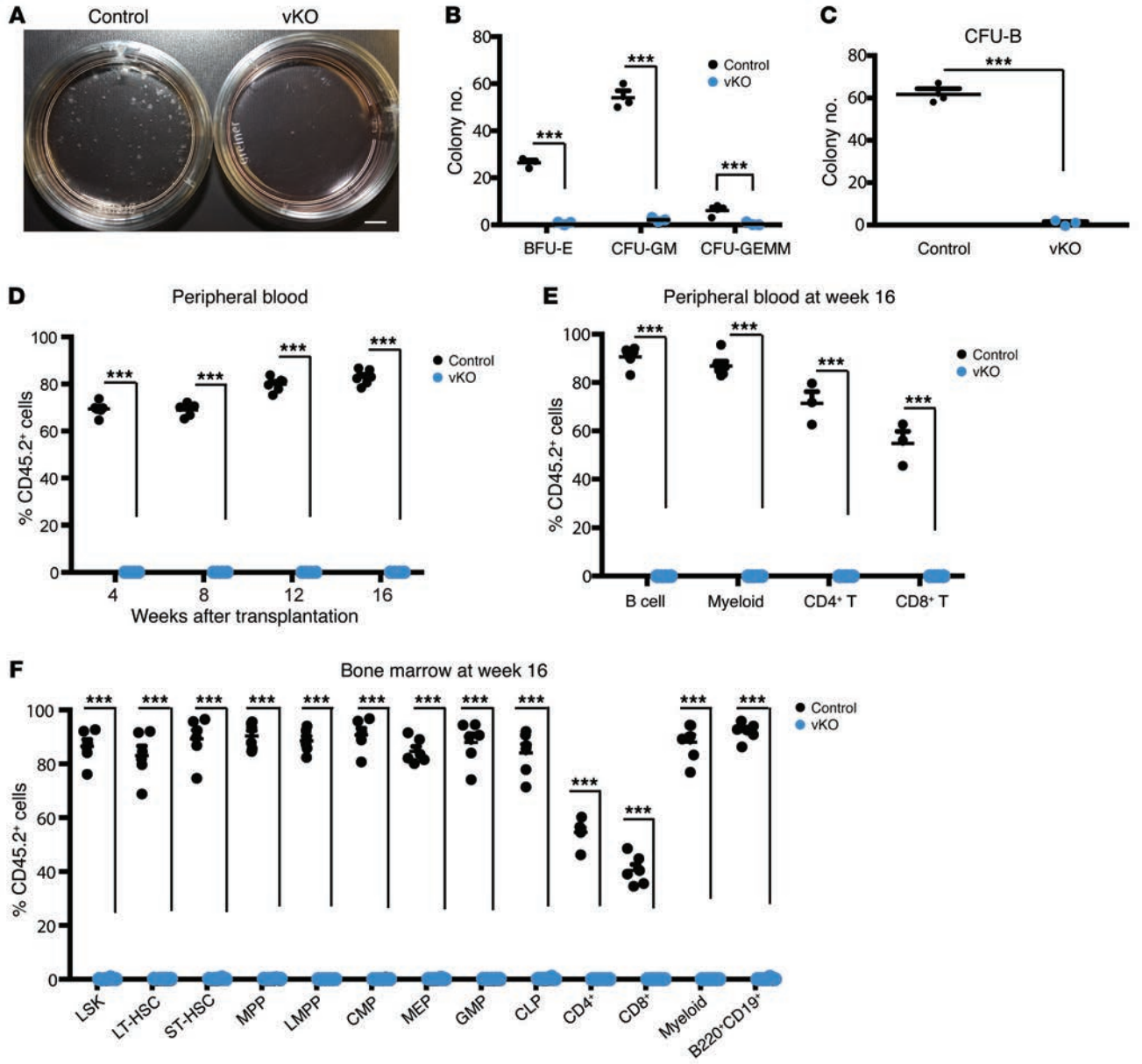

Figure 4. *Brpf1* disruption impairs colony formation and bone marrow reconstitution activities in the neonatal bone marrow. (**A**) Myeloid progenitor cell colony formation. Bone marrow cells (6×10^4) isolated from control and *Brpf1*$^{fl/fl}$ *Vav1-iCre* (vKO) pups at P6 were plated and cultured in MethoCult M3434 and colonies were analyzed on days 8–10. Representative images of the plates are shown. (**B**) Myeloid progenitor cell colony formation assays were performed as in **A**. Three different types of colonies, burst-forming unit-erythroid (BFU-E), colony-forming unit-granulocyte/monocyte (CFU-GM), and colony-forming unit-granulocyte/erythrocyte/monocyte/megakaryocyte (CFU-GEMM), were enumerated on days 8–10. Average values were calculated from 3 pairs of control and vKO pups. (**C**) B cell progenitor colony formation. Bone marrow cells (1.5×10^5) from control and vKO pups at P6 were cultured in MethoCult M3630 (see Supplemental Methods) and pre-B cell colonies were counted on days 8–10. Average values from 3 pairs of control and vKO pups are shown. (**D**) Long-term hematopoietic reconstitution was impaired in the mutant bone marrow. Contribution of donor (CD45.2$^+$) cells in the recipients' peripheral blood was determined at 4 to 16 weeks after transplantation. (**E**) At week 16 after transplantation, multilineage engraftment in the peripheral blood was analyzed. Note the robust contribution of the control but not the mutant CD45.2$^+$ bone marrow cells to formation of B cells (B220$^+$), myeloid cells (Gr1$^+$Mac1$^+$), and T cells (CD4$^+$ or CD8$^+$). (**F**) Fractions of donor-derived cells in HSCs, progenitors, and lineage cells in the recipient bone marrow at week 16 after transplantation. For **D**–**F**, $n = 6$ for each group; $^{***}P < 0.001$. Unpaired 2-tailed Student's t tests were performed and average values are shown as the mean + SEM in **B**–**F**. LT-HSC, long-term HSC; ST-HSC, short-term HSC.

ents' blood system might be due to a homing defect. To test this, CD45.2$^+$ mutant or control bone marrow cells harvested from pups at P6 were injected via tail vein into γ-irradiated CD45.1$^+$ recipient mice. At 40 hours after transplantation, bone marrow cells from recipient mice were collected and analyzed by flow cytometry. The results show that the number of control donor-derived cells in the bone marrow of recipient mice was similar to that of mutant donor-derived cells (Supplemental Figure 6), indicating that the mutant bone marrow cells are normal in homing to the bone marrow of the host.

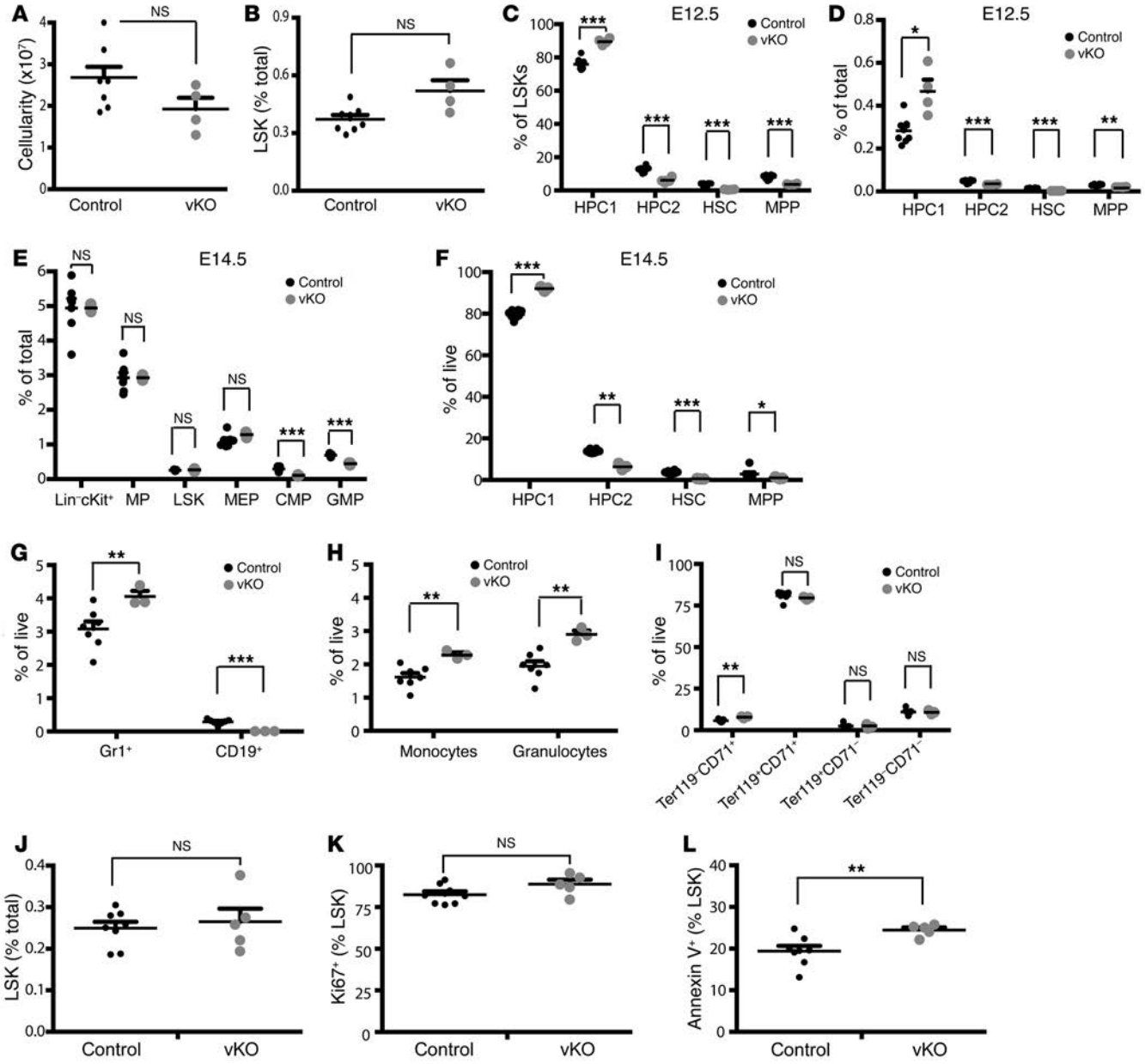

Figure 5. *Brpf1* deletion reduces HSC and B cell populations in the fetal liver. (**A**–**D**) Total cellularity (**A**), LSK cells (**B**), and 4 stem/progenitor populations (HPC1, HPC2, HSC, and MPP; **C** and **D**) in the fetal liver of control vs. *Brpf1*$^{fl/fl}$ *Vav1-iCre* (vKO) mice at E12.5. (**E**) Percentage values of LSK cells, myeloid progenitor, and different fractions (CMP, GMP, and MEP) in the E14.5 fetal liver. Numbers of CMPs and GMPs, but not LSK cells, MPs, or MEPs, decreased in the mutant. (**F**) Percentage values of the 4 fractions gated according to expression of CD48 and CD150. Despite the similar cell number of LSKs (**E**), the HSC fraction declined, whereas the HPC1 fraction slightly increased in the mutant. (**G**–**I**) B lymphoid (**G**), myeloid (**H**), and erythroid cells (**I**) were compared between control and vKO fetal livers at E14.5. Percentage values of Gr1$^+$ cells, CD19$^+$ B lineage cells, Mac1$^+$Gr1^{lo} monocytes, Mac1$^+$Gr1^{hi} granulocytes, and 4 erythroid fractions are shown. B lineage cells disappeared but myelopoiesis showed a mild increase in the mutant. (**J**–**L**) Proliferation and apoptosis of LSK cells in the E14.5 fetal liver. n = 8 for control and n = 4 for vKO in **A**–**D**; n = 7 for control and n = 3 for vKO in **E**–**I**; n = 8 for control and n = 5 for vKO in **J**–**L**; *P < 0.05, **P < 0.01, ***P < 0.001. For statistical analysis, unpaired 2-tailed Student's t tests were performed and average values are presented here as the mean + SEM.

Brpf1 deletion reduces HSC and progenitor populations in the fetal liver. To identify the reasons for the HSC and progenitor defects (Figures 3 and 4), we traced the developmental origins. Definitive hematopoiesis initiates at the aorta-gonad-mesonephros (AGM) region, colonizes the fetal liver, and eventually migrates to the thymus, spleen, and bone marrow (5, 6). Defective HSCs and progenitors in the mutant bone marrow (Figures 3 and 4) raised the question of whether similar defects are present in the mutant fetal liver, a major site of definitive hematopoiesis in the fetus (5, 6). To investigate this, we performed flow cytometry with hematopoietic cells from the fetal liver. At E12.5, the total cellularity and cell number of the LSK population in the mutant fetal liver were similar to those in the control (Figure 5, A and B). Upon separation of LSK cells into 4 different populations, an interesting picture

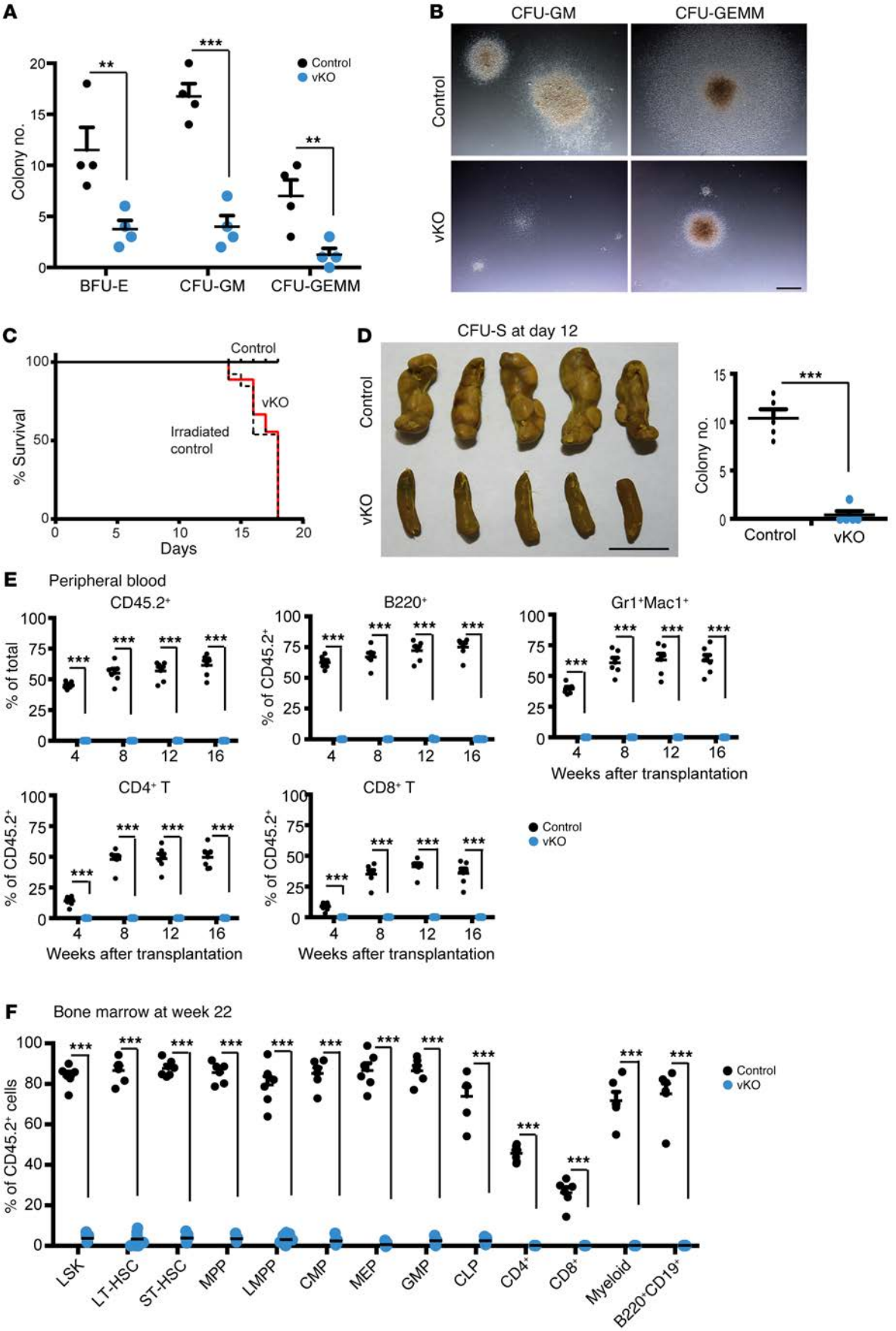
A
Colony no.
Control
vKO
BFU-E
CFU-GM
CFU-GEMM
B
CFU-GM
CFU-GEMM
Control
vKO
C
% Survival
Control
vKO
Irradiated control
Days
D
CFU-S at day 12
Control
vKO
Colony no.
E
Peripheral blood
CD45.2+
B220+
Gr1+Mac1+
CD4+ T
CD8+ T
% of total
% of CD45.2+
Weeks after transplantation
F
Bone marrow at week 22
% of CD45.2+ cells
LSK
LT-HSC
ST-HSC
MPP
LMPP
CMP
MEP
GMP
CLP
CD4+
CD8+
Myeloid
B220+CD19+

Figure 6. *Brpf1* inactivation impairs colony formation and bone marrow repopulating activities in the fetal liver. (**A**) Myeloid progenitor cell colony formation of fetal liver cells (6×10^4) from control and *Brpf1*$^{fl/fl}$ *Vav1-iCre* (vKO) embryos at E15.5. Colonies were examined at day 9, and average numbers of burst-forming unit-erythroid (BFU-E), colony-forming unit-granulocyte/monocyte (CFU-GM), and colony-forming unit-granulocyte/erythrocyte/monocyte/megakaryocyte (CFU-GEMM) colonies are presented. $n = 4$ for each group. (**B**) Morphology of representative individual colonies formed from control and vKO fetal liver cells. Images were obtained with an AxioCam HRc digital camera and a 20× objective on an AXIO Zoom.V16 microscope. Scale bar: 1 mm. (**C**) Survival curves of irradiated C57BL/6 mice without transplantation (dashed line) or transplanted with 2×10^5 control (solid black line) or vKO (solid red line) fetal liver cells at E14.5. $n = 13$ for the group without transplantation and $n = 9$ for each transplanted group. (**D**) CFU-S analysis at day 12. Images of spleens are shown on the left and the colony numbers are presented in the graph on the right. $n = 5$ for each group. Scale bar: 5 mm. (**E** and **F**) *Brpf1* inactivation impairs long-term hematopoietic reconstitution potential in the fetal liver. Fetal liver cells were collected for tail-vein injection into irradiated C57BL/6.SJL mice. Flow cytometric analysis of the contribution of donor (CD45.2$^+$) cells and multilineage engraftment in the recipients' peripheral blood at 4 to 16 weeks after transplantation is shown in **E**, whereas fractions of donor-derived cells in specific cell populations in the recipients' bone marrow at 22 weeks are presented in **F**. E12.5 and E15.5 mutant fetal liver cells showed similar defects in hematopoietic reconstitution, and the data are from 6 pairs of wild-type and mutant embryos (3 pairs at E12.5 and 3 pairs at E15.5). $^{**}P < 0.01$, $^{***}P < 0.001$. For **A**, **D** (right), **E**, and **F**, unpaired 2-tailed Student's *t* tests were performed and average values are shown as the mean + SEM.

emerged. While the HPC1 population slightly expanded, a significant decrease was found with the HPC2, HSC, and MPP fractions (Figure 5, C and D). At E14.5, the mutant MP, LSK, and MEP populations were comparable with those from the control fetal liver, whereas the mutant CMP and GMP fractions were compromised (Figure 5E). As found for E12.5 (Figure 5D), the HPC1 fraction slightly expanded, but a significant decrease was found with the remaining 3 fractions (Figure 5F). At E14.5, B cell differentiation was compromised, whereas myelopoiesis increased (Figure 5, G and H). By contrast, erythropoiesis appeared largely normal in the mutant fetal liver (Figure 5I). Thus, BRPF1 is required for early stages of definitive hematopoiesis in the fetal liver.

BRPF1 is required for the bone marrow reconstitution potential of fetal liver cells. The immunophenotyping results from flow cytometry (Figure 5) suggest that deficiency in HSCs and some progenitors in the fetal liver is the cause for the eventual bone marrow failure after birth (Figures 1 and 2). One remaining question is whether residual HSCs and progenitor populations are still functional. To investigate this, we performed methylcellulose colony formation assays. When cultured in Methocult M3434, the number of colonies formed by the mutant fetal liver cells was much smaller than that from the control (Figure 6, A and B), indicating fewer functional myeloid and erythroid progenitor cells in the mutant fetal liver. Thus, *Brpf1* is critical for functions of fetal hematopoietic progenitors in vitro.

To determine short-term repopulating potential, we transplanted X-ray–irradiated C57BL/6.SJL young mice with wild-type or mutant fetal liver cells. The wild-type, but not the mutant, fetal liver cells conferred survival advantage over the irradiated control mice, which received the same dose of radiation but no transplantation (Figure 6C). Unlike the wild-type, the mutant fetal liver cells yielded few colony-forming units in the spleen (CFU-S) at day 12 (Figure 6D), suggesting that at the fetal stage, *Brpf1* loss impairs functions of fetal short-term hematopoietic stem/progenitor cells in vivo.

To assess the long-term repopulating potential, we performed competitive bone marrow transplantation by injecting wild-type (or mutant) CD45.2$^+$ fetal liver cells, premixed with CD45.1$^+$ liver fetal cells, into γ-irradiated CD45.1$^+$ recipient mice. As shown in Figure 6E, at 4 to 16 weeks after the bone marrow transplantation, cytometric analysis revealed that the mutant fetal liver cells were unable to contribute to multiple lineages in the recipients' peripheral blood, whereas the control contributed 10% to 80% of the cells in the recipients' blood. At week 22, almost no contribution of the mutant fetal liver cells to different stem/progenitors cells and differentiated lineages in the recipients' bone marrow was detected (Figure 6F). These results indicate that *Brpf1* is essential for long-term repopulating activities of fetal liver cells.

BRPF1 regulates fetal HSC signature gene expression. To elucidate the underlying cellular mechanisms, we investigated whether *Brpf1* deletion alters proliferation of LSK cells. Simultaneous staining of cell surface markers and the intracellular nuclear protein Ki67 was performed for subsequent quantification by flow cytometry. At P6, the proportion of Ki67$^+$ cells in the mutant LSK population was significantly lower (Figure 7, A and B), indicating that there are fewer cycling LSK cells in the mutant bone marrow. By contrast, the proliferation index was normal in LSK cells from the mutant fetal liver (Figure 5, J and K). Related to this, the cell cycle profile was not affected (Supplemental Figure 7). These results suggest no obvious alteration of cell cycle progression at least in a majority of LSK cells from the mutant fetal liver.

We also examined survival of LSK cells by annexin V staining and cytometric analysis. As shown in Figure 7C, the LSK population in the mutant bone marrow displayed apoptosis as indicated by a significantly elevated amount of annexin V$^+$ cells. Apoptosis also slightly increased in the fetal liver (Figure 5L), but it was much less severe than that in the bone marrow (Figure 7C). Moreover, increased levels of ROS (Figure 7D and Supplemental Figure 8A) and cellular senescence (Figure 7E and Supplemental Figure 8B) were also detected in LSK cells from the mutant bone marrow. A similar increase was present in HSC-containing CD150$^+$ LSK cells (Figure 7, D and E). This population also showed some increase in the ROS level in the mutant fetal liver at E14.5 (Supplemental Figure 8C). These results support that elevated ROS and senescence are 2 cellular mechanisms contributing to defects in mutant LSK cells.

To understand the molecular mechanism underlying the functional defects in mutant HSCs and progenitors, we sorted LSK cells from the wild-type or mutant fetal liver at E14.5 for RNA isolation, oligo(dT)–primed reverse transcription, and deep sequencing. Two independent sets of RNA-Seq results revealed that multiple genes important for HSC stemness were downregulated in the mutant LSK cells (Table 1, Supplemental Figure 9, and Supplemental Table 4). These genes include *Slamf1*, *Evi1*, *Mds1*, *Sox17*, *Hoxa9*, *Hoxa7*, *Meis1*, *Hlf*, *Gfi1*, *Rora*, and *Gata3*. Among them, *Slamf1* encodes CD150, which has been frequently used as an HSC surface marker (48). The *Mds1* and *Evi1* complex locus (also known as *Mecom*) encodes MDS1, EVI1, and their fusion protein, and is important for long-term HSC function (49, 50). SOX17 is an HMG-

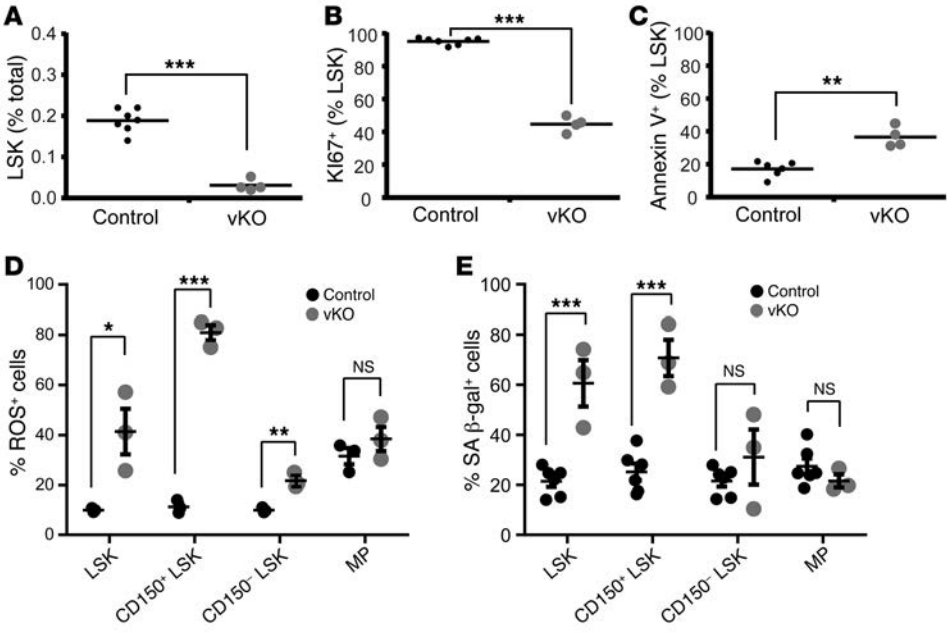

Figure 7. *Brpf1* deletion alters LSK cell programs. (**A** and **B**) After staining with antibodies against lineage-specific markers (PerCPCy5.5-conjugated CD3ε, B220, Gr1, and Ter119) together with antibodies specific for HSC markers (Sca1-APC and cKit-Pacific blue), P6 bone marrow cells were fixed, permeabilized, and restained with Ki67-FITC. n = 7 for control and n = 4 for *Brpf1*$^{fl/fl}$ *Vav1-iCre* (vKO) pups. (**C**) Bone marrow cells were stained with the antibodies as in **A** and **B**, except that Ki67-FITC was replaced with annexin V-PECy7. n = 6 for control and n = 4 for vKO. (**D**) Percentage of ROS-positive cells in LSK, CD150$^+$LSK, CD150$^-$LSK, and MP populations in the control and mutant bone marrows at P9. n = 3 for each group. (**E**) Percentage of senescent cells in LSK, CD150$^+$LSK, CD150$^-$LSK, and MP fractions in the control and mutant bone marrows at P9. n = 6 for control pups and n = 3 for vKO pups. *P < 0.05, **P < 0.01, ***P < 0.001. For statistical analysis, unpaired 2-tailed Student's t tests were performed; average values are presented as the mean + SEM in **A**–**C** and as the mean ± SEM in **D** and **E**.

box transcription factor crucial for fetal HSCs (51). The zinc finger transcription factor GFI1 is important for HSC self-renewal (52, 53). The homeodomain transcription factor HOXA9 interacts with MEIS1 and PBX1/2 to form a trimeric DNA-binding complex that is important for HSC proliferation (54–57). HOXA7 has functions similar to those of HOXA9 (58). HLF (hepatic leukemia factor) is a bZIP transcription factor important for HSC identity (59). Interestingly, *Mecom*, *Hoxa9*, and 4 other downregulated genes (*Ets1*, *Myct1*, *Eya1*, and *Egr*; Table 1) were shown to be direct targets of the histone methyltransferase MLL in an HSC-rich cell population (60), suggesting a potential interaction between BRPF1 and MLL. In addition, RNA-Seq revealed defective transcription of multiple genes specific to hematopoietic progenitors (Supplemental Figure 9). For example, consistent with defects in B cell lineage (Supplemental Figure 3, C and D, and Figure 5G), transcription of *Ebf1*, *Lef1*, and *Pou2af1*, which encode 3 transcription factors important for B cell development, was dramatically reduced (Supplemental Figure 9). Thus, the RNA-Seq results suggest that BRPF1 loss leads to transcriptional reduction of genes important for HSCs and hematopoietic progenitors.

To verify this conclusion based on RNA-Seq, we performed RT-qPCR with RNA from sorted fetal liver LSK cells at E14.5. RT-qPCR analysis confirmed reduction in a majority of targets selected for analysis (Table 1 and Supplemental Figure 9). Moreover, transcript levels of 2 BRPF1 paralogs (BRPF2 and BRPF3) and 3 interacting histone acetyltransferases (MOZ, MORF, and HBO1) (26–28) were unaltered in mutant fetal liver LSK cells at E14.5 (Supplemental Table 4) and in mutant fetal liver HSCs at E12.5 (Supplemental Figure 10A), indicating that the defects are not due to the lack of these BRPF1-related or -interacting proteins. Consistent with minimal effects on the cell cycle profile at E14.5 (Supplemental Figure 7), no changes were detected in transcripts of multiple cell cycle regulators (Supplemental Table 4).

Immunophenotyping and functional analysis revealed that HSC and progenitor defects are evident at E12.5 (Figures 5 and 6), raising the question of whether molecular defects are also present at this developmental stage. To investigate this, we performed RT-qPCR to analyze RNA from wild-type and mutant fetal liver LSK cells at E12.5. As shown in Table 1 and Supplemental Figure 9, transcriptional defects were already severe at E12.5. These results indicate that *Brpf1* loss results in developmental abnormality of HSCs and progenitors starting at E12.5. Thus, BRPF1 is a chromatin regulator with an essential role in early HSC development.

BRPF1 is essential for hematopoietic histone H3 acetylation. Molecular and cell-based studies have established that BRPF1 stimulates activities of the histone acetyltransferases MOZ, MORF, and HBO1 towards histone H3 in vitro (26, 28, 61), so we investigated how *Brpf1* loss might affect histone H3 acetylation in vivo. For this, we first harvested bone marrow cells from wild-type and mutant pups at P7 for protein extract preparation and immunoblotting. As shown in Figure 8A, *Brpf1* loss led to dramatic reduction of histone acetylation at lysines 9, 14, and 23 in the bone marrow. By contrast, acetylation at lysine 18 of histone H3 was not affected in the mutant bone marrow (Figure 8B), indicating that the effect is specific to certain sites. There were some effects on histone H4 acetylation at lysine 16 (Figure 8B), but they were much milder compared with those on lysines 9, 14, and 23 of histone H3 (Figure 8A). Consistent with hematopoietic-specific effects, no changes in lysine 23 acetylation were detected in the mutant kidney (Figure 8C). Lysines 9 and 14 of histone H3 are well known to be important for marking active genes. By contrast, much less is known for acetylation at lysine 23 of histone H3. Interestingly, this mark has recently been shown to be highly abundant in U2OS osteosarcoma and HeLa cells (62, 63) and was reported in 2010 to serve as a unique ligand for the important chromatin reader TRIM24 in breast cancer (64), suggesting the importance of lysine 23 acetylation in vivo. Moreover, MORF and a related *Drosophila* protein acetylate histone H3 at lysine 23 (65, 66). In light of these

Table 1. Reduced transcription of known and potential HSC signature genes

Gene	RNA-Seq (fold change)	RT-qPCR (fold change)	
	E14.5	E14.5	E12.5
Slamf1/Cd150	0.05/0.25	0.46 ± 0.12[A]	0.25
Oit3/EF9	0.07/0.17	?	?
Cecr2	0.11/0.14	0.17 ± 0.01[C]	0.29
Hoxb5	0.16/2.0	0.71 ± 0.11[D]	0.52
Vldlr	0.16/nd	?	?
Runx1t1/Eto	0.16/0.26	0.49 ± 0.10[B]	0.24
Ets1	0.19/0.27	0.20 ± 0.02[C]	0.42
Hemgn	0.18/0.77	1.22 ± 0.26	0.22
Mecom/Mds1-Evi1	0.23/0.27	0.53 ± 0.08[B]	0.22
Sox17	0.25/nd	?	?
Myct1	0.26/0.4	0.56 ± 0.15[A]	0.25
Vegfa	0.26/0.5	?	?
Hoxa9	0.28/0.25	0.25 ± 0.16[B]	0.24
Hoxa5	0.31/0.5	?	?
Hlf	0.33/0.5	0.38 ± 0.06[C]	0.31
Hoxa10	0.34/0.42	0.80 ± 0.77[D]	0.02
Eya1	0.36/0.59	?	?
Meis1	0.37/0.4	0.48 ± 0.09[B]	0.36
Hoxa7	0.37/1.11	?	0.09
Rora	0.38/0.45	?	?
Gfi1	0.42/0.56	0.64 ± 0.07[B]	0.30
Egr	0.43/0.59	?	?
Gata3	0.45/0.5	?	?
Brpf1	0.28/0.62	0.30 ± 0.13[B]	0.01
Brpf1-N		0.35 ± 0.11[B]	0.10

Wild-type and mutant LSK cells were prepared from control and mutant fetal livers at E14.5 for RNA-Seq. Selected multipotency genes with reduced expression in 2 different RNA-Seq experiments were used for validation by RT-qPCR with RNA from wild-type and mutant LSK cells sorted from E12.5 and E14.5 fetal livers. The values are shown as the fold change in the mutant when compared to the control. For each gene, numbers in the "RNA-Seq" column represent fold change in 2 different RNA-Seq experiments. For RT-qPCR at E14.5, the data were derived from 3 different sets of pooled LSK cells and are shown as the mean ± SEM; $n = 7$ for the control and $n = 5$ for *Brpf1*$^{fl/fl}$ *Vav1-iCre* embryos. For statistical analysis, unpaired 2-tailed Student's *t* tests were performed. [A]$P < 0.05$, [B]$P < 0.01$, [C]$P < 0.001$. [D]Not statistically significant. For RT-qPCR at E12.5, the data were based on 1 set of sorted fetal LSK cells pooled from 4 wild-type or mutant embryos. Genes regulated by MLL are highlighted in gray. See the main text and Supplemental Figure 9 for discussion about known and potential roles of the listed genes in HSCs and progenitors. nd, not detectable; ?, not investigated.

findings, we performed indirect immunofluorescence microscopy to analyze this epigenetic mark in sorted bone marrow LSK cells and on bone marrow sections. The fluorescence signal for lysine 23 acetylation was undetectable in sorted mutant LSK cells at P7 (Figure 8D). Moreover, the lysine 23 acetylation level was low in the mutant bone marrow at P5, but the fluorescence signal was not affected in the adjacent bone (Supplemental Figure 11). Together, these results indicate that BRPF1 is important for specific histone H3 acetylation in the bone marrow.

Discussion

BRPF1 is a multivalent chromatin reader crucial for fetal HSC development. Because of its multiple histone-binding domains and the ability to activate 3 different histone acetyltransferases, BRPF1 is a unique chromatin reader with the potential to mediate crosstalk between different chromatin modifications (26–28). The results presented herein demonstrate that BRPF1 is highly expressed in HSCs from the fetal liver (Supplemental Figure 1C) and serves as an essential regulator in the HSC and hematopoietic progenitor compartments (Figures 2–6). The results also support its function upstream from multiple multipotency genes important for HSC stemness (Table 1 and Supplemental Figure 9). Because HSCs emerge at the AGM region and start to migrate to the liver at E10.5 (1), it is intriguing to note that effects of *Brpf1* deletion become evident at E12.5 (Figures 5 and 6). Notably, *Vav1-iCre* fails to initiate complete excision at E11.5 (67), so it will be necessary to utilize a different Cre line, such as Vec-Cre (67), to examine the function of BRPF1 at the time window between E10.5 and E12.5. The important role of BRPF1 in HSC development is potentially novel because little is known about functions of chromatin readers in HSC homeostasis (Figure 8E). These readers, such as the BET family of bromodomain proteins (68), have been shown to be valuable as drug targets, so the important role of BRPF1 in HSCs and hematopoietic progenitors suggests its potential as a molecular target for developing therapeutic means for treating hematopoiesis-related disorders.

Roles in HSC homeostasis have been reported for enzymatic chromatin modifiers: the DNA methyltransferase DNMT3a in promoting HSC differentiation (69); the DNA demethylase TET2 in repressing HSC expansion (70); 3 histone methyltransferases (MLL1, EZH1 and EZH2) and a subunit of a histone H2A ubiquitin ligase complex (BMI1) in HSC self-renewal and maintenance (71–76); the acetyltransferase MOZ in HSC development (77, 78); and the deacetylase HDAC3 in HSC proliferation (79). Among them, MOZ, BMI1, and MLL regulate fetal HSC functions (Figure 8E). Our results indicate that BRPF1 plays an essential role at the fetal stage (Figure 8E). It remains to be determined whether BRPF1 has any roles in postnatal maintenance of HSCs. Interestingly, BRPF1 loss led to decreased expression of multiple genes, such as *Mecom*, *Hoxa9*, *Ets1*, *Myct1*, *Eya1*, and *Egr* (Table 1), that are also regulated by MLL (60). This similarity suggests potential interaction between BRPF1 and MLL.

Bone marrow transplantation (Figure 6, E and F) and gene expression profiling (Table 1 and Supplemental Figure 9) indicate that BRPF1 acts on HSC development starting at or prior to E12.5, which is quite intriguing in light of HSC emergence at the AGM region and subsequent migration to the fetal liver around E10.5 (Figure 8E) (1). Further investigation of its role within this narrow time window shall yield new insights into epigenetic networks important for HSC ontogeny (80).

Brpf1 deletion causes bone marrow failure through a potentially new mechanism. One striking phenotype of *Brpf1* mutant pups is

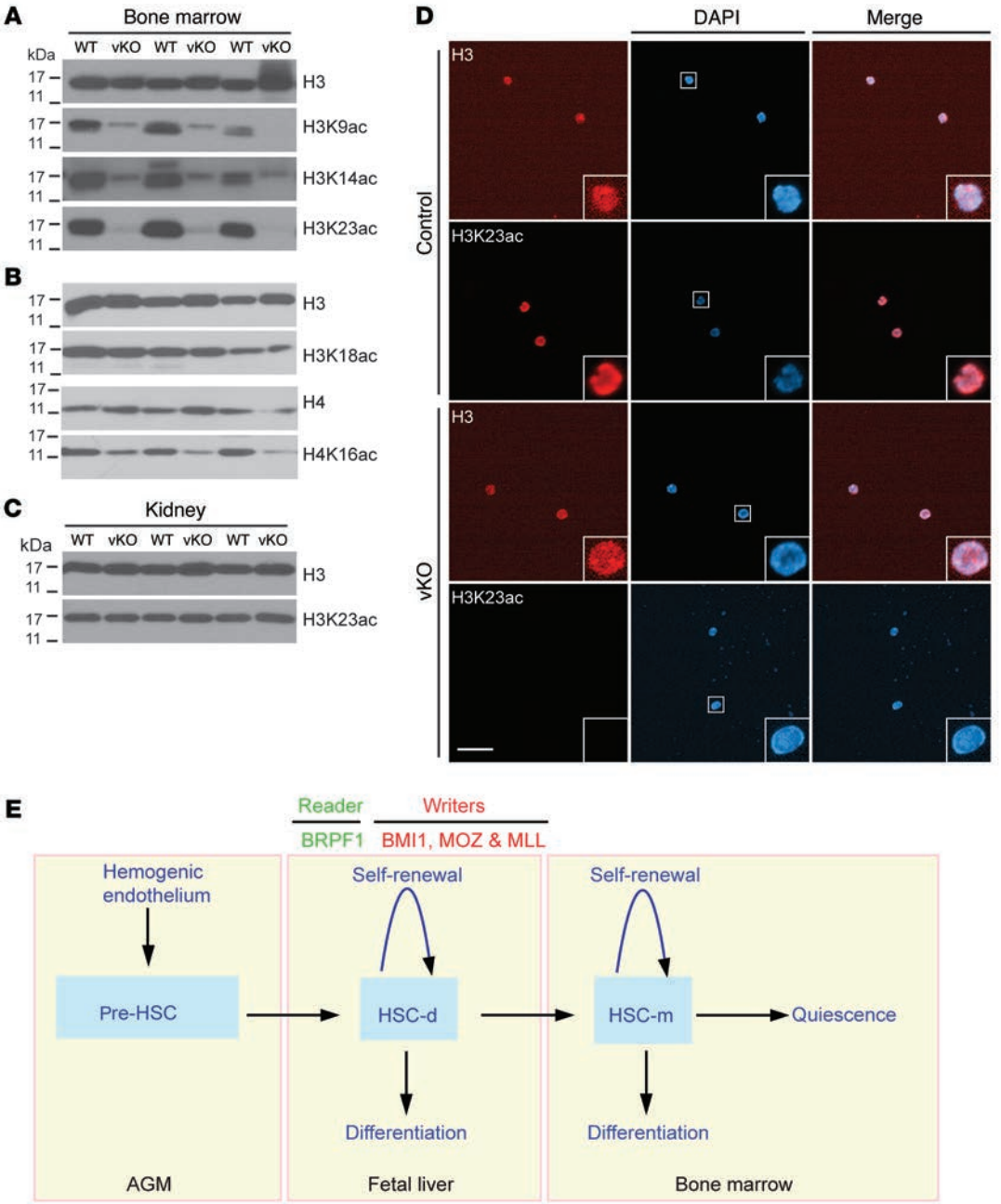

Figure 8. BRPF1 regulates histone acetylation in the bone marrow and LSK cells. (**A** and **B**) Immunoblotting analysis of histone H3 and H4 acetylation in wild-type and *Brpf1*$^{fl/fl}$ *Vav1-iCre* (vKO) bone marrow cell extracts at P7. (**C**) Immunoblotting for histone H3 acetylation at lysine 23 in kidney protein extracts at P7. (**D**) Immunofluorescence microscopic analysis of histone H3 acetylation at lysine 23 in LSK cells sorted from the wild-type or mutant bone marrow at P7. Scale bar: 50 μm. In **A** and **B**, results were similar for bone marrow cells from 3 pairs of wild-type and mutant pups. The experiment in **D** was repeated 3 times, and similar results were obtained with over 100 wild-type or mutant cells. (**E**) Cartoon explaining the roles of BRPF1 and 3 other chromatin regulators important for fetal HSC homeostasis. The hemogenic endothelium at the AGM region gives rise to pre-HSCs for subsequent migration to the fetal liver, where definitive HSCs (HSC-d) merge and travel to the bone marrow for eventual maturation to generate mature HSCs (HSC-m). In addition to its role as a chromatin reader due to its multiple histone-binding domains, BRPF1 acts as a co-writer to activate the acetyltransferases MOZ, MORF, and HBO1 (107). Thus, BRPF1 is a unique multivalent chromatin reader (23–25).

that they were healthy in postnatal week 1 but all dead in week 3 (Figure 1). Immunophenotyping and functional transplantation assays indicate that deficient HSCs and hematopoietic progenitors in the fetal liver and bone marrow contribute to bone marrow failure (Figures 2–6). Bone marrow failure has been reported for pups lacking the deacetylase SIRT6 (81). Interestingly, the pups exhibit premature aging due to defective glucose metabolism. By contrast, the glucose level was normal in *Brpf1* mutant pups (Supplemental Figure 12). Although not examined directly, the bone marrow of *Sirt6*$^{-/-}$ pups may be histologically normal, as their HSCs are functional (81). Bone marrow failure is a key feature of diseases with aplastic anemia. In a mouse model of Fanconi anemia, the p53/

p21 DNA damage response is exacerbated (82). Synergy of p53 mutants with loss of the inhibitor MDM2 or MDM4 also leads to bone marrow failure (83, 84). Due to defective telomere functions, bone marrow failure is also a feature of dyskeratosis congenita. As a model of this genetic disease, mice lacking POT1B, a subunit of a complex required for telomere protection, exhibit bone marrow failure and defective HSCs due to p53-dependent apoptosis (85, 86). Of relevance, hematopoietic-specific *Brpf1* deletion promoted apoptosis (Figures 5L and 7C), but there were no obvious defects in p53-dependent processes such as *Cdkn1a* expression (Supplemental Table 4). Together, these considerations suggest that bone marrow failure in *Brpf1* mutant pups occurs through a previously unrecognized mechanism.

BRPF1 regulates histone H3 acetylation in stem cells and human diseases. BRPF1 is conserved from *Caenorhabditis elegans* to humans (42). It regulates neuron asymmetry, hindgut development, and fecundity in worms (87). Fish Brpf1 maintains pharyngeal segmental identity and skeletal development (88). Thus, an important role in mouse HSCs is unexpected. Whether fish Brpf1 regulates hematopoiesis is presently unclear. Mammalian BRPF1 is paralogous to BRPF2 and BRPF3 (26, 27). Deletion of mouse *Brpf2* leads to embryonic lethality at E15.5 and faulty erythropoiesis (89). By contrast, *Brpf3* is dispensable (90). Thus, despite their sequence similarity, the 3 BRPF proteins have distinct roles in vivo. Related to their differences, BRPF1 interacts with the acetyltransferases MOZ, MORF, and HBO1 (26–28), whereas BRPF2 and BRPF3 target predominantly (if not exclusively) HBO1 (89–91). In mammals, there are 3 JADE proteins, each of which shares similarity with BRPF1 in 2 PHD fingers and 2 small motifs (26). However, JADE proteins do not show any homology to the bromodomain and PWWP domain of BRPF1 (26). Moreover, JADEs activate only HBO1 (26, 28). Thus, compared with BRPF2, BRPF3, and JADEs, BRPF1 is unique.

Known interactions of BRPF1 with MOZ, MORF, and HBO1 are based on cell-based assays in vitro (89–91), so an important question is which acetyltransferases BRPF1 activates in HSCs and other hematopoietic cells in vivo. Among the 3 acetyltransferases, MOZ is critical in HSCs (77, 78, 92). Through interacting with BRPF2, HBO1 is important for development of erythrocytes and thymocytes (89, 93). Its role in HSCs remains unclear. Similarly, the function of MORF in hematopoiesis also awaits investigation (94). Our results show that BRPF1 is crucial for histone H3 acetylation at lysines 9, 14, and 23 (Figure 8, A and D). The finding about lysine 23 acetylation is exciting and potentially novel, as this histone mark is poorly characterized but highly abundant, at least in 2 human cell lines (62, 63). Moreover, enok (a fly acetyltransferase homologous to MOZ and MORF) is crucial for histone H3 acetylation at lysine 23 in vivo and MORF targets the same site in lung cancer cells (65, 66). MOZ is paralogous to MORF (42), so it is expected to acetylate histone H3 at lysine 23. By contrast, mouse *Hbo1* is crucial for acetylation of histone H3 at lysine 14 in vivo (93). At their mRNA levels, mouse *Morf* appears to be expressed at a much lower level than *Moz* and *Hbo1* in fetal liver HSCs at E12.5 (Supplemental Figure 10B) and fetal liver LSK cells at E14.5 (Table S4), so it is tempting to propose that BRPF1 mainly targets MOZ and HBO1 to control histone H3 acetylation in HSCs and hematopoietic progenitors. Further studies are needed to substantiate this interesting possibility.

Pathologically, BRPF1 regulates leukemogenesis and aberrant MOZ-containing proteins, and has been shown to be essential for self-renewal of leukemic stem cells (39, 40, 95). Like the *MOZ* gene, the *MORF* gene is rearranged in leukemia (41, 42). This gene is also mutated in leiomyoma (96), prostate cancer (97), and breast cancer (98). Moreover, the *MOZ* and *MORF* genes are also amplified in different types of cancer (99) and mutated in developmental disorders with intellectual disability (100–106). Related to these developmental disorders, BRPF1 is important for murine neural stem cells (35, 37). In addition, it will be important to investigate whether the *BRPF1* gene is also mutated in patients with related developmental disorders. Thus, how BRPF1 interacts with MOZ, MORF, and other partners to regulate stem cells in leukemia and other diseases is an exciting question awaiting further investigation.

Methods

Mice. Mice were in the C57BL/6J background except that the γ-irradiated recipient mice used for competitive bone marrow transplantation were the congenic strain C57BL/6.SJL-Ptprc^{a} Pepc^{b}/BoyJ (Jackson Laboratory, stock 002014). Heterozygous *Brpf1*^{LacZ} mice were originally obtained from the European Mutant Mouse Archive (ID 04257) to produce *Brpf1*$^{fl/fl}$ mice as described previously (34). The *Brpf1*^{fl} allele contains 2 loxP sites flanking exons 4–6 of the *Brpf1* gene (34). To generate hematopoietic-specific knockouts, *Brpf1*$^{fl/fl}$ mice were bred with the *Vav1-iCre* strain (Jackson Laboratory, stock 008610) (46).

Knockout efficiency was verified by genomic PCR, RT-PCR, and/or RT-qPCR. Genomic PCR was carried out as described (35–37). For RT-PCR or RT-qPCR, cells were harvested from the bone marrow, thymus, spleen, kidney, or fetal liver. After staining with different combinations of fluorophore-conjugated antibodies (Supplemental Table 5, see below), different hematopoietic lineages were sorted on a FACSAria sorter (BD Biosciences) directly into tubes containing QIAzol (QIAGEN) or TRIzol (Thermo Fisher). RNA was extracted with an miRNeasy or RNeasy Mini Kit (QIAGEN). RT-PCR and RT-qPCR were performed as described previously (35–37). Primers are listed in Supplemental Table 6.

Flow cytometry. Total bone marrow cells were flushed out of femurs and tibias with DMEM containing 2% FBS and penicillin/streptomycin (Gibco). Spleen, thymus, and fetal liver tissues were minced in the same medium. Single-cell suspensions were prepared by passing them through 40-μm cell strainers (StemCell Technologies). Red blood cells were lysed with Red Blood Cell (RBC) Lysis Buffer (eBioscience). The nucleated cell number was counted on an automated cell counter (Bio-Rad, TC10). FVD-eFluor 506 (eBioscience) was used as a viability dye to exclude dead cells. For lineage labeling, fetal liver, neonatal bone marrow, or spleen cells were stained with PerCPCy5.5-conjugated monoclonal antibodies against 4 lineage (Lin)-specific cell surface markers (CD3ε, B220, Gr1, and Ter119; eBioscience; Supplemental Table 5), whereas for adult bone marrow cells, 5 markers (CD3ε, B220, Gr1, Ter119, and Mac1; eBioscience) were used. For detection of HSCs and progenitors, cells were stained with respective combinations of fluorophore-conjugated monoclonal antibodies (cKit-PECy7 or cKit-Pacific Blue, Sca1-APC, Flt3-PE, CD34-FITC, IL-7Rα-PE, CD150-PE, CD48-FITC, and CD16/32-PE; eBioscience; Supplemental Table 5). Combinations of fluorophore-conjugated monoclonal antibodies specific for cell surface markers were: long-term HSC, CD34^{-}Flt3^{-}LSK; short-term HSC, CD34^{+}Flt3^{-}LSK; MPP,

$CD48^-CD150^-LSK$ (Figure 3F and Supplemental Figure 1C) or $CD34^+Flt3^+LSK$ (Figures 4F and 6F); HPC1, $CD48^+CD150^-LSK$; HPC2, $CD48^+CD150^+LSK$; LMPP, $Lin^-Sca1^+cKit^+Flt3^{hi}$; CLP, $Lin^-IL\text{-}7R\alpha^+Sca1^{lo}cKit^{lo}$; CMP, $Lin^-Sca1^-cKit^+CD34^+CD16/32^-$; GMP, $Lin^-Sca1^-cKit^+CD34^+CD16/32^+$; MEP, $Lin^-Sca1^-cKit^+CD34^-CD16/32^-$; and fetal liver HSC, $Lin^-Sca1^+cKit^+CD48^-CD150^+$. Three pairs of conjugated monoclonal antibodies (CD19-PE vs. Gr1-PerCPCy5.5, Mac1-PerCP-Cy5.5 vs. Gr1-PE, and Ter119-PerCPCy5.5 vs. CD71-PE) were used to assess B lineage, myeloid differentiation, and erythroid differentiation, respectively. For thymocyte differentiation, CD4-PE and CD8a-FITC were used. All fluorophore-conjugated monoclonal antibodies were from eBioscience. Flow cytometry was performed with a 3-laser LSR II or 4-laser LSR Fortessa flow cytometer (BD Biosciences). FACSDiva (BD Biosciences) and FlowJo (TreeStar Inc.) software packages were used for data analysis. Sorting of HSCs, LSK cells, and other hematopoietic cells was performed on the FACSAria cell sorter.

Statistics. Statistical analysis was performed with unpaired 2-tailed Student's *t* tests, with the exception of Supplemental Figure 7, in which 1-way ANOVA was used for multiple comparisons in cell cycle analyses. *P* values less than 0.05 were considered to be statistically significant, and data are presented as the mean ± SEM or mean + SEM. Graphs were generated with Prism 6 (GraphPad Software).

Animal study approval. Animal-related procedures used in this study were carried out according to the Animal Use Protocol 5786, which was reviewed and approved by the Facility Animal Care Committee of McGill University, Montreal, Quebec, Canada.

Supplemental information. Information about antibodies and additional experimental procedures is included in the Supplemental Information section, which also contains Supplemental Tables 1–6 and Supplemental Figures 1–12.

Author contributions

LY initiated the project. LL finished the project. LY and LL carried out all experiments. KY provided ideas on H3K23 acetylation. JZ and EW performed bioinformatics analysis. JB and AN helped design flow cytometric experiments. LY and LL prepared drafts of the manuscript. XJY supervised the project and finalized the manuscript.

Acknowledgments

The research was supported by operating grants from Canadian Institutes for Health Research (CIHR to AN and XJY) and Natural Sciences and Engineering Research Council of Canada (NSERC to XJY).

Address correspondence to: Xiang-Jiao Yang, Goodman Cancer Center, Room 413, 1160 Pine Avenue West, Montreal, Quebec H3A 1A3, Canada. Phone: 514.398.5883; E-mail: xiang-jiao.yang@mcgill.ca.

1. Orkin SH, Zon LI. Hematopoiesis: an evolving paradigm for stem cell biology. *Cell*. 2008;132(4):631–644.
2. Doulatov S, Notta F, Laurenti E, Dick JE. Hematopoiesis: a human perspective. *Cell Stem Cell*. 2012;10(2):120–136.
3. Copley MR, Beer PA, Eaves CJ. Hematopoietic stem cell heterogeneity takes center stage. *Cell Stem Cell*. 2012;10(6):690–697.
4. Morrison SJ, Scadden DT. The bone marrow niche for haematopoietic stem cells. *Nature*. 2014;505(7483):327–334.
5. Dzierzak E, Speck NA. Of lineage and legacy: the development of mammalian hematopoietic stem cells. *Nat Immunol*. 2008;9(2):129–136.
6. Medvinsky A, Rybtsov S, Taoudi S. Embryonic origin of the adult hematopoietic system: advances and questions. *Development*. 2011;138(6):1017–1031.
7. Rossi DJ, Jamieson CH, Weissman IL. Stems cells and the pathways to aging and cancer. *Cell*. 2008;132(4):681–696.
8. Biffi A, et al. Lentiviral hematopoietic stem cell gene therapy benefits metachromatic leukodystrophy. *Science*. 2013;341(6148):1233158.
9. Aiuti A, et al. Lentiviral hematopoietic stem cell gene therapy in patients with Wiskott-Aldrich syndrome. *Science*. 2013;341(6148):1233151.
10. Naldini L. Ex vivo gene transfer and correction for cell-based therapies. *Nat Rev Genet*. 2011;12(5):301–315.
11. Hütter G, et al. Long-term control of HIV by CCR5 Delta32/Delta32 stem-cell transplantation. *N Engl J Med*. 2009;360(7):692–698.
12. Appel SH, et al. Hematopoietic stem cell transplantation in patients with sporadic amyotrophic lateral sclerosis. *Neurology*. 2008;71(17):1326–1334.
13. Copelan EA. Hematopoietic stem-cell transplantation. *N Engl J Med*. 2006;354(17):1813–1826.
14. McKinney-Freeman S, et al. The transcriptional landscape of hematopoietic stem cell ontogeny. *Cell Stem Cell*. 2012;11(5):701–714.
15. Novershtern N, et al. Densely interconnected transcriptional circuits control cell states in human hematopoiesis. *Cell*. 2011;144(2):296–309.
16. Rossi L, et al. Less is more: unveiling the functional core of hematopoietic stem cells through knockout mice. *Cell Stem Cell*. 2012;11(3):302–317.
17. Li B, Carey M, Workman JL. The role of chromatin during transcription. *Cell*. 2007;128(4):707–719.
18. Kouzarides T. Chromatin modifications and their function. *Cell*. 2007;128(4):693–705.
19. Ronan JL, Wu W, Crabtree GR. From neural development to cognition: unexpected roles for chromatin. *Nat Rev Genet*. 2013;14(5):347–359.
20. Bonasio R, Tu S, Reinberg D. Molecular signals of epigenetic states. *Science*. 2010;330(6004):612–616.
21. Suganuma T, Workman JL. Signals and combinatorial functions of histone modifications. *Annu Rev Biochem*. 2011;80:473–499.
22. Kohli RM, Zhang Y. TET enzymes, TDG and the dynamics of DNA demethylation. *Nature*. 2013;502(7472):472–479.
23. Taverna SD, Li H, Ruthenburg AJ, Allis CD, Patel DJ. How chromatin-binding modules interpret histone modifications: lessons from professional pocket pickers. *Nat Struct Mol Biol*. 2007;14(11):1025–1040.
24. Latham JA, Dent SY. Cross-regulation of histone modifications. *Nat Struct Mol Biol*. 2007;14(11):1017–1024.
25. Musselman CA, Lalonde ME, Côté J, Kutateladze TG. Perceiving the epigenetic landscape through histone readers. *Nat Struct Mol Biol*. 2012;19(12):1218–1227.
26. Doyon Y, et al. ING tumor suppressor proteins are critical regulators of chromatin acetylation required for genome expression and perpetuation. *Mol Cell*. 2006;21(1):51–64.
27. Ullah M, et al. Molecular architecture of quartet MOZ/MORF histone acetyltransferase complexes. *Mol Cell Biol*. 2008;28(22):6828–6843.
28. Lalonde ME, et al. Exchange of associated factors directs a switch in HBO1 acetyltransferase histone tail specificity. *Genes Dev*. 2013;27(18):2009–2024.
29. Qin S, et al. Recognition of unmodified histone H3 by the first PHD finger of bromodomain-PHD finger protein 2 provides insights into the regulation of histone acetyltransferases monocytic leukemic zinc-finger protein (MOZ) and MOZ-related factor (MORF). *J Biol Chem*. 2011;286(42):36944–36955.
30. Klein BJ, et al. Bivalent interaction of the PZP domain of BRPF1 with the nucleosome impacts chromatin dynamics and acetylation. *Nucleic Acids Res*. 2016;44(1):472–484.
31. Poplawski A, et al. Molecular insights into the recognition of N-terminal histone modifications by the BRPF1 bromodomain. *J Mol Biol*. 2014;426(8):1661–1676.
32. Vezzoli A, et al. Molecular basis of histone H3K36me3 recognition by the PWWP domain of Brpf1. *Nat Struct Mol Biol*. 2010;17(5):617–619.
33. Wu H, et al. Structural and histone binding ability characterizations of human PWWP domains. *PLoS ONE*. 2011;6(6):e18919.
34. You L, Chen L, Penney J, Miao D, Yang XJ. Expression atlas of the multivalent epigenetic regulator Brpf1 and its requirement for survival of mouse

embryos. *Epigenetics*. 2014;9(6):860–872.
35. You L, et al. The lysine acetyltransferase activator Brpf1 governs dentate gyrus development through neural stem cells and progenitors. *PLoS Genet*. 2015;11(3):e1005034.
36. You L, et al. The chromatin regulator Brpf1 regulates embryo development and cell proliferation. *J Biol Chem*. 2015;290(18):11349–11364.
37. You L, et al. Deficiency of the chromatin regulator BRPF1 causes abnormal brain development. *J Biol Chem*. 2015;290(11):7114–7129.
38. Borrow J, et al. The translocation t(8;16)(p11;p13) of acute myeloid leukaemia fuses a putative acetyltransferase to the CREB-binding protein. *Nat Genet*. 1996;14(1):33–41.
39. Deguchi K, et al. MOZ-TIF2-induced acute myeloid leukemia requires the MOZ nucleosome binding motif and TIF2-mediated recruitment of CBP. *Cancer Cell*. 2003;3(3):259–271.
40. Huntly BJ, et al. MOZ-TIF2, but not BCR-ABL, confers properties of leukemic stem cells to committed murine hematopoietic progenitors. *Cancer Cell*. 2004;6(6):587–596.
41. Chinen Y, et al. The leucine twenty homeobox (LEUTX) gene, which lacks a histone acetyltransferase domain, is fused to KAT6A in therapy-related acute myeloid leukemia with t(8;19)(p11;q13). *Genes Chromosomes Cancer*. 2014;53(4):299–308.
42. Yang XJ, Ullah M. MOZ and MORF, two large MYSTic HATs in normal and cancer stem cells. *Oncogene*. 2007;26(37):5408–5419.
43. Perfetto SP, Chattopadhyay PK, Roederer M. Seventeen-colour flow cytometry: unravelling the immune system. *Nat Rev Immunol*. 2004;4(8):648–655.
44. Mayle A, Luo M, Jeong M, Goodell MA. Flow cytometry analysis of murine hematopoietic stem cells. *Cytometry A*. 2013;83(1):27–37.
45. Oguro H, Ding L, Morrison SJ. SLAM family markers resolve functionally distinct subpopulations of hematopoietic stem cells and multipotent progenitors. *Cell Stem Cell*. 2013;13(1):102–116.
46. de Boer J, et al. Transgenic mice with hematopoietic and lymphoid specific expression of Cre. *Eur J Immunol*. 2003;33(2):314–325.
47. Vosshenrich CA, Cumano A, Müller W, Di Santo JP, Vieira P. Thymic stromal-derived lymphopoietin distinguishes fetal from adult B cell development. *Nat Immunol*. 2003;4(8):773–779.
48. Kiel MJ, Yilmaz OH, Iwashita T, Yilmaz OH, Terhorst C, Morrison SJ. SLAM family receptors distinguish hematopoietic stem and progenitor cells and reveal endothelial niches for stem cells. *Cell*. 2005;121(7):1109–1121.
49. Kataoka K, et al. Evi1 is essential for hematopoietic stem cell self-renewal, and its expression marks hematopoietic cells with long-term multilineage repopulating activity. *J Exp Med*. 2011;208(12):2403–2416.
50. Zhang Y, et al. PR-domain-containing Mds1-Evi1 is critical for long-term hematopoietic stem cell function. *Blood*. 2011;118(14):3853–3861.
51. Kim I, Saunders TL, Morrison SJ. Sox17 dependence distinguishes the transcriptional regulation of fetal from adult hematopoietic stem cells. *Cell*. 2007;130(3):470–483.
52. Hock H, et al. Gfi-1 restricts proliferation and preserves functional integrity of haematopoietic stem cells. *Nature*. 2004;431(7011):1002–1007.
53. Zeng H, Yücel R, Kosan C, Klein-Hitpass L, Möröy T. Transcription factor Gfi1 regulates self-renewal and engraftment of hematopoietic stem cells. *EMBO J*. 2004;23(20):4116–4125.
54. Thorsteinsdottir U, et al. Overexpression of the myeloid leukemia-associated Hoxa9 gene in bone marrow cells induces stem cell expansion. *Blood*. 2002;99(1):121–129.
55. Shen WF, Rozenfeld S, Kwong A, Köm ves LG, Lawrence HJ, Largman C. HOXA9 forms triple complexes with PBX2 and MEIS1 in myeloid cells. *Mol Cell Biol*. 1999;19(4):3051–3061.
56. LaRonde-LeBlanc NA, Wolberger C. Structure of HoxA9 and Pbx1 bound to DNA: Hox hexapeptide and DNA recognition anterior to posterior. *Genes Dev*. 2003;17(16):2060–2072.
57. Lawrence HJ, et al. Loss of expression of the Hoxa-9 homeobox gene impairs the proliferation and repopulating ability of hematopoietic stem cells. *Blood*. 2005;106(12):3988–3994.
58. So CW, Karsunky H, Wong P, Weissman IL, Cleary ML. Leukemic transformation of hematopoietic progenitors by MLL-GAS7 in the absence of Hoxa7 or Hoxa9. *Blood*. 2004;103(8):3192–3199.
59. Komorowska M, Mikkola HKA, Larsson J, Magnusson M. Hepatic leukemia factor is an important regulator of hematopoietic stem cell activity and identity. *Blood*. 2013;122:2410.
60. Artinger EL, et al. An MLL-dependent network sustains hematopoiesis. *Proc Natl Acad Sci U S A*. 2013;110(29):12000–12005.
61. Lalonde ME, Cheng X, Côté J. Histone target selection within chromatin: an exemplary case of teamwork. *Genes Dev*. 2014;28(10):1029–1041.
62. Chen S, et al. The PZP domain of AF10 senses unmodified H3K27 to regulate DOT1L-mediated methylation of H3K79. *Mol Cell*. 2015;60(2):319–327.
63. Zhou T, Chung YH, Chen J, Chen Y. Site-specific identification of lysine acetylation stoichiometries in mammalian cells. *J Proteome Res*. 2016;15(3):1103–1113.
64. Tsai WW, et al. TRIM24 links a non-canonical histone signature to breast cancer. *Nature*. 2010;468(7326):927–932.
65. Simó-Riudalbas L, et al. KAT6B is a tumor suppressor histone H3 lysine 23 acetyltransferase undergoing genomic loss in small cell lung cancer. *Cancer Res*. 2015;75(18):3936–3945.
66. Huang F, et al. Histone acetyltransferase Enok regulates oocyte polarization by promoting expression of the actin nucleation factor spire. *Genes Dev*. 2014;28(24):2750–2763.
67. Chen MJ, Yokomizo T, Zeigler BM, Dzierzak E, Speck NA. Runx1 is required for the endothelial to haematopoietic cell transition but not thereafter. *Nature*. 2009;457(7231):887–891.
68. Filippakopoulos P, Knapp S. Targeting bromodomains: epigenetic readers of lysine acetylation. *Nat Rev Drug Discov*. 2014;13(5):337–356.
69. Challen GA, et al. Dnmt3a is essential for hematopoietic stem cell differentiation. *Nat Genet*. 2012;44(1):23–31.
70. Moran-Crusio K, et al. Tet2 loss leads to increased hematopoietic stem cell self-renewal and myeloid transformation. *Cancer Cell*. 2011;20(1):11–24.
71. Xie H, et al. Polycomb repressive complex 2 regulates normal hematopoietic stem cell function in a developmental-stage-specific manner. *Cell Stem Cell*. 2014;14(1):68–80.
72. Hidalgo I, et al. Ezh1 is required for hematopoietic stem cell maintenance and prevents senescence-like cell cycle arrest. *Cell Stem Cell*. 2012;11(5):649–662.
73. Jude CD, Climer L, Xu D, Artinger E, Fisher JK, Ernst P. Unique and independent roles for MLL in adult hematopoietic stem cells and progenitors. *Cell Stem Cell*. 2007;1(3):324–337.
74. McMahon KA, et al. Mll has a critical role in fetal and adult hematopoietic stem cell self-renewal. *Cell Stem Cell*. 2007;1(3):338–345.
75. Lessard J, Sauvageau G. Bmi-1 determines the proliferative capacity of normal and leukaemic stem cells. *Nature*. 2003;423(6937):255–260.
76. Park IK, et al. Bmi-1 is required for maintenance of adult self-renewing haematopoietic stem cells. *Nature*. 2003;423(6937):302–305.
77. Katsumoto T, et al. MOZ is essential for maintenance of hematopoietic stem cells. *Genes Dev*. 2006;20(10):1321–1330.
78. Thomas T, et al. Monocytic leukemia zinc finger protein is essential for the development of long-term reconstituting hematopoietic stem cells. *Genes Dev*. 2006;20(9):1175–1186.
79. Summers AR, et al. HDAC3 is essential for DNA replication in hematopoietic progenitor cells. *J Clin Invest*. 2013;123(7):3112–3123.
80. Cullen SM, Mayle A, Rossi L, Goodell MA. Hematopoietic stem cell development: an epigenetic journey. *Curr Top Dev Biol*. 2014;107:39–75.
81. Mostoslavsky R, et al. Genomic instability and aging-like phenotype in the absence of mammalian SIRT6. *Cell*. 2006;124(2):315–329.
82. Ceccaldi R, et al. Bone marrow failure in Fanconi anemia is triggered by an exacerbated p53/p21 DNA damage response that impairs hematopoietic stem and progenitor cells. *Cell Stem Cell*. 2012;11(1):36–49.
83. Abbas HA, et al. Mdm2 is required for survival of hematopoietic stem cells/progenitors via dampening of ROS-induced p53 activity. *Cell Stem Cell*. 2010;7(5):606–617.
84. Simeonova I, et al. Mutant mice lacking the p53 C-terminal domain model telomere syndromes. *Cell Rep*. 2013;3(6):2046–2058.
85. Hockemeyer D, Palm W, Wang RC, Couto SS, de Lange T. Engineered telomere degradation models dyskeratosis congenita. *Genes Dev*. 2008;22(13):1773–1785.
86. Wang Y, Shen MF, Chang S. Essential roles for Pot1b in HSC self-renewal and survival. *Blood*. 2011;118(23):6068–6077.
87. O'Meara MM, Zhang F, Hobert O. Maintenance of neuronal laterality in Caenorhabditis elegans through MYST histone acetyltransferase complex components LSY-12, LSY-13 and LIN-49. *Genetics*. 2010;186(4):1497–1502.
88. Laue K, et al. The multidomain protein Brpf1 binds histones and is required for Hox gene expression and segmental identity. *Development*. 2008;135(11):1935–1946.
89. Mishima Y, et al. The Hbo1-Brd1/Brpf2 complex is responsible for global acetylation of H3K14

and required for fetal liver erythropoiesis. *Blood*. 2011;118(9):2443–2453.
90. Yan K, et al. The chromatin regulator BRPF3 preferentially activates the HBO1 acetyltransferase but is dispensable for mouse development and survival. *J Biol Chem*. 2016;291(6):2647–2663.
91. Feng Y, et al. BRPF3-HBO1 regulates replication origin activation and histone H3K14 acetylation. *EMBO J*. 2016;35(2):176–192.
92. Perez-Campo FM, Borrow J, Kouskoff V, Lacaud G. The histone acetyl transferase activity of monocytic leukemia zinc finger is critical for the proliferation of hematopoietic precursors. *Blood*. 2009;113(20):4866–4874.
93. Kueh AJ, Dixon MP, Voss AK, Thomas T. HBO1 is required for H3K14 acetylation and normal transcriptional activity during embryonic development. *Mol Cell Biol*. 2011;31(4):845–860.
94. Thomas T, Voss AK, Chowdhury K, Gruss P. Querkopf, a MYST family histone acetyltransferase, is required for normal cerebral cortex development. *Development*. 2000;127(12):2537–2548.
95. Shima H, et al. Bromodomain-PHD finger protein 1 is critical for leukemogenesis associated with MOZ-TIF2 fusion. *Int J Hematol*. 2014;99(1):21–31.
96. Moore SD, et al. Uterine leiomyomata with t(10;17) disrupt the histone acetyltransferase MORF. *Cancer Res*. 2004;64(16):5570–5577.
97. Grasso CS, et al. The mutational landscape of lethal castration-resistant prostate cancer. *Nature*. 2012;487(7406):239–243.
98. Lynch H, et al. Can unknown predisposition in familial breast cancer be family-specific? *Breast J*. 2013;19(5):520–528.
99. Zack TI, et al. Pan-cancer patterns of somatic copy number alteration. *Nat Genet*. 2013;45(10):1134–1140.
100. Kraft M, et al. Disruption of the histone acetyltransferase MYST4 leads to a Noonan syndrome-like phenotype and hyperactivated MAPK signaling in humans and mice. *J Clin Invest*. 2011;121(9):3479–3491.
101. Clayton-Smith J, et al. Whole-exome-sequencing identifies mutations in histone acetyltransferase gene KAT6B in individuals with the Say-Barber-Biesecker variant of Ohdo syndrome. *Am J Hum Genet*. 2011;89(5):675–681.
102. Simpson MA, et al. De novo mutations of the gene encoding the histone acetyltransferase KAT6B cause Genitopatellar syndrome. *Am J Hum Genet*. 2012;90(2):290–294.
103. Campeau PM, et al. Mutations in KAT6B, encoding a histone acetyltransferase, cause Genitopatellar syndrome. *Am J Hum Genet*. 2012;90(2):282–289.
104. Yu HC, Geiger EA, Medne L, Zackai EH, Shaikh TH. An individual with blepharophimosis-ptosis-epicanthus inversus syndrome (BPES) and additional features expands the phenotype associated with mutations in KAT6B. *Am J Med Genet A*. 2014;164A(4):950–957.
105. Arboleda VA, et al. De novo nonsense mutations in KAT6A, a lysine acetyl-transferase gene, cause a syndrome including microcephaly and global developmental delay. *Am J Hum Genet*. 2015;96(3):498–506.
106. Tham E, et al. Dominant mutations in KAT6A cause intellectual disability with recognizable syndromic features. *Am J Hum Genet*. 2015;96(3):507–513.
107. Yang XJ. MOZ and MORF acetyltransferases: Molecular interaction, animal development and human disease. *Biochim Biophys Acta*. 2015;1853(8):1818–1826.